

# PACIFIC EARTHQUAKE ENGINEERING RESEARCH CENTER

## **Application Guide for the Design of Flexible and Rigid Bus Connections between Substation Equipment Subjected to Earthquakes**

**Jean-Bernard Dastous**

Institut de Recherche d'Hydro-Québec

**Armen Der Kiureghian**

University of California, Berkeley

# **Application Guide for the Design of Flexible and Rigid Bus Connections between Substation Equipment Subjected to Earthquakes**

**Jean-Bernard Dastous**

Expertise Mécanique, Métallurgie et Hydro-Éolien  
Institut de Recherche d'Hydro-Québec

**Armen Der Kiureghian**

Department of Civil and Environmental Engineering  
University of California, Berkeley

PEER Report 2010/04  
Pacific Earthquake Engineering Research Center  
College of Engineering  
University of California, Berkeley

September 2010

## **ABSTRACT**

Interaction between equipment subjected to earthquakes is an area of major concern to engineers intent on seismically hardening a substation. The buswork connections installed between equipment greatly affect the seismic performance of that equipment. If the buswork is not properly designed, equipment that would otherwise survive may fail, resulting in unnecessary financial losses or reliability impact. The use of seismically designed connections, whether flexible, rigid, or a combination of both, increases the probability that a facility will still be operational after an earthquake.

This application guide addresses the design of flexible and rigid buswork connections to incorporate the seismic interaction between equipment. A complete design process is presented along with a detailed description of the required input, and details for a proper installation. The guide also addresses the concept of developing standard details to use for most common types of flexible connections as opposed to custom designing all connections. Practical design examples are provided for flexible and rigid buses. Available data on the dynamic properties of substation equipment are provided as well.

## **ACKNOWLEDGMENTS**

This study was sponsored by the Pacific Earthquake Engineering Research Center's Program of Applied Earthquake Engineering Research of Lifelines supported by the Pacific Gas and Electric Company, California Energy Commission, and California Department of Transportation. Opinions, findings, and conclusions or recommendations expressed in this material are those of the authors and do not necessarily reflect those of the sponsors.

The authors wish to thank Eric Fujisaki of Pacific Gas and Electric Company for his valuable support during the course of this project.

# CONTENTS

<b>ABSTRACT</b> .....	<b>iii</b>
<b>ACKNOWLEDGMENTS</b> .....	<b>iv</b>
<b>TABLE OF CONTENTS</b> .....	<b>v</b>
<b>LIST OF FIGURES</b> .....	<b>ix</b>
<b>LIST OF TABLES</b> .....	<b>xiii</b>
<b>1 INTRODUCTION</b> .....	<b>1</b>
1.1 Overview .....	1
1.2 Scope .....	2
1.3 Purpose .....	2
1.4 Practical References .....	2
1.5 Definitions, Abbreviations, and Acronyms.....	2
1.5.1 Definitions.....	2
1.5.2 Abbreviations and Acronyms.....	5
<b>2 INTERACTION OF SUBSTATION EQUIPMENT DURING EARTHQUAKES</b> .....	<b>7</b>
2.1 General Description .....	7
2.2 Observations from Past Earthquakes .....	8
2.3 Main Research Results on Interaction.....	8
<b>3 GENERAL DESIGN PROCESS</b> .....	<b>11</b>
3.1 Overview of Main Design Criteria.....	11
3.1.1 Permitting Differential Displacement between Equipment .....	11
3.1.2 Meeting Electrical Clearances.....	12
3.1.3 Multi-Connected Equipment Effects.....	13
3.1.4 Forces Expected at the Terminals .....	13
3.1.5 Stability to Operational Loads .....	15
3.2 Design Process for Seismic Connections.....	15
<b>4 DETERMINATION OF SEISMIC INPUT</b> .....	<b>17</b>
4.1 General Characterization of Seismic Input .....	17
4.2 Concept of Response Spectrum .....	18
4.2.1 Normalized and Local Response Spectra.....	21

<b>5</b>	<b>DETERMINATION OF BASIC CONNECTION GEOMETRY .....</b>	<b>25</b>
<b>6</b>	<b>DETERMINATION OF ELONGATION DEMAND.....</b>	<b>27</b>
6.1	Required Components of Displacement to Establish the Elongation Demand.....	28
6.2	Determination of Differential Displacement of Stand-Alone Equipment.....	31
6.2.1	Introduction .....	31
6.2.2	Available Analytical/Numerical Methods .....	32
6.2.3	Comparison and Use of the Different Analytical Methods.....	36
6.2.4	Values of the First Modal Participation Factor for the Generalized SDOF Method .....	38
6.2.5	Evaluation of Stand-Alone Equipment Displacement through Testing.....	48
6.3	Combination of Individual Displacements to Obtain Elongation Demand .....	50
<b>7</b>	<b>FLEXIBLE BUSWORK SEISMIC DESIGN.....</b>	<b>53</b>
7.1	Advantages and Limitations of Flexible Connections .....	53
7.2	Available Shapes, Required Conductor Length, and Qualitative Behavior.....	54
7.2.1	Typical Shapes .....	54
7.2.2	Required Conductor Length.....	55
7.2.3	Qualitative Investigation on the Flexibility of the Different Shapes under Stretching .....	57
7.2.4	Qualitative Effects of Adding Slack .....	63
7.3	Verification of Clearances, Flexibility, and Stability Using the Nonlinear Finite Element Method.....	65
7.3.1	Introduction.....	65
7.3.2	Required Software for Flexible Conductor Analysis.....	68
7.3.3	Required Types of Elements in Flexible Conductor Modeling .....	68
7.3.4	Determination of Input Properties for the Beam Element Representing the Conductor.....	69
7.3.5	Calculation of the Initial Configuration of the Conductor .....	74
7.3.6	Verification of Clearances.....	84
7.3.7	Verification of Stability.....	85
7.3.8	Verification of Flexibility .....	93
7.4	Verification of Clearances, Stability, and Flexibility Experimentally.....	96
7.4.1	Verification of Clearances.....	96

7.4.2	Verification of Stability.....	97
7.4.3	Verification of Flexibility .....	98
7.5	Flexible Connection Design: Example 1.....	99
7.5.1	Determination of Elongation Demand .....	100
7.5.2	Preliminary Shape .....	102
7.5.3	Required Conductor Length.....	102
7.5.4	Verification of Clearances, Flexibility, and Stability.....	102
7.6	Flexible Connection Design: Example 2.....	107
7.6.1	Determination of Elongation Demand .....	108
7.6.2	Preliminary Shape: Trial 1 .....	110
7.6.3	Required Conductor Length: Trial 1 .....	110
7.6.4	Verification of Clearances, Flexibility, and Stability: Trial 1.....	110
7.6.5	Preliminary Shape: Trial 2 .....	112
7.6.6	Required Conductor Length: Trial 2.....	112
7.6.7	Verification of Clearances, Flexibility, and Stability: Trial 2.....	113
7.6.8	Preliminary Shape: Trial 3 .....	114
7.6.9	Required Conductor Length: Trial 3.....	114
7.6.10	Verification of Clearances, Flexibility, and Stability: Trial 3.....	115
7.7	Flexible Connection Design: Example 3.....	119
7.7.1	Determination of Elongation Demand .....	121
7.7.2	Preliminary Shape: Trial 1 .....	122
7.7.3	Required Conductor Length: Trial 1 .....	122
7.7.4	Verification of Clearances, Flexibility, and Stability: Trial 1.....	122
7.7.5	Preliminary Shape: Trial 2 .....	123
7.7.6	Required Conductor Length: Trial 2.....	124
7.7.7	Verification of Clearances, Flexibility, and Stability: Trial 2.....	125
7.8	Standardized Design of Flexible Buswork.....	129
7.8.1	How to Establish Standardized Design Tables .....	130
7.8.2	Example of a Standardized Design Table for Flexible Configurations .....	133
7.9	Installation of Flexible Buswork.....	138
<b>8</b>	<b>SEISMIC DESIGN OF RIGID BUSWORK .....</b>	<b>141</b>
8.1	Introduction.....	141

8.1.1	General Description of Rigid Bus Connections .....	141
8.1.2	Design Principles of Rigid Bus Conductors .....	144
8.1.3	Available Methods to Evaluate the Interaction Effect .....	144
8.2	Determination of Rigid Bus Connection Properties .....	145
8.2.1	Experimental Determination .....	145
8.2.2	Numerical Determination .....	148
8.3	Evaluation of Interaction between Equipment Connected by Rigid Bus Using Simplified Analysis Methods .....	148
8.3.1	Basic Assumptions .....	148
8.3.2	Seismic Interaction in Linearly Connected Equipment .....	149
8.3.3	Deformation of the Rigid Bus–Flexible Connector (RB–FC) .....	155
8.3.4	Simplified Method to Analyze Interaction due to Nonlinear Rigid Bus Connections .....	157
8.4	Rigid Bus Connection Design: Example 1 .....	161
8.4.1	Linear Analysis .....	162
8.4.2	Nonlinear Analysis .....	162
8.5	Rigid Bus Connection Design: Example 2 .....	167
8.5.1	Linear Analysis .....	168
8.5.2	Nonlinear anaLysis .....	171
<b>9</b>	<b>OTHER CONSIDERATIONS .....</b>	<b>173</b>
9.1	Considerations of Interest in Other Standards .....	173
9.2	Bird Caging of Flexible Conductors .....	174
9.3	Prevention of Clearance Violation with Flexible Bus Using Rigid Bus Extensions .....	174
	<b>REFERENCES.....</b>	<b>177</b>
	<b>APPENDIX A: GENERAL DESIGN TREE FOR FLEXIBLE CONNECTION FROM IEEE STD 1527-2006</b>	
	<b>APPENDIX B: FEAP INPUT FILES FOR FLEXIBLE CONFIGURATION EXAMPLES</b>	

## LIST OF FIGURES

Fig. 2.1	Displacement between interconnected equipment during an earthquake .....	7
Fig. 3.1	Schematic view of electrical clearance distance requirements .....	12
Fig. 3.2	Practical example of required clearances.....	13
Fig. 3.3	Flowchart for design of seismic connections.....	16
Fig. 4.1	90° component of horizontal ground acceleration from the 1989 Loma Prieta earthquake $M_w$ 7.0 recorded at station no. 58222 (San Francisco Presidio).....	17
Fig. 4.2	Idealization of equipment by a single-degree-of-freedom system.....	19
Fig. 4.3	Construction of response spectrum.....	20
Fig. 4.4	IEEE 693 performance-level response spectrum for the moderate level (0.5 g) .....	22
Fig. 4.5	Montreal response spectrum from the National Building Code of Canada 2005 .....	22
Fig. 5.1	Basic connection geometry .....	25
Fig. 5.2	Determination of basic geometry from connector extremities .....	26
Fig. 5.3	Example of basic connection geometry .....	26
Fig. 6.1	Theoretical maximum elongation demand.....	29
Fig. 6.2	Ratio of estimated elongation $D_L$ over “real” elongation $e_o$ when $D_L=D_T$ ( $D_V=0$ ) .....	30
Fig. 6.3	Generalized single-degree-of-freedom system .....	33
Fig. 6.4	Example of equipment and corresponding finite element model .....	34
Fig. 6.5	Example of modal superposition (Clough and Penzien 1975).....	35
Fig. 6.6	Cantilever beam (a) and its first three modes (b) (Clough and Penzien 1975).....	36
Fig. 6.7	Models used for theoretical evaluation of first modal participation factor in Dastous et al. (2004) .....	39
Fig. 6.8	First modal participation factor for a beam of constant property with lumped mass on top .....	40
Fig. 6.9	First modal participation factor for equipment on a support (beams of constant properties along their height) .....	43
Fig. 6.10	First modal participation factor versus frequency for all equipment surveyed .....	45
Fig. 6.11	Upper-bound displacement according to IEEE 693 required spectra for 2% damping.....	46
Fig. 6.12	Difference between required response spectrum and time history input spectrum .....	49

Fig. 7.1	Basic flexible conductor configurations .....	54
Fig. 7.2	Alternative flexible conductor configurations (Opsetmoen 1998) .....	55
Fig. 7.3	Results of flexibility testing at BC Hydro on different configurations (Opsetmoen 1998) .....	58
Fig. 7.4	General behavior of flexible connections under stretching .....	59
Fig. 7.5	Effect of shape on flexibility for a constant $\beta$ value of 0.8 (span 4 m, $e_o=30$ cm, slack=37.5 cm for all shapes (except parabola half circle).....	61
Fig. 7.6	Effect of shape on flexibility for a constant $\beta$ value of 0.5 (span 4 m, $e_o=30$ cm, slack=60 cm for all shapes (except parabola half circle).....	62
Fig. 7.7	Effect of adding slack for catenary shapes of different spans (1796 KCM conductor, safety clearances for 170 kV, insulator length 1.7 m) .....	64
Fig. 7.8	Effect of adding slack on sag for catenary configurations of different spans.....	65
Fig. 7.9	Comparison between calculated and measured shape of a catenary configuration .....	67
Fig. 7.10	Clearance check with the finite element method with double-curvature configurations of different spans .....	67
Fig. 7.11	Comparison between calculated and measured forces of static push-pull tests on catenary configurations.....	68
Fig. 7.12	General procedure to establish the initial configuration of the conductor.....	75
Fig. 7.13	Snap-back and snap-through.....	81
Fig. 7.14	Unstable and stable solutions for snap-back.....	82
Fig. 7.15	Geometric points required to check clearances .....	87
Fig. 7.16	Calculated configuration without weight.....	92
Fig. 7.17	Load-displacement curve using the arc length continuation method.....	92
Fig. 7.18	Calculated configuration with weight using the arc length method .....	93
Fig. 7.19	Load-displacement curve with 0.25 m cyclic displacement.....	94
Fig. 7.20	Load-displacement curve with 1.0 m cyclic displacement .....	95
Fig. 7.21	Load-displacement curve with 1.35 m cyclic displacement.....	96
Fig. 7.22	Measured geometry of a configuration under its self-weight (Stevenson and Beattie 1990).....	97
Fig. 7.23	Experimental investigation of stability using water-filled tubes (Stevenson and Beattie 1990).....	97

Fig. 7.24	Experimental investigation of stability to wind load using water-filled tubes (Stevenson and Beattie 1990) .....	98
Fig. 7.25	Schematic of experimental setup to investigate flexibility (Stevenson and Beattie 1990) .....	98
Fig. 7.26	Experimental setup to investigate flexibility (Bhuyan et al. 2001) .....	99
Fig. 7.27	Example 1: general description and main dimensions (mm).....	100
Fig. 7.28	Verification of clearances for example 1 .....	104
Fig. 7.29	Force-elongation curve for example 1 at equipment terminals .....	105
Fig. 7.30	Equilibrium position for example 1 under 45 mm of radial ice.....	106
Fig. 7.31	Equilibrium position for example 1 with 160 km/hr wind .....	107
Fig. 7.32	Example 2 general description and main dimensions (mm).....	109
Fig. 7.33	Verification of clearances for example 2, trial 1.....	112
Fig. 7.34	Verification of clearances for example 2, trial 2.....	115
Fig. 7.35	Verification of clearances for example 2, trial 3.....	117
Fig. 7.36	Force-elongation curve for example 2, trial 3, at equipment terminals .....	118
Fig. 7.37	Equilibrium position for example 2, trial 3, with 90 km/hr wind.....	119
Fig. 7.38	Example 3 general description and main dimensions (mm).....	120
Fig. 7.39	Verification of clearances for example 3, trial 1.....	124
Fig. 7.40	Verification of clearances for example 3, trial 2.....	127
Fig. 7.41	Force-elongation curve for example 3, trial 2, at equipment terminals .....	127
Fig. 7.42	Equilibrium position for example 3 with 48 km/hr wind and 6.35 mm radial ice.....	129
Fig. 7.43	Bus bar dimensions for 145 kV standardized table example.....	134
Fig. 7.44	Double-curvature configurations for 145 kV standardized table example .....	136
Fig. 7.45	Triple-curvature configurations for 145 kV standardized table example .....	136
Fig. 7.46	Catenary configurations for 145 kV standardized table example.....	137
Fig. 7.47	Geometry to determine length to cut for flexible connections .....	138
Fig. 8.1	Rigid bus with flexible connector (Filiatrault et al. 1999).....	141
Fig. 8.2	Flexible strap connectors (Song et al. 2006).....	142
Fig. 8.3	Slider connectors (Song et al. 2006).....	142
Fig. 8.4	Custom-made BPA flexible connector (courtesy of Leon Kempner, Bonneville Power Administration).....	143
Fig. 8.5	ATC-24 test protocol .....	146

Fig. 8.6	Load displacement response of a spring connector at different ductility levels (Filiatrault et al. 1999) .....	147
Fig. 8.7	Model of two equipment items connected by a linear RB–FC .....	150
Fig. 8.8	Influence of dynamic interaction on seismic demand of low-frequency (left) and high-frequency (right) equipment items. Parameter values are $f_2 = \omega_2 / 2\pi = 10$ Hz, $m_1 / m_2 = 2$ , $\zeta_1 = \zeta_2 = 0.02$ , $\alpha_1 = \alpha_2 = 1$ , and $c_0 = 0$ . .....	153
Fig. 8.9	Influence of ratio of equipment masses on the seismic demand of the high- frequency equipment. Parameter values are $f_2 = \omega_2 / 2\pi = 10$ Hz, $k_0 / (k_1 + k_2) = 0.2$ , $\zeta_1 = \zeta_2 = 0.02$ , $\alpha_1 = \alpha_2 = 1$ , and $c_0 = 0$ . .....	154
Fig. 8.10	Influence of damping of RB–FC on the seismic demand of the high-frequency equipment. Parameter values are $f_2 = \omega_2 / 2\pi = 10$ Hz, $k_0 / (k_1 + k_2) = 0.2$ , $m_1 / m_2 = 2$ , $\zeta_1 = \zeta_2 = 0.02$ , and $\alpha_1 = \alpha_2 = 1$ . .....	155
Fig. 8.11	Influence of participation factors on the seismic demand of the high-frequency equipment. Parameter values are $f_2 = \omega_2 / 2\pi = 10$ Hz, $k_0 / (k_1 + k_2) = 0.2$ , $m_1 / m_2 = 2$ , $\zeta_1 = \zeta_2 = 0.02$ , and $c_0 = 0$ . .....	155
Fig. 8.12	Deformation of the RB–FC relative to the differential displacement between stand-alone equipment items. Parameter values are $f_2 = \omega_2 / 2\pi = 10$ Hz, $m_1 / m_2 = 2$ , $\zeta_1 = \zeta_2 = 0.02$ , $\alpha_1 = \alpha_2 = 1$ and $c_0 = 0$ . .....	157
Fig. 8.13	Hysteretic behavior of two FCs under quasi-static tests (Song et al. 2006) .....	158
Fig. 8.14	Definition of equivalent stiffness of RB–FC .....	159
Fig. 9.1	Clamps used to prevent bird caging .....	174

## LIST OF TABLES

Table 2.1	Maximum forces measured during experiments with flexible connections .....	10
Table 3.1	Design forces from seismically induced dynamic effects of flexible conductors, for IEEE 693 moderate and high qualification performance levels .....	15
Table 4.1	Spectral displacements comparison between IEEE 693 for the moderate level and Montreal spectra, for 5% damping .....	23
Table 6.1	Practical values of $D_L/e_o$ for a span of 3 m (10 ft) with $H/L=0$ .....	30
Table 6.2	Modal participation factor of a cantilever beam of constant properties .....	37
Table 6.3	Natural frequencies and spectral displacements of a cantilever beam using the high performance level IEEE 693 response spectrum at 2% damping.....	37
Table 6.4	Example comparison of the SDOF, generalized SDOF, and MDOF methods .....	37
Table 6.5	First modal participation factor for beam of constant property with lumped mass....	40
Table 6.6	Set of parameters used for studying the influence of support .....	42
Table 6.7	Results of survey on first modal participation factor.....	45
Table 6.8	Upper-bound displacement according to IEEE 693 required spectra for 2% damping .....	47
Table 7.1	Summary of basic flexible configurations characteristics.....	55
Table 7.2	Properties of the Bersimis 42/7 conductor.....	70
Table 7.3	Common conductor input properties for finite element calculations .....	74
Table 7.4	Properties of the 4000 kcmil conductor.....	90
Table 7.5	Computational parameters for example of stability using <i>FEAP</i> .....	91
Table 7.6	Example 1: basic data .....	99
Table 7.7	Computational parameters for example 1 using <i>FEAP</i> software.....	103
Table 7.8	Example 2: basic data .....	108
Table 7.9	Computational parameters for example 2 using <i>FEAP</i> software, trial 1 .....	111
Table 7.10	Computational parameters for example 2 using <i>FEAP</i> software, trial 2 .....	113
Table 7.11	Computational parameters for example 2 using <i>FEAP</i> software, trial 3 .....	116
Table 7.12	Example 3: basic data .....	121
Table 7.13	Computational parameters for example 3, trial 1, using <i>FEAP</i> software .....	123
Table 7.14	Computational parameters for example 3 using <i>FEAP</i> software, trial 2 .....	125
Table 7.15	Example of standardized rigid bus bar dimensions for a given utility .....	131

Table 7.16	Length and availability for inverse parabola configuration.....	135
Table 7.17	Length and availability for double-curvature configuration.....	135
Table 7.18	Length and availability for triple-curvature configuration .....	136
Table 7.19	Length and availability for catenary configuration .....	137
Table 7.20	Standardized table for the 145 kV example.....	138
Table 8.1	Available load-displacement curves for rigid bus flexible connector .....	147
Table 8.2	Summary of iterations for rigid bus design example 1 .....	165
Table 8.3	Summary of iterations for rigid bus design example 2.....	171

# 1 Introduction

## 1.1 OVERVIEW

Interaction between equipment subjected to earthquakes is an area of major concern to engineers intent on seismically hardening a substation. The buswork connections installed between equipment greatly affect the seismic performance of that equipment. If the buswork is not properly designed, equipment that would otherwise survive can fail, compromising the reliability of the system and resulting in unnecessary financial losses. The use of seismically designed connections, whether flexible, rigid, or a combination of both, increases the probability that a facility will still be operational after an earthquake.

This application guide addresses the design of flexible and rigid buswork connections to incorporate the seismic interaction between equipment. A complete design process is presented along with a detailed description of the required input, and details for a proper installation. The guide also addresses the concept of developing standard details to use for the most common types of flexible connections as opposed to custom designing all connections. Practical design examples are provided for flexible and rigid buses. Available data on the dynamic properties of substation equipment are provided as well.

This application guide does not address the particular case of interconnections with air core reactors, which require special considerations due to, among others, their special construction and proximity to the significant electrical field around such equipment.

This application guide was intentionally presented presuming a minimum knowledge of mathematics and structural dynamics. Therefore, as much as possible, it focuses on the concepts and the use of specific software (whenever applicable), rather than on the underlying mathematics.

## 1.2 SCOPE

The scope of this document is the engineering and design of flexible and rigid bus connections for substation equipment subjected to earthquakes.

## 1.3 PURPOSE

This document was prepared to provide practical guidelines to the substation designer on seismic design of buswork connections. The intent is to complement and extend the content of IEEE Std 1527-2006 (IEEE 2006) by providing details, information, and guidelines that will permit a user to apply in a practical way the methods, sometimes complex, that form the basis of this standard. An additional aim is to sensitize equipment manufacturers and utility engineers to the dynamic forces that are transmitted from flexible and rigid bus connections at the attachment points of equipment items during earthquakes.

## 1.4 PRACTICAL REFERENCES

This application guide complements the following publications:

- IEEE Std 605-2008, *IEEE Guide for Design of Substation Bus Structures*
- IEEE Std 693-2005, *IEEE Recommended Practice for the Seismic Design of Substations*
- IEEE Std 1527-2006, *IEEE Recommended Practice for the Design of Flexible Buswork Located in Seismically Active Areas*

## 1.5 DEFINITIONS, ABBREVIATIONS, AND ACRONYMS

### 1.5.1 Definitions

**Basketing of flexible conductors (also called “bird caging”):** The unraveling or untwisting of outer and inner strands. Basketing can be caused by the following:

- minimum bending radius is violated
- ends being twisted opposite to direction of lay angle

**Bundled conductor:** An assembly of two or more conductors used as a single conductor and employing spacers to maintain a predetermined configuration. The individual conductors of this assembly are called subconductors.

**Complete quadratic combination (CQC method):** A modal combination method, especially useful for systems with closely spaced natural frequencies.

**Conductor configuration:** The generic term for a flexible buswork connection geometry that has been designed to accommodate a certain amount of movement at end points, without putting undue strain or stress on these end points.

**Critical damping:** The least amount of viscous damping that causes a single-degree-of-freedom system to return to its original position without oscillation after initial disturbance.

**Damping:** An energy-dissipation mechanism that reduces the response amplification and broadens the vibratory response over frequency in the region of resonance. Damping is usually expressed as a percentage of critical damping. See also: critical damping.

**Differential displacement between equipment:** The maximum absolute relative displacement between two equipment items moving toward or away from each other during an earthquake, or for design purposes.

**Drops:** The field or construction term for the flexible buswork connection made between a high buswork section, either rigid or strained and a piece of equipment or lower buswork section.

**Flexible buswork or flexible buswork connections:** Terms given to the section of buswork that is usually made up of stranded bare conductors (as opposed to rigid conductors) electrically interconnecting two pieces of equipment, a piece of equipment and a section of rigid bus, or two sections of rigid bus.

**g:** Acceleration due to gravity, i.e., 9.81 m/s<sup>2</sup>.

**Ground acceleration:** The acceleration of the ground resulting from the motion of a given earthquake. The maximum or peak ground acceleration is the zero period acceleration (ZPA) of the ground response spectrum.

**Natural frequency:** A frequency at which a body or system vibrates due to its own physical characteristics (mass and stiffness) when the body or system is distorted and then released.

**Pinch effect:** The “pinch effect” is caused by the bending of the conductor during a high-velocity movement caused by short-circuit forces near where a spacer or equipment terminal clamp is attached.

**Push-pull tests:** The name given to a test to determine how flexible a certain conductor configuration is when its end points are pulled apart or pushed together. The results of this test are units of force per displacement of the connection point of the conductor.

**Response spectrum:** A plot of the maximum absolute response of an array of single-degree-of-freedom (SDOF) identically damped oscillators with different frequencies, all subjected to the same base excitation. See also: single-degree-of-freedom system.

**Seismically decouple:** A term to describe how two pieces of equipment or a piece of equipment and a rigid bus section can be interconnected electrically by a flexible buswork connection, which ideally allows independent movement, or at least, minimized interaction between the two components.

**Seismicity:** Seismic activity; the occurrence of earthquakes in time and space.

**Single-degree-of-freedom (SDOF) system:** The idealization of a physical system in which its mass, its elastic properties (flexibility or rigidity), its energy-loss mechanism (damping), and its external source of excitation (loading) are assumed to be concentrated in a single physical element.

**Slack (or “conductor slack”):** The difference between the conductor length and the straight-line distance between its attachment points; the amount of displacement that a conductor in a given configuration can be stretched into a straight configuration.

**Square root of the sum of squares method (SRSS method):** A modal combination method used to obtain an estimation of the complete response of a system, by summing up the square of each modal response considered in the analysis (such as displacement, force, etc.) and then taking the square root of the result. This method assumes that individual maximum modal responses are not correlated, which is approximately the case when modal frequencies are spaced by more than 20% of each other. See also: complete quadratic combination (CQC method).

**Stand-alone equipment displacement:** The motion of equipment without conductors attached, i.e., without interconnection to other equipment.

**Time history:** A record of earthquake ground motion (either natural or artificial), usually in terms of acceleration, as a function of time.

### **1.5.2 Abbreviations and Acronyms**

CQC	complete quadratic combination
MDOF	multi-degree-of-freedom
PGA	peak ground acceleration
SDOF	single-degree-of-freedom
SRSS	square root of sum of squares
ZPA	zero period acceleration

## 2 Interaction of Substation Equipment during Earthquakes

### 2.1 GENERAL DESCRIPTION

Substation equipment is generally seismically qualified on a stand-alone basis, without consideration of the conductor (rigid or flexible) that normally interconnects them. However, during an earthquake, interconnected equipment will move relative to one another, stretching and compressing the connection between (Fig. 2.1). This differential displacement between equipment items will result in additional forces transmitted from the conductor to their attachment points. These forces in turn translate into moments at the bases of the equipment insulators, which may be vulnerable if not qualified accordingly; hence equipment that would otherwise survive in a stand-alone configuration may fail. Also, the connection itself creates to some degree interaction between equipment that may adversely modify their seismic behavior, as compared to stand-alone behavior. The use of properly designed and installed connections increases the probability that a facility will remain operational after an earthquake.

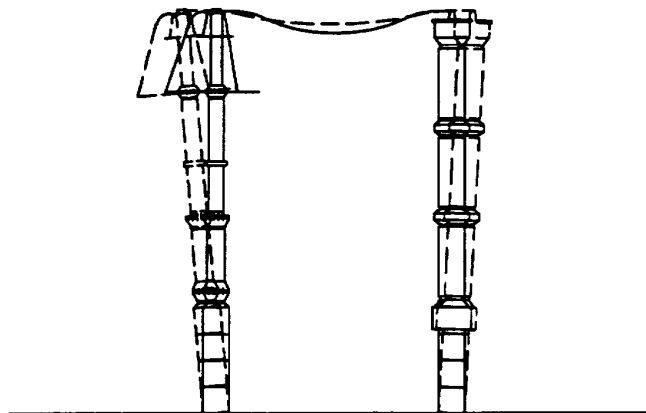


**Fig. 2.1 Displacement between interconnected equipment during an earthquake**

## 2.2 OBSERVATIONS FROM PAST EARTHQUAKES

In past earthquakes, it has been suspected that the presence of conductors between equipment experiencing differential displacement might be responsible for generating destructive forces at the tops of such apparatus. For example, during the 1978 Miyagi, Japan, earthquake, many units of interconnected equipment failed, even though they were individually qualified to withstand the effects of an event of that magnitude; connections were then identified as one of the important causes of destruction (Okada et al. 1986). Similar conclusions were drawn after the 1986 North Palm Springs, California, earthquake (EPRI 1998); the 1988 Saguenay, Quebec, Canada, earthquake (Pierre 1991); and the 1995 Kobe, Japan, earthquake (NIST 1996). From these observations basic recommendations to provide at least adequate conductor slack have been provided in some guides and standards (e.g., IEEE 2005; Schiff 1998) although it is only recently that more specific guidance has been formally provided through IEEE 1527.

## 2.3 MAIN RESEARCH RESULTS ON INTERACTION

To our knowledge, the first research on conductor interaction was initiated in Japan about 25 years ago, after observations from the Miyagi earthquake (Okada et al. 1986). In the early 1990s, research began in Hydro-Quebec, where the dynamics of conductors was experimentally investigated (Dastous and Pierre 1996). Since then, several groups have begun and/or pursued research on the subject, either analytically and/or experimentally: Hydro-Quebec, BPA, BC Hydro, and PEER (UC San Diego and UC Berkeley). Many methods recommended in IEEE 1527, as well as in this application guide, have evolved from these results. It is not the purpose of this application guide to present and discuss in depth these research results. A summary on flexible conductor research can be found in the appendix of IEEE 1527, and the bibliography of this guide refers, to the best of our knowledge, to the main publications in the domain, including studies on rigid bus connections. However, some of the main results that support the understanding behind this application guide are summarized here.

**Flexible and rigid conductors are dynamic rather than static systems:** Experimental and numerical simulation results have demonstrated that a connection responds dynamically rather than statically when excited from the motion of interconnected equipment. The response is not only a function of being stretched to a given elongation, but also of inertia and the energy-dissipation characteristics of the connection and the connected equipment.

**Significant interaction effects may take place when not enough slack is provided in a flexible connection:** In a pair of interconnected equipment, the response of the higher-frequency item may be adversely amplified as compared to its stand-alone behavior when insufficient slack is provided. In some cases this may also happen to the lower-frequency item due to the inertia of the conductor.

**Significant interaction effects may take place using rigid bus connections:** When a rigid bus connection is used, the higher-frequency equipment item motion may be amplified under certain conditions as compared to its stand-alone behavior; in the same way, the lower-frequency equipment item motion may be de-amplified. The interaction effect is strongly conditioned by the dynamic properties of the coupled system. The amplification of the higher-frequency item response tends to increase with increasing stiffness of the connecting element, increasing mass of the lower-frequency item, increasing separation between equipment frequencies, and increasing differential displacement between the stand-alone equipment items. Damping in the connecting element has a significant effect on reducing the amplification due to the interaction.

**The level of dynamic forces generated at the ends of a single flexible conductor may be on the order of 1000 N for a 0.5g PGA ground motion:** The forces generated at the ends of connections during a dynamic elongation can be much higher than under the corresponding static elongation. Analytical as well as experimental results on typical flexible conductor configurations have shown that the level of forces obtained during interconnected behavior is of the order of 1000 N (225 lbs) for a ground acceleration of 0.5g PGA, *even* when sufficient slack is provided (Table 2.1). The actual level of generated forces varies greatly and depends on many factors, including the shape and the amount of slack, the frequencies of the interconnected equipment, and the input used, among others. At this time, it is not possible to predict in a simplified fashion (without either experimentation or simulation) the forces that would be obtained under a given set of these parameters. The level of 1000 N/conductor is at this time the best estimate of the average maximum force that can be obtained when sufficient slack is provided, for one or two conductors, from 1796 kcmil to 4000 kcmil.

**The stand-alone differential displacement of equipment items is usually a conservative estimate of the interconnected equipment differential displacement when items are connected with a flexible or rigid bus connection.**

For flexible connections, the minimum required slack is the one that permits the expected maximum differential displacement between equipment items in their stand-alone configurations.

When sufficient slack is provided in a flexible connection, the frequencies of interconnected equipment are not significantly modified compared to their stand-alone frequencies provided that the mass of the bus is small relative to the equipment mass.

The frequencies of equipment items interconnected with a rigid bus are always greater than the corresponding frequencies of equipment items in their stand-alone configurations.

**Table 2.1 Maximum forces measured during experiments with flexible connections<sup>1</sup>**

Type of test / configuration--span-type of conductor	Equivalent maximum input acceleration to IEEE Std 693 (g)	Maximum horizontal force <sup>3</sup>	Reference
<ul style="list-style-type: none"> <li>• harmonic out of phase / catenary—5 m—1796 kcmil</li> <li>• harmonic out of phase / catenary—5 m—4000 kcmil</li> <li>• harmonic out of phase / catenary—3 m—1796 kcmil</li> </ul>	0.48 0.48 0.48	750 N 1590 N 1114 N	(Dastous and Pierre 1996)
<ul style="list-style-type: none"> <li>• 3 cycles sine wave / parabola—3 m—1796 kcmil</li> <li>• 3 cycles sine wave / parabola—4 m—4000 kcmil</li> <li>• 3 cycles sine wave / double curvature—5 m—4000 kcmil</li> <li>• 3 cycles sine wave / triple curvature —5 m—4000 kcmil</li> </ul>	0.48 0.48 0.48 0.48	1040 N 1140 N 720 N 620 N	(Dastous and Paquin 2003)
<ul style="list-style-type: none"> <li>• shake table time history test / catenary—4.6 m—2300 kcmil</li> <li>• shake table time history test / catenary—4.6 m—Lupine</li> <li>• shake table time history test / catenary—4.6 m—2300 kcmil</li> <li>• shake table time history test / catenary—4.6 m—Lupine</li> </ul>	0.5 0.5 0.5 0.5	1060 N 810 N 1330 N 1430 N	(Filiatrault and Stearns 2002)
<ul style="list-style-type: none"> <li>• shake table time history test / catenary—3.2 m—2300 kcmil</li> <li>• shake table time history test /catenary—3.2 m—2300 kcmil</li> <li>• shake table time history test / catenary—3.2 m—2300 kcmil</li> </ul>	0.5 0.5 0.5 <sup>2</sup>	693 N 730 N 948 N	(Gualifabian et al. 2004)

1. The results reported in this table were for flexible connections with sufficient slack to permit the differential displacement to be applied at the conductor's ends. No cases of resonance or strong interaction are reported in this table.
2. The actual experiment was conducted at 0.38g. The traction reported in this table for 0.5g is obtained by linear extrapolation from the measured traction for 0.38g.
3. Force per subconductor when multi-conductors were used (up to 2).
4. All conductors in these studies are all-aluminum conductors (AAC).

## 3 General Design Process

### 3.1 OVERVIEW OF MAIN DESIGN CRITERIA

This chapter presents an overview of the main mechanical criteria that a seismically designed connection must meet in order to be adequate. The establishment and/or verification of these criteria are expanded in the following clauses, along with practical examples.

#### 3.1.1 Permitting Differential Displacement between Equipment

It is intuitively obvious that an adequate flexible connection must allow the interconnected equipment to displace without sudden impact due to loss of all slack. To do so, the *maximum differential displacement* that can occur during an earthquake between interconnected equipment must be evaluated. From this quantity the *elongation demand* on the connection, i.e., the maximum stretch to which a connection would be submitted, can be determined. It has been established for flexible conductors that the amount of required slack, defined as the *availability* i.e., the stretch that a connection can tolerate without a sudden impact on the attached equipment, *must be at least equal* to the *elongation demand*. Due to the stiffness and the inertia of flexible conductors, the elongation demand is the *minimum* amount of required slack; depending on the conductor shape and/or flexibility, an additional length is needed in order for the transmitted forces to be within acceptable levels.

Rigid buses with a flexible connector should also allow for the differential displacement to take place without sudden impact. However, the dynamic properties of the coupled system, i.e., the equipment items and the connection, have a strong influence on the differential displacement and may reduce it, as compared to the differential displacement between the stand-alone equipment items.

### 3.1.2 Meeting Electrical Clearances

As with any air-insulated buswork, it is important that a flexible buswork connection maintain the minimum electrical clearances as specified in such documents as the National Electrical Safety Code (IEEE 2001) to ensure the proper operation and integrity of the facility and safety.

The required electrical clearances of a given configuration in its plane are illustrated in Figure 3.1 for a flexible bus; the same requirements apply to a rigid bus. These clearances are the *phase-to-ground* and the *minimum safety* clearances.

The phase-to-ground clearance appears as a radius from the base of the insulator (top of the metallic support) that is equal to or shorter than the insulator length. For proper clearance of this type, no part of the flexible connection should fall within the shaded area indicated in Figure 3.1. The minimum safety clearance appears as a vertical distance from the ground under which the conductor should not fall. For a given configuration, this translates into a maximum sag value that should not be exceeded. The flexible buswork design must also assure that the minimum phase-to-phase and phase-to-ground clearances will be maintained during and after a seismic event.

An example of the required clearances for a connection between a dead tank circuit breaker and a disconnect switch is presented in Figure 3.2.

Rigid buses should at all times meet clearances as well. Even though they deform much less than flexible buses, their flexible connectors add flexibility to the assembly and therefore should be checked for the required clearances.

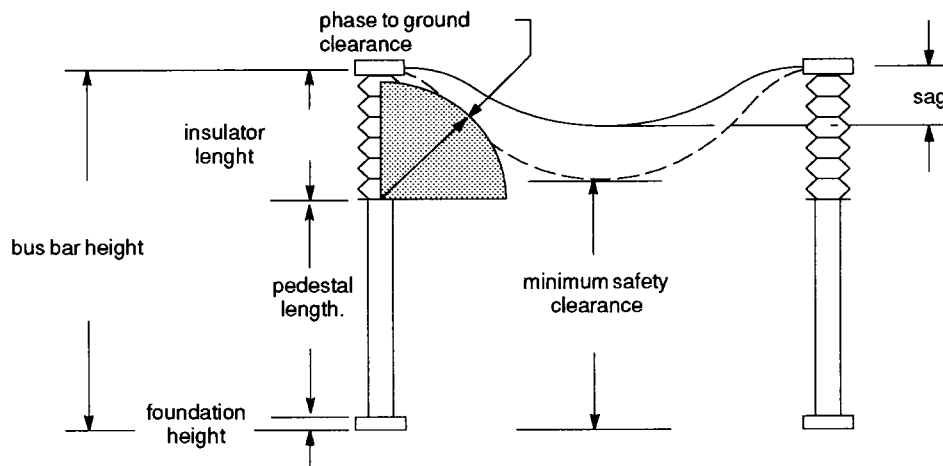
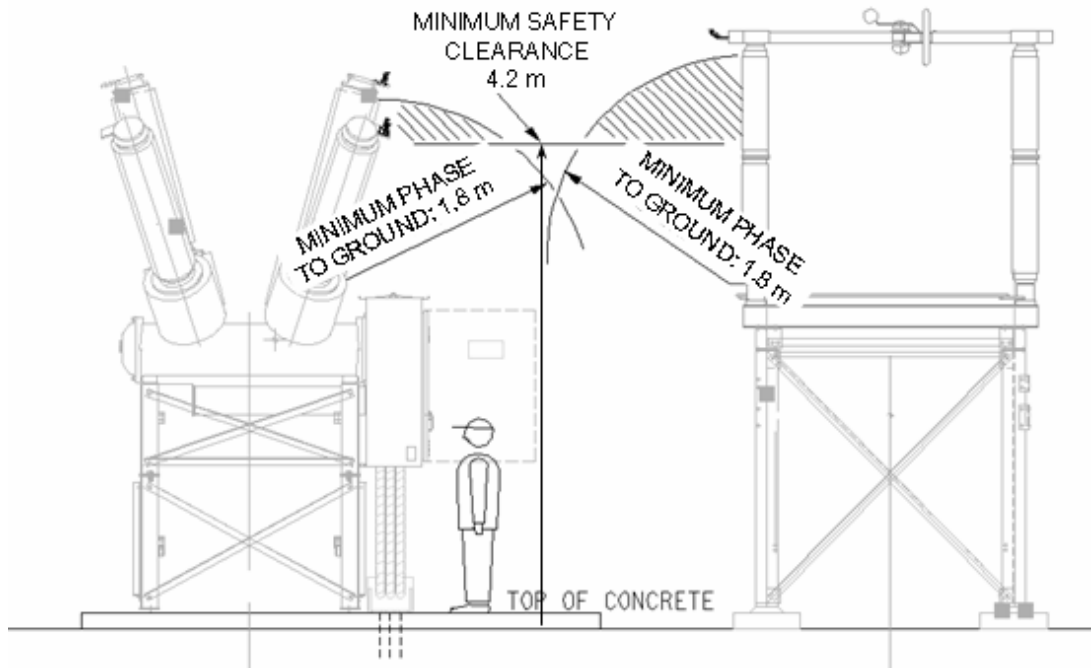


Fig. 3.1 Schematic view of electrical clearance distance requirements



**Fig. 3.2 Practical example of required clearances**

### 3.1.3 Multi-Connected Equipment Effects

It is important that in a given electrical phase, all connections are designed such that sufficient slack and/or flexibility are provided *between all interconnected equipment pairs*. Otherwise, impacts may be transferred between equipment, from pairs where slack is insufficient. In addition, for equipment items in a given electrical phase interconnected with rigid buses, it is important that the interaction effect between all pairs of items be within the permissible limits, particularly when the motion of connected equipment is amplified due to the interaction as compared to its stand-alone response.

### 3.1.4 Forces Expected at the Terminals

As discussed earlier, even for a flexible connection with sufficient slack or a rigid bus with a flexible connector, significant forces may be transferred to the terminals due to dynamic effects during a seismic event. Therefore, terminal hardware as well as equipment should be designed to withstand those loads in addition to normal and exceptional operating loads. These additional, normal, and exceptional loads are

- the weight of the connection system,
- the forces due to wind,
- ice loading,
- electrical fault condition (short-circuit forces), and
- normal operating forces.

Several of these loads can occur simultaneously thereby having a cumulative effect on the equipment terminal pads. *The probability of simultaneous occurrence of these loads must be reviewed on a case-by-case basis.* Short-circuit loads have not been found to be a significant cause of failure during past earthquakes (IEEE 2005).

Since the seismic qualification of equipment is done on a stand-alone basis, the effect of the loads (stresses) listed above must be included in the design in *direct combination* (i.e., *additional*) to the maximum stresses either measured or calculated in the seismic qualification process. The effect of many of these loads is to add an additional bending stress at the base of the insulator(s) of the equipment, since they are applied near the tops.

To account for dynamic effects of *flexible* conductors, design forces have been established based on available experimental (Table 2.1) and analytical results at this time (Dastous 2007); these design forces are presented in Table 3.1 according to the seismic input defined in the IEEE 693 Std. These forces are defined per subconductor, *for a maximum of two subconductors in a given connection*. In case of more than two subconductors, a separate study should be undertaken to evaluate these forces. As discussed in Section 4.3, the forces in Table 2.1 were obtained with the following all-aluminum conductors: 1796 kcmil, 2300 kcmil, 2500 kcmil, and 4000 kcmil, which are typical conductors used in interconnecting substation equipment. Note that the physical characteristics of the first three conductor types are relatively similar, while the 4000 kcmil conductor is relatively heavier but of similar minimum bending stiffness.

As an example, suppose that two equipment items qualified for the moderate level of IEEE-693 will be interconnected by a bundle of two subconductors. In such a case, additional vertical and horizontal forces of 2000 N (1000 N per subconductor) must be included as additional loads in the seismic design.

It is recognized that the forces in Table 3.1 might be especially significant for lower voltage and lighter equipment (230 kV and below). However, even for higher voltage, they cannot be neglected in most cases.

**Table 3.1 Design forces from seismically induced dynamic effects of flexible conductors, for IEEE 693 moderate and high qualification performance levels**

Design force <sup>a</sup>	Qualification level	
	moderate (0.5g)	high (1.0g)
Horizontal (at terminal pad in line direction)	1000 N per subconductor	2000 N per subconductor
Vertical (at terminal pad)	1000 N per subconductor	2000 N per subconductor

<sup>a</sup> These forces include the static forces due to conductor's weight

### 3.1.5 Stability to Operational Loads

Flexible or rigid connections must be designed such that their shapes regain their original form after the application of any normal and exceptional loads; i.e., they should not sustain any permanent deformation. For example, a connection must be designed so that it does not collapse laterally after the application of high wind.

## 3.2 DESIGN PROCESS FOR SEISMIC CONNECTIONS

Appendix A presents the general flowchart from IEEE Std. 1527 for the seismic design of flexible connections, including electrical requirements. Assuming that all electrical parameters (such as number and dimensions of conductors, clearance requirements, etc.) have been determined beforehand, Figure 3.3 shows a more precise flowchart for the mechanical design of connections valid for rigid and flexible connections.

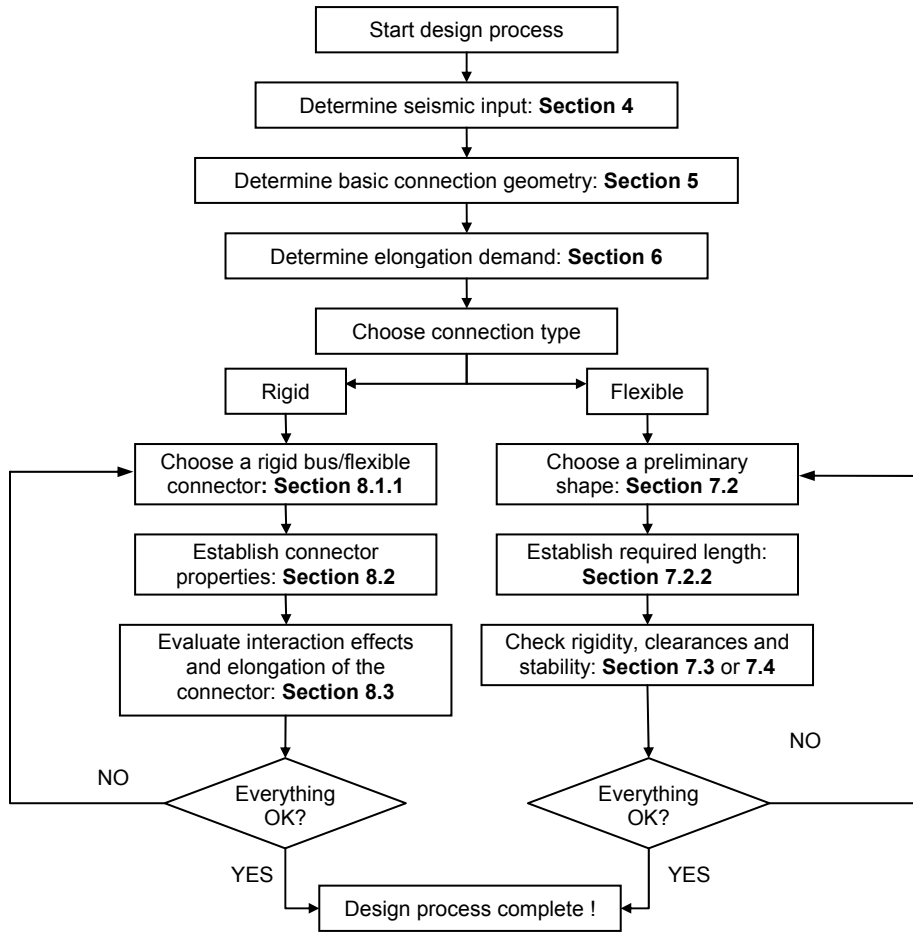


**Fig. 3.3 Flowchart for design of seismic connections**

## 4 Determination of Seismic Input

### 4.1 GENERAL CHARACTERIZATION OF SEISMIC INPUT

During an earthquake, a structure experiences ground shaking at its base. This shaking is usually characterized by two orthogonal components of horizontal motion in translation (sometimes called the longitudinal and transverse components) and one vertical component.

For engineering purposes, these components of motion can be defined in two ways to characterize the seismic input required for analysis or testing:

- by the time variation of ground acceleration
- by a response spectrum

The time variation of ground acceleration is obtained from the recording of a given earthquake (or sometimes artificially generated using dedicated software). One example of historical recording is presented in Figure 4.1. It is observed that the maximum ground acceleration (PGA) of this record is 0.20 g.

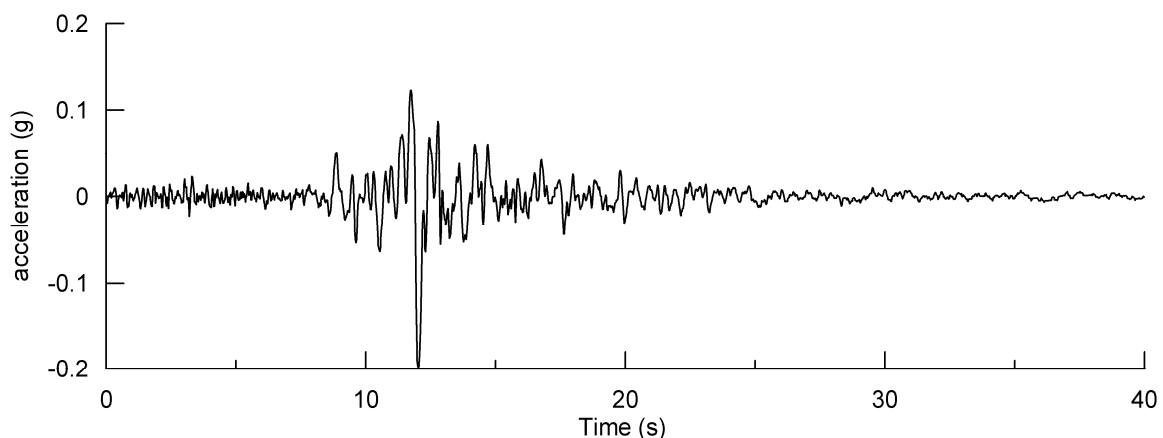


**Fig. 4.1** 90° component of horizontal ground acceleration from the 1989 Loma Prieta earthquake  $M_w$  7.0 recorded at station no. 58222 (San Francisco Presidio)

Since the time variation of ground acceleration from a given recording is an historical event that is unlikely to recur, more than one recording is usually needed in order to adequately characterize the variability of the expected input at a given location. These records are also usually scaled up or down to represent the expected intensity of the ground motion at a given distance from the expected earthquake source(s).

As an alternative to the time variation of ground acceleration, the concept of *response spectrum* is now widely used in standards and seismic guidelines to describe the seismic input. This concept is the one used in this application guide and is detailed in the following clauses.

The first design step, establishing the seismic input as per the flowchart in Figure 3.3, consists therefore of determining the response spectrum at the location where the electrical equipment and connections will be installed.

## 4.2 CONCEPT OF RESPONSE SPECTRUM

The time variation of ground acceleration can be used as input to obtain the time variation of a given response quantity of a structure; e.g., the displacement at the top. This can be done numerically using computer models or experimentally using shake table testing. For design of new structures or evaluation of existing ones, however, it is generally sufficient to know only the absolute peak value of the response quantity of interest. This can be accomplished through the concept of response spectrum. A response spectrum is a plot of the peak absolute-value response of a single-degree-of-freedom (SDOF) system as a function of its natural frequency, for a specified value of its damping.

A single-degree-of-freedom system is the idealization of a structure in which its mass, elastic property (*flexibility* or *rigidity*), and energy-loss mechanism (*damping*) are assumed to be concentrated in a single physical element allowed to move in a single direction only (simple oscillator). Figure 4.2 illustrates this idealization.

A SDOF system is characterized by (1) a unique *natural frequency* of vibration (denoted by  $f$ ), corresponding to the frequency at which the system would vibrate if distorted (into the dotted line in Fig. 4.2) then released and (2) a unique value of damping (denoted by  $\zeta$ ), which causes the initial amplitude of vibration to decay with time. It is important to note that the natural frequency of a SDOF idealization is a function of the *combination* of the mass and rigidity

properties of the structure under consideration. Therefore, very dissimilar structures of different mass and rigidity may have the same natural frequency when idealized as a SDOF system.

The SDOF idealization is very useful in dynamic analysis, as responses of most structures in the linear domain can be realistically obtained using one or an assemblage of SDOF systems. For the seismic design of connections, this idealization is used to obtain the maximum differential displacement of interconnected equipment under a specified earthquake input and, thereby, the maximum elongation demand of the connection.

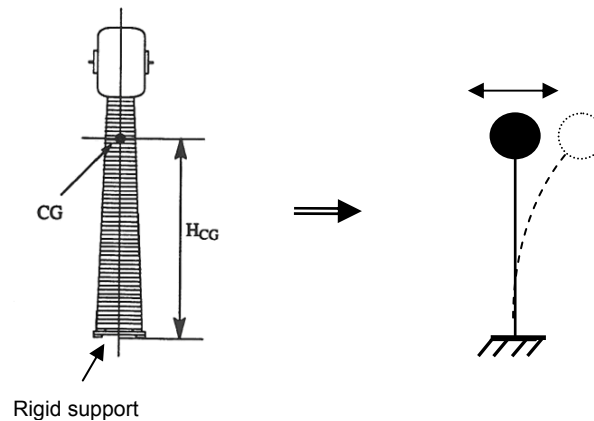


**Fig. 4.2 Idealization of equipment by a single-degree-of-freedom system**

Figure 4.3 illustrates the construction of a response spectrum from the time variation responses of SDOF systems of different frequencies under the Loma Prieta recording (Fig. 4.1). It is observed that the response spectrum presents only the maximum absolute response of SDOF systems as stated earlier.

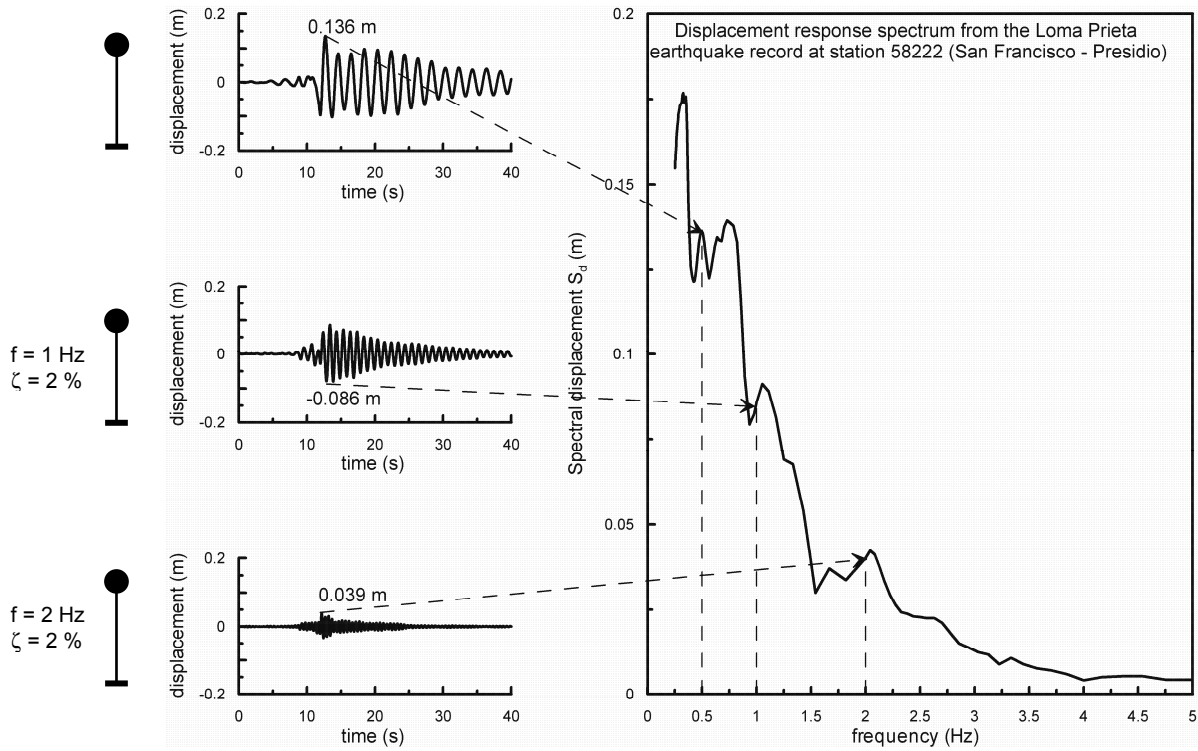


**Fig. 4.3 Construction of response spectrum**

Earthquake response spectra are typically presented in three ways, depending on the response quantity of interest:

- spectral displacement response spectrum giving the maximum absolute value of the “exact” displacement of the SDOF system relative to its moving base, denoted  $S_d$
- pseudo-velocity response spectrum giving an estimation of the maximum velocity of the SDOF system relative to its moving base, denoted  $S_v$
- pseudo-acceleration response spectrum giving an estimation of the maximum absolute acceleration of the SDOF system, denoted  $S_a$

These quantities are related through the following relationships:

$$S_v = (2 \cdot \pi \cdot f) \cdot S_d \quad (4.1)$$

$$S_a = (2 \cdot \pi \cdot f)^2 \cdot S_d \quad (4.2)$$

The term *pseudo* is used for the velocity and acceleration spectra obtained from Equations (4.1) and (4.2), since they provide approximations to, respectively, the maximum

exact relative velocity and the absolute acceleration that would be obtained using the mathematics of SDOF responses.

In the evaluation of the maximum displacement of equipment items, Equations (4.1) and (4.2) can be used to obtain the spectral displacement  $S_d$  when the input is either a pseudo-velocity or a pseudo-acceleration response spectrum, as is most often the case in seismic guidelines and standards.

#### 4.2.1 Normalized and Local Response Spectra

The response spectrum from a given input record has the same limitation as the time history variation of the ground motion from which it originates: it represents only *one* historical event. Therefore, more than one response spectrum is needed in design to represent the probable earthquake excitation that could happen at a given location, from different earthquake scenarios expected in the lifetime of the considered structure. For this reason, in practice a *design* response spectrum is used that “envelops” all the different response spectra that would be expected. Two types of design response spectra are generally used:

- normalized design response spectrum
- local (also called site-specific) design response spectrum

The normalized response spectrum is a general spectrum that envelops all the possible responses that are expected over a wide area from earthquakes with different magnitudes, distances, site-soil conditions, etc., to provide a design that would allow structures (or equipment in our case) to be safely designed for all possible inputs in this area. For example, the IEEE 693 response spectrum for the moderate level is presented in Figure 4.4; it is valid for all areas in Mexico, Canada, and the United States for which the maximum expected ground acceleration (ZPA) at the site is equal to or less than 0.5 g. The advantage is that equipment designed according to such a spectrum could be safely interchanged between all areas for which the design criterion applies.

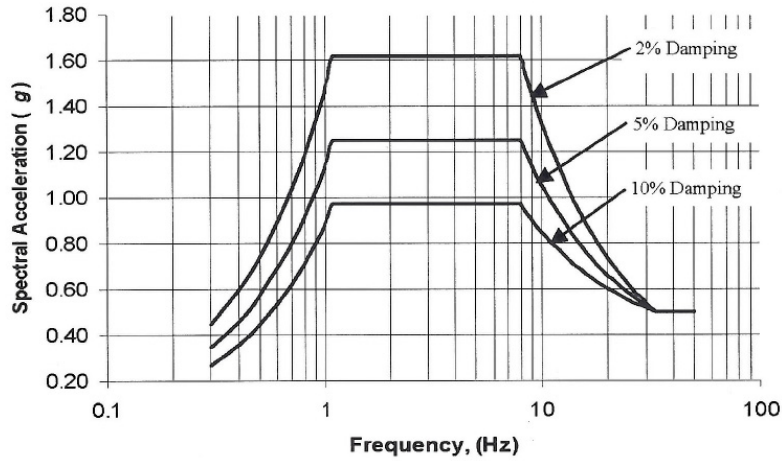


**Fig. 4.4 IEEE 693 performance level response spectrum for the moderate level (0.5g)**

The disadvantage of the normalized design response spectrum is that, for many regions, it overestimates the response that could locally be expected. For this reason, local spectra are also available that represent more closely the expected responses at a given site. Similar to the normalized spectrum, they envelop all the predicted inputs at a site. An example of a local response spectrum is presented in Figure 4.5.

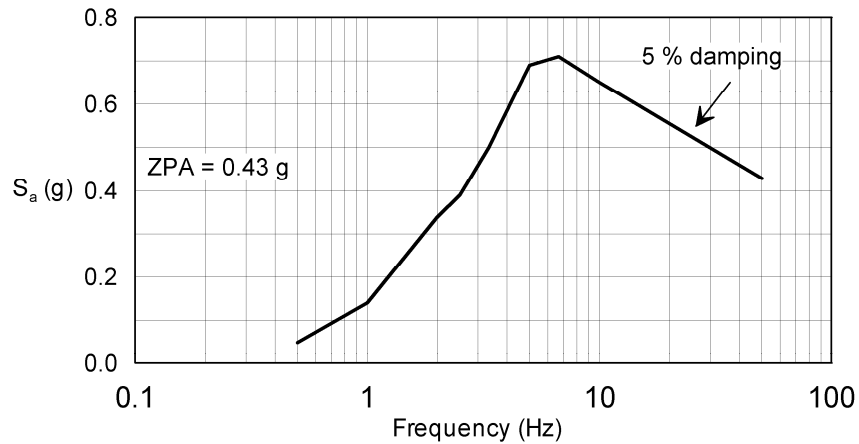


**Fig. 4.5 Montreal response spectrum from the National Building Code of Canada 2005**

When custom-designing connections at a given substation, it is recommended whenever possible to use the local spectrum, since it will generally lead to less equipment displacements and therefore will demand less elongation from a connection. This is particularly important in the design of flexible connections for equipment of low natural frequencies, such as 330 kV and above, as a demand of a large elongation (resulting in large connection slack) can sometimes be

difficult to meet in practice when the conductor is too long and violates the required electrical clearances.

As an example, in Table 4.1 we present the spectral displacements  $S_d$  from the IEEE spectrum and the Montreal spectrum (both spectra could have been used interchangeably for a substation in Montreal), for frequencies of 1, 2, and 5 Hz and a damping value of 5%. It is observed that the displacements from the IEEE spectrum are far greater than the ones from the Montreal spectrum<sup>1</sup>. This is especially true at frequencies of 1 Hz and below. However, it is observed that as the frequency increases, the displacements become small and for the related equipment these differences will not be of practical importance.

**Table 4.1 Spectral displacements comparison between the IEEE 693 (at the performance level) for the moderate level and Montreal spectra, for 5% damping**

<b>Spectrum</b>	<b>1 Hz</b>	<b>2 Hz</b>	<b>5 Hz</b>
IEEE 693 (ZPA=0.5 g)	28 cm	8 cm	1.2 cm
Montreal (ZPA=0.43g)	4 cm	2 cm	0.7 cm

---

<sup>1</sup> Earthquakes in Eastern North America have usually far less energy content in the low-frequency range than earthquakes on the West Coast. This explains here the large differences between the IEEE and Montreal spectra.

## 5 Determination of Basic Connection Geometry

A simple but important step in establishing an adequate seismic connection is to define the connection geometry. The basic geometry (Fig. 5.1) of a connection is defined by

- the horizontal distance between its attachment points:  $L$ ,
- the vertical separation between its attachment points:  $H (= h_2 - h_1)$ ,
- the straight-line distance between attachment points (chord length):  $L_1$ .

as schematized in Figure 5.1. Note that the attachment points refer to the extremities of connectors (Fig. 5.2) and will be input to determine the “free” conductor length required, i.e., the conductor length outside the connectors free to deform. As will be discussed later, additional conductor length should be provided for installation of flexible buswork to include the required length *inside* the connectors.

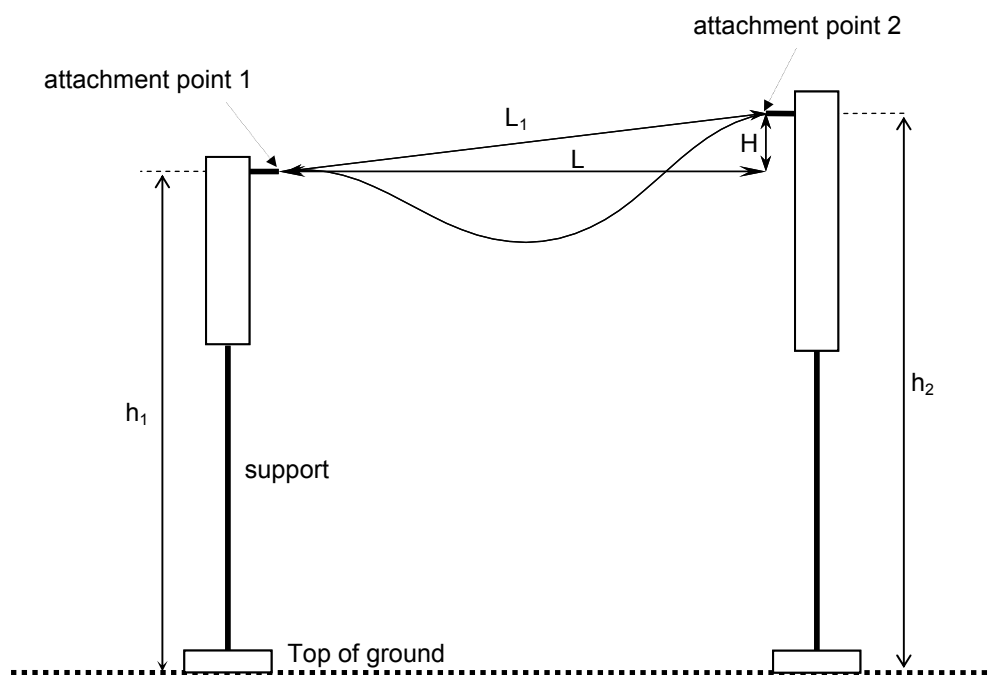
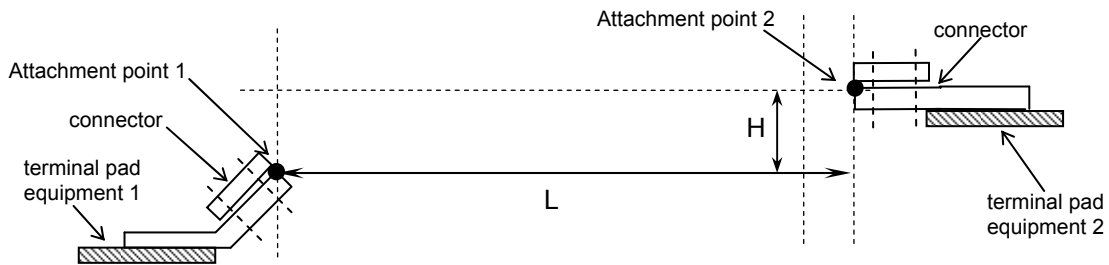


Fig. 5.1 Basic connection geometry

According to Figure 5.1:

$$L_1 = \sqrt{L^2 + H^2} \quad (5.1)$$

which is a required input to establish the necessary conductor length for a flexible connection; it is of course a necessary quantity to design a rigid connection as well.



**Fig. 5.2 Determination of basic geometry from connector extremities**

A practical example is illustrated in Figure 5.3 for which we have

$$L_1 = \sqrt{3^2 + 0.4^2} = 3.027 \text{ m}$$

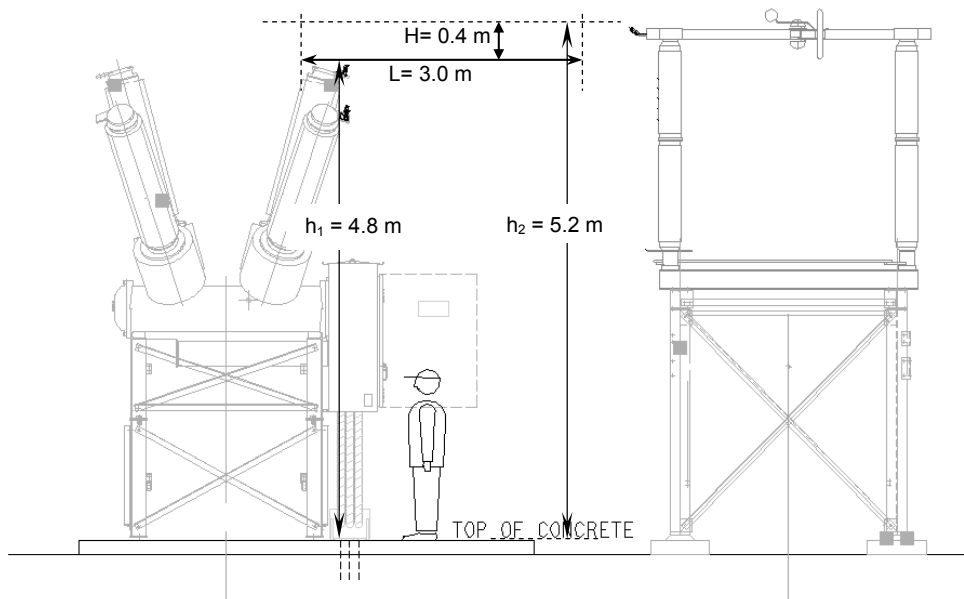


**Fig. 5.3 Example of basic connection geometry**

## 6 Determination of Elongation Demand

As introduced in Section 3.1.1, the elongation demand (denoted from now on by the simpler term “demand”) is the amount of stretch that a massless connector with zero stiffness would experience under the displacement of its two interconnected equipment.

Due to the non-zero mass and stiffness of the conductor and the resulting interaction with the connected equipment, the displacements of equipment items in their connected configuration cannot be evaluated in a simple fashion. Sophisticated methods, such as the nonlinear finite element method or analytical/numerical methods are required to obtain representative results. Therefore, it is easier and preferable for design purposes to use the equipment displacements in their stand-alone configurations, i.e., without conductors connected. Moreover, the stand-alone displacements are more readily available from equipment seismic qualification tests or analytical qualification, which are usually conducted on the stand-alone equipment.

It has been demonstrated that the stand-alone differential displacement is usually a conservative estimate of the differential displacement between connected equipment in cases of flexible connections (Dastous et al. 2004), and, therefore an estimation of the elongation demand can be obtained from it. For equipment interconnected by a rigid bus/flexible connector system, it has been shown that depending on the connector properties, the response of the higher-frequency equipment in a pair can be amplified, while the response of the lower-frequency item is usually de-amplified. However, the net result is that the differential displacement between the interconnected items is most often smaller than the stand-alone differential displacement (Song et al. 2007). Therefore, using the stand-alone differential displacements of equipment items is also a conservative estimate of the elongation demand for rigid bus/flexible connector systems; however, this estimate can produce too conservative an estimate of the force generated in a rigid bus that lacks a flexible connector.

## 6.1 REQUIRED COMPONENTS OF DISPLACEMENT TO ESTABLISH THE ELONGATION DEMAND

Since the nature of earthquake excitation is three dimensional, the stand-alone displacement input to establish the elongation demand should theoretically comprise two horizontal orthogonal components and a vertical one.

In this guide we will define the *horizontal* components of ground motion as follows:

- The *longitudinal* component is the horizontal ground motion in the direction from one equipment to the other (or more precisely from one attachment point to the other on each pair of interconnected equipment).
- The *transverse* component is the horizontal ground motion perpendicular to the longitudinal component.

For a flexible bus, the elongation demand is the difference between the straight-line distance between the attachment points of equipment in their installed (non-moving) positions and the maximum straight-line distance between the same points under the seismic input. Since for a rigid bus, compression is as bad as tension, the larger absolute difference based on either the maximum or minimum straight-line distance between the attachment points under the seismic input governs the design. The elongation demand is computed as

$$e_o = |L_1^* - L_1| \quad (6.1)$$

where  $e_o$  is the elongation demand,  $L_1^*$  is the maximum (for flexible bus) or the maximum or minimum (for rigid bus) straight-line distance between the attachment points of equipment under the seismic input, and  $L_1$  is the straight-line distance between the attachment points in their non-moving positions.

Let  $D_L$ ,  $D_T$ , and  $D_V$  denote the maximum differential displacements between the attachments points in the longitudinal (L), transverse (T), and vertical (V) directions, respectively, under a given seismic input. The maximum net elongation under the assumption that the three differential displacement components reach their maxima at the same time during an earthquake is illustrated in Figure 6.1(a) for two equipment attachment points separated by an horizontal distance of  $L$  and a vertical distance of  $H$ .

For all practical purposes, the differential displacement in the vertical direction,  $D_V$ , is zero, since electrical substation equipment is usually very rigid in this direction. As a result, the individual vertical displacement experienced by each equipment item is the ground displacement

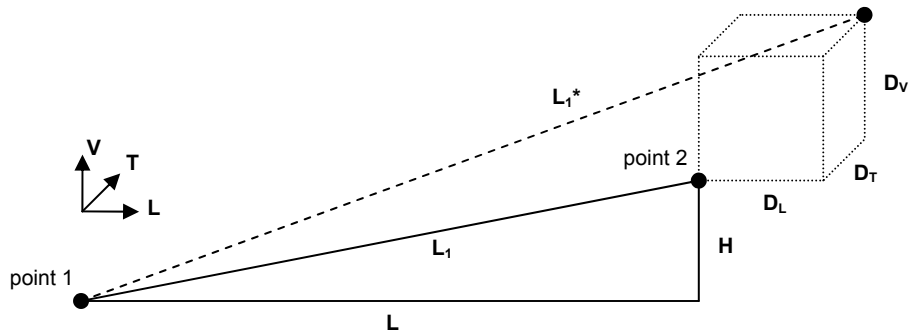
during the earthquake, which is the same for both and is usually very small (unless a foundation moves due to liquefaction). Therefore, the maximum elongation demand in practice comprises the two horizontal components only, as illustrated in Figure 6.1(b). According to Figure 6.1(b), the elongation  $e_o$  (still assuming that the maximum values of  $D_L$  and  $D_T$  occur at the same time) is given by

$$e_o = L \cdot \left[ \sqrt{\left(1 + \frac{D_L}{L}\right)^2 + \left(\frac{D_T}{L}\right)^2 + \left(\frac{H}{L}\right)^2} - \sqrt{1 + \left(\frac{H}{L}\right)^2} \right] \quad (6.2)$$

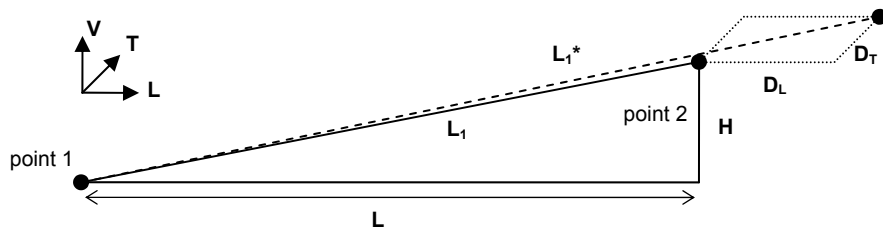
Expansion of the squared terms in the above equations shows that a good approximation to  $e_o$  is the maximum longitudinal differential displacement  $D_L$  between the two attachment points

$$e_o \approx D_L \quad (6.3)$$

and that the contribution of  $D_T$  to the elongation demand  $e_o$  is negligible provided that the ratio  $D_T/L$  is much smaller than 1, which is normally the case.



(a) Theoretical 3D maximum differential displacement between attachment points



(b) Maximum differential displacement between attachment points with  $D_V = 0$

**Fig. 6.1 Theoretical maximum elongation demand**

To gauge how close  $D_L$  is to  $e_o$ , we present in Figure 6.2 the ratio  $D_L/e_o$  against the ratio  $D_L/L$  (maximum longitudinal differential displacement over the horizontal span) for different ratios of  $H/L$ , under the realistic assumption that  $D_L=D_T$  (still with  $D_V=0$ ), i.e., the two horizontal

maximum differential displacement components are of the same order and reach their maxima at the same time.

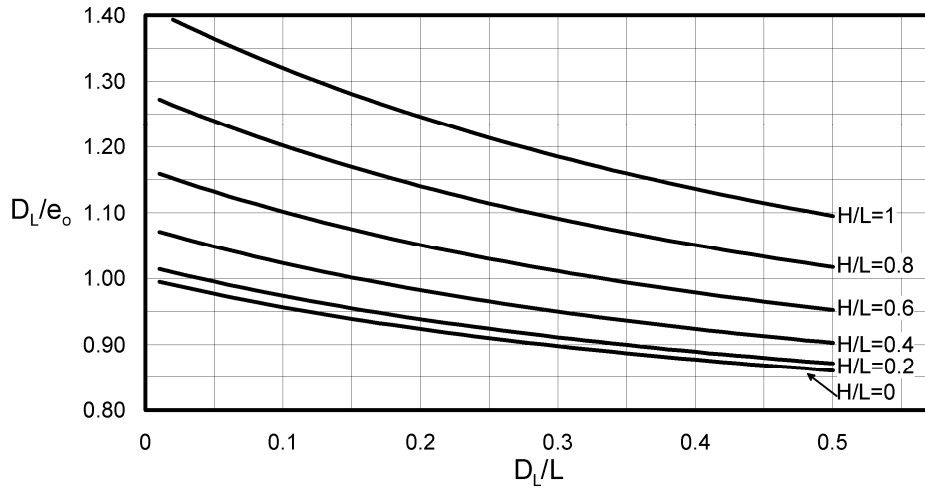


**Fig. 6.2 Ratio of estimated elongation  $D_L$  over "real" elongation  $e_o$  when  $D_L=D_T$  ( $D_V=0$ )**

It is observed from Figure 6.2 that even for a very large ratio  $D_L/L = 0.5$  (longitudinal differential displacement component *half* the horizontal span—an unlikely situation unless the span is small and the equipment displacements are large)— $D_L$  provides 86% of the "real" value of the elongation  $e_o$  when attachment points are at the same height ( $H/L=0$ ). Furthermore, it is observed that as the difference of height between attachment points increases, the ratio  $D_L/e_o$  increases, with values over one, for which  $D_L$  is then a conservative estimate of  $e_o$ .

In practice, the values of  $D_L/L$  are usually much smaller than 0.5. This is illustrated in Table 6.1 where we present values of  $D_L/e_o$  for average values of  $D_L$  derived using the IEEE 693 spectrum for both moderate and high levels, for a typical span of 3 m (10 ft) with  $H/L=0$ , using realistic values of expected differential displacements. It is observed that in the worst possible case, the approximation of  $D_L$  provides a 90% estimate of the real value of  $e_o$ , which confirms that the contribution of  $D_T$  to the elongation is rather small in realistic practical cases.

**Table 6.1 Practical values of  $D_L/e_o$  for a span of 3 m (10 ft) with  $H/L=0$**

Average frequency of interconnected equipment	IEEE 693 moderate level (0.5 g)			IEEE 693 high level (1 g)		
	$D_L$	$D_L/L$	$D_L/e_o$	$D_L$	$D_L/L$	$D_L/e_o$
1 Hz	45 cm	0.15	0.94	90 cm	0.30	0.90
2 Hz	15 cm	0.05	0.97	30 cm	0.10	0.96
5 Hz	2 cm	0.007	$\cong 1$	4 cm	0.013	0.99

It is also noteworthy that during a seismic event, it is unlikely that both  $D_L$  and  $D_T$  reach their maxima at the same time, since the time variations of the orthogonal components of horizontal ground motion usually have low correlation. Hence, the ratio of  $D_L/e_o$  will likely be higher than presented by the above analysis, and therefore the value of the differential displacement in the longitudinal direction,  $D_L$ , provides a good estimate in practice of the real expected elongation.

In summary, the elongation demand can generally be well approximated using Equation (6.3), but Figure 6.2 can always be used to gauge the accuracy of the approximation given by  $D_L$ . If desired, Equation (6.2) can be used to obtain a more accurate estimate using the two horizontal differential displacement components at their maximum values at the same time.

## **6.2 DETERMINATION OF DIFFERENTIAL DISPLACEMENT OF STAND-ALONE EQUIPMENT**

The way to determine the maximum differential displacement of stand-alone equipment is the same for either the horizontal longitudinal direction (connection direction) or the transversal direction (perpendicular to the connection). Therefore, in what follows we will use  $x_{max}$  to describe the maximum differential displacement in either direction; however they are not necessarily the same, depending on the equipment configuration.

### **6.2.1 Introduction**

It is only recently that the evaluation of the displacement at the attachment point has been formally required in the seismic qualification of substation equipment (IEEE 2005). Prior to this requirement, this information was often not readily available in reports, and is therefore missing for a large portion of equipment presently installed.

Whenever the maximum displacement is available from a seismic qualification report, it is recommended to use it directly as long as the qualification has been done analytically/numerically (usually with the *finite element method*), provided of course that the model used is deemed representative and that the damping used is equal to or less than the actual physical damping of the fundamental vibration mode (as defined below) of the equipment. When the information on the maximum displacement comes from a qualification done experimentally (usually through a shake table test), care must be exercised in its use as discussed in Section

6.2.5. When the information on the displacement is missing from the qualification report, different analytical/numerical methods are available to estimate it, as discussed below in Clauses 6.2.2–6.2.4.

## 6.2.2 Available Analytical/Numerical Methods

Different analytical methods are available to estimate the maximum displacement of structures under seismic loading, as described in many textbooks such as Clough and Penzien (1975). Also, the finite element method can be used, based on numerical approximations. It is to be recognized that even though mathematically exact, these methods are all approximate in the sense that they rely on a discretization of the equipment and assumptions regarding their properties. Nevertheless, they are representative of the real behavior of structures when the latter are properly modeled.

We present here different methods that can be used, followed by some approximations. The choice of which method to use depends on how much information is available to the user regarding the equipment at hand. The basic input required in all these methods is the *fundamental frequency* of the equipment and its *damping*. If not available, these quantities must be either estimated and/or obtained experimentally.

### 6.2.2.1 Single-Degree-of-Freedom Method

The simplest approximation is to assume that the equipment behaves essentially as a single-degree-of-freedom (SDOF) system of frequency  $f$  and critical damping ratio  $\zeta$ , as described earlier (Fig. 4.2). Using a response spectrum to define the seismic input in the desired horizontal direction, the maximum displacement of such a system is directly given in terms of the ordinate of the response spectrum as

$$x_{\max} = S_d(f, \zeta) = \frac{S_v(f, \zeta)}{2 \cdot \pi \cdot f} = \frac{S_a(f, \zeta)}{(2 \cdot \pi \cdot f)^2} \quad (6.4)$$

depending on the way the spectrum is specified, i.e., displacement spectrum ( $S_D$ ), pseudo-velocity spectrum ( $S_v$ ), or acceleration spectrum ( $S_a$ ).

This method gives a good approximation of the displacement if the center of gravity (CG) of the equipment (Fig. 4.2) is close to its interconnection point and if the response of the system

is defined essentially by the first vibration mode. Examples of such equipment are live-tank circuit breakers for which the mass is concentrated at the top.

### 6.2.2.2 Generalized Single-Degree-of-Freedom Method

A more accurate approximation is to assume that the system behaves as a generalized SDOF system (Fig. 6.3) and that it oscillates principally in one vibration mode or mode shape  $\psi(y)$ . The mode shape is simply the predominant displacement pattern of the equipment under the earthquake input. It is intuitively obvious that for most tall and slender equipment, this pattern is similar to a cantilever deflection. This pattern is similar to the one that the structure would take if a displacement were applied at its attachment point and then suddenly released: the structure would then essentially oscillate at its *fundamental frequency*, in its *fundamental mode*.

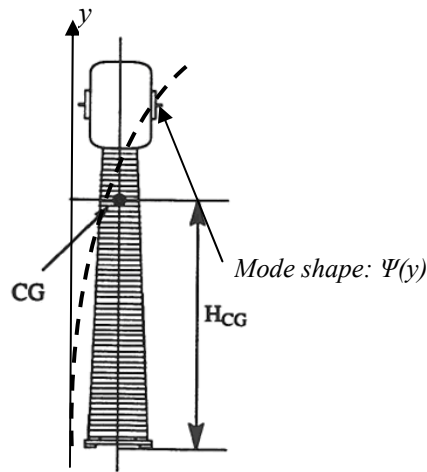


**Fig. 6.3 Generalized single-degree-of-freedom system**

Using the response spectrum method, the displacement at any point  $y$  of such a system is given by

$$x_{\max} = \alpha_1 \cdot S_d(f, \zeta) = \alpha_1 \cdot \frac{S_v(f, \zeta)}{2 \cdot \pi \cdot f} = \alpha_1 \cdot \frac{S_a(f, \zeta)}{(2 \cdot \pi \cdot f)^2} \quad (6.5)$$

where  $\alpha_1$  is the modal-participation factor associated with the *fundamental* frequency and mode when its shape  $\psi(y)$  is normalized to unity at the attachment point.

This factor can be calculated if the mass and stiffness distributions of the system (leading to a correct evaluation of the mode shape) are known with sufficient accuracy. The modal-

participation factor  $\alpha$  characterizes the difference between the SDOF system and the *generalized* SDOF, as it is generally different from 1. Average and bound values of this factor for different equipment are given in Section 6.2.4.

### 6.2.2.3 Multi-Degree-of-Freedom Method

The most precise numerical approximation is to model the equipment as a multi-degree-of-freedom (MDOF) system using the finite element method. This method consists of dividing a structure into smaller elements of given properties (finite elements) connected to each other by nodes. A proper division (the meshing) along with representative physical properties of the different parts (insulator, support, etc.) ensures that the structure at hand is properly modeled and representative of the behavior of the real one. This method is now well established and numerous finite element programs are commercially available. An example of a finite element model for a 230 kV circuit breaker is presented in Figure 6.4.

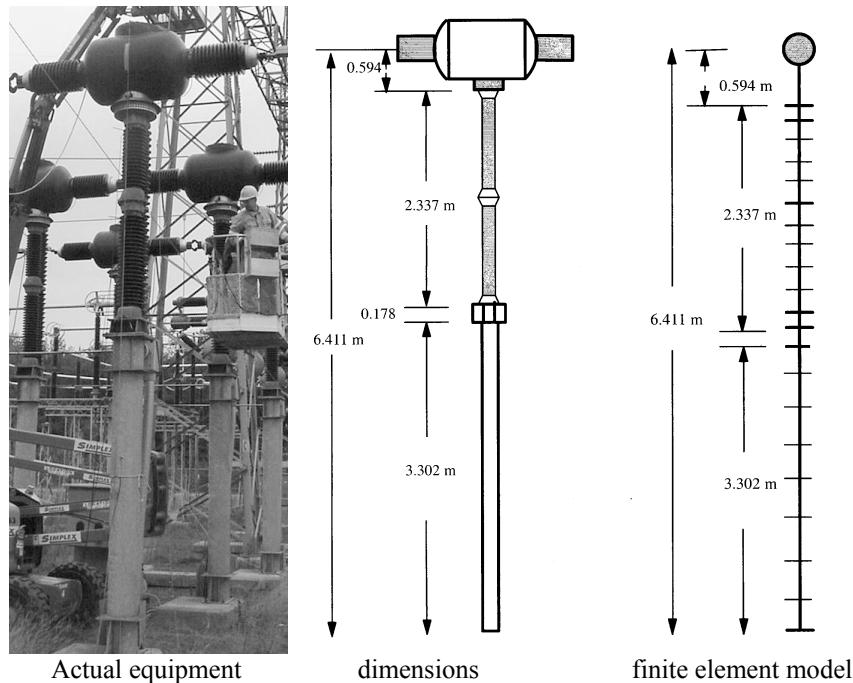


**Fig. 6.4 Example of equipment and corresponding finite element model**

Substation equipment can usually be represented using *linear* models for which the displacements and deformations are assumed small and for which the material properties are assumed constant (not varying when the structure deforms). The displacement at any nodal point

$j$  of such models can be obtained using the principle of *modal superposition* and an appropriate combination method of the *modal responses*. The principle of modal superposition is based on the theory that the deformation of a structure under a dynamic loading can be represented by the sum of different spatial patterns (the *modes*), each of a unique harmonic vibration frequency. It is qualitatively equivalent to a *Fourier* analysis, where any signal can be represented by a summation of sine and cosine functions of different frequencies. Figure 6.5 exemplifies the method where the displacement of the cantilever structure at the left is represented by the sum of its first three vibration modes.

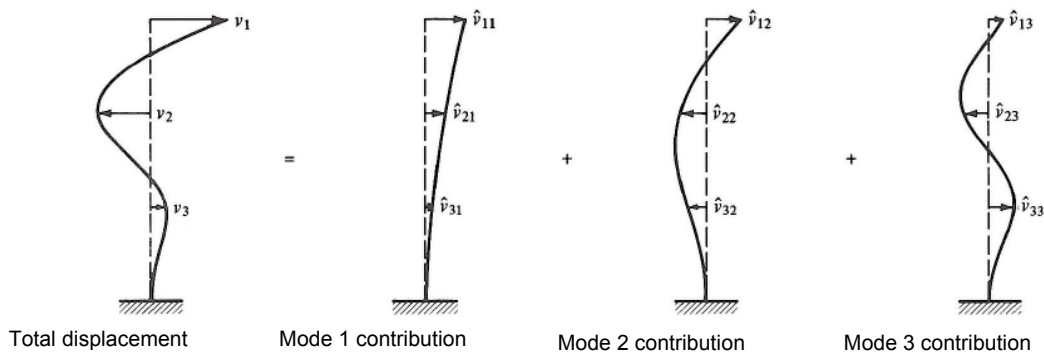


**Fig. 6.5 Example of modal superposition (Clough and Penzien 1975)**

It is not the purpose of this guide to discuss this method in depth, since, as we will shortly see, that it is seldom necessary in the evaluation of the displacement, and since finite element software will perform the calculations automatically anyway. It suffices to say that this method is an extension of the *generalized* SDOF method where the displacement at the top using the *SRSS* combination rule (appropriate when modal frequencies are well spaced) is given by the sum of the squares of the different modal responses of the structure as

$$x_{\max} = \sqrt{(\alpha_1 \cdot S_{d1})^2 + (\alpha_2 \cdot S_{d2})^2 + \dots + (\alpha_n \cdot S_{dn})^2} \quad (6.6)$$

where  $\alpha_j$  are the modal participation factors of all modes used (up to  $n$ ) and where  $S_{dj}$  is the spectral displacement for mode  $j$  of frequency  $f_j$  and damping ratio  $\zeta_j$ . It can be observed by comparison with Equation (6.5) that the latter is simply a special case of the multi-degree-of-freedom method where only the first mode is used.

In the case of the multi-degree-of-freedom method, the precision of the solution is dependent on the number of modes used, where the modes are numbered from 1 to  $n$  in the order of increasing frequency. We will see in the next section that, for most cases, the number of

modes to use for a precise estimation of the displacement is usually very small and that, in fact, the use of only one mode (usually the *fundamental mode* corresponding to the *fundamental frequency* of the structure) is often sufficient.

### 6.2.3 Comparison and Use of the Different Analytical Methods

To qualitatively compare the different methods, we consider the simple example of a cantilever beam of constant properties because most substation equipment that is tall and/or slender has behavior similar to that of a cantilever beam. Two cases are considered. The first is a beam with a fundamental frequency of 1 Hz which would represent tall and heavy equipment, such as some of those found at 500 kV and above. The second is for a fundamental frequency of 4 Hz, which would be representative of lighter equipment, such as those found at 230 kV and below.

For the MDOF method, we limit our analysis to the first three vibration modes as illustrated in Figure 6.6, where  $EI$  is the bending stiffness of the beam,  $\bar{m}$  is the mass per unit length, and  $\omega_i$  is the *circular* frequency of mode  $i$  equal to  $2 \cdot \pi \cdot f_i$ .

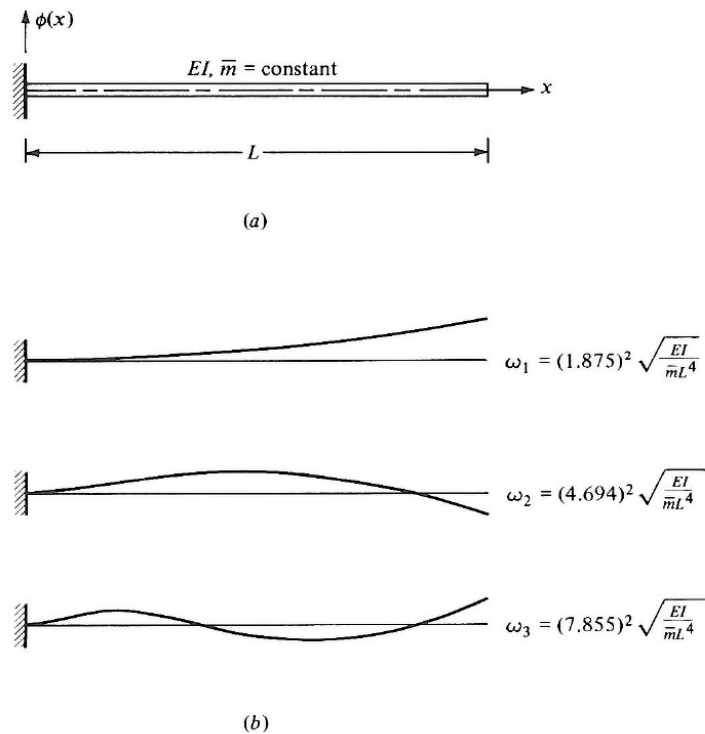


**Fig. 6.6 Cantilever beam (a) and its first three modes (b) (Clough and Penzien 1975)**

The modal participation factors of the first three modes of a cantilever beam, normalized to obtain unit displacement at the top of the beam, are given in Table 6.2.

**Table 6.2 Modal participation factor of a cantilever beam of constant properties**

Mode	$\alpha_i$
1	1.566
2	0.867
3	0.509

As seismic input, we will use the IEEE 693 spectrum at 2% damping for the high-performance level at 1 g PGA (twice the spectral values in Fig. 4.4). The first three modal frequencies and spectral displacements for the two cases studied are presented in Table 6.3.

**Table 6.3 Natural frequencies and spectral displacements of a cantilever beam using the high performance level IEEE-693 response spectrum at 2% damping**

Case 1			Case 2		
Mode	f (Hz)	S <sub>d</sub> (m)	Mode	f (Hz)	S <sub>d</sub> (m)
1	1.0	0.736	1	4	0.0503
2	6.3	2.03E-2	2	25	4.89E-4
3	18	1.22E-3	3	70	5.07E-5

The comparison between the SDOF, the generalized SDOF, and the MDOF methods for the two cases studied is presented in Table 6.4. The displacement at the top of the beam is the response quantity of interest.

**Table 6.4 Example comparison of the SDOF, generalized SDOF, and MDOF methods**

Case	SDOF Equation (6.4)	Generalized SDOF Equation (6.5)	MDOF (3 modes) Equation (6.6)
1	0.736 m	1.153 m	1.153 m
2	5.03 cm	7.877 cm	7.877 cm

It is first observed that the SDOF method underestimates the displacement for both cases, as expected, since the first modal participation factor is 1.566 as opposed to 1.0 with the SDOF approximation. This is because the mass of the cantilever is not concentrated at its tip. It is next observed that there is practically no difference between the generalized SDOF and MDOF methods. This is typical of most substation equipment that are tall and/or slender and therefore,

*the generalized SDOF method provides a realistic estimation of the displacement of most substation equipment when using the first or fundamental mode of the system<sup>2</sup>.*

The *preferred method* to establish the stand-alone displacement in this guide is therefore the generalized SDOF method. Practical values of the first modal participation factors for this method are presented next.

#### **6.2.4 Values of the First Modal Participation Factor for the Generalized SDOF Method**

In the following subclauses different methods are presented to determine the first modal participation factors for practical cases. All methods assume that the first fundamental frequency of equipment is known. The equipment damping is also assumed to be known. In case of uncertainty in the damping value, the recommended value for substation equipment is 2% of critical damping (IEEE 2005).

##### ***6.2.4.1 Theoretical Values of First Modal Participation Factor***

Theoretical values of the first modal participation factor have been determined by Dastous et al. (2004) for the cases illustrated in Figure 6.7(a), (b), and (c), corresponding, respectively, to a beam of constant properties, a beam of constant properties with lumped mass on the top, and two connected beams each of different but constant properties.

---

<sup>2</sup> Note that for certain types of structures (e.g., disconnect switches), the mode and frequency of vibration of interest to obtain the displacement are not necessarily the fundamental (or first) mode and corresponding frequency of the structure when the modes are ordered in increasing order of frequency. In particular, the fundamental (first) mode may correspond to a local vibration pattern that is irrelevant to the global behavior of the connected equipment. By fundamental (or first) mode we imply here the one corresponding to the first bending mode of the structure in the direction of interest, which is usually shaped as a cantilever pattern. As a relevant example, see Chapter 2 of Song et al. (2006), where the determination of the most representative mode for a disconnect switch on a 3D lattice supporting structure is discussed.

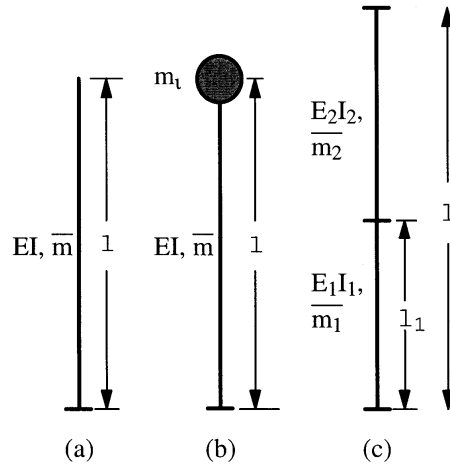


**Fig. 6.7 Models used for theoretical evaluation of first modal participation factor in Dastous et al. (2004)**

In Section 6.2.3 the results were presented for (a), for which  $\alpha_1=1.566$  (Table 6.2). This situation would correspond in practice to an equipment of constant cross-sectional area on a rigid base, e.g., an insulator column or a lightning arrester on a rigid support. The term “rigid base” is somewhat relative, as it practically implies that the fundamental frequency of the equipment is much lower than that of its stiff support, e.g., an insulator of 2 Hz over a support of 30 Hz. Another example where this model is applicable is the case of an equipment item with additional dampers between its base and support. For such a system, the fundamental mode is often related only to the motion of the insulator-equipment itself, while the support is relatively motionless.

Case (b) demonstrates the effect of an added rigid lumped mass at the top of an equipment of constant cross-sectional area, while supposing that the support is relatively rigid compared to the insulator column. Practical examples of such equipment are live tank circuit breakers, for which the tank at the top corresponds to adding a rigid mass on a flexible column. For such a case, the first modal participation factor is a function of the ratio of the added mass  $m_l$  to the mass of the column itself:  $m = \bar{m} \cdot l$ , with  $\bar{m}$  being the linear mass and  $l$  the equipment length. The variation of the first modal participation as a function of this ratio is given in Table 6.5 and illustrated in Figure 6.8. It is observed that as the ratio of the lumped mass to the mass of the beam increases, the modal participation factor decreases up to the theoretical case of the SDOF system with a factor of 1. Inversely, as the lumped mass diminishes, the case of a beam of constant property with no lumped mass is eventually attained (factor of 1.566).

**Table 6.5 First modal participation factor for beam of constant property with lumped mass**

$m_1/m$	0.01	0.05	0.1	0.5	1	2	5	10
$\alpha_1$	1.562	1.475	1.408	1.190	1.113	1.062	1.027	1.014

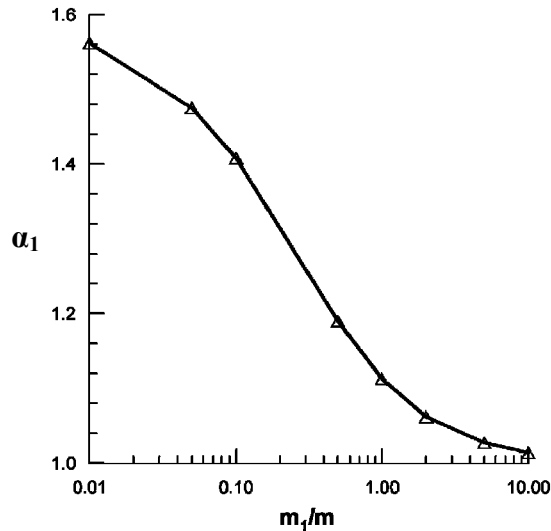


**Fig. 6.8 First modal participation factor for a beam of constant property with lumped mass on top**

In practice, most equipment items have supports offering some degree of flexibility. Contrary to the two previous cases, for which a theoretical solution was relatively easy to obtain, determination of the modal-participation factor for equipment resting on its support is less straightforward and can be obtained only numerically or by means of approximate methods. Case (c) illustrates the common case of an equipment of constant cross section over a support of constant property, thus demonstrating the effect of the support flexibility. Practical examples of this case are an insulator over a tubular support or a constant cross-section lattice support and a lightning arrester or a voltage/current transformer over similar supports.

For case (c), it can be shown that the first modal participation factor is a function of three dimensionless parameters:

$$\alpha_1 = f\left(\frac{l_1}{l}, \frac{\bar{m}_1}{\bar{m}_2}, \frac{E_1 I_1}{E_2 I_2}\right) \quad (6.7)$$

where  $\frac{l_1}{l}$  is the ratio of the support length to the total length of the equipment-support combination,  $\frac{\bar{m}_1}{\bar{m}_2}$  is the ratio of the linear mass of the support over the linear mass of the equipment, and  $\frac{E_1 I_1}{E_2 I_2}$  is the ratio of the bending stiffness of the support over the bending stiffness of the equipment.

In order to study the variation of the modal-participation factor with the dimensionless parameters given in Equation (6.7), a parametric study was performed by calculating all possible combinations of a given set of values for the support and the equipment properties (Dastous et al. 2004). Five different cross sections were used for the support, and three for the equipment. Three values of  $l_1/l$  were used. Apart from the two extreme values of the support cross section, all values were chosen as representative values that are actually found in practice. The extreme values were artificially chosen to correspond, respectively, to a very flexible and a very rigid support in an aim to study bounding values of the  $E_1 I_1/E_2 I_2$  ratio. It was assumed that the support was a circular tubular steel cross section, and that the equipment was made of porcelain with a solid circular cross section. It is to be noted that in this study (as in practice), the linear mass  $\bar{m}_i$  and the rigidity  $E_i I_i$  are correlated, since they are both obtained with the same cross section. However, in order to study the possible case of oil-filled equipment, the linear mass of the equipment  $\bar{m}_2$  was also varied for a given cross section by multiplying its nominal value obtained with the solid porcelain cross section, by factors up to three; five factors between one and three were used. This allowed studying the effect of adding mass to equipment of constant rigidity and, hence, the effect of varying the ratio  $\bar{m}_1/\bar{m}_2$  for a constant ratio of  $E_1 I_1/E_2 I_2$ . The parameters that served in this study are presented in Table 6.6. All possible combinations led to a set of 225 different simulations. It is to be noted that some combinations will seldom be used in practice: e.g., a support diameter of 0.5 m with a porcelain diameter of 0.15 m. However, the objective here was to obtain a general idea of the possible variations of the modal-participation factor including extreme values, so such combinations are still of interest.

**Table 6.6 Set of parameters used for studying the influence of support**

Parameter	Values used
$l_1/l$	0.33, 0.5, 0.6
Support diameter (m) (thickness in in.)	0.1 (1/4), 0.2 (1/4), 0.3 (1/4), 0.4 (1/4), 0.5 (1/2)
Equipment diameter (m)	0.15, 0.25, 0.35
Factor multiplying the porcelain linear mass $\bar{m}_2$	1, 1.5, 2, 2.5, 3

The results of this study are presented in Figure 6.9 as a function of the ratio  $\bar{m}_1/\bar{m}_2$  for a factor of 1 only for  $\bar{m}_2$  and the three values of  $l_1/l$ . In this figure, the ratio  $\bar{m}_1/\bar{m}_2$  is therefore correlated to the ratio  $E_1I_1/E_2I_2$ .

It is first observed that the modal-participation factor varies between 1.37 and 2.09 for all combinations and increases with an increase in  $\bar{m}_1/\bar{m}_2$ . The value of 1.37 corresponds to the combination of the lightest support (also the most flexible) and the heaviest equipment (also the most rigid). The value of 2.09 corresponds to the opposite combination, i.e., the heaviest support and lightest equipment. It is next observed that for a  $\bar{m}_1/\bar{m}_2$  ratio less than 1, the modal-participation factor decreases with an increase of  $l_1/l$ , while the opposite occurs for the values of  $\bar{m}_1/\bar{m}_2$  greater than 1. It is also observed that for the same ratio of less than 1, the modal-participation factor is bound by a value of approximately 1.6. In practice, the equipment is often heavier (and less flexible) than the support (when of tubular type), which means that the value of 1.6 can be regarded as a realistic bounding value. Compared to the value of 1.566 for a beam of constant properties with fixed support, it can therefore be deduced that, in many practical cases, the effect of the flexible support will be to decrease the modal-participation factor. However, it is important to note that as the support becomes more flexible, the fundamental frequency of the support-equipment combination will decrease, leading to a higher spectral displacement than in the opposite case. From the point of view of obtaining the smallest displacement for limiting the required slack, it is therefore advisable to avoid too much flexibility in the support relative to the equipment. In other words, it is better to have a higher modal-participation factor with a high frequency than the opposite.

Next, the effect of increasing the value of  $\bar{m}_2$  while keeping a constant ratio  $E_1I_1/E_2I_2$  was studied. It was observed (but not shown here) that the modal-participation factor is reduced for all values of  $\bar{m}_1/\bar{m}_2$  and that this effect is more marked for higher ratios of  $E_1I_1/E_2I_2$  than for smaller ones, where the reduction is almost negligible. The maximum decrease observed in this study was 21%, obtained with the longest support ( $l_1/l=0.6$ ) with the highest value of the ratio

$E_1I_1/E_2I_2$ . However, since the fundamental frequency will also decrease with an increase of  $\bar{m}_2$  for a constant ratio of  $E_1I_1/E_2I_2$ , this reduction will be largely offset by the increase in spectral displacement.

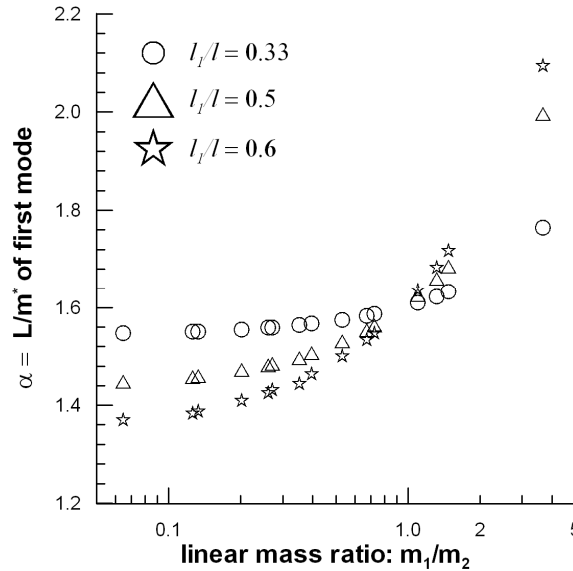


**Fig. 6.9 First modal participation factor for equipment on a support (beams of constant properties along their height)**

In summary, the effect of the support, apart from always decreasing the fundamental frequency, is to modify the modal-participation factor. In practical cases where  $\bar{m}_1/\bar{m}_2$  is often less than 1, a bounding value of 1.6 was established. For ratios  $\bar{m}_1/\bar{m}_2$  over 1, a bounding value of 2.09 was obtained. Since this was done with an extreme combination of rigid support-flexible equipment, it can be safely assumed that the modal-participation factor will always be less than 2 for equipment on a support that can be assimilated as two beams of constant properties. However, care must be applied in interpreting this result when the equipment-support combination diverges from the case of two simple beams, e.g.. a bushing on a transformer top.

#### 6.2.4.2 Survey of First Modal Participation Factor from Equipment Database

An important survey of the first modal participation from seismic qualification reports has been performed and detailed in Dastous et al. (2004). In this survey, reports where qualification had been done analytically/numerically with the response spectrum method have been reviewed.

Since, as seen above, the contribution of the first mode is dominant in the displacement, the first modal participation factor can be extracted from this report as

$$\alpha_1 \cong \frac{x_{max}}{S_d(f, \zeta)} \quad (6.8)$$

where  $x_{max}$  is the reported maximum displacement at the attachment point in a given direction, and  $S_d(f, \zeta)$  is the spectral displacement from the response spectrum used in the qualification for the fundamental frequency,  $f$ , and damping ratio,  $\zeta$ , of the equipment.

The equipment retained in this study were high-voltage apparatus mostly rated over 120 kV, which could be idealized as generalized SDOF systems (candle-like or frame type). Equipment not considered were dead tank circuit breakers and equipment with added dampers, as the behavior of these equipment is somewhat different from that of the generalized SDOF system. A total of 181 factors were obtained comprising 161 factors for equipment on flexible supports and 20 without flexible supports. The results are presented in Table 6.7 and illustrated in Figure 6.10 against the fundamental frequency of the equipment.

It is observed that the first modal participation factor is in the range of 0.65–1.98 with a mean value of 1.34. For disconnect switches (vertical opening in this survey only), the modal participation factor was observed to be significantly higher in the closed position, which suggests that this position should be used in the evaluation of the first modal participation factor. Figure 6.10 reveals that the first modal participation factor is not correlated with the frequency of the equipment, which varies here from 0.4 Hz to 17 Hz with an average of 3.9 Hz.

**Table 6.7 Results of survey on first modal participation factor**

Equipment type	nb. of values	nb. with support	nb. without support	$\alpha_1$ all values			$\alpha_1$ With support only			$\alpha_1$ Without support only		
				min	max	mean	min	max	mean	min	max	mean
Current transformers	19	14	5	1.18	1.84	1.43	1.18	1.84	1.44	1.34	1.51	1.40
Circuit breakers/live tank	38	38	0	0.65	1.82	1.25	0.65	1.82	1.25			
Circuit switcher	1	1	0	-	-	1.44	-	-	1.44			
Disconnect switches: hinge end open	8	8	0	0.88	1.82	1.21	0.88	1.82	1.21			
Disconnect switches: jaw end open	8	8	0	0.71	1.82	1.15	0.71	1.82	1.15			
Disconnect switches: hinge end closed	9	9	0	1.16	1.91	1.45	1.16	1.91	1.45			
Disconnect switches: jaw end closed	9	9	0	1.09	1.91	1.42	1.09	1.91	1.42			
Ground disconnect switches (column type)	1	1	0	-	-	1.44	-	-	1.44			
Lightning/surge arresters	24	17	7	1.08	1.59	1.43	1.08	1.59	1.40	1.49	1.56	1.51
Reactors	3	3	0	1.28	1.29	1.29	1.28	1.29	1.29			
Shunt capacitors on rack	49	49	0	0.80	1.98	1.32	0.80	1.98	1.32			
Voltage transformers	12	4	8	1.3	1.63	1.45	1.44	1.60	1.52	1.30	1.63	1.41
<b>All values</b>	<b>181</b>	<b>161</b>	<b>20</b>	<b>0.65</b>	<b>1.98</b>	<b>1.34</b>	<b>0.65</b>	<b>1.98</b>	<b>1.33</b>	<b>1.30</b>	<b>1.63</b>	<b>1.44</b>

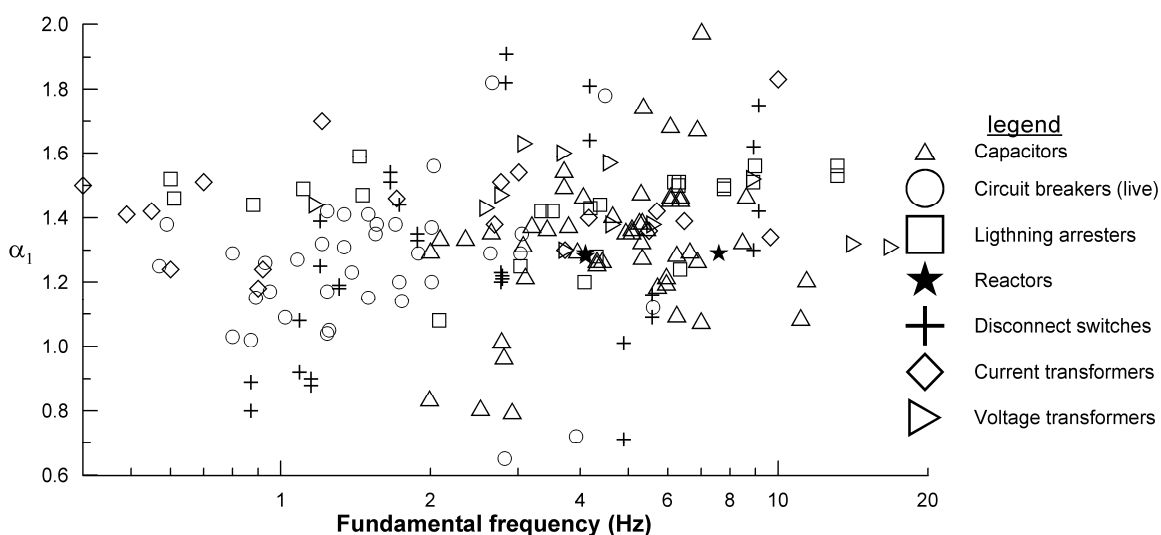


**Fig. 6.10 First modal participation factor versus frequency for all equipment surveyed**

#### 6.2.4.3 Average and Bounding Values of the First Modal Participation Factor

Based on the above survey, it was found that the distribution of the first modal participation factor for a randomly selected equipment on support was approximately *Gaussian (Normal)*, with a *mean value of 1.35* and a standard deviation of 0.15 (Dastous et al. 2004). Based on this, the following equation predicts an upper-bound value on the maximum displacement that covers 95% of equipment surveyed:

$$x_{\max}|_{95\%} = 1.62 \cdot S_d(f, \zeta) \quad (6.9)$$

It is noted that the above 95% upper-bound estimate assumes no uncertainty in the determination of  $S_d$ . It is recommended that in the absence of data other than the fundamental frequency of the equipment and its damping, this equation be used to obtain a conservative estimate of the equipment maximum displacement for connection design. Based on this equation, Figure 6.11 provides upper-bound values for the equipment displacement as a function of the equipment fundamental frequency for 2% damping, according to the spectral displacements from the IEEE 693 required response spectra for the moderate- and high-performance levels. Table 6.8 provides values from this graph at selected frequencies.

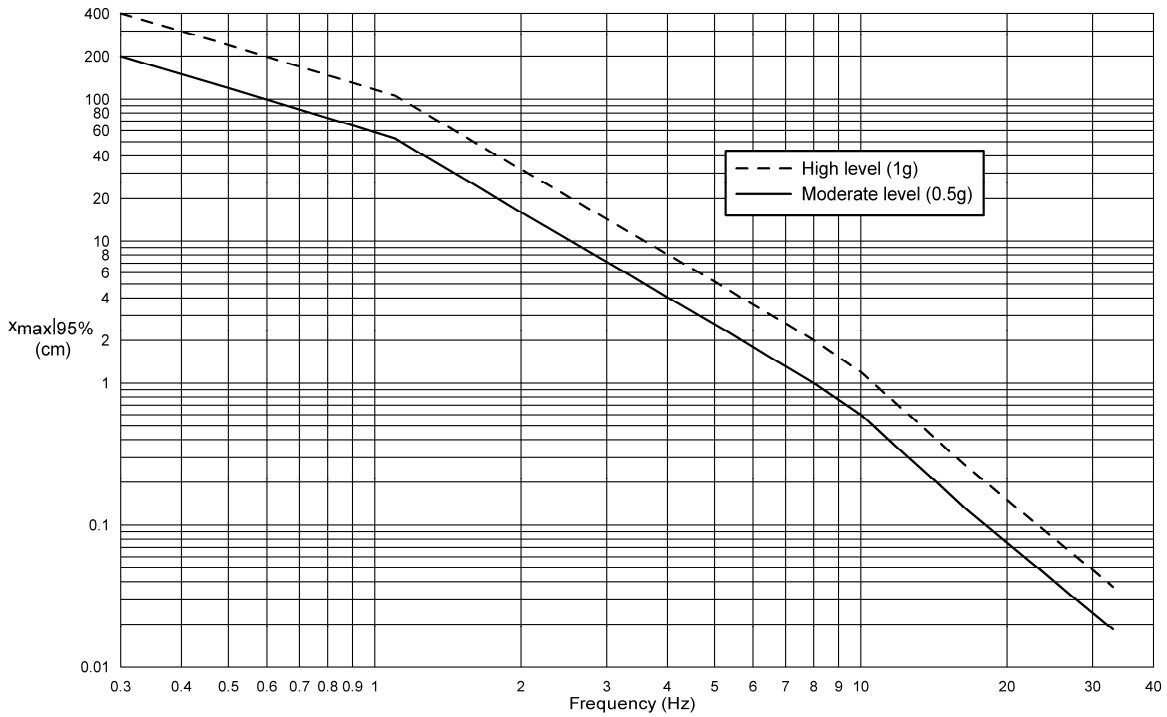


**Fig. 6.11 Upper-bound displacement according to IEEE 693 required spectra for 2% damping**

**Table 6.8 Upper-bound displacement according to IEEE 693 required spectra for 2% damping**

f (Hz)	$X_{\max 95\%}$ IEEE-693 moderate performance level (0.5 g) (cm)	$X_{\max 95\%}$ IEEE-693 high- performance level (1 g) (cm)
0.5	120	240
1	60	120
2	16	32
3	8	15
5	2.6	5.2
10	0.6	1.2
16.7	0.13	0.25
33	0.019	0.037

#### 6.2.4.4 Application of the Generalized SDOF Method

As discussed, the generalized SDOF method applies to all equipment that are tall and slender (candle-like) as well as those which are of frame type such as disconnect switches and capacitor banks on simple supports. For the first category (candle-like), the first modal participation factor and the fundamental frequency<sup>2</sup> are generally similar in both the longitudinal and transverse directions of the equipment, as long as the equipment support and insulator are symmetric. For the latter category (frame type), the first modal participation factor (as well as the fundamental frequency) is generally different between the longitudinal and transverse directions. However, even though such equipment appears more complex, their fundamental vibration modes are often of cantilever type in both directions and contribute most to the displacement response.

A few types of equipment generally cannot be adequately represented by a generalized SDOF model:

- dead tank circuit breakers
- bushings on power transformer or on reactors
- equipment such as disconnect switches that are supported on complex 3D lattice or truss structures

The reasons are that

- The reported fundamental frequency of the equipment may not correspond to the motion of the bushing itself.
- The attachment conditions of the bushing on the equipment are often complex and the vibration behavior of the bushing-equipment may deviate from the simple cantilever behavior of a generalized SDOF system.

- The 3D nature of the support involves more complex mode shapes than equipment on simple supports.

For the first two types, the displacement at the top of the bushing can be estimated in a simple fashion as follows:

- Evaluate the fundamental frequency and modal participation factor of the bushing *alone* on a *rigid base* and obtain an intermediate value of displacement using the generalized SDOF method.
- Multiply this intermediate value of displacement by a factor of 2 to get the final displacement at the top.

The factor of 2 has been established empirically to account for the amplification from the attachment conditions at the base of the bushings<sup>3</sup> (see IEEE 2005).

An alternative and more precise method for the three types of equipment identified above is to do a representative finite element analysis of the equipment and its support; such a method, however, is time consuming and requires appropriate skill and software. Care must also be taken to represent in the most precise way the attachment conditions of the bushing on the equipment, which are often complex and include the effects of different parts such as the flange, the rubber ring, and the bolts.

### **6.2.5 Evaluation of Stand-Alone Equipment Displacement through Testing**

Shake table testing can be used to determine the equipment displacement when the equipment falls within the physical size and load limits of the table. Time history data obtained from an earthquake record on the site (if available) or for a geologically similar site may be scaled up or down for input to the testing to match the qualification level selected, but usually more than one is used. A geoscientist should be consulted on the selection and scaling of the ground motion record. The stand-alone displacement can be obtained if *measured directly* using an appropriate *displacement* sensor (*not* from the double integration of an accelerometer signal as discussed below). However, the maximum displacement thus obtained may not always correspond to the required response spectrum as the *test response spectrum*, i.e., the actual response spectrum from the motion of the shake table itself, does not always match the required response spectrum at all

---

<sup>3</sup> The recommended factor of 2 is not definitive, as it is presently under investigation by different research projects focusing on the complex behavior of bushing-support arrangements.

frequencies. This is due to the limitations of shake table controls and/or the time history signal itself, whereby the spectrum cannot *precisely* match the required response spectrum at all frequencies, as illustrated in Figure 6.12. Shown here is the difference between the response spectrum from a time history signal compatible with the target high level IEEE 693 response spectrum.

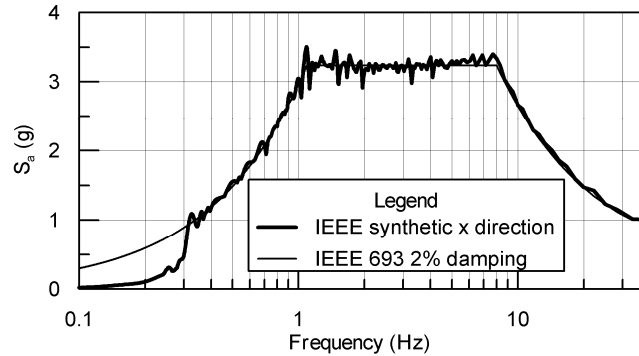


**Fig. 6.12 Difference between required response spectrum and time history input spectrum**

If the test response spectrum is lower than the required response spectrum at or close to the fundamental frequency of the equipment, it is advisable to correct the measured displacement to match the required response spectrum as follows:

1. From the *test response spectrum*, obtain the spectral displacement at the fundamental frequency of the equipment:  $S_{d\_TRS}$ .
2. Obtain an approximation of the modal participation as

$$\alpha_1 \cong \frac{x_{\max\_measured}}{S_{d\_TRS}} \quad (6.10)$$

3. Obtain the corrected displacement corresponding to the required response spectrum as

$$x_{\max} = \alpha_1 \cdot S_d \quad (6.11)$$

where  $S_d$  corresponds to the spectral displacement from the required response spectrum at the fundamental frequency of the equipment.

This approach is of course valid inasmuch as the actual damping of the first vibration mode is close to the damping assumed in the evaluation of the test response spectrum. Otherwise, the modal participation factor from Equation (6.10) could be biased.

Recovery of the displacement from double integration of the measured acceleration at the top of the equipment (through an accelerometer) is *not recommended* because the obtained displacement could be seriously biased. Also, one may be tempted to obtain the first modal

participation using the measurement of the maximum acceleration  $\ddot{x}_{\max\_measured}$  as  $\alpha_1 \equiv \frac{\ddot{x}_{\max\_measured}}{S_{a\_TRS}}$ ,

where  $S_{a\_TRS}$  is the spectral acceleration from the test response spectrum at the fundamental frequency. However, this approach may be *seriously flawed*, since unlike the displacement, the maximum acceleration is most often made up of the contributions of more than one vibration mode; usually the first three account for a representative approximation in the case of candle-like or frame structures.

### 6.3 COMBINATION OF INDIVIDUAL DISPLACEMENTS TO OBTAIN ELONGATION DEMAND

In order to evaluate the elongation demand, the stand-alone displacements of a pair of interconnected equipment must be combined in order to obtain the maximum differential displacement between them in both horizontal directions:  $D_L$  for the longitudinal direction and  $D_T$  for the transversal direction. However, as discussed in Section 6.1, in most cases  $D_L$  alone provides an excellent estimate of the elongation demand. In what follows we denote by  $x_{\max\_1}$  and  $x_{\max\_2}$  as the stand-alone displacements in a given horizontal direction for equipment items 1 and 2.

Three methods are theoretically available to obtain the maximum differential displacement, which we denote by  $D$  for either direction:

1. the absolute sum method:

$$D = x_{\max\_1} + x_{\max\_2} \quad (6.12)$$

2. the SRSS combination:

$$D = \sqrt{x_{\max\_1}^2 + x_{\max\_2}^2} \quad (6.13)$$

3. an adaptation of the CQC combination rule (Der Kiureghian et al. 1999):

$$D = \sqrt{x_{\max\_1}^2 - 2 \cdot \rho_{12} \cdot x_{\max\_1} \cdot x_{\max\_2} + x_{\max\_2}^2} \quad (6.14)$$

where  $\rho_{12}$  is the correlation coefficient between  $x_{\max\_1}$  and  $x_{\max\_2}$

$$\rho_{12} = 8\zeta^2(1+r)r^{3/2} / [(1-r^2)^2 + 4\zeta^2r(1+r)^2] \quad (6.15)$$

where  $r$  is the ratio of the fundamental frequencies of the stand-alone equipment items:  $f_1/f_2$ . Note that the numbering of the equipment items is immaterial. The same numerical result is obtained

for  $\rho_{12}$  when  $r$  is replaced by  $1/r$  (i.e., for  $f_2/f_1$  instead) and  $\zeta$  is the critical damping ratio, which is assumed to be the same for the two equipment.

It is to be noted that when the frequencies of interconnected equipment of light damping are separated by more than 20% relative to each other, the CQC and SRSS methods yield basically identical results, since the correlation coefficient  $\rho_{12}$  is then nearly zero.

In Dastous (2007), the three methods are compared based on numerical simulations of 325 different pairs of substation equipment of varying fundamental frequencies under 12 different time history inputs, for a total of 3,900 combinations. In this study, the “true” differential displacement obtained during the simulations was compared to estimations from the above three methods. The results showed that

- when the frequencies of the two equipment items are within 20% or less of each other, the best overall method is the CQC method;
- when the frequencies are separated by 20% or more, the CQC and SRSS methods provide the same precision;
- in all cases, the absolute sum method provides the poorest estimate of the true differential displacement, with sometimes very large absolute errors for equipment at low frequencies (for which stand-alone displacements are also large).

The main reasons why the absolute sum method provides poor estimates are that

- it assumes that the equipment reach their maximum stand-alone displacements at the same time during an earthquake—an unlikely situation unless they have the same fundamental frequency and damping;
- it also assumes that the two equipment items are oscillating out of phase (in opposite directions) at the moment they simultaneously reach their maximum displacements—a very unlikely situation indeed; if they have the same frequency and damping, they theoretically oscillate in phase and will therefore have *no* (zero) differential displacement between them.

Since the CQC and SRSS methods are statistical methods, they provide only an average value of the maximum differential displacement over an ensemble of ground motions and may, therefore, underestimate the true differential displacement for a given ground motion. To counteract this possibility, a factor of 1.25 was empirically obtained in Dastous (2007) to cover 95% of the true differential displacement using the SRSS method. Therefore, the differential displacement in this

application guide using the SRSS method with displacements obtained from a *mean* response spectrum of an ensemble of ground motions should be obtained as

$$D=1.25 \cdot \sqrt{x_{\max\_1}^2 + x_{\max\_2}^2} \quad (6.16)$$

Such a factor has not been determined yet for the CQC method but we recommend using the same when this method is applied:

$$D=1.25 \cdot \sqrt{x_{\max\_1}^2 - 2 \cdot \rho_{12} \cdot x_{\max\_1} \cdot x_{\max\_2} + x_{\max\_2}^2} \quad (6.17)$$

*However, if the displacements are obtained from a response spectrum corresponding to the mean plus one standard deviation (as is the case in most design response spectra), the 1.25 factor may not be needed in both equations above (i.e., the use of a factor of 1 may be more adequate).*

As discussed, the CQC method is the most precise and will be particularly useful when expected displacements are large and fundamental frequencies of interconnected equipment are closer than 20%, so that a reduced and more realistic value of the demand will be obtained by comparison with the SRSS method. It is noted that when the two equipment items have identical frequencies and damping ratios, the CQC formulation correctly predicts zero differential displacement. This is not the case with either the absolute sum or the SRSS combination method.

## 7 Flexible Buswork Seismic Design

This chapter describes the design of flexible connections between equipment items in order to satisfy the requirements of sufficient flexibility, displacement capacity to meet demand, electrical clearances, and span.

### 7.1 ADVANTAGES AND LIMITATIONS OF FLEXIBLE CONNECTIONS

Flexible connections are often used to interconnect substation equipment due to the following advantages:

- When properly designed, they provide sufficient flexibility between equipment, especially in the case of large expected differential displacements, thus avoiding transfer of forces.
- They naturally provide sufficient provision for thermal expansion movements arising from heating of the conductors.
- More than one conductor can be used in a bundle to allow the passage of high current density.
- They are relatively easy to install.

Flexible connections have the following limitations:

- For short spans (less than 1–2 m, depending on the conductor size), they can be relatively rigid due to their inherent axial and bending stiffness.
- Due to their flexibility, they sag and thus may lead to clearance violations.
- Due to the two previous limitations, and depending on shape and rigidity, they can be used only for span lengths over certain intervals.
- They may be subjected to large lateral movements under short circuit and wind conditions, thus allowing the possibility of compromising phase-to-phase clearances during such events.

## 7.2 AVAILABLE SHAPES, REQUIRED CONDUCTOR LENGTH, AND QUALITATIVE BEHAVIOR

### 7.2.1 Typical Shapes

As a result of analysis and actual physical tests with AAC conductors aimed at establishing the flexibility characteristics, four basic configurations and slight variations of each (such as attachment at other angles) were found to be most suitable. These basic configurations are shown in Figure 7.1. These configurations provide the necessary conductor “stretch” and permit “compression” without applying excessive force to the bus and equipment terminations when their length is appropriately determined (next section).

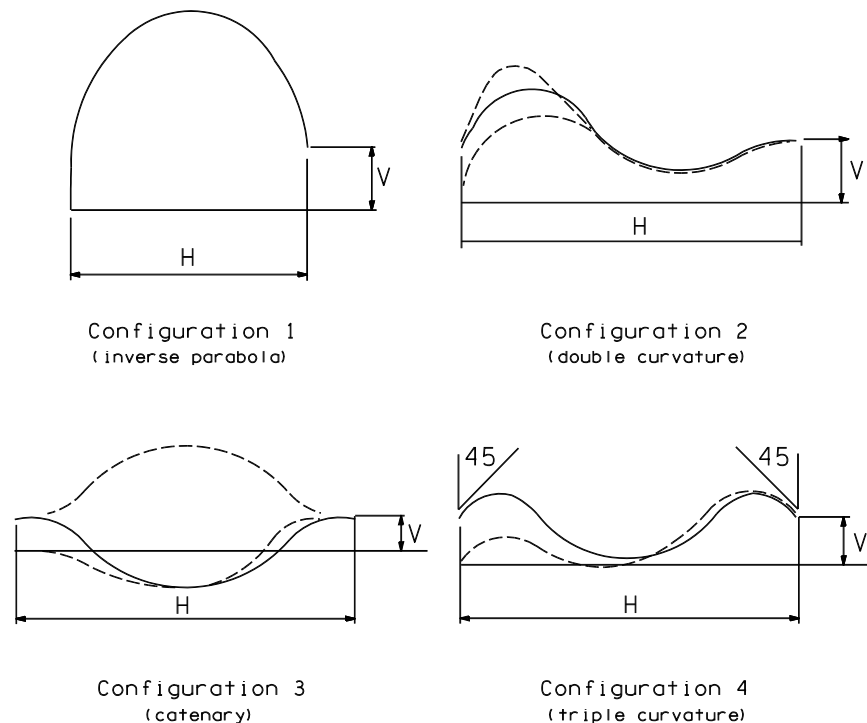


**Fig. 7.1 Basic flexible conductor configurations**

All presented configurations maintain their assumed shapes within a specified span interval, outside of which the shapes may become unstable (Dastous and Paquin 2003). The recommended use, advantages, and limitations of each configuration are summarized in Table 7.1. Alternative configurations and variations have also been installed, such as those presented in Figure 7.2.



Fig. 7.2 Alternative flexible conductor configurations (Opsetmoen 1998)

Table 7.1 Summary of basic flexible configurations characteristics

Configuration	Recommended use for	Advantages	Limitations
1: inverse parabola	<ul style="list-style-type: none"> <li>large required slack</li> <li>clearance problems with other shapes</li> </ul> <p>(Length should be defined such that it corresponds to a <b>half circle</b> when both ends are at the same height).</p>	<ul style="list-style-type: none"> <li>most flexible of all configurations <b>when</b> designed as a half circle, for the same elongation demand</li> <li>automatically meets clearances</li> <li>permits elongation without abrupt change of stiffness over a large range</li> </ul>	<ul style="list-style-type: none"> <li>Limited in maximum span as may collapse under weight or climatic loading</li> <li>Recommended to use in a bundle of two with spacers to provide lateral stability to wind</li> <li>requires 90° connector hardware</li> </ul>
2: double curvature	<ul style="list-style-type: none"> <li>clearance problems with catenary</li> <li>one end must be attached horizontally</li> </ul>	<ul style="list-style-type: none"> <li>may need to be pre-shaped for smaller spans</li> <li>may satisfy clearances not possible with catenary</li> </ul>	<ul style="list-style-type: none"> <li>may lead to large sags for longer spans</li> <li>requires 45° or 90° connector hardware</li> </ul>
3: catenary	<ul style="list-style-type: none"> <li>smaller elongation demand</li> </ul>	<ul style="list-style-type: none"> <li>simple</li> <li>most flexible of all configurations for the same ratio of elongation demand over available slack (however the inverse parabola is usually more flexible when formed as a half circle as prescribed in this guide)</li> <li>conventional installation with conventional hardware</li> <li>easy acceptance by field personnel as “business as usual”</li> </ul>	<ul style="list-style-type: none"> <li>may lead to abrupt change of stiffness if all slack is used up</li> <li>may lead to clearance violations if a large slack is required</li> </ul>
4 triple curvature	<ul style="list-style-type: none"> <li>clearance problems with catenary</li> <li>large spans where inverse parabola not suitable</li> </ul>	<ul style="list-style-type: none"> <li>may satisfy clearances not possible with catenary with same required slack</li> <li>takes conductor away from phase to ground radius clearance</li> </ul>	<ul style="list-style-type: none"> <li>Limited in minimum span as may become too stiff</li> <li>requires 45° connector hardware</li> <li>not recommended with 90° hardware as may lead to “bird caging”</li> </ul>

## 7.2.2 Required Conductor Length

In addition to permitting the required amount of differential displacement, i.e., “meeting” the elongation demand, it is necessary to choose a practical conductor configuration that will provide sufficient flexibility. Although the seismically induced equipment movements will initially be in the same direction, later movements may oppose each other, depending on the natural frequency of each piece of equipment. It is, therefore, necessary to choose a conductor configuration that

will provide the necessary flexibility, in both the “pushing” and “pulling” directions, to accommodate the expected maximum differential displacement. Since configurations where the amount of available slack equals the elongation demand will become abruptly stiff when stretched close to that limit, an additional length is necessary so that the configuration provides the required flexibility for the entire range of expected motions.

The required conductor length for a flexible conductor is given by

$$L_0 = L_1 + e_o + L_2 \quad (7.1)$$

where  $L_0$  is the necessary conductor length,  $L_1$  is the straight-line distance between the attachment points,  $e_o$  is the elongation demand, and  $L_2$  is an additional provision for the conductor shape under consideration to avoid abrupt stiffening when stretched close to the elongation demand and to ensure that the loads transferred to the terminals are within equipment and terminal pad connection capacities.

Also, for each conductor configuration, a minimum span exists below which the conductor becomes increasingly more rigid and, therefore, lacks the necessary flexibility to accommodate the expected differential displacement. Depending on the required amount of slack, some configurations may also sag in a way that they will violate the clearance requirements.

Therefore, in addition to determining  $L_2$ , the user must determine

- the minimum span below which the configuration becomes too rigid,
- the maximum span at which the configured shape will collapse under its own weight or under the additional effects of climatic loading such as wind and ice whenever this applies,
- the satisfaction of the clearance requirements.

The methods to check these requirements are presented below.

Regarding configuration 1, the inverse parabola, it is recommended to form it as a half circle, whenever possible, since it will then be more stable to vertical loads, such as its own weight and additional ice loading if present. In terms of the parameters defined in Figure 7.1, the recommended length of the conductor in this configuration is

$$L_{0\_parabola} = \frac{\pi \cdot H}{2} + V \quad (7.2)$$

where  $L_{0\_parabola}$  is the necessary conductor length for the inverse parabola,  $H$  is the horizontal distance between attachment points, and  $V$  is the vertical distance between attachment points.

This length will be adequate as long as it can permit without abrupt stiffening the elongation demand  $e_0$ , as discussed in the next section. In general, this configuration is suitable for large displacements, as the slack provided by the half-circle configuration is important and often much larger than the elongation demand. When the vertical difference between the supports ( $V$ ) is of the order of the horizontal span between them ( $H$ ), i.e.,  $V \approx H$ , it is recommended instead to use a configuration closer to a quarter circle, which would be more stable than the full inverse parabola. In such a case, the required length to use is closer to

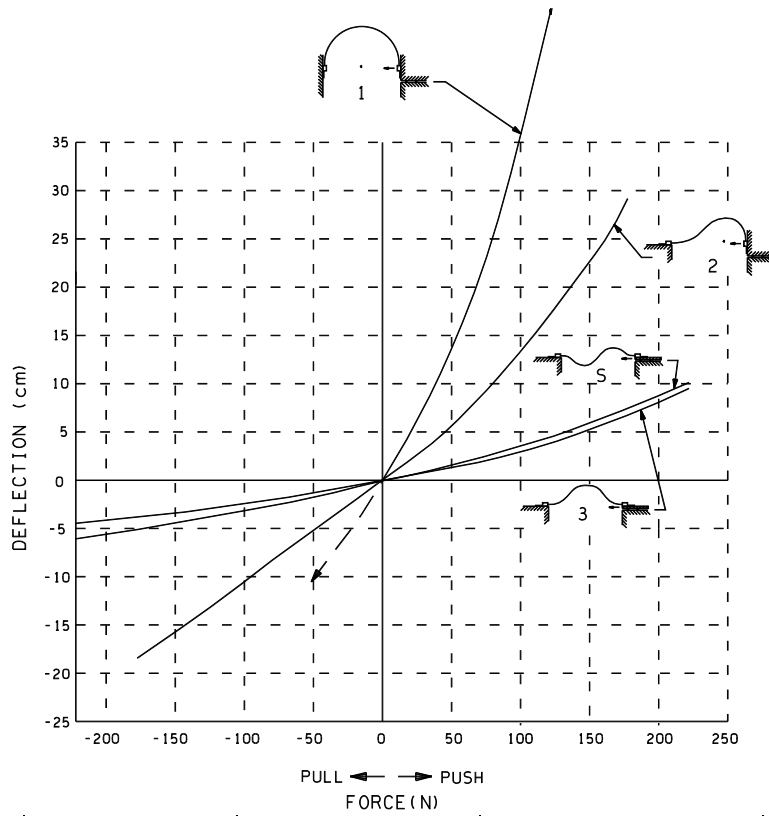
$$L_{0\_quarter\_circle} \approx \frac{\pi \cdot H}{2} \quad (7.3)$$

The quarter-circle configuration provides less slack than the full inverse parabola and can therefore accommodate less displacement than the latter.

### 7.2.3 Qualitative Investigation on the Flexibility of the Different Shapes under Stretching

The flexibility of some of the recommended shapes (or their variations) has been investigated experimentally by static push-pull tests, where both ends were rigidly clamped in position (Fig. 7.3). Although limited in scope, since each configuration was tested with only one span length and with a unique amount of slack, this figure demonstrates qualitatively that the inverse parabola is the most flexible configuration, followed by the double curvature.

However, this figure is also somewhat misleading, as it is not possible to assess based on the actual shape alone, a definitive or quantitative conclusion on the flexibility of the different shapes. The main reason is that any shape will be relatively flexible over a given range of elongation but, as discussed in Section 7.2.2, will ultimately and often abruptly become stiff when the elongation reaches the available slack. It is then more precise to say that all configurations have a range of elongation over which their behavior is somewhat linear, and a nonlinear range where their flexibility diminishes rapidly (or their rigidity increases abruptly), as shown in Figure 7.4, for both ranges from the results of a push-pull test on a catenary shape. Note that the boundary between the quasi-linear and nonlinear ranges, here 5.2 m, is specific to the conductor cross section and configuration and has been qualitatively selected.



Configuration	Span Length (m)	Conductor Length (m)
1	0.70	2.21
2	1.37	1.85
3	1.37	1.58
S	1.37	1.58

Note: Vertical separation of terminals was zero for the above configuration.

**Fig. 7.3 Results of flexibility testing at BC Hydro on different configurations (Opsetmoen 1998)**

General test description:

- Slow application of a cyclic displacement at one end of the conductor with the other end fixed
- The horizontal force applied at the fixed end is measured, along with the sag at mid-span

Description of specimen tested:

- Conductor type: 1796 kcmil
- Cross section area: 910 mm<sup>2</sup>
- Length: 5.52 m
- Both ends clamped horizontally

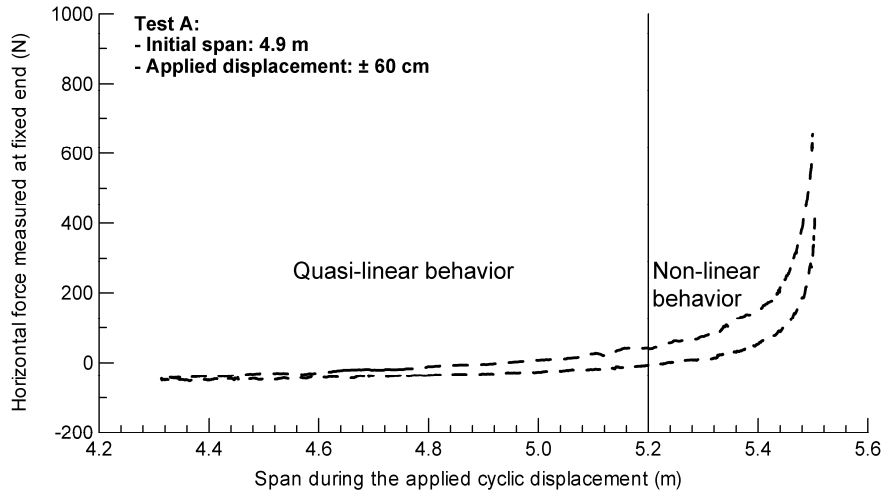


**Fig. 7.4 General behavior of flexible connections under stretching**

An alternative way to assess the flexibility of the different shapes is to compare their behavior for the same ratio of demand over available slack, given by

$$\beta = \frac{e_o}{L_0 - L_1} \quad (7.4)$$

where  $\beta$  is the ratio of demand over available slack, also defined as the interaction parameter (Der Kiureghian et al. 1999),  $e_o$  is the elongation demand, and  $L_0 - L_1$  is the available slack or “availability,” the difference between the conductor length and the straight-line distance between attachment points.

As  $\beta$  approaches 1, clearly, any configuration will be less flexible (or more rigid). To illustrate the flexibility of the different shapes proposed in this guide according to  $\beta$ , we present in the following figures the results of quasi-static push-pull finite element simulations using values of  $\beta = 0.8$  and  $0.5$  for a unique span of 4 m and a demand of 30 cm; scaled initial shapes of all configurations are also illustrated. For the inverse parabola, we also present the case where its length corresponds to a half circle as recommended in this guide (which corresponds to  $\beta = 0.13$  here).

Figure 7.5 illustrates that for  $\beta = 0.8$ , the most flexible configuration for all ranges of elongations is the catenary, followed by the double curvature, the triple curvature, and finally the parabola. This is understandable, as configurations with ends attached at angles will rapidly become stiffer when stretched, due to the bending stiffness of the conductor near the attachment points. The bending stiffness resists any elongation that tends to flatten the conductor to achieve an angle of  $0^\circ$  at the attachment points. This can also be inferred by examining the initial position of the different shapes on the figure, especially the inverse parabola at  $\beta = 0.8$  (not the half-circle shaped one), since as observed, it is already quite flat except near its attachment points at  $90^\circ$ ; any increase in elongation will therefore be resisted by the bending stiffness of the conductor there. We note that for this inverse parabola configuration, the generated force for the complete elongation of 30 cm is of the order of 20,000 N and well outside the range of the figure.

As also indicated in the figure, the triple-curvature configuration was transformed in a kind of parabola shape at  $45^\circ$  attachment points through a “snap-through” phenomenon. The weight of the conductor was not sufficient to keep it in the desired configuration because due to its bending stiffness, the conductor moved upward when its attachment points were rotated  $45^\circ$ . This phenomenon was induced here by the way the shape was formed through the finite element simulation (as presented and discussed later), but would probably occur in practice unless the conductor was pre-shaped before its installation. This phenomenon can also take place when stretching a connection, as is observed here for the double-curvature shape: the jump observed around 0.06 m in the elongation curve for this shape is due to this effect.

The results in Figure 7.5 suggest that due to the bending stiffness of the conductor, it is necessary to increase the additional length  $L_2$  in Equation (7.1) when the ends of the conductor are attached at an angle (from  $45^\circ$  to  $90^\circ$  here). It is also observed that the rigidity of the inverse parabola formed as a half circle is almost constant and close to zero for the elongation range considered; this is understandable, as the corresponding value of  $\beta$  is only 0.13, which signifies that a lot of slack is available in relationship to the demand.

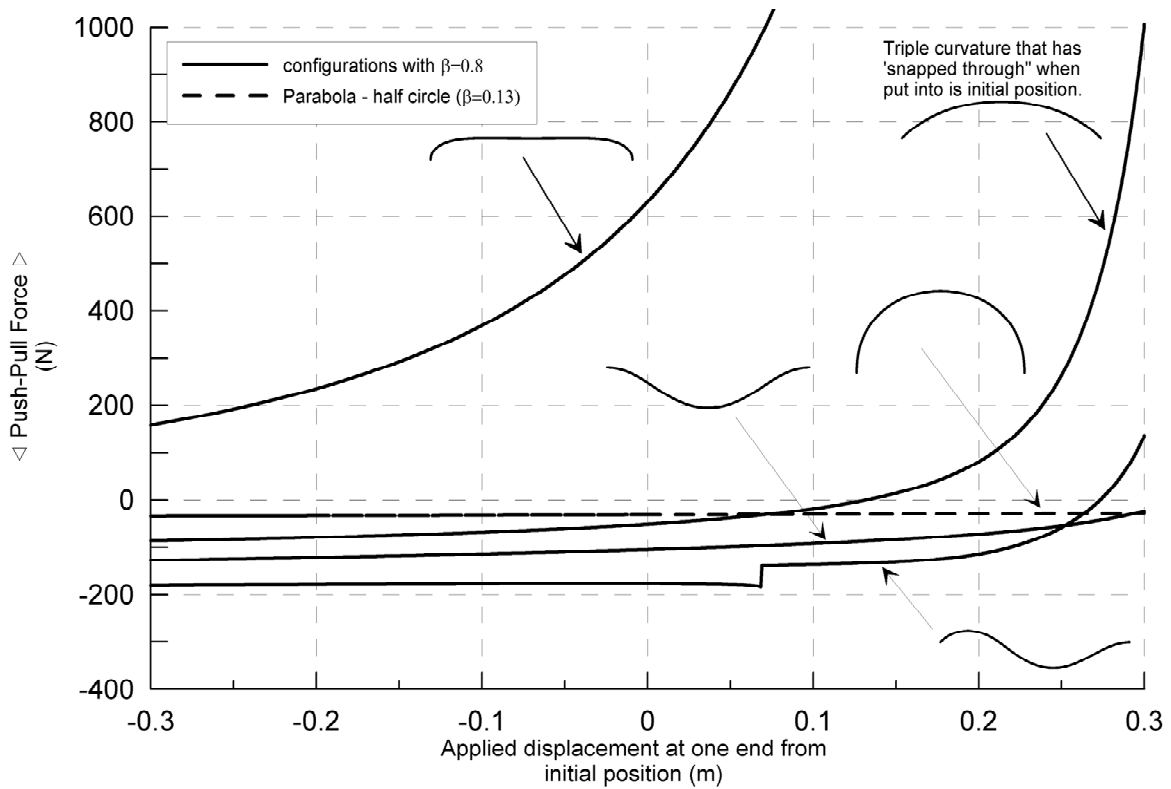


**Fig. 7.5 Effect of shape on flexibility for a constant  $\beta$  value of 0.8 (span 4 m,  $e_o=30$  cm, slack=37.5 cm for all shapes (except parabola half circle))**

Figure 7.6 illustrates the case where  $\beta=0.5$ . It is observed that except for the inverse parabola, all other shapes are in the quasi-linear behavior and thus have sufficient slack for the required elongation demand (here assumed to be 30 cm). Also, by comparison with the previous figure, it is observed that the inverse parabola with  $\beta=0.5$  is much more flexible than with  $\beta = 0.8$ .

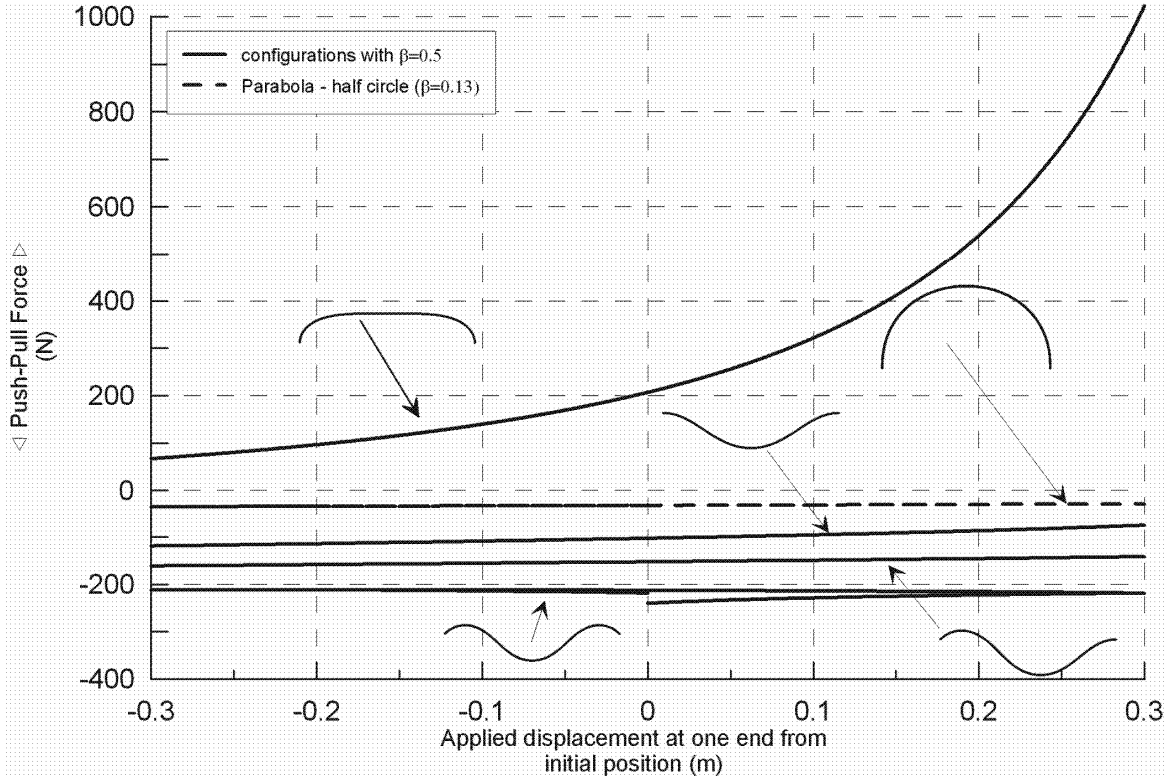


**Fig. 7.6 Effect of shape on flexibility for a constant  $\beta$  value of 0.5 (span 4 m,  $e_o=30$  cm, slack=60 cm for all shapes (except parabola half circle))**

The preceding observations lead to the following conclusions regarding the flexibility of available configurations:

- All configurations possess a range of elongations over which they are relatively flexible but after which their stiffnesses gradually and then rapidly increase (quasi-linear vs. nonlinear behavior).
- A ratio of demand over availability under 1 [ $\beta$  – Eq. (7.4)] is mandatory to avoid the nonlinear range and corresponding abrupt stiffening.
- For the same value of  $\beta$  (under 1), the most flexible configuration is the catenary, followed in order by the double curvature, the triple curvature, and the inverse parabola.
- All configurations require an additional length  $L_2$  to provide sufficient flexibility, especially when attachment points are at an angle.
- The flexibility of a configuration generally increases with decreasing  $\beta$ .
- When the inverse parabola is formed under a half circle as recommended, it is generally very flexible as long as the demand is easily permitted.

## 7.2.4 Qualitative Effects of Adding Slack

The main effects of adding slack to a flexible conductor are

- increase of sag (in the cases of configurations 2–4 above) and, therefore, of the possibility that phase-to-ground and minimum safety clearances may be violated;
- decrease of forces applied at the terminals in the static configuration of the conductor under its own weight;
- increase in the flexibility of the conductor for the same demand (e.g., decrease in the value of  $\beta$ );
- increase in the possibility that the conductor will collapse under its own weight or additional vertical (ice) or transversal (wind) loads, particularly in the case of the inverse parabola; and
- increase in the mass of the conductor, which may decrease the fundamental frequency of light equipment connected to it.

Regarding the first point, of increased sag and the possibility of violating clearance, it may not be obvious that sometimes *adding only a few more centimeters* of slack can make the difference between a configuration that meets the clearances requirements and one that does not. Among other factors, the effect of adding slack depends on the span. This is illustrated in Figure 7.7, where scaled representations of a catenary<sup>4</sup> shape under its own weight for different amounts of slack are represented for spans of 2, 4, and 6 m. These figures have been developed using finite element calculations as described below. For each span, the effect of adding slack by increments of 15 cm (approximately 6 in.) is illustrated. It is observed that the span of 2 m is quickly limited by the phase-to-ground clearance as it is augmented, while the span of 6 m is limited by the minimum safety clearance for the same increments of slack. It is observed here that the span of 4 m is the one that provides the maximum amount of permitted slack while respecting clearances (with a maximum amount of permitted slack of about 40 cm), whereas the spans of 2 and 6 m allow less than 30 cm of slack while satisfying both clearances.

---

<sup>4</sup> The term “catenary” here is not exact due to the bending stiffness of the conductor, which has a significant influence on the deformations in the vicinity of the attachment points. However, this term is retained in this guide to describe a conductor with ends attached horizontally.

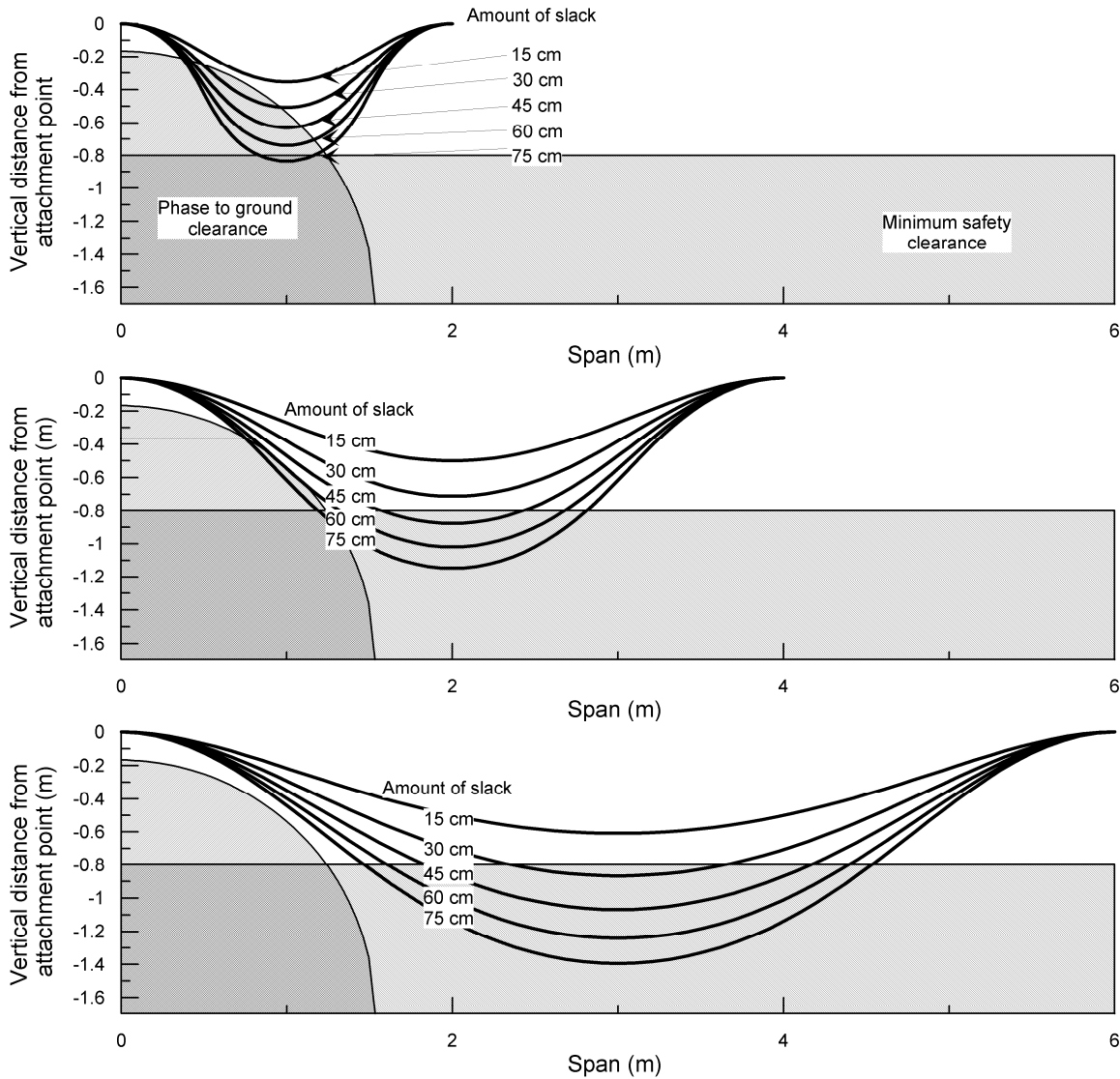


**Fig. 7.7 Effect of adding slack for catenary shapes of different spans (1796 KCM conductor, safety clearances for 170 kV, insulator length 1.7 m)**

The preceding calculations and figures also underscore that the required slack must be estimated as precisely as possible, as it may be difficult to meet the clearances depending on the span (and also the conductor shape). By comparison with the estimated upper-bound displacements from the IEEE 693 spectrum (Table 6.8), we see that for frequencies in the vicinity of 1 Hz or less, it might be difficult to provide sufficient slack for these displacements while meeting the clearances.

It is also inferred from the preceding figures that the effect of added slack on the sag is proportional to the span; i.e., the greater the span, the more the sag increases for the same increase in slack. This is illustrated in Figure 7.8, where we present the sag as a function of slack

for the three spans above. It is observed that the greater the span, the greater the sag for the same amount of slack and the faster the sag increases with the slack.

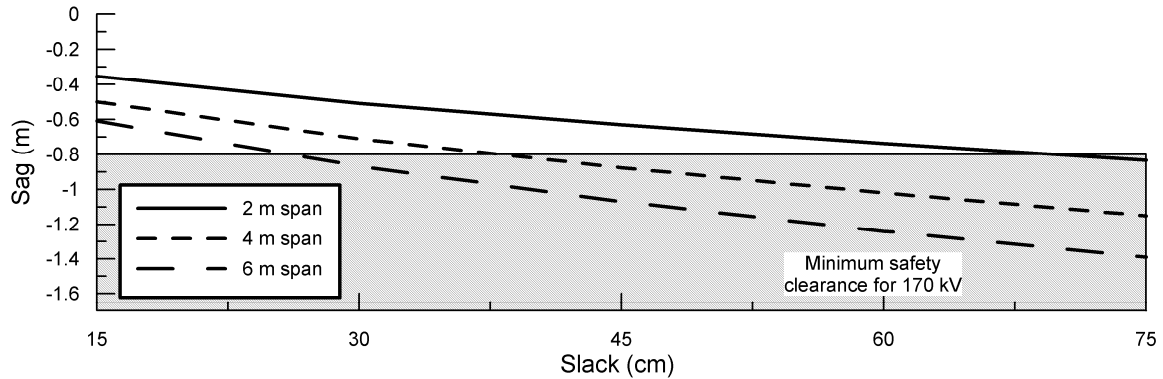


**Fig. 7.8 Effect of adding slack on sag for catenary configurations of different spans**

### 7.3 VERIFICATION OF CLEARANCES, FLEXIBILITY, AND STABILITY USING THE NONLINEAR FINITE ELEMENT METHOD

Once the elongation demand has been established and the conductor configuration has been selected, the additional length  $L_2$  must be determined in order to establish the required conductor length  $L_0$ . This additional length is a function of the desired flexibility upon application of the elongation demand  $e_0$  to ensure that the loads transferred to the terminals are within equipment and terminal pad connection capacities. Once the total length has been established, one must check that the corresponding configuration under its own weight (and ice if applicable) is able to meet the required clearances and is also stable (will not collapse) under its weight (and ice if applicable) and lateral loading due to wind. The nonlinear finite element method is suitable for these verifications. When used properly, it provides a realistic prediction of the conductor shape in its installed configuration under operational loads, and, gives a reasonable estimate of the static forces applied at the terminals. The present section introduces this method, describes how to use it, and provides representative calculation examples.

#### 7.3.1 Introduction

The finite element method is a widely used computational method, whereby a structure is divided into small (finite) elements of given properties—a process called “meshing”—the assembly of which represents the physical behavior of the real structure under arbitrary loading. Different types of elements are available to model structures, namely linear elements such as

beams, surface type such as shells, and solid type such as tetrahedrons. An element is defined geometrically by the position of its *nodes*—the points at its boundaries—and physically by its dimensions and the physical properties of the material assigned to it.

The analysis process of any structure generally consists of the following steps:

1. determination of the required mechanical properties: cross section, elastic moduli, etc.;
2. discretization of the structure into  $n$  finite elements—the meshing;
3. application of the boundary conditions of the structure: the points that will remain fixed in given directions such as connections to foundations;
4. application of the considered loads at the nodes of the model: self-weight, ice weight, wind, displacement of a point, etc.;
5. computation of the structure's response to the loads; and
6. analysis of the results: displacements, internal forces, stresses, etc.

For structures, two main types of finite element analysis are available: linear and nonlinear. Linear analysis generally applies when the material deformation remains within the elastic range and when the deformation of the structure remains small compared to its dimensions. Conversely, nonlinear analysis applies outside the elastic range behavior and/or when deformations are not small.

Flexible conductors are similar to beams due to their bending stiffness, which has a definite influence on their behavior, especially in the areas close to their attachment points. However, as opposed to regular beams used in building structures, flexible conductors may experience large deformations under the influence of their own weight and other loads. It is therefore not possible to predict beforehand their final installed position. For this reason, this position must be found starting from a straight horizontal line configuration, by gradual application of the weight and displacement of the attachments points to reach the desired span, vertical offset, and attachment angles of the installed configuration. Therefore, flexible connections require *nonlinear analysis*. Since their deformations are large in the process to establish their equilibrium position—technically, this behavior is said to be *geometrically nonlinear*. Furthermore, flexible connections are also *materially nonlinear*, due to their construction in layers of wires where each wire can be either slipping or sticking to the adjacent ones, leading to a variable bending stiffness (Dastous 2005; Hong et al. 2005). However, as we will see below, this type of nonlinearity can be avoided in a conservative way in static calculations by considering an effective bending stiffness as an approximation.

The selected results of nonlinear finite element calculations are presented in the following figures as typical applications of the method for flexible connections. Figure 7.9 illustrates the prediction of a given geometry and is representative of the typical results of this method. When a configuration “falls” in its final shape under its own weight (without need of pre-shaping), the finite element method produces quite accurate results and thus may be used with confidence to check clearances, as illustrated in Figure 7.10. It is observed that at the attachment point, the conductor, due to its bending stiffness is initially straight before “falling” under its own weight. This bending stiffness cannot be neglected as discussed above.

Figure 7.11 illustrates the prediction of end forces during static push-pull tests for two different catenary configurations and shows a relatively good agreement. However, the precision of the prediction of forces by the method can be somewhat different from case to case, depending on, among other factors, the properties of the model used and the history of how the final configuration of the conductor was formed during the installation. Therefore, it is safe to say that *for predicting forces, the nonlinear finite element method generally provides a realistic but not always precise estimate.*

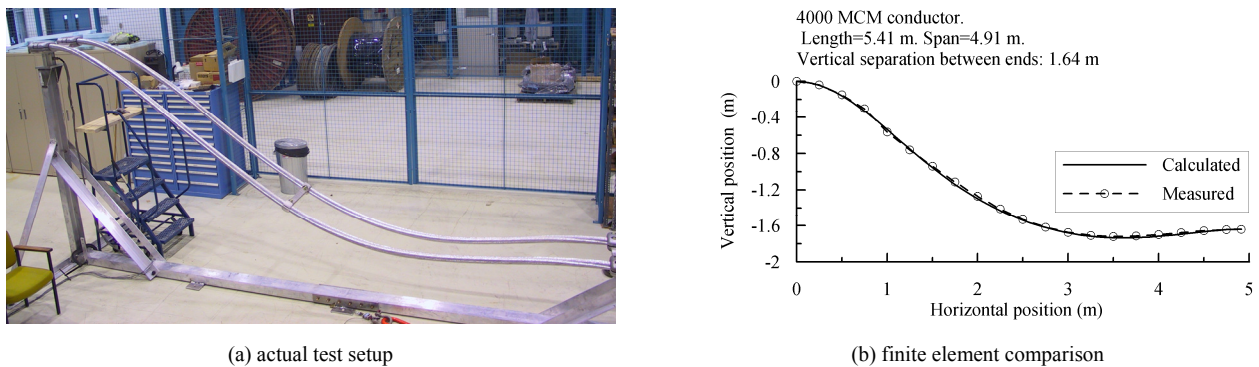


**Fig. 7.9 Comparison between calculated and measured shape of a catenary configuration**

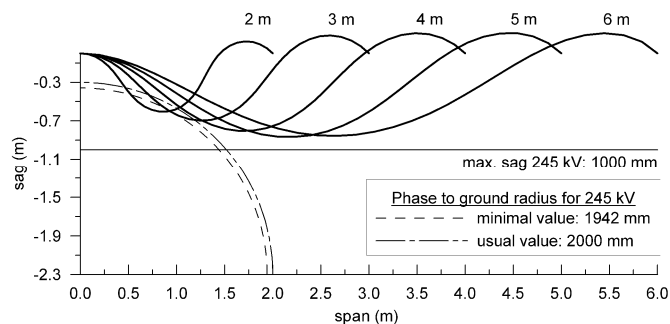


**Fig. 7.10 Clearance check with the finite element method with double-curvature configurations of different spans**

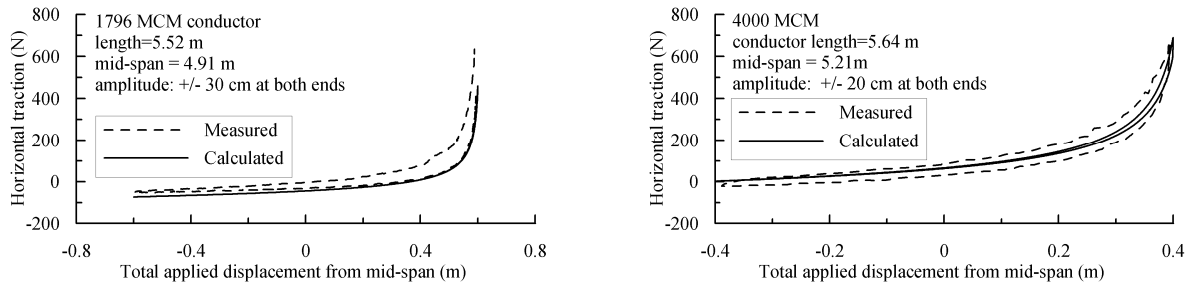


**Fig. 7.11 Comparison between calculated and measured forces of static push-pull tests on catenary configurations**

### 7.3.2 Required Software for Flexible Conductor Analysis

To analyze flexible connections, a finite element program with large displacement nonlinear capabilities is necessary. Most commercial finite element packages now have such capabilities. The cost and functionalities of these programs may vary greatly but they are generally expensive, on the order of several thousand dollars.

For an excellent introductory low-cost program, we recommend using the educational program *FEAP*, which is available at

<http://www.ce.berkeley.edu/~rlt/feap/>

This program provides state-of-the-art numerical methods and elements but is not as sophisticated in terms of its interface as commercial programs because its input must be defined through a text file. However, it is entirely adequate to perform nonlinear calculations of flexible connections as described in this guide. A free version of this software, *FEAPpv*, is also available at the same link as above but is more limited in its capabilities. It can be used only to perform 2D nonlinear calculations of a flexible connection under its own weight in a vertical plane, which is, however, sufficient to check clearances and the geometry that a configuration would take under gravitational loading.

### 7.3.3 Required Types of Elements in Flexible Conductor Modeling

As stated earlier, a structure should be divided prior to analysis into a finite number of elements (the meshing). Different types of elements are available for that purpose (mainly beams, shells, and solids). To adequately model the behavior of a flexible conductor, a beam element is

necessary and sufficient, since as discussed above, flexible conductors are similar to beams with finite deformations.

Ideally, a specialized beam element accounting for the construction in layers of conductors and the corresponding slipping or sticking of the individual wires could be used. However, such elements are complex and not readily available in commercial finite element software unless the user is willing to develop and implement a custom-made element. Before doing so, the user should also qualify his model through comparisons with experiments to ensure realistic results. Since this is not possible for most users of this guide, one must instead use a regular beam element which is normally readily available in the program at hand.

The method in this guide is based on the use of geometrically nonlinear beam elements with constant material properties, e.g., bending stiffness; the required properties for a representative calculation are discussed next.

Depending on the program, a geometrically nonlinear beam element is named in different ways, such as *finite deformation beam*, or most often *nonlinear beam*. The user must only verify that the beam element used accounts for large displacements and/or deformations in a geometrically nonlinear way.

### **7.3.4 Determination of Input Properties for the Beam Element Representing the Conductor**

The following properties of a flexible conductor must be evaluated as input to the beam element used in the model:

- cross-sectional area:  $A$
- equivalent Young's modulus:  $E_{eq}$
- equivalent bending moment of inertia:  $I$
- mass property of the element: linear mass:  $\bar{m}$  or density  $\rho$

#### **7.3.4.1 Cross-Sectional Area**

The cross-sectional area  $A$  of a flexible conductor is approximately equal to the sum of the cross-sectional areas of its individual wires. This approximation neglects the contribution of the lay angle of the wires, which is usually small. For the general case of a conductor made of wires of different diameters, the cross-sectional area is given by

$$A = \frac{\pi}{4} \cdot \sum_{i=1}^n \delta_i^2 \quad (7.5)$$

where  $n$  is the number of wires in the conductor, and  $\delta_i$  is the diameter of wire  $i$ .

For the case where a conductor is made of wires of identical diameter  $\delta$ , Equation (7.5) simplifies to

$$A = n \cdot \pi \cdot \frac{\delta^2}{4} \quad (7.6)$$

For example, consider a 2300 kcmil conductor made of 61 identical wires of diameter  $\delta_i=4.939$  mm. Equation (7.6) is used to obtain

$$A = 61 \cdot \pi \cdot \frac{4.939^2}{4} = 1169 \text{ mm}^2$$

As an example of a conductor made of different wire sizes, consider the ACSR *Bersimis* 42/7 conductor made of 42 aluminum strands, 6 steel strands, and 1 steel wire for the core. The properties of this conductor are summarized in Table 7.2.

**Table 7.2 Properties of the Bersimis 42/7 conductor**

layer	material	number of wires	wire diameter (mm)	Young's modulus (GPa)	material density (kg/m <sup>3</sup> )
core	steel	1	2.54	200	7800
1	steel	6	2.54	200	7800
2	aluminum	8	4.57	69	2700
3	aluminum	14	4.57	69	2700
4	aluminum	20	4.57	69	2700

Here we have two different wire diameters, so Equation (7.5) is used and simplified to

$$A = \frac{\pi}{4} \cdot \sum_{i=1}^n \delta_i^2 = \frac{\pi}{4} \cdot [7 \cdot 2.54^2 + 42 \cdot 4.57^2] = 725 \text{ mm}^2$$

### 7.3.4.2 Equivalent Young's Modulus

The equivalent Young's modulus  $E$  of a conductor of given cross section is derived from its axial stiffness  $EA$  as

$$E_{eq} = \frac{EA}{A} \quad (7.7)$$

The axial stiffness of an arbitrary cross-sectional area composed of a single material is given by the product of its area and the *Young's* (or elasticity) modulus of its material  $E$ . In the case of flexible conductors made of layers, the axial stiffness is in theory also a function of the lay angle of each layer. However, since the axial stiffness is not a dominant factor in the conductor behavior under static loading (unless the conductor is stretched to a straight-line or beyond), the product of the area  $A$  times the Young's modulus  $E$  provides an adequate approximation of the axial stiffness for finite element analyses purposes.

Therefore, when a conductor is made of wires of the same material, the equivalent Young's modulus is simply the Young's modulus  $E$  of the material itself. In the case where the core and layers are made of different materials (e.g., an ACSR conductor), the axial stiffness is given by

$$EA = E_c \cdot A_c + E_l \cdot A_l \quad (7.8)$$

where  $E_c$  is the Young's modulus of the core material,  $A_c$  is the area of the core,  $E_l$  is the Young's modulus of the material in the layers, and  $A_l$  is the total area of all the layers. In this case, the equivalent Young's modulus is a weighted average of  $E_c$  and  $E_l$ .

As an example of a conductor made of different materials, consider again the ACSR Bersimis 42/7 conductor (Table 7.2). The area of the core and the first layer  $A_c$  are given by

$$A_c = 7 \cdot \pi \cdot \frac{(2.54)^2}{4} = 35.5 \text{ mm}^2$$

The total area of all the other layers is given by

$$A_l = 42 \cdot \pi \cdot \frac{(4.57)^2}{4} = 689 \text{ mm}^2$$

Thus, the axial stiffness of the conductor is given by (using proper units for the quantities above)

$$EA = E_c \cdot A_c + E_l \cdot A_l = 200 \cdot 10^9 \cdot 35.5 \cdot 10^{-6} + 69 \cdot 10^9 \cdot 689 \cdot 10^{-6} = 5.46 \cdot 10^7 \text{ N}$$

The total area of the conductor was computed as  $725 \text{ mm}^2$  and, therefore, the equivalent Young's modulus is given by

$$E_{eq} = \frac{EA}{A} = \frac{5.46 \cdot 10^7}{725 \cdot 10^{-6}} = 75.4 \text{ GPa}$$

### 7.3.4.3 Equivalent Bending Moment of Inertia

The bending behavior of a conductor under loading is a complex phenomenon because individual wires may either slip or stick to the adjacent ones. When all wires are in the slip state, the bending stiffness of the conductor is at its minimal value and is given by the sum of the bending stiffnesses of individual wires around their respective neutral axes. For a conductor made of  $n$  wires, the minimum bending stiffness is given by

$$EI_{\min} = \sum_{i=1}^n E_i \cdot \pi \cdot \frac{\delta_i^4}{64} \quad (7.9)$$

where  $n$  is the total number of wires in the conductor,  $E_i$  is the Young's modulus of wire  $i$ , and  $\delta_i$  is the diameter of wire  $i$ .

When all the individual wires are sticking together, the bending stiffness is at its maximal value  $EI_{\max}$ . The ratio of  $EI_{\max}$  to  $EI_{\min}$  can be large. For example, for the 1796 kcm AAC conductor, which is made of 61 aluminum wires, this ratio is close to 80.

It has been shown that for short-span substation conductors (typically between 2 and 7 m), which have relatively low tension as opposed to transmission lines, the bending stiffness is generally close to its minimal value (Stearns and Filiatrault 2005). Furthermore, since we are interested in verifying the electrical clearances, it would be conservative to use the minimum bending stiffness, as this would lead to the maximum deflection of the conductor configuration. Similarly, to verify stability under loading, the use of the minimum bending stiffness will be conservative. *Therefore, the use of the minimum bending moment of inertia is recommended in this application guide for such calculations.* When more precision is required, the user is referred to more complex models such as those described in Dastous (2005) and Hong et al. (2005).

The minimum bending moment of inertia should be obtained using the equivalent Young's modulus used in the model, since the finite element input requires  $I_{\min}$  instead of  $EI_{\min}$ . Using Equation (7.9), this is given by

$$I_{\min} = \frac{EI_{\min}}{E_{eq}} \quad (7.10)$$

For example, consider a 2300 kcmil conductor made of 61 identical aluminum wires of diameter  $\delta_i=4.939$  mm and Young's modulus equal to 69 GPa. Using Equation (7.9) we obtain directly the minimum bending stiffness as

$$EI_{\min} = \sum_{i=1}^n E_i \cdot \pi \cdot \frac{\delta_i^4}{64}$$

$$\frac{EI_{\min}}{E} = I_{\min} = \sum_{i=1}^n \pi \cdot \frac{\delta_i^4}{64} = n \cdot \pi \cdot \frac{\delta_i^4}{64} = 61 \cdot \pi \cdot \frac{4.939^4}{64} = 1782 \text{ mm}^4 = 1.782 \cdot 10^{-9} \text{ m}^4$$

As an example of a conductor of different wire properties, consider again the Bersimis 42/7 conductor (Table 7.2). Using Equation (7.9) we first obtain the value of the minimum bending stiffness as

$$EI_{\min} = \sum_{i=1}^n E_i \cdot \pi \cdot \frac{\delta_i^4}{64} = \sum_{i=1}^7 200 \cdot 10^9 \cdot \pi \cdot \frac{(2.54 \cdot 10^{-3})^4}{64} + \sum_{i=1}^{42} 69 \cdot 10^9 \cdot \pi \cdot \frac{(4.57 \cdot 10^{-3})^4}{64} = 65.72 \text{ N} \cdot \text{m}^2$$

Using Equation (7.10) and the value of  $E_{eq}$  previously found, we obtain the bending moment of inertia as

$$I_{\min} = \frac{EI_{\min}}{E_{eq}} = \frac{65.72}{75.4 \cdot 10^9} = 8.72 \cdot 10^{-10} \text{ m}^4$$

#### 7.3.4.4 Mass Property

Depending on the finite element software at hand, the mass property of the conductor cross section could be specified either through the density of the material  $\rho$  or the linear mass of the conductor cross section  $\bar{m}$ .

In the general case of a conductor cross section made of different materials for the core and the outer layers, the linear mass is given by

$$\bar{m} = \rho_c \cdot A_c + \rho_l \cdot A_l \quad (7.11)$$

where  $\rho_c$  is the mass density of the core material,  $A_c$  is the cross-sectional area of the core,  $\rho_l$  is the mass density of the outer layer material, and  $A_l$  is the cross-sectional area of the outer layers.

When the density is required as input, an equivalent density  $\rho_{eq}$  must be input in the case where two materials are used in the conductor. This equivalent density can be obtained using Equation (7.11), and the total conductor cross section  $A$  as

$$\rho_{eq} = \frac{\bar{m}}{A} \quad (7.12)$$

For example, the linear mass of the 2300 kcmil conductor with density  $2700 \text{ kg/m}^3$  is given, using its previously calculated area of  $1169 \text{ mm}^2$ , by

$$\bar{m} = \rho \cdot A = 2700 \cdot 1169 \cdot 10^{-6} = 3.16 \text{ kg/m}$$

As another example, consider again the Bersimis 42/7 conductor using areas for the steel and aluminum outer layers as previously computed. Using (7.11), the linear mass is obtained as

$$\bar{m} = \rho_c \cdot A_c + \rho_l \cdot A_l = 7800 \cdot 35.5 \cdot 10^{-6} + 2700 \cdot 689 \cdot 10^{-6} = 2.137 \text{ kg/m}$$

Using Equation (7.12), the equivalent density is given by

$$\rho_{eq} = \frac{\bar{m}}{A} = \frac{2.137}{724.5 \cdot 10^{-6}} = 2950 \text{ kg/m}^3$$

### 7.3.4.5 Common Conductor Properties

Table 7.3 shows the properties of commonly used substation conductors according to the nomenclature and calculations above. All conductors in this table are made of the same material (all copper or all aluminum) and have identical wire diameters ( $\delta_i$ ).

**Table 7.3 Common conductor input properties for finite element calculations\***

Size (kcmil)	Material	N	$\delta_i$ (mm)	A (mm <sup>2</sup> )	$E_{eq}$ (GPa)	$I_{min}$ (mm <sup>4</sup> )	$\rho$ (kg/m <sup>3</sup> )	$\bar{m}$ (kg/m)
250	Copper	19	2.916	127	120	67.4	8955	0.343
500	Copper	37	2.950	253	120	138	8955	0.683
715.5	Aluminum	37	3.534	363	69	283	2700	0.980
1113	Aluminum	61	3.432	564	69	415	2700	1.524
1796	Aluminum	61	4.359	910	69	1080	2700	2.458
2300	Aluminum	61	4.939	1169	69	1782	2700	3.155
4000	Aluminum	270	3.090	2025	69	1208	2700	5.470

\* All conductors listed are made of only one material as stated (e.g., aluminum conductors are AAC).

### 7.3.5 Calculation of the Initial Configuration of the Conductor

The first step in analyzing a flexible connection is to obtain its equilibrium position under its own weight in its installed position. To do so, we start with the configuration initially in a straight horizontal line and apply the required weight and displacement(s) / rotation(s) of the end points to obtain the final span, the required vertical offset, and the attachment angles. Since the deformations of the conductor from a straight line are large, the final configuration cannot be obtained in only one calculation step by applying all the weight and displacement at once, as this would lead to computational, or *convergence*, problems, in the terminology of the finite element method, since the final configuration is too far from the original one. We must therefore apply the weight and required displacements in small increments and, for each increment, calculate the corresponding equilibrium position until the final position is obtained. One recommended

procedure, particularly applicable to the catenary shape, is to first incrementally apply the weight on the initial straight line and then to incrementally move either one or both end points to obtain the final position (see Fig. 7.12).

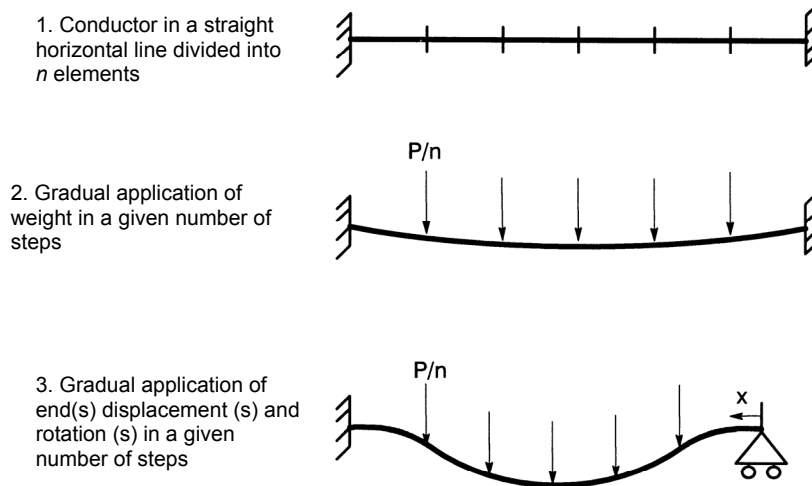


**Fig. 7.12 General procedure to establish the initial configuration of the conductor**

We will now describe this procedure in details to illustrate the main features of a nonlinear calculation. However, other paths may or sometimes need to be applied to reach *convergence*, as described later.

### 7.3.5.1 Straight-line Initial Configuration and Required Number of Elements

The configuration must first be modeled as a straight line with a length equal to the conductor length  $L_0$ . This line must be divided into a sufficient number of elements in order to obtain a proper representation of the behavior of the real conductor. In theory the finer the *meshing*, the more accurate is the representation. However in practice, 20–100 elements would provide a sufficient discretization to obtain accurate results.

It is a good practice to start with a relatively coarse mesh (for example 20 elements) and to gradually increase the number until the difference between the calculation results is insignificant. In the process we can compare the convergence of the results, such as sag at mid-span and forces applied at the terminals. Generally, in finite element calculations displacements (such as the mid-span sag) converge more rapidly than forces. For example 20 elements might

already provide the final sag with good accuracy, while 60 elements may be required to obtain the convergence of the applied forces at the terminals. It is therefore recommended to experiment with the number of elements until all results of interest have converged.

It is noted that too many elements may lead to numerical problems and convergence difficulties. This is due to the internal representation of the different stiffnesses of a beam element, e.g., axial and bending stiffnesses, which are inversely proportional to the length and cubic length of the element, respectively. When this happens, one may get a message from the program that the stiffness matrix is *ill-conditioned*. For example, dividing a configuration into several thousand elements may lead to such a problem. Therefore the refinement of the mesh must be sufficient while not being excessive.

### ***7.3.5.2 Numerical Method to Establish Equilibrium in the Calculation Process and Path***

As described earlier, the solution to the desired equilibrium position must be obtained in a step-by-step fashion, by following a certain “path.” Using the example from Figure 7.12, a possible path is to

1. apply incrementally the total weight in 20 increments,
2. apply incrementally the required displacement of the right end to reach the desired span in 100 increments.

The number of increments provided here is just for example. In practice one must also experiment with the chosen path and its division into steps to make sure *convergence* of the solution is obtained. By *convergence*, we mean that at each step of the process along the path, the related intermediary equilibrium positions obtained are qualitatively similar to what would happen in practice if the conductor weight and displacement were applied along the same path, so that the final position is realistic. Indeed, due to the nonlinear calculation process, it is possible that the obtained solution does not correspond to the physical reality, or even that no solution can be obtained following a certain path and/or a certain division in number of steps. We now discuss the recommended numerical method to obtain convergence and the notion of convergence criteria. Next we will discuss the recommended path.

## Recommended Numerical Method and Convergence Criteria

To explain the nonlinear computation process and to verify that we have obtained a “converged” solution, we must first explain some basics. In a nonlinear calculation, the equation solved by the finite element program can be generalized as

$$K(x) \cdot x = F \quad (7.13)$$

where  $K(x)$  is the *stiffness* matrix of the system and represents the resistance of the structure to loads,  $x$  is a vector representing the displacements at every node of the model, and  $F$  is a vector representing the loads applied at every node of the model (either actual loads or those resulting from imposed displacements).

The left-hand side of this equation represents the internal forces resisting the external forces  $F$  (right-hand side). It is observed that the stiffness matrix  $K$  is written as a function of  $x$ , the displacements. This is because under nonlinear behavior, the resistance of the system varies as it deforms. For example, a catenary configuration with a small sag will resist differently a given conductor weight than a configuration with a larger sag. Since  $K(x)$  varies as a function of  $x$ , the solution of Equation (7.13) cannot be obtained directly. It must be obtained gradually by following, as stated above, a given path where the applied load  $F$  is divided into increments and an intermediate solution is obtained for each increment step.

The intermediate solution at each increment (or step) along a given path is obtained in an iterative way in finite element programs by attempting successive evaluations of the stiffness matrix  $K(x)$  and finding the corresponding solution  $x$  until the two sides of Equation (7.13) are more or less equal, i.e., until the difference between the two sides becomes acceptably small (different criteria to verify this are discussed below). Different numerical methods exist to perform this analysis, the most common being the *Newton-Raphson*, *modified Newton-Raphson*, and *BFGS* methods. All these methods involve evaluations in a certain pattern of the stiffness matrix during the iterations in one computational step (or increment) and differ in their advantages and disadvantages. The numerical method recommended in this guide for the calculation of flexible connections is the Newton-Raphson method, which is generally robust and provides fast convergence.

Due to the finite precision of computers and the approximations involved in any numerical method, Equation (7.13) can never be solved perfectly and some differences between its left and right hand sides will always remain. This is why a finite convergence criterion is set in programs that ensure a sufficient but not unattainable precision without demanding extensive

computational resources. Generally, in finite element programs, the convergence criterion can be based on different measures, the most common and also the recommended one in this guide being the one based on the “energy norm” or simply the energy, which is often the default criterion in programs. The energy norm is made of the square root of the product of the incremental displacement times the difference between the right and left sides of Equation (7.13) for the same given increment. The convergence is usually checked at a given step by comparing the energy norm obtained at the first iteration with the norm at the current iteration until

$$dE^i \leq \varepsilon \cdot dE^1 \quad (7.14)$$

where  $dE^1$  is the energy norm obtained at the first iteration of the current increment,  $dE^i$  is the energy norm at iteration I, and  $\varepsilon$  is the convergence criterion ( $\ll 1$ ) (also called the *tolerance level* or simply, the *tolerance* of the solution). The recommended values for the convergence criterion (or tolerance)  $\varepsilon$  are from  $1 \cdot 10^{-8}$  to  $1 \cdot 10^{-16}$ . In general, a smaller value will correspond to more iterations and longer computation times and vice-versa. However, smaller values are sometimes necessary, as convergence of the final results cannot be reached using bigger values.

### **Recommended Path**

In theory, a nonlinear solution can be obtained by different paths and different subdivisions (also called load steps) of each part of a path. However, to obtain convergence and a sound solution for flexible conductors, a basic rule of thumb should be followed.

This rule is that the chosen path must correspond to what one would do physically to install a configuration and/or what makes sense in a physical way. For example, to obtain the catenary configuration as per Figure 7.12, it would make less sense to first apply the displacements on a massless conductor, followed by the application of the weight, as this has no physical counterpart (the weight is always present) unless the configuration is first shaped on the surface of the ground and then lifted and rotated for its installation.

One possible path for a general configuration with vertical offset between the end points and the latter installed at angles consists in carrying out the following successive “segments”:

1. Apply the weight on the straight line.
2. Move one end horizontally to obtain the desired span.
3. Displace one end vertically to obtain the required vertical difference.
4. Apply the required rotation at each end (either simultaneously or one after the other when both ends are attached at angles).

The advantage in the above procedure of first applying the weight is that this “conditions” the conductor to fall under its own weight when one end is moved horizontally to obtain the desired span. If instead we tried to apply the horizontal displacement first, we would run into convergence problems, as this would simply compress the conductor along its length. This direction corresponds to a very high stiffness (axial stiffness) and, therefore, would lead to convergence problems.

However, the above procedure does not always work well when ends are at angles and the span is short, and/or when angles of  $90^\circ$  are present at one or both ends, such as for the inverse parabola. Sometimes convergence problems are met under a given path, and a different one must be tried in order to obtain a stable solution. For such cases, an alternative path, which works particularly well for the inverse parabola, is the following:

1. Apply a small fraction of the required rotation at both ends, such as 5%, to condition the conductor to move in the required direction once the horizontal displacement is applied (next step).
2. Move one end to obtain the desired span while applying the remainder of the required rotation(s).
3. Displace one end vertically to obtain the required vertical offset.
4. Apply the weight of the conductor.

This procedure corresponds physically to first shaping the configuration on the surface of the ground, lifting it from the ground, and then rotating it in a vertical plane for its installation. The first step of applying a small fraction of the rotation is similar to applying the weight in the preceding procedure, as this conditions the conductor to move upwards in the case of the inverse parabola when the horizontal displacement will be applied. In the examples that follow, we will see that both above procedures are used.

As for the division of each “segment” of the above paths in increments or load steps (we will use the simple term “step”), one must choose a sufficiently fine division to facilitate convergence. In general the number of steps to apply the weight can be 20–100, while the other segments may each require from 100 to a few 1000 steps. In general the more steps, the easier it is to obtain convergence, as the change between one increment to another is smaller. However, in cases of convergence problems, refining the division does not always work, as discussed in the next section. Again one must experiment and the final number of steps or segments depends on,

among other factors, the convergence criteria, the physical property of the conductor, and the required displacements and rotations if applicable.

### ***7.3.5.3 Instabilities and Convergence Difficulties in Nonlinear Calculations***

#### **Snap-back and Snap-through**

During a nonlinear calculation, a configuration can sometimes abruptly change its shape (or displace a large amount) and move to a new equilibrium position between two load steps, technically called a *bifurcation point*. The solution of such phenomena can sometimes be difficult and lead to convergence problems (or numerical instabilities), which make the solution difficult and may even result in the impossibility of attaining a converged solution, using the standard Newton-Raphson method as recommended earlier. In such cases, refining the division of the segment where the bifurcation happens does not generally help, as the instability is real no matter how slowly it is attained. In the analysis of flexible conductors, two similar phenomena of instability can occur:

- “snap-back,” when an initially concave part switches to a convex shape
- “snap-through,” when an initially convex part switches to a concave part

The two situations are illustrated in Figure 7.13. A snap-back generally occurs when rotations are applied at one end or both ends and, due to the bending stiffness of the conductor, the conductor abruptly moves upwards; this may happen, e.g., when forming a double- or triple-curvature configuration, as it suddenly moves into an inverse parabola shape. A snap-through generally occurs when the weight of the conductor, or the additional weight of ice, is applied over an inverse parabola, and the conductor abruptly moves downwards a certain distance. In both cases, a transitory loss of stiffness (the structure “softens”) or stability (the structure “buckles”) occurs until a new equilibrium position is reached, where the new corresponding stiffness is then able to sustain the applied loads again.

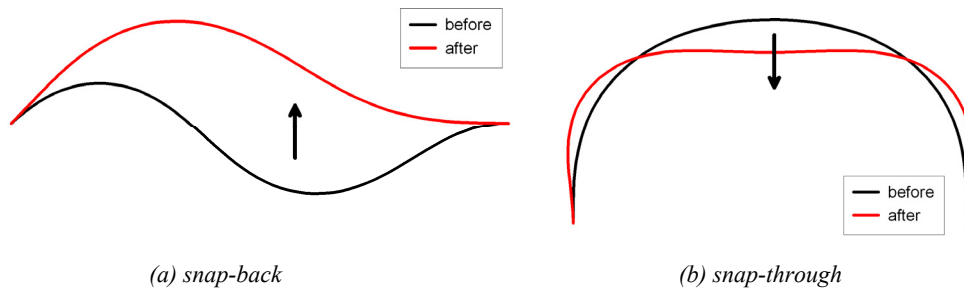


**Fig. 7.13 Snap-back and snap-through**

Using the standard Newton-Raphson equilibrium scheme with the possibility of continuing the analysis when the stiffness matrix becomes *non-positive definite*—the technical term employed in structural analysis (and in most finite element software) to define the loss of stability of the structure under consideration—two behaviors can generally be observed when a bifurcation point is reached:

- a sudden loss of stability and *no* stable equilibrium position attained afterwards
- a sudden loss of stability followed by a stable equilibrium position

The first behavior is shown in Figure 7.14(a), where we plot the resulting shape of a double-curvature configuration that is currently being formed by rotating its left end from the moment the bifurcation point (denoted by  $i$  in the figure) is attained to two steps later in the computational process (denoted by  $i+2$ ). It is observed that within two load steps the configuration deforms abnormally and an unstable solution is obviously reached; observe the scale of the last shape from the top. For this case, obviously it will not be possible to come back to a stable solution (after  $i+2$ ). The second behavior is shown in Figure 7.14(b). It is observed that even though the displacement is large between the steps, a sound physical position is finally attained; for such a case the solution is controlled and nothing more has to be done even though there was a momentary loss of stability in the computational process.

In both snap-back and snap-through phenomena where the solution is unstable, different numerical techniques have been devised and can be used to circumvent difficulties. While it is beyond the scope of this guide to present all numerical techniques that are available for that purpose, we recommend, among others, the use of a continuation method to obtain a stable and converged solution. A *continuation method* consists of controlling the increment of the load applied such that the variation of displacement is small (or of controlled amplitude) from one

time step to the other; in other words, the variation of the configuration shape is controlled such that large sudden displacements cannot happen between load steps. Such a continuation method is commonly called an *arc length* method or a *load-displacement-control* method. One possibility is to run the analysis until just before the bifurcation point using the Newton-Raphson method, and then switch to the continuation method afterwards. An example is presented below.

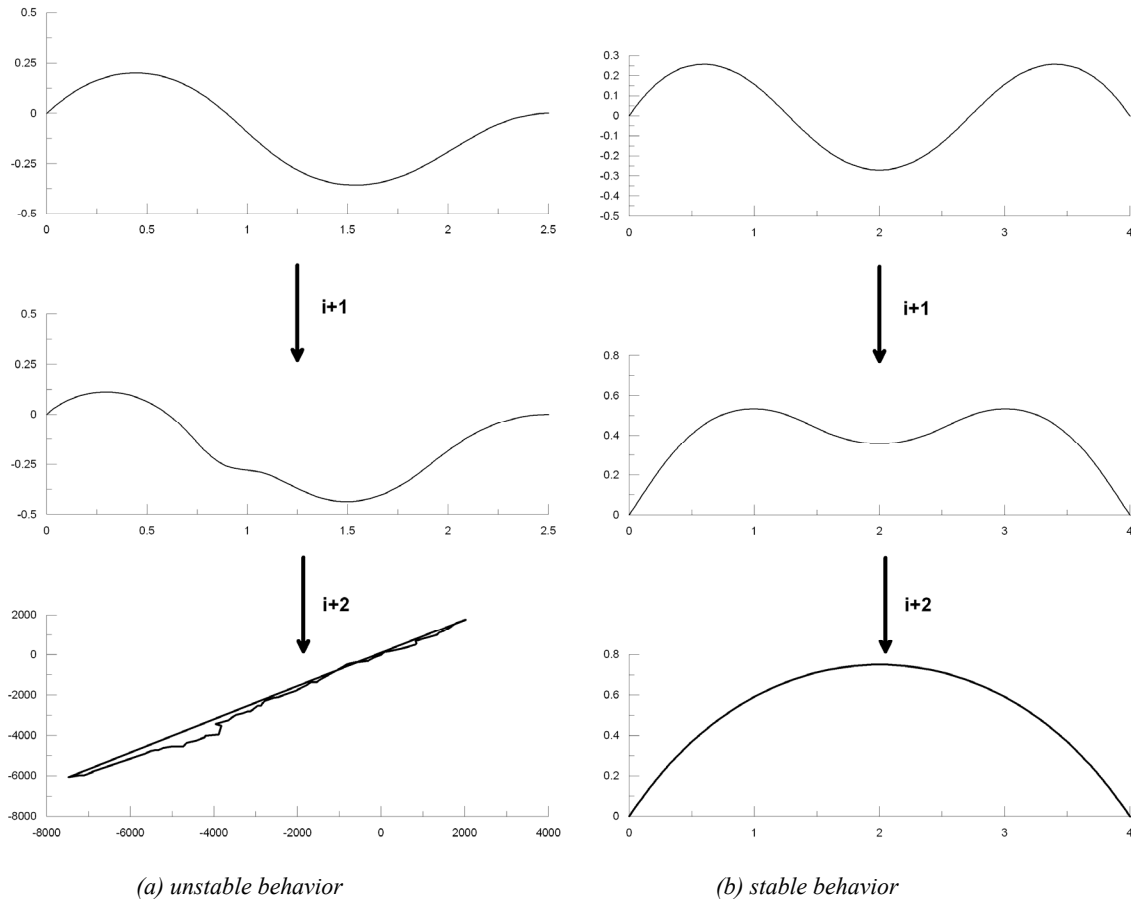


**Fig. 7.14 Unstable and stable solutions for snap-back<sup>5</sup>**

### Convergence Difficulties

Sometimes the solution does not converge at a certain step and the program terminates abruptly or indicates so by a message, or the solution “blows up” (meaning that divergence of the solution happens because the computer cannot precisely handle the very large or very small numbers generated in the numerical solution). This may happen without the attainment of a bifurcation point. The main reasons are usually one or more of the following:

<sup>5</sup> In these figures, the vertical axis represents the vertical position of the conductor at each horizontal position represented by the horizontal axis. Note that in figure (a) at iteration  $i+2$ , the calculation strongly diverges and this is why the vertical and horizontal axis span values are in the order of the thousandth, showing that the numerical solution there “blew up.”

1. The load or displacement increment between steps is too large and does not allow the possibility of attaining equilibrium.
2. The specified number of iterations is not sufficient, so that equilibrium cannot be reached at the tolerance level specified (convergence is slow).
3. The specified convergence criterion  $\varepsilon$  is too small and cannot be attained.
4. The convergence criterion  $\varepsilon$  is too big and the solution has therefore diverged along the steps as the solution has progressed.
5. The path chosen (e.g., application of weight, then displacements, then rotations) leads to sudden or abrupt increase of stiffness.
6. The structure “softens” over a certain range and increasing the load eventually leads to instability problems.

In nonlinear analysis, there are no universal means to solve such problems because solutions are most often problem dependent. The suggestions discussed below often work.

Regarding the first point, it can often easily be corrected by simply refining the division of the steps for the segment under consideration; e.g., changing the division of an applied displacement of 0.5 m from 100 to 500 steps. Some commercial programs also allow the possibility of automatically dividing a given step if convergence is not reached, through the use of an *automatic-time-stepping* scheme, which subdivides a time step until convergence is attained.

Considering the second point, it can often be corrected by simply increasing the number of iterations. We recommended 20 load step iterations but sometimes more are required when the convergence is slow.

Regarding the third point, it can often be corrected by setting the convergence criterion  $\varepsilon$  higher. We recommended earlier using values of  $\varepsilon$  from  $1 \cdot 10^{-8}$  to  $1 \cdot 10^{-16}$ , but sometimes values as high as  $1 \cdot 10^{-3}$  work well and give stable solutions. However, the danger in setting the tolerance too high is that the solution can slowly diverge as it progresses, since equilibrium is not attained with sufficient precision. This also addresses the fourth point above, the solution of which is to decrease the value of the criterion until divergence disappears.

With respect to the fifth point, as discussed earlier, the path chosen must somehow have physical meaning. As described in an earlier example provided of a horizontal straight-line configuration, we cannot displace one end of the conductor horizontally towards the other because this would correspond to compressing a very rigid structure. If, for this example, the

weight is first applied, the line will be “conditioned” to go downwards as soon as we displace one end, thus avoiding compression of a straight line along its axis. Most such problems occur when the displacement applied is in a direction of increased or of initially high rigidity. The solution then is to change the path to avoid such a situation. Sometimes combinations of different segments are necessary to obtain convergence; e.g., applying a small amount of the end rotations, then of the horizontal displacement, then of the combined rotations and displacement, followed by the application of the weight. Below we will present examples of some of the schemes that were required for different shapes.

For many of the convergence problems above, a solution is sometimes to change the numerical method used in establishing the equilibrium or to complement it with some algorithms that help the solution to converge. Among such methods are the modified-Newton-Raphson method and the BFGS algorithm to establish equilibrium, and the *line search* method to complement the *Newton-Raphson* or *BFGS* or *modified-Newton-Raphson* algorithms.

For the sixth point, which is similar to the snap-back and snap-through phenomena, the use of the continuation method is often useful in case of a softening behavior. An introduction to these alternative methods can be found in Zienkiewicz and Taylor (2000) or in the user’s manuals of many commercial programs.

### **7.3.6 Verification of Clearances**

To check the clearance requirements (phase-to-ground and minimum safety clearances), the equilibrium position calculated must be extracted from the finite element results and plotted against these requirements according to the geometry of the installation. The following points must be extracted from the geometry of the installation in order to plot the configuration and check clearances:

- coordinates of attachment points on both sides, in order to locate the calculated configuration relative to the base of the insulator parts and from the minimum safety clearance;
- coordinates of the base of insulator parts (or the “grounded” points closest to the configuration) in order to set the origins for the phase to ground radii that will be plotted to check the phase-to-ground clearances;

- location of the minimum safety clearance baseline relative to the coordinates of attachments points.

The origin of the coordinate system used does not matter as long as all points above are measured according to it. For the sake of simplicity, we recommend using as origin the first attachment point at the left of the configuration.

Figure 7.15 presents an example of how the required points are extracted and placed in the coordinate system used (here, the  $x,y$  system for, respectively, the horizontal and the vertical axis), and how the configuration is checked for the required clearances. This example is taken from Figure 3.2 with the difference that both attachment points are horizontal, rather than at an angle from the horizontal. This example shows a hypothetical configuration and demonstrates that the minimum safety clearance is just met, while it easily meets phase-to-ground clearances on both sides.

### **7.3.7 Verification of Stability**

#### **7.3.7.1 Introduction**

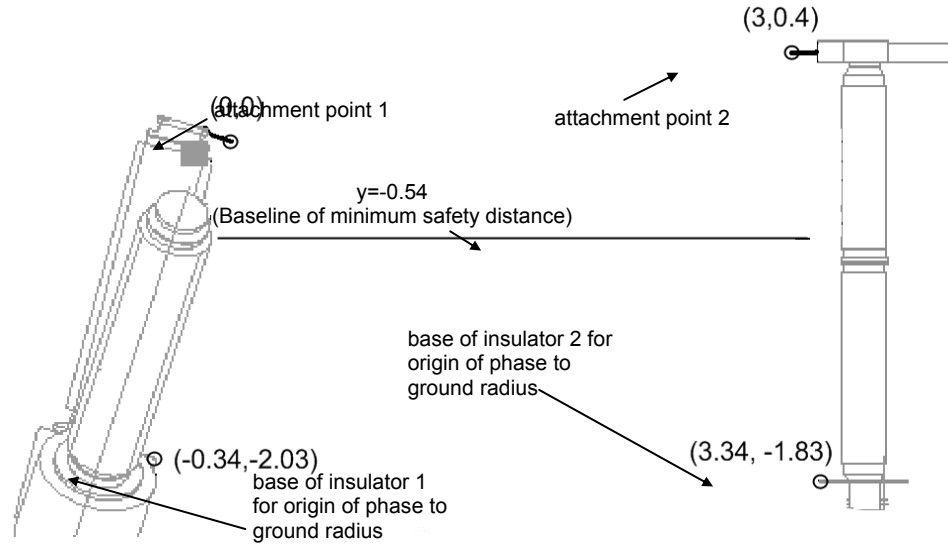
The stability of a configuration should be verified under two types of loads:

- under the self-weight of the conductor (normal operational load)
- under self-weight plus ice and wind design loads (extreme loads), as applicable

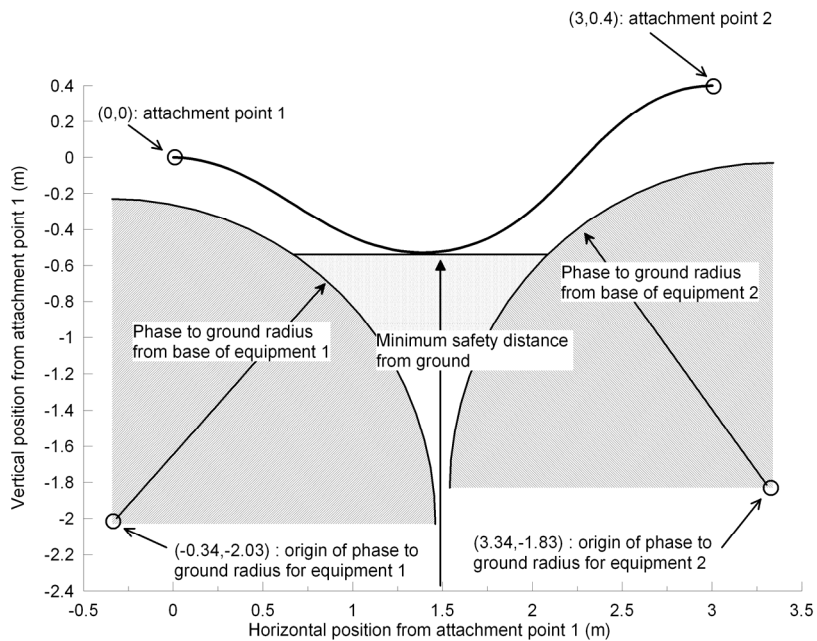
Under the first type of load, the check of stability generally serves to verify the maximum span that a given configuration can take while holding its assumed shape. For example, one should check the maximum span that an inverse parabola can take without collapsing under its own weight into a triple-curvature shape. Such verification is done while calculating the initial equilibrium position with the finite element method, as described above. If the obtained position does not correspond to the assumed shape, then it is probably a good indication that the span used is too long for this type of configuration.

The second type of load (ice and/or wind) may displace the configuration away from its equilibrium position. This may cause a violation of clearances previously met and/or deform a conductor permanently. The new position that a configuration may take under such loads can be calculated by supposing that these loads act in a static way, and by performing a finite element analysis from the calculated initial position under their application. However, because the calculation method presented earlier is limited to the assumption that the material behavior is

linear and perfectly elastic, it therefore does not permit predicting if the configuration will be deformed permanently. One may refine this analysis by modeling the nonlinear material behavior, but in the absence of tests to support the validity of such models, it is risky to use them to predict the permanent deformation in a conductor. Furthermore, due to the construction of conductors in layers, a precise model would have to take account of the behavior of each strand individually. The finite element method presented here should therefore be used to check the influence of such loads over the initially calculated equilibrium position. If the configuration displaces to such extent that concerns arise regarding the violation of clearances, testing such a configuration experimentally, as described in the next section, can verify if the conductor would then be permanently deformed. Also, since ice and wind load levels used for design occur generally with a long return period (e.g., 50 years), one should decide if a permanent deformation under such extreme events can be tolerated until the configuration is replaced. If this is the case, then the only concern that remains is that the configuration is stable under its normal operating conditions (i.e., it maintains its assumed shape). But effects from smaller and more frequent winds or ice loads are possible, and it is therefore essential to make sure that the conductor configuration meets the corresponding required criteria.



(a) Geometric points in the chosen coordinate system



(b) Plot of configuration in the coordinates system along with clearances

**Fig. 7.15 Geometric points required to check clearances**

### 7.3.7.2 Wind and Ice Load Determination and Their Introduction in the Calculation Process

Ice and wind loads correspond to uniform loads on a configuration in the same way as the self-weight of the conductor. The determination of these loads will be done in this guide according to IEEE Std 605-2008 (IEEE 2008); alternatively, ASCE Manual no. 113 may be used as well

(ASCE 2008). We will present here only the basic equations; the user is referred to IEEE Std-605-2008 or ASCE no. 113 for further information regarding the parameters used as input.

### Ice Load

For engineering design purposes, it is assumed that the conductor is covered with a uniform ice thickness. The ice weight on a circular conductor is given as

$$F_I = \pi w_I r_I (D_o + r_I) \quad (7.15)$$

where  $F_I$  is the weight of ice per unit length of the conductor (N/m) (lbf/in.),  $w_I$  is the weight density of ice (8820 N/m<sup>3</sup>) (0.0330 lbf/in.<sup>3</sup>),  $r_I$  is the equivalent uniform radial thickness of ice due to freezing rain (m) (in.), and  $D_o$  is the outside diameter of the conductor (m)(in.).

Note: multiply result in lbf/in. by 12 to get result in lbf/ft.

For sections other than circular, the ice weight is given as

$$F_I = w_I A_I \quad (7.16)$$

where  $A_I$  is the area covered by ice on the cross section considered (m<sup>2</sup>) (in.<sup>2</sup>).

The ice thickness used by the utility for transmission line design should be considered as the criterion for the ice loading on conductors between equipment. The thickness of ice will depend on the operator's standard; it could be 6.4 mm (1/4 in.) to 12.7 mm (1/2 in.) or higher depending on the winter conditions or the location of the installation, for it cannot be assumed that ice will not accumulate even with a conductor temperature above zero degrees Celsius. The only exceptions to this general rule of thumb are regions where the ambient temperature does not fall below zero degrees Celsius and regions that are too dry to prevent ice from forming.

Alternatively, the minimum ice thickness for the United States can be determined according to the 50-year mean recurrence interval uniform ice thickness due to freezing rain with concurrent 3-s gust wind speeds used in ASCE 7-05 (the corresponding maps are reproduced in IEEE-605-2008).

### Wind Loads

The maximum force due to wind may occur during extreme wind conditions with no ice or high wind conditions with ice. In general, the extreme wind conditions result in higher loads than the high wind conditions with ice. However, it is recommended to calculate wind loads with both

types of wind in order to evaluate the maximum scenario, as it might not always be the case depending on particular local conditions.

Factors that affect wind forces are the speed and gust of wind, the conductor size and shape, the height and exposure of the conductor, and the radial thickness of ice. Wind loads should be evaluated in the horizontal direction that produces the maximum load.

In the case of extreme wind speed (without ice), the wind load by unit length on a conductor is given as

$$F_w = CV^2 D_o C_f K_z G_f I \quad (7.17)$$

where  $F_w$  is the wind load by unit length (N/m) [lbf/ft],  $C$  is a constant (SI: 0.613, British:  $2.132 \times 10^{-4}$ ),  $V$  is the extreme wind speed without ice (m/s) (mi/h),  $D_o$  is the conductor outside diameter or the height of the profile used as conductor (m) (in.),  $C_f$  is the force coefficient,  $K_z$  is the height and exposure factor,  $G_f$  is the gust response factor, and  $I$  is the importance factor of the structure.

Note: the results in British units are directly in lbf/ft (divide result by 12 to get results in lbf/in.)

In the case of high wind with ice, the wind load by unit length on a conductor is given as

$$F_{wI} = CV_I^2 (D_o + 2 \times r_I) C_f K_z G_f I \quad (7.18)$$

where  $F_{wI}$  is the wind load with ice by unit length (N/m) [lbf/ft],  $V_I$  is the high wind speed with ice (m/s) [mi/h],  $r_I$  is the equivalent uniform radial thicknesses of ice due to freezing rain (m) (in.), and  $G_f$  is the gust response factor which is equal to 1.0 for ice and concurrent wind.

### **Introduction of These Loads in the Finite Element Model**

The ice and wind loads given above are loads by unit length. They may be applied as such in the finite element model if the program used allows the specification of uniform loading. Otherwise, they may be translated as point loads at each node of the model by obtaining the net load on the total length of conductor used and dividing it by the number of elements in the model.

For example, let's consider that the wind load by unit length calculated is 20 N/m, that the conductor length is 5 m, and that a total of 64 elements are used in the model. The corresponding point load at each node of the model is therefore  $20 \times 5 / 64 = 1.563$  N.

As for the application of the self-weight in the calculation of the equilibrium position, the application of wind and ice loads should be done *incrementally* in a given number of steps, since the calculation is nonlinear.

### 7.3.7.3 Example

#### Stability under Self-Weight

This first example corresponds to the verification of stability for an inverse parabola planned to be used for a span of 6 m; the selected span is purposely long in order to illustrate the instability of the configuration under its own weight. We suppose here that a 4000 kcmil conductor is used and that the two ends are at the same height.

First we need to determine the conductor properties required as input. The basic conductor properties are summarized in Table 7.4. Since the conductor is an aluminum conductor made of the same wires in all layers, a detailed description is not necessary and we therefore present only the necessary properties for the calculations.

**Table 7.4 Properties of the 4000 kcmil conductor**

layer	material	number of wires (total)	wire diameter (mm)	Young's modulus (GPa)	material density (kg/m <sup>3</sup> )
all	aluminum	270	3.09	69	2700

Using this data, we now determine the properties required as input for the finite element calculation.

- cross-sectional area [Eq. (7.6)], since the material is the same in all layers and strand diameter is constant)

$$A = n \cdot \pi \cdot \frac{\delta^2}{4} = 270 \cdot \pi \cdot \frac{3.09^2}{4} = 2025 \text{ mm}^2 = 2.025 \times 10^{-3} \text{ m}^2$$

- minimum bending moment of inertia [combining Eqs. (7.9) and (7.10), since the material is the same in all layers]

$$I_{\min} = \sum_{i=1}^n \pi \cdot \frac{\delta_i^4}{64} = 270 \cdot \pi \cdot \frac{3.09^4}{64} = 1208 \text{ mm}^4 = 1.208 \times 10^{-9} \text{ m}^4$$

- Young's modulus = 69 GPa = 6.9 x 10<sup>10</sup> Pa
- linear mass [using Eq. (7.12)]

$$\bar{m} = \rho \cdot A = 2700 \cdot 2.025 \times 10^{-3} = 5.467 \text{ kg / m}$$

- The required conductor length is evaluated using Equation (7.2):

$$L_{0\_parabola} = \frac{\pi \cdot H}{2} + V = \frac{\pi \cdot 6.0}{2} + 0 = 9.425 \text{ m}$$

To check if the configuration is holding its assumed shape under its own weight, we try to calculate its equilibrium position in three main steps using the *FEAP* software:

1. application of 2.5% of the final rotations ( $2.0^\circ$ ) in 100 increments;
2. simultaneous application of the horizontal displacement of 2.37 m, vertical displacement of  $-0.90$  m, and the remaining rotations ( $98\% = 88^\circ$ ) in 3900 increments;
3. application of the weight in 100 increments.

The path chosen here is similar to the one discussed above and recommended for the inverse parabola. The computational parameters are summarized in Table 7.5. The *FEAP* input is given in Appendix B.

**Table 7.5 Computational parameters for example of stability using *FEAP***

Parameter	Value or description
Starting position	Straight line of length 9.425 m
Number of elements	64
Number of increments to apply initially 2.5 % of rotations	100
Number of increments to apply horizontal displacement, vertical displacement and remaining of rotations	3900
Number of increments to apply weight of conductor	100 but the solution is unstable (see below)
Method used to reestablish equilibrium at each step	Newton-Raphson ( <i>tang</i> in <i>FEAP</i> )
Solution tolerance	$10^{-12}$

The weight of the conductor was not input directly as a uniform load but replaced by a downward force at each node, equivalent to the total weight of the conductor ( $5.470 \text{ kg/m} \times 9.81 \text{ m/s}^2 \times 9.425 \text{ m} = 505.8 \text{ N}$ ) divided by the number of elements:  $505.8 \text{ N} / 64 = 7.903 \text{ N}$ . This force was applied gradually.

The calculation of the equilibrium position led to the snap-through phenomena in calculation step 3, indicating that physically, the configuration would lose its assumed inverse parabola shape under its own weight. The first two calculation steps above (forming the shape of the parabola without the application of weight) led to the assumed shape; the result is presented in Figure 7.16 (clearly this is a half circle as assumed). However in the third step of gradually applying the conductor weight, the snap-through phenomenon took place, and then convergence problems related to the snap-through phenomenon occurred and it was not possible to converge to the final equilibrium position using the standard Newton-Raphson equilibrium method no

matter how much we refined the application of the load. A solution can be obtained from this shape by using a continuation method as discussed earlier, where the load is controlled such that the displacement increases in a stable way, without abrupt changes. To do so using *FEAP*, the equilibrium position obtained without weight was input as the starting position and the arc length method was used; the corresponding program input is also given in Appendix B. Figure 7.17 shows the relationship between the proportion of the weight applied (1 being equal to the total weight) and the downwards displacement at mid-span. It is observed that the structure softens as the load is applied and then becomes stiffer as the load increases again until the total weight is applied. The final configuration is presented in Figure 7.18; it is observed that clearly the obtained triple-curvature shape does not correspond to the desired parabola shape and that a violation of the minimum safety clearance would probably occur, as the sag is around 2.5 m. Therefore, the span chosen here of 6 m is definitively too long to install an inverse parabola.

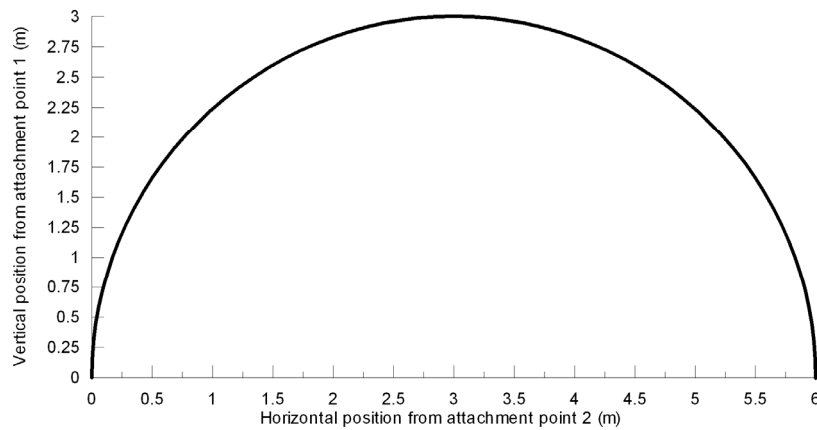


**Fig. 7.16** Calculated configuration without weight

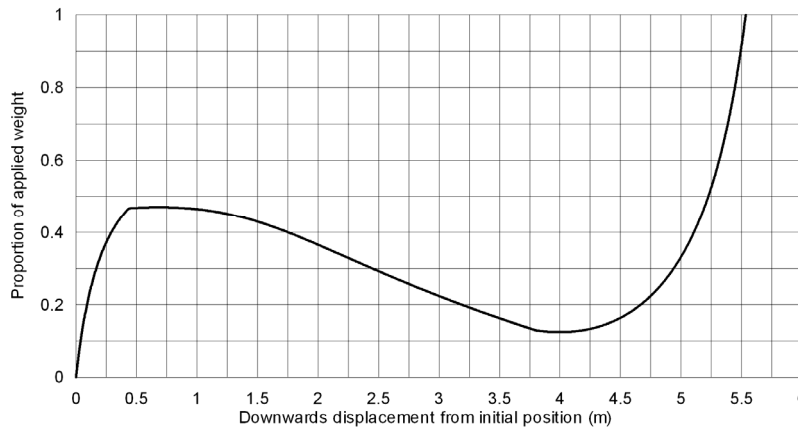


**Fig. 7.17** Load displacement curve using the arc length continuation method

## Stability under Wind and Ice Loads

The stability problems illustrated in the previous example could occur under the influence of wind and/or ice. Since the phenomenon and the solution to compute the final equilibrium position are similar, there is no need to present an example of instability under wind and/or ice. We will present later design examples where the stability under wind and ice is investigated.

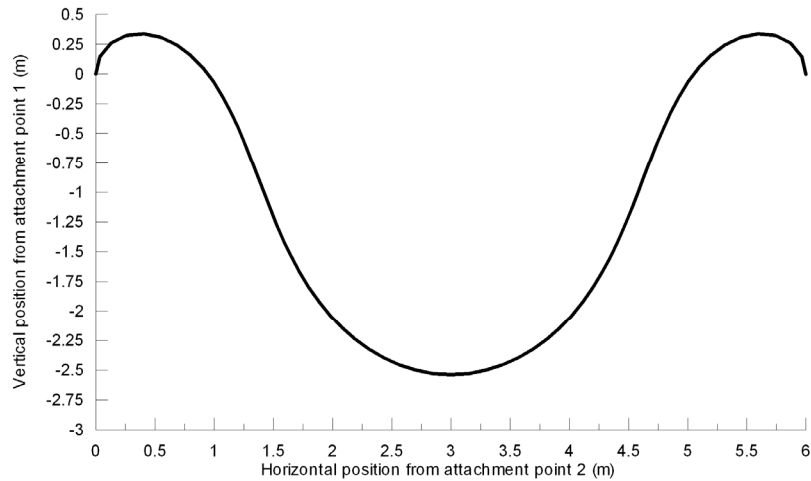


**Fig. 7.18** Calculated configuration with weight using the arc length method

### 7.3.8 Verification of Flexibility

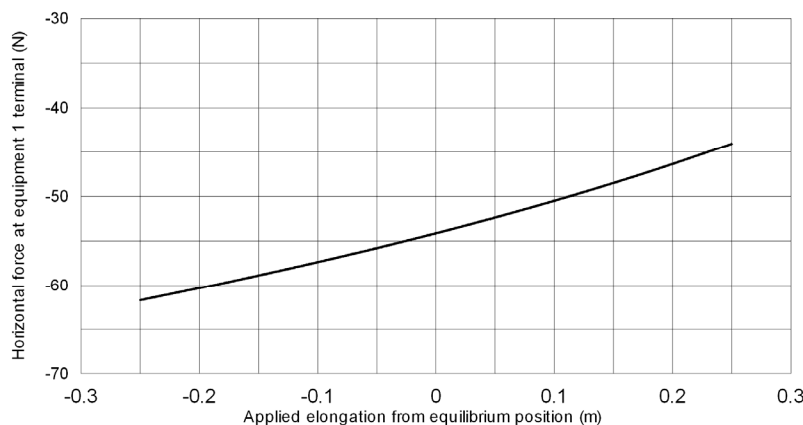
Once the equilibrium position is calculated, the flexibility of a configuration can be verified with the finite element model by applying a cyclic displacement at one end of the conductor, equal to the assumed elongation, and by obtaining the horizontal force at the displaced end during the process. The plot of the load-displacement data obtained permits checking the flexibility of the configuration. The flexibility is considered adequate when there is no significant or abrupt increase of force for a small increase of displacement over the elongation range considered. The flexibility of a configuration can be considered adequate for a given elongation range but not for another, as we discussed and exemplified in Section 7.2.3. Also, the actual value of the maximum force should be considered in relation to the acceptable forces at the terminals, as well as the terminal pad connection capacities, and by noting that the obtained forces are static forces, and therefore that the actual dynamic forces during a seismic event will most likely exceed those.

The load-displacement curve does not necessarily have to be linear over the full range of elongation to consider the flexibility adequate; what we want to avoid is a significant increase of force for a small increase of displacement. A monotonous increase of force will often be

observed with a more pronounced increase near the full positive elongation range, while the flexibility may still be considered adequate. At this time, there is no definite criterion or statute on the adequacy of the flexibility and one must somehow rely on judgment. As a general rule of thumb, the more linear the load-displacement curve, the better, and as discussed earlier, it is recommended that as much slack be added as permitted by the electrical clearances. If a significant increase of force is found over the elongation range considered, a solution is to increase the additional length  $L_2$  in Equation (7.1) [in some cases an additional provision could also be added for the inverse parabola length given by Eq. (7.2)]. Some examples are presented next.

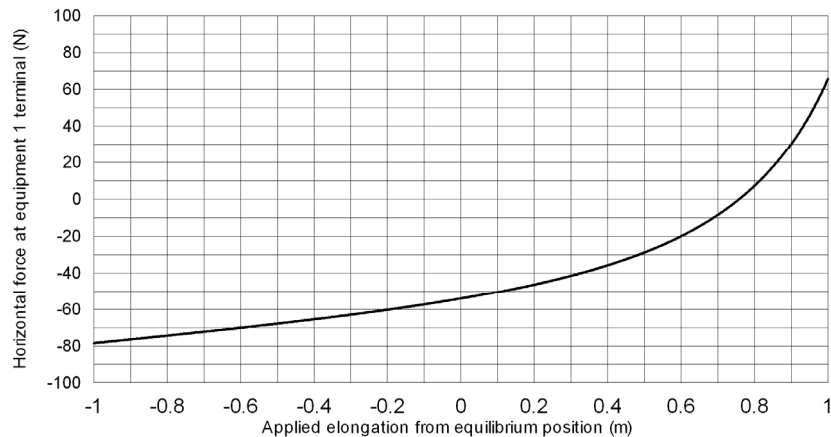
### 7.3.8.1 Finite Element Examples of Verification of the Flexibility

Figure 7.19 presents a load-displacement curve obtained for a cyclic displacement of 0.25 m applied on an inverse parabola of 3 m span, using a 4000 kmil conductor. The conductor length is calculated with Equation (7.2) and equals 4.712 m. It is observed from the figure that the behavior is almost linear and that there is no abrupt change of stiffness (the stiffness corresponds to the slope of the curve), so the flexibility of the configuration is considered adequate. The net increase of force over the full elongation range is from  $-62$  to  $-44$  N:  $+18$  N which is definitely negligible. Here the negative values of the force correspond to a configuration in a compressed state over the full range of elongation (i.e., the configuration “pushes” on the terminals instead of “pulling” them).



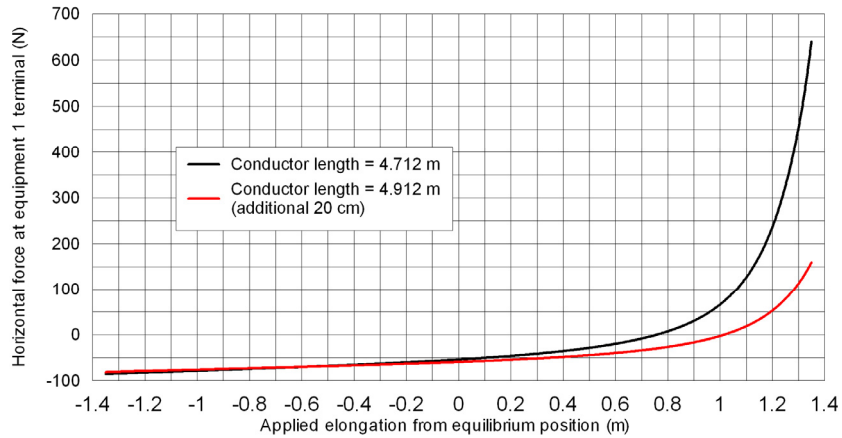
**Fig. 7.19 Load-displacement curve with 0.25 m cyclic displacement**

Figure 7.20 shows a load-displacement curve for the same configuration as above, but this time with a cyclic displacement of 1.0 m (four times the preceding). There is now a departure from linearity in the positive range of elongation. The net increase of force over the elongation range is around 150 N. Again, the flexibility here is considered more than adequate, as the net increase of force is small and there is no abrupt increase of the force even though the curve is clearly nonlinear.



**Fig. 7.20 Load-displacement curve with 1.0 m cyclic displacement**

We present in Figure 7.21 a load-displacement curve again for the same configuration, but this time with a cyclic displacement of 1.35 m. There is now a strong departure from linearity in the positive range of elongation. The net increase of force over the elongation range is around 750 N. The flexibility is not considered adequate here, as the net increase of force is too significant to be considered acceptable. Also, from the slope of the curve in the positive range of elongation, it can be deduced that any further small increase of elongation would lead to a very significant increase in force. A solution here to withstand the 1.35 m elongation range would be to add some additional length to the configuration. As an example, we added 20 cm of slack to the configuration used, for a net length now of 4.912 m, and then calculated the corresponding load-displacement curve as illustrated in red in the same figure. It is now observed that the net increase of force over the elongation range is around 230 N, a configuration considered having adequate flexibility.



**Fig. 7.21 Load-displacement curve with 1.35 m cyclic displacement**

## 7.4 VERIFICATION OF CLEARANCES, STABILITY, AND FLEXIBILITY EXPERIMENTALLY

Clearances, stability, and flexibility of a configuration can also be verified experimentally. The obvious advantage of doing so is to diminish the uncertainties associated with finite element modeling, such as the assumption that the material behavior of the conductor is linear, the minimum bending stiffness assumption, and the assumed “perfect” in-plane shape assumption. However, the main disadvantages are the need to prepare an experimental setup and the corresponding increased costs. Also, as with finite element modeling, some idealistic assumptions are still present in testing, notably the uniformity of ice and the constant pressure of wind.

### 7.4.1 Verification of Clearances

Clearances can be checked by installing a configuration between supports (or in-between existing equipment) and measuring the obtained geometry, and then checking the distances from the configuration to the phase-to-ground radii and the minimum safety distance in the same way as with the finite element results. A test setup as illustrated in Figure 7.9 could be used. An example of measured geometry is presented in Figure 7.22.

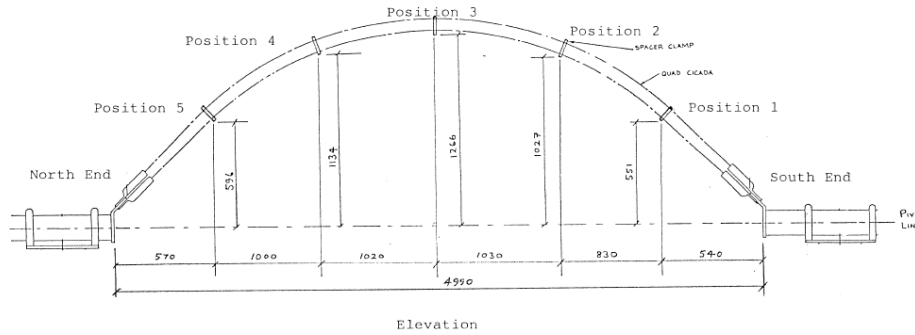


**Fig. 7.22 Measured geometry of a configuration under its self-weight (Stevenson and Beattie 1990)**

#### 7.4.2 Verification of Stability

Stability under self-weight will be immediately checked upon installation of the desired configuration on the test setup. Stability to ice can be checked by simulating experimentally the corresponding additional weight upon the installed configuration by various means. One way would be to attach small weights at uniformly spaced points, approximately every 0.25 m. Care must be taken that the attachment hardware used is not so rigid as to modify the bending stiffness of the conductor locally. The weights used would correspond to the discretized effect of the uniform weight upon the total length of the conductor (i.e., total load divided by number of points used). Another way would be to attach water-filled tubes to the configuration, dimensioned to reproduce the uniform load from ice; care must be taken that the stiffness of the tubes is not significant and that the tubes are attached so that they do not modify the stiffness of the conductor. An example is presented in Figure 7.23.



**Fig. 7.23 Experimental investigation of stability using water-filled tubes (Stevenson and Beattie 1990)**

Stability to wind load can be investigated in the same way as to ice, using either weights at points or water-filled tubes, with the difference of installing the configuration sideways; an example is presented in Figure 7.24. This method, however, does not permit testing for the simultaneous application of ice and wind.



**Fig. 7.24 Experimental investigation of stability to wind load using water-filled tubes (Stevenson and Beattie 1990)**

### 7.4.3 Verification of Flexibility

Verification of flexibility can be done experimentally by push-pull tests on the conductor and by recording the load-displacement curve. Usually, one end is fixed to a strong floor (or wall) and the other end is moved using an actuator. Attention must be given to minimizing the additional resistance from the test setup itself that might “contaminate” the measured load (e.g., the friction effect when one end is displaced on a roller). The next two figures present examples of actual setups used.

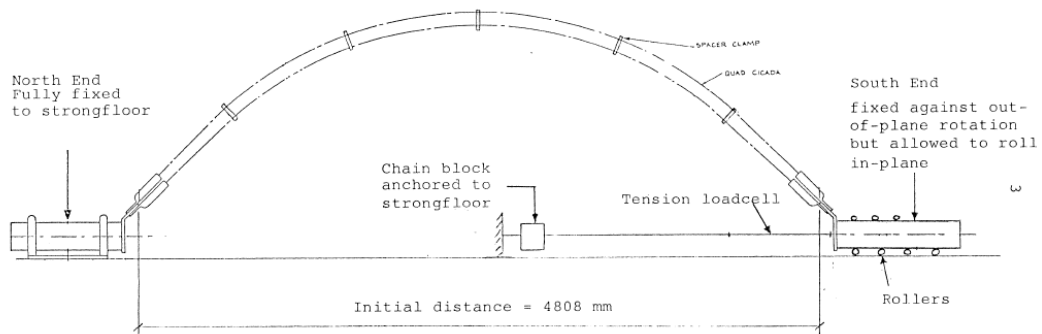


**Fig. 7.25 Schematic of experimental setup to investigate flexibility (Stevenson and Beattie 1990)**



**Fig. 7.26 Experimental setup to investigate flexibility (Bhuyan et al. 2001)**

## 7.5 FLEXIBLE CONNECTION DESIGN: EXAMPLE 1

A 230 kV disconnect switch—equipment 1—and a current-voltage transformer (CVT)—equipment 2, need to be connected by a 2300 kcmil flexible conductor. The general description of the equipment and the main dimensions of the setup are illustrated in Figure 7.27. The configuration must also withstand separately the effect of a given ice thickness and wind. The basic data of the example are given in Table 7.6. The seismic input is defined according to the IEEE 693 moderate performance level (0.5g) as per Figure 4.4.

**Table 7.6 Example 1: basic data**

Data		Description	Value
Basic connection geometry according to 0	$h_1$	Height of attachment point 1	6.471 m
	$h_2$	Height of attachment point 2	6.717 m
	L	Horizontal distance between attachment points	2.958 m
	H	Vertical distance between attachment points	0.246 m
Seismic input	-	Required response spectrum	IEEE 693 0.5 g (perf. level)
Extreme wind	V	Extreme wind speed (100 mph)	160 km/h (44.44 m/s)
	$D_o$	Conductor diameter for wind force calculation	4.445 cm (1.750 in.)
	-	Surface Roughness according to IEEE-605	C
	-	Height above ground for wind calculation	7.6 m (25 ft)
	$K_z$	Exposure factor according to IEEE-605 for surface roughness C and Height of 7.6 m	0.94
	$G_f$	Gust response factor according to IEEE-605 for wire and surface exposure C	0.95
	$C_f$	Force coefficient for cable (drag coefficient)	1.0
Ice thickness	I	Importance factor of structure for 2% annual probability of return and 50 year mean return period.	1.0
	$r_i$	radial ice thickness (1.772 ")	45 mm

We follow the flowchart illustrated in Figure 3.3, where certain steps are simultaneously considered for simplicity. The seismic input and basic connection geometry have already been described above, so the next step is the determination of the elongation demand.

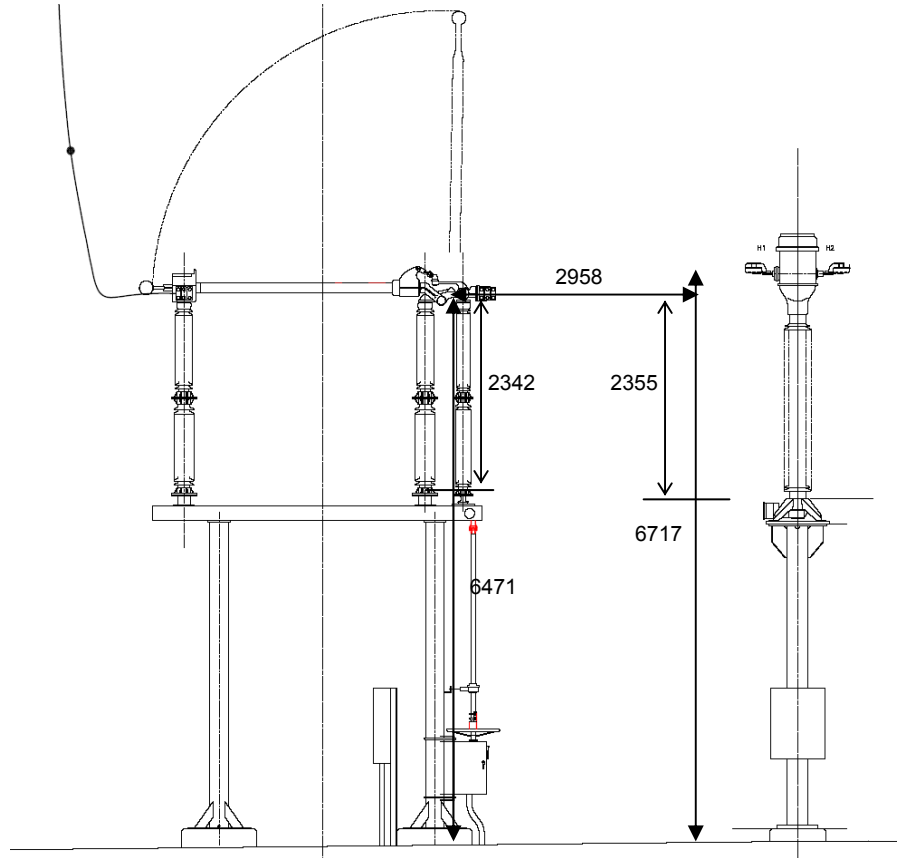


**Fig. 7.27 Example 1: general description and main dimensions (mm)**

### 7.5.1 Determination of Elongation Demand

To determine the elongation demand, we first obtain the dynamic properties of the equipment in order to determine their stand-alone displacements. In this case, the only available information from the seismic qualification reports is the fundamental frequency of each equipment item in the first bending mode (Fig. 6.3), in the longitudinal direction:

- disconnect switch in open position:  $f_1 = 2.2$  Hz
- CVT:  $f_2 = 1.8$  Hz

No information being available on the damping, we assume a critical damping ratio of 2% for both equipment items. This is a conservative value for substation equipment.

Both equipment items can be described by the generalized single-degree-of-freedom model, since they are beam and frame types. To determine their stand-alone displacements, we use Equation (6.9), since we have no information on their first modal participation factor:

$$x_{\max}|_{95\%} = 1.62 \cdot S_d(f, \zeta)$$

To determine the spectral displacement  $S_d(f, \zeta)$ , we first obtain the spectral acceleration from the IEEE moderate performance level (Fig. 4.4), which is equal to  $1.62g$  for both  $f_1=2.2$  Hz and  $f_2 = 1.8$  Hz (flat portion of the spectra—note that there is no relationship between the 1.62 factor above for  $x_{\max}$  and the  $1.62g$  from the IEEE spectrum). Using Equation (4.2), we then obtain

$$S_d(2.2\text{Hz}, 2\%) = \frac{S_a(2.2\text{Hz}, 2\%)}{(2 \cdot \pi \cdot f)^2} = \frac{1.62 \cdot 9.81}{(2 \cdot \pi \cdot 2.2)^2} = 0.0832\text{m}$$

$$S_d(1.8\text{Hz}, 2\%) = \frac{S_a(1.8\text{Hz}, 2\%)}{(2 \cdot \pi \cdot f)^2} = \frac{1.62 \cdot 9.81}{(2 \cdot \pi \cdot 1.8)^2} = 0.124\text{m}$$

Therefore, the stand-alone displacements are

$$x_{\max,1}|_{1.62} = 1.62 \cdot 0.0832 = 0.135\text{m}$$

$$x_{\max,1}|_{1.62} = 1.62 \cdot 0.124 = 0.201\text{m}$$

We establish the elongation demand  $e_o$  using the maximum differential displacement  $D_L$  in the longitudinal direction between the two equipment in Equation (6.3):

$$e_o \approx D_L$$

The maximum differential displacement is determined with the CQC rule [Eq. (6.14)] and the 1.25 factor recommended in Equation (6.16):

$$D_L = 1.25 \cdot \sqrt{x_{\max,1}^2 - 2 \cdot \rho_{12} \cdot x_{\max,1} \cdot x_{\max,2} + x_{\max,2}^2}$$

The correlation coefficient  $\rho_{12}$  is first obtained using  $r=f_1/f_2 = 2.2/1.8 = 1.222$ , as

$$\rho_{12} = \frac{8\zeta^2(1+r)r^{3/2}}{[(1-r^2)^2 + 4\zeta^2r(1+r)^2]} = \frac{8 \cdot 0.02^2(1+1.222) \cdot 1.222^{3/2}}{[(1-1.222^2)^2 + 4 \cdot 0.02^2 \cdot 1.222 \cdot (1+1.222)^2]} = 0.0378$$

Hence, the elongation demand is given by

$$e_o \approx 1.25 \cdot \sqrt{x_{\max,1}^2 - 2 \cdot \rho_{12} \cdot x_{\max,1} \cdot x_{\max,2} + x_{\max,2}^2} = 1.25 \cdot \sqrt{0.135^2 - 2 \cdot 0.0378 \cdot 0.135 \cdot 0.201 + 0.201^2} = 0.297\text{m}$$

## 7.5.2 Preliminary Shape

As a preliminary shape, we choose the flexible catenary configuration 3 from Figure 7.1 where both ends are attached at  $0^\circ$ .

## 7.5.3 Required Conductor Length

The required length is given by Equation (7.1):

$$L_0 = L_1 + e_o + L_2$$

$L_1$  is the straight-line distance between the two attachment points and is given by Equation (5.1):

$$L_1 = \sqrt{L^2 + H^2}$$

Using the data in Figure 7.27, we obtain

$$L_1 = \sqrt{L^2 + H^2} = \sqrt{2.958^2 + (6.717 - 6.471)^2} = 2.968 \text{ m}$$

Based on experience, we choose a tentative value of  $L_2$  equal to 0.05 m. We will later check to see if this value provides sufficient flexibility. Using the previous values, the required length is

$$L_0 = L_1 + e_o + L_2 = 2.968 + 0.297 + 0.05 = 3.315 \text{ m}$$

which we round up to 3.32 m.

## 7.5.4 Verification of Clearances, Flexibility, and Stability

We first check for the clearance requirements. If the configuration satisfies these requirements, we will then check the flexibility and the stability; otherwise, another configuration shape must be chosen.

### 7.5.4.1 Clearances

At the 230 kV level, the required clearances for the utility concerned are given by

- minimum safety distance: 5.600 m
- phase-to ground clearance: 1.942 m

To check these we will establish the equilibrium position of the configuration using the nonlinear finite element method with the *FEAP* software.

The basic properties of the 2300 kcmil conductor needed as input were calculated previously in Section 7.3.4 and are summarized in Table 7.3.

To check the clearances, we first compute the equilibrium position of the conductor under its own weight, using the procedure illustrated in Figure 7.12 and the *FEAP* software. The final position is calculated in three main steps:

1. application of weight in 100 increments on a straight-line configuration equal to the total conductor length of 3.32 m
2. application of a horizontal displacement of  $-0.362$  m to the right end support (left end fixed) to get the desired span of 2.958 m
3. application of a vertical displacement of  $+0.246$  m to the right end support to achieve the required vertical offset between the supports ( $6.717$  m  $-$   $6.471$  m  $=$   $0.246$  m)

The program input is given in Appendix B and the computational parameters are summarized in Table 7.7.

**Table 7.7 Computational parameters for example 1 using *FEAP* software**

Parameter	Value or description
Starting position	Straight line of length 3.32 m
Number of elements	64
Number of increments to apply weight of conductor	100
Number of increments to apply horizontal displacement	2000
Number of increments to apply vertical displacement	500
Method used to reestablish equilibrium at each step	Newton-Raphson ( <i>tang</i> in <i>FEAP</i> )
Solution tolerance	$10^{-8}$

Note that in the simulation, the weight of the conductor was not input directly but replaced by an equivalent downward force at each node equivalent to the total weight of the conductor ( $3.155$  kg/m  $\times$   $9.81$  m/s<sup>2</sup>  $\times$   $3.32$  m  $=$   $102.8$  N) divided by the number of elements:  $102.8$  N /  $64 = 1.606$  N. This force was applied gradually in the first step discussed above.

Once the calculation is done, the clearances are checked graphically by plotting the obtained equilibrium position against the phase to ground radius from the base of each equipment item and the minimum safety clearance (the position of each node of the conductor model under its equilibrium position must be extracted from the output of the computer program used). Here, the base position of the phase to ground radius for each equipment item has been assumed to be 30 cm away in the horizontal direction from the attachment point. Vertically, the base position is the bottom position of the porcelain part of each insulator. This is illustrated in Figure 7.28 where the (0,0) reference position is assumed to be the attachment point of the

disconnect switch. It is observed that both clearances are satisfied, so the configuration is adequate from this standpoint.

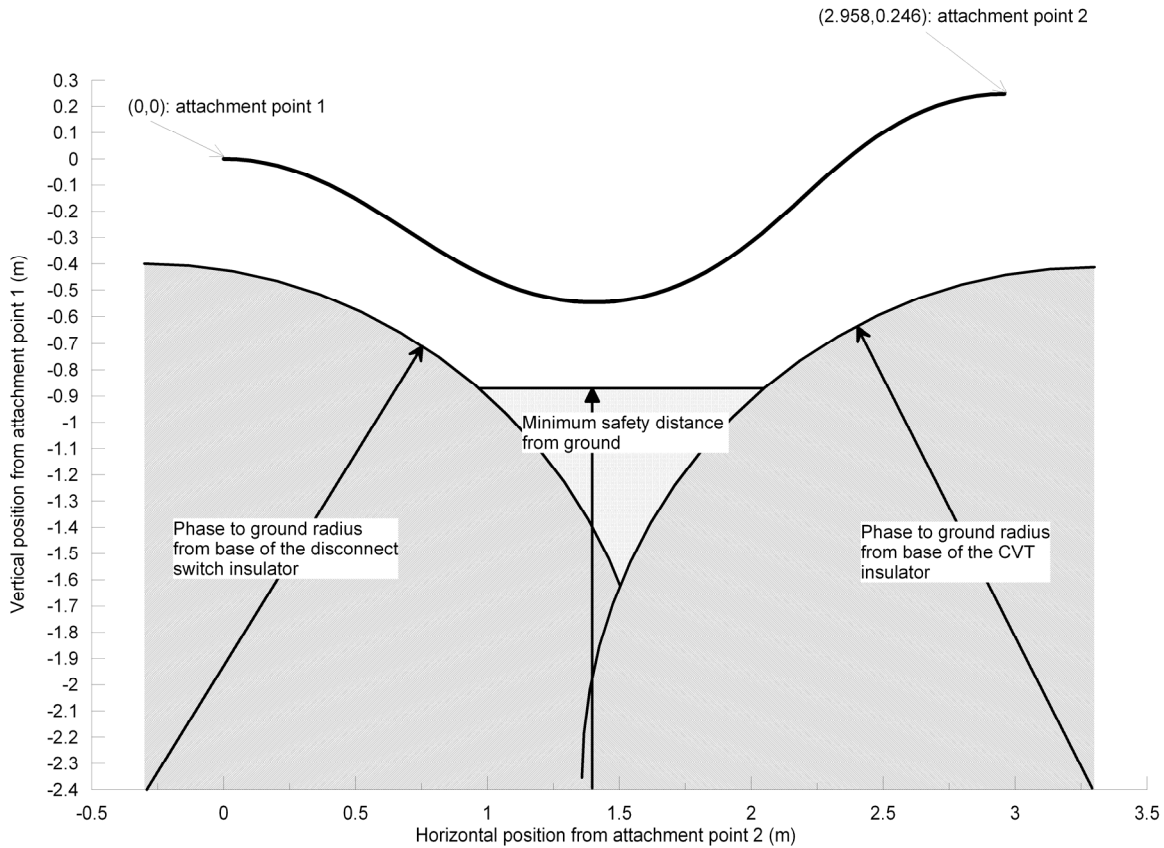


**Fig. 7.28 Verification of clearances for example 1**

#### 7.5.4.2 Flexibility

As discussed, the required flexibility must be such that the force-elongation behavior of the conductor under the elongation demand remains approximately linear without an abrupt change of stiffness. To check that, we use the same finite element model as above, and starting from the computed equilibrium position, apply a cyclic displacement in a quasi-static fashion (without dynamic effects) equal to the elongation demand of 0.297 m identified earlier. To do so, one end of the conductor is kept fixed in the simulation while the other is moved back and forth with an amplitude equal to the elongation demand. The program input is given in Appendix B.

The resulting force-elongation curve is given in Figure 7.29. It is observed that the curve is nearly linear without abrupt change of stiffness, so the configuration is adequately flexible. The negative sign of the forces here indicates that the configuration is in compression on the elongation range considered; this is normal and due to the bending stiffness of the conductor.

Therefore, the configuration here applies a pushing force at both terminal ends in its installed position.

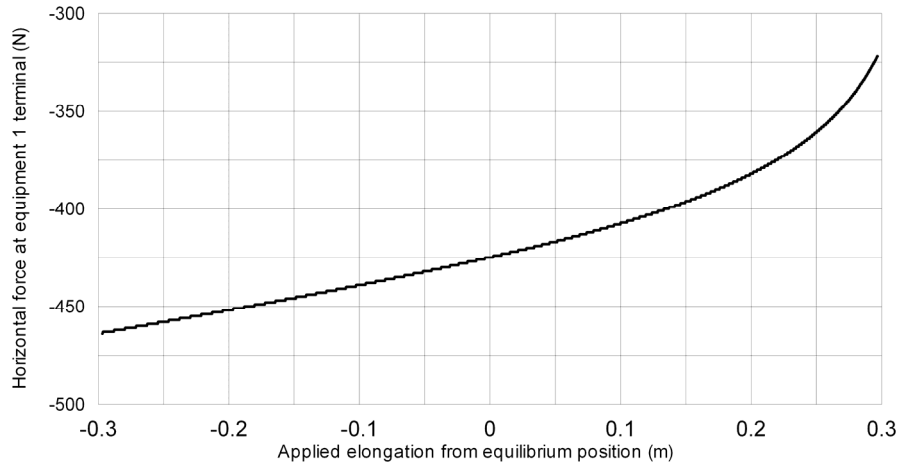


**Fig. 7.29 Force-elongation curve for example 1 at equipment terminals**

#### 7.5.4.3 Stability

It is necessary to check that the considered configuration will not collapse due to the effects of ice and wind, and that it will maintain its clearances under these effects. The climatic loads to consider in this example are the separate effects of 45 mm of ice around the conductor and a wind of 160 km/h. According to IEEE-605-2008, these loads are considered static (without dynamic effects).

The effect of ice is to add an additional uniform downward load on the conductor, equal to the weight of ice around the conductor. Using Equation (7.15), the additional weight by unit length on the conductor is

$$F_I = \pi w_I r_I (D_o + r_I) = \pi \cdot 8820 \cdot 0.045 \cdot (0.0445 + 0.045) = 111.6 \text{ N/m}$$

To calculate the final shape of the conductor with the additional weight of ice, we follow the same procedure as for calculating the equilibrium position, changing only the forces applied downward at all nodes to take account of the additional ice weight. Since we have 64 elements, the additional force applied at each node is equal to the ice unit weight times the conductor length divided by the number of elements:  $111.6 \text{ N/m} \times 3.32 \text{ m} / 64 = 5.789 \text{ N}$ . This force is added to the one simulating the weight of the conductor alone, for a total of 7.395 N at each node, downwards. The program input is given in Appendix B.

The result is shown in Figure 7.30, where the initial equilibrium position without ice is also plotted. It is observed that the configuration is only slightly deformed by the additional ice weight and it is then obvious that the clearances are still satisfied as needed.

The effect of wind on the conductor is to generate a uniform lateral load. Using Equation (7.17) and the values from Table 7.6 we obtain

$$F_w = CV^2 D_o C_f K_z G_f I = 0.613 \cdot 44.44^2 \cdot 0.0445 \cdot 1.0 \cdot 0.94 \cdot 0.95 \cdot 1 = 48.11 \text{ N/m}$$

The lateral displacements and the deformed position are again obtained from the finite element simulation, starting from the initial position calculated without ice. The wind force by unit length is replaced at each node by an equivalent point load, equal to the total force applied on the conductor divided by the number of elements. In the case here, the total force is given by  $48.11 \text{ N/m} \times 3.32 \text{ m} = 159.7 \text{ N}$  and, therefore, the nodal load is  $159.7 / 64 = 2.496 \text{ N}$ . This load is applied using 100 increments. The program input is given in Appendix B.

The corresponding maximum lateral displacement is 0.559 m and the final equilibrium position under the wind is illustrated in Figure 7.31. It is observed that even though the lateral displacement is significant, it should not compromise the phase-to-phase clearance, as other phases would experience a similar displacement under the same wind and time.

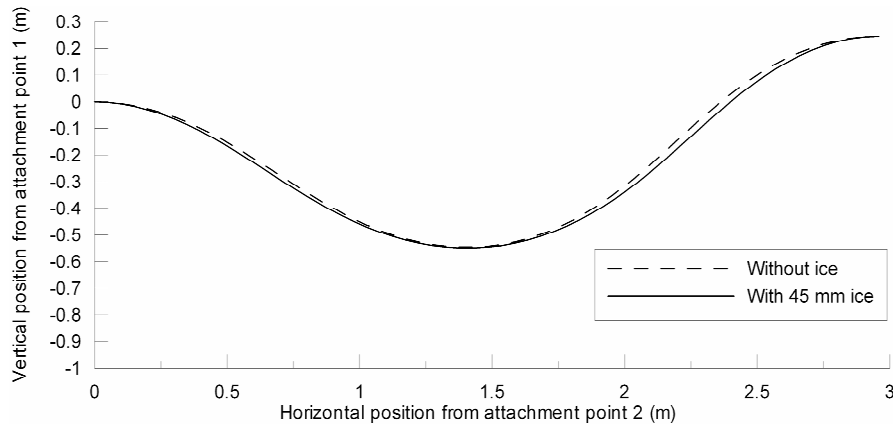


**Fig. 7.30** Equilibrium position for example 1 under 45 mm of radial ice

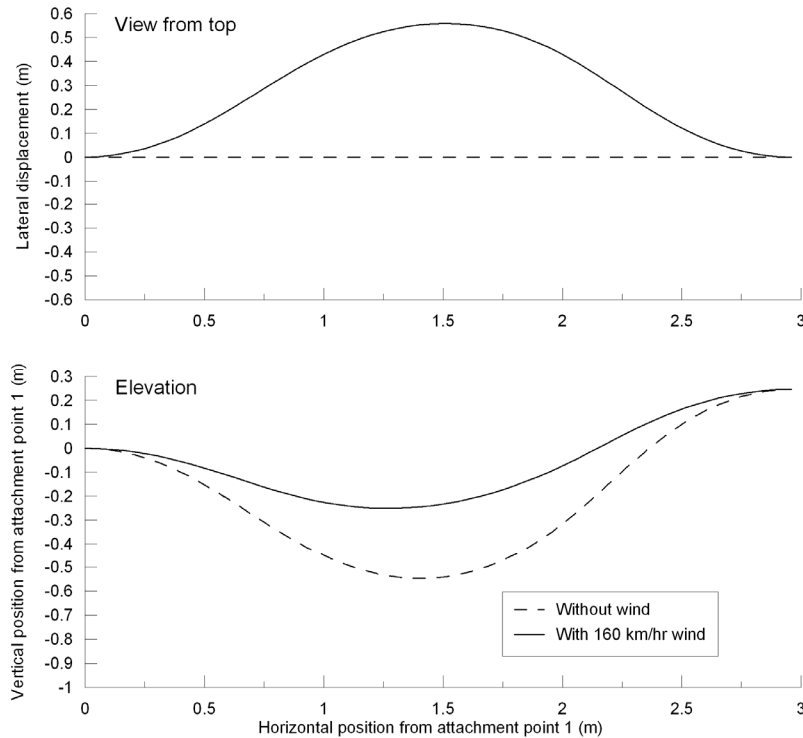


**Fig. 7.31 Equilibrium position for example 1 with 160 km/hr wind**

#### 7.5.4.4 Conclusion of Example 1

The tentative catenary shape meets all requirements and is therefore accepted as final design.

## 7.6 FLEXIBLE CONNECTION DESIGN: EXAMPLE 2

A 330 kV rigid bus—equipment 1—and a circuit breaker—equipment 2—need to be connected by a 4000 kcmil flexible conductor. A schematic description of the equipment and main dimensions are illustrated in Figure 7.32. The configuration must also withstand separately the effect of wind (no effect of ice is present). The basic data for the example are given in Table 7.8. The seismic input is defined according to the IEEE 693 moderate performance level (0.5g) as per Figure 4.4.

We will follow the flowchart illustrated in Figure 3.3. As for the previous example, certain steps will be considered at the same time for simplicity. The seismic input and basic connection geometry have already been described above, so the next step is the determination of the elongation demand.

### 7.6.1 Determination of Elongation Demand

To determine the elongation demand, we first obtain the dynamic properties of the equipment in order to determine their stand-alone displacements. Here, the fundamental frequencies of the two equipment items in their first bending mode (Fig. 6.3), in the longitudinal direction, have been obtained from finite element models as

- rigid bus:  $f_1 = 4.33$  Hz
- circuit breaker:  $f_2 = 0.80$  Hz

We assume a critical damping ratio of 2% for both equipment items.

**Table 7.8 Example 2: basic data**

Data		Description	Value
Basic connection geometry according to Figure 5.1	$h_1$	Height of attachment point 1	7.000 m
	$h_2$	Height of attachment point 2	6.910 m
	L	Horizontal distance between attachment points	4.000 m
	H	Vertical distance between attachment points	-0.090 m
Seismic input	-	Required response spectrum	IEEE 693 0.5 g performance level
Extreme wind	V	Extreme wind speed (56.25 mph)	90 km/h (25.0 m/s)
	$D_o$	Conductor diameter for wind force calculation	5.863 cm (2.308 in.)
	-	Surface Roughness according to IEEE-605	C
		Height above ground for wind calculation	approximated to 7.6 m (25 ft) to use given values in IEEE-605
	$K_z$	Exposure factor according to IEEE-605 for surface roughness C and Height of 7.6 m	0.94
	$G_f$	Gust response factor according to IEEE-605 for wire and surface exposure C	0.95
	$C_f$	Force coefficient for cable (drag coefficient)	1.0
	I	Importance factor of structure for 2% annual probability of return and 50 year mean return period.	1.0
Ice thickness	$r_i$	radial ice thickness	0

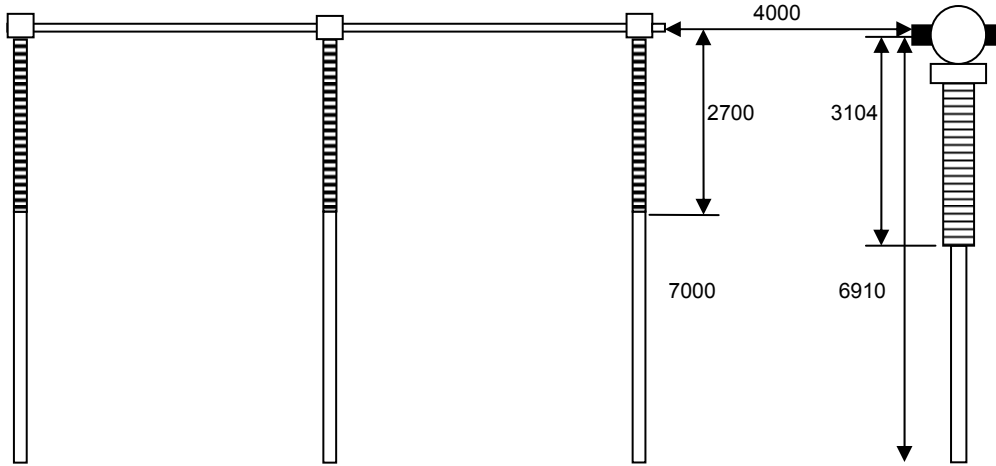


**Fig. 7.32 Example 2 general description and main dimensions (mm)**

The stand-alone displacements of the two equipment items are obtained using the IEEE 0.5 g performance level at 2% damping as input to the finite element models:

$$x_{\max,1} = 0.035 \text{ m}$$

$$x_{\max,2} = 0.598 \text{ m}$$

We establish the elongation demand  $e_o$  using the maximum longitudinal displacement  $D_L$  between the two equipment [Eq. (6.3)]:

$$e_o \approx D_L$$

Since the frequencies are spaced by more than 20% relative to each other, the SRSS summation method is used to determine the expected differential longitudinal displacement using Equation (6.16):

$$D_L = 1.25 \cdot \sqrt{x_{\max,1}^2 + x_{\max,2}^2}$$

Hence, the elongation demand is given by

$$e_o \approx 1.25 \cdot \sqrt{x_{\max,1}^2 + x_{\max,2}^2} = 1.25 \cdot \sqrt{0.035^2 + 0.598^2} = 0.748 \text{ m}$$

We observe that the elongation demand is rather high. This is because the frequency of equipment 2 is very low, at 0.8 Hz, and because the IEEE response spectrum has significant energy in the low-frequency range.

### 7.6.2 Preliminary Shape: Trial 1

As a preliminary shape, we choose the flexible catenary configuration 3 from Figure 7.1, where both ends are attached at  $0^\circ$ , since this is the most simple and common shape.

### 7.6.3 Required Conductor Length: Trial 1

The required length is given by Equation (7.1):

$$L_0 = L_1 + e_o + L_2$$

$L_1$  is the straight-line distance between the two attachment points and is given by Equation (5.1):

$$L_1 = \sqrt{L^2 + H^2}$$

Using the data from Figure 7.32, we obtain

$$L_1 = \sqrt{L^2 + H^2} = \sqrt{4.000^2 + (7.000 - 6.910)^2} = 4.001 \text{ m}$$

Based on experience, we choose a tentative value of  $L_2$  equal to 0.05 m. We will later check to see if this value provides sufficient flexibility if the configuration is found to meet the electrical clearance requirements.

Therefore, using the previous values, the required length is

$$L_0 = L_1 + e_o + L_2 = 4.001 + 0.748 + 0.05 = 4.799 \text{ m}$$

which we round up to 4.80 m.

### 7.6.4 Verification of Clearances, Flexibility, and Stability: Trial 1

We first check to see if the clearance requirements are satisfied. If the configuration meets these requirements, we will then check the flexibility and the stability; otherwise, we will have to choose another shape.

#### 7.6.4.1 Clearances

At the 330 kV level, the required clearances for the utility concerned are given by

- minimum safety distance: 6.400 m
- phase-to ground clearance: 2.401 m

To check if the configuration can satisfy these clearances, we establish the equilibrium position using the *FEAP* software as in example 1, using the properties for the 4000 kcmil conductor determined in Section 7.3.7.3. To check the clearances, we first compute the equilibrium position of the conductor under its own weight, using the procedure illustrated in Figure 7.12. The final position is calculated in three main steps:

1. application of the weight in 100 increments on a straight horizontal line configuration equal to the total conductor length of 4.80 m
2. application of the horizontal displacement of  $-0.800$  m in 4000 increments to the right end support (left end is fixed) to get the desired span of 4.000 m
3. application of the vertical displacement of  $-0.090$  m in 500 increments to the right end support to achieve the specified vertical offset between supports

The program input is given in Appendix B and the computational parameters are summarized in Table 7.9.

**Table 7.9 Computational parameters for example 2 using *FEAP* software, trial 1**

Parameter	Value or description
Starting position	Straight line of length 4.800 m
Number of elements	64
Number of increments to apply weight of conductor	100
Number of increments to apply horizontal displacement	4000
Number of increments to apply vertical displacement	500
Method used to reestablish equilibrium at each step	Newton-Raphson ( <i>tang</i> in <i>FEAP</i> )
Solution tolerance	$10^{-8}$

Note that in the simulation, the weight of the conductor was not input directly but replaced by an equivalent downward force at each node equivalent to the total weight of the conductor ( $5.470 \text{ kg/m} \times 9.81 \text{ m/s}^2 \times 4.80 \text{ m} = 257.6 \text{ N}$ ) divided by the number of elements:  $257.6 \text{ N} / 64 = 4.025 \text{ N}$ . This force was applied gradually in the first step discussed above.

Once the calculation is done, we check the clearances graphically by plotting the obtained equilibrium position against the phase to ground radius from the base of each equipment item and the minimum safety clearance. Here, the base position of the phase to ground radius has been assumed to be 30 cm away in the horizontal direction from the attachment point for the rigid bus and 45 cm away for the circuit breaker. Vertically, the base position for the origin of the phase to ground radius is the bottom position of the porcelain part of each insulator (top of steel support). This is illustrated in Figure 7.33 where the (0,0) reference position is taken to be the attachment

point of the rigid bus. It is observed that both clearances are violated, so the configuration is not adequate from this standpoint; we therefore need to select a new shape to meet the clearances.

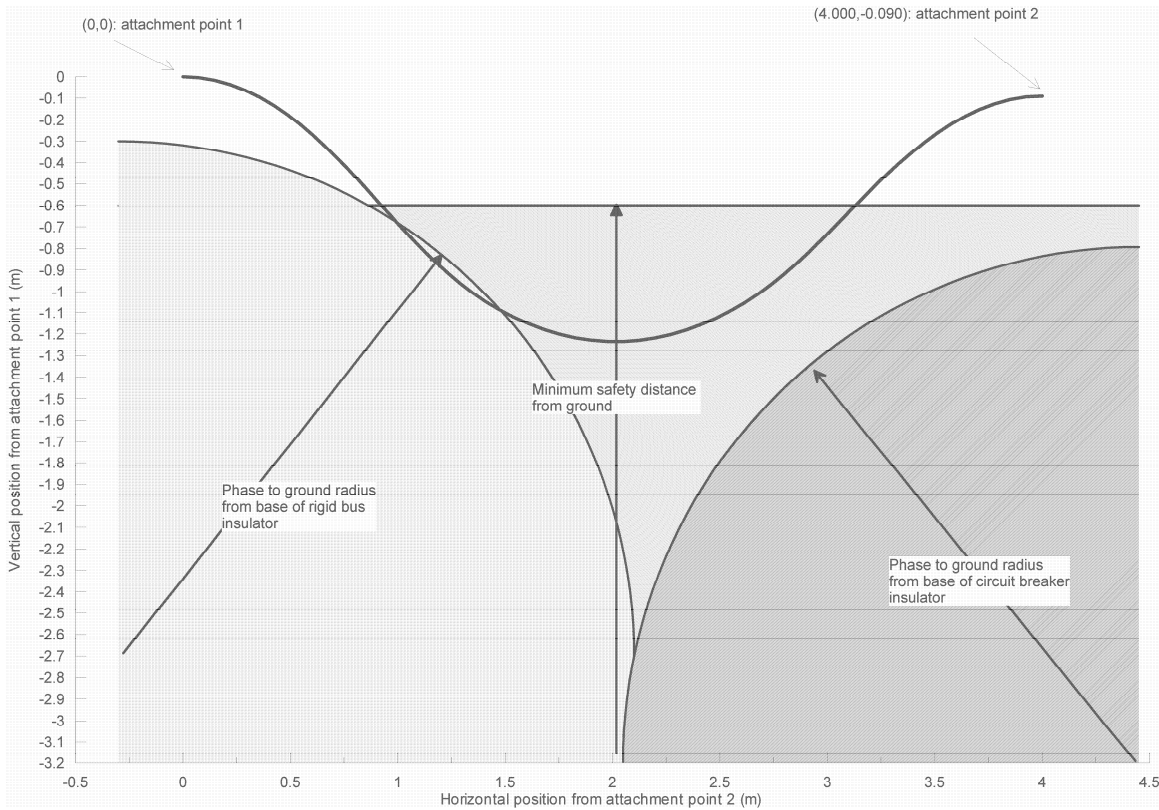


**Fig. 7.33 Verification of clearances for example 2, trial 1**

### 7.6.5 Preliminary Shape: Trial 2

As a second trial, we choose the triple-curvature configuration 4 from Figure 7.1, where both ends are attached at  $45^\circ$ . This configuration will move the conductor away from the phase to ground radius from the base of the rigid bus insulator, and will also diminish the sag so that it may satisfy the minimum safety clearance as well.

### 7.6.6 Required Conductor Length: Trial 2

The required length is given by Equation (7.1):

$$L_0 = L_1 + e_o + L_2$$

Based on experience with the triple-curvature shape, we choose a tentative value of  $L_2$  equal to 0.15 m; we will later check if this value provides sufficient flexibility.

Using the previous values, the required length is therefore:

$$L_0 = L_1 + e_o + L_2 = 4.001 + 0.748 + 0.15 = 4.899 \text{ m}$$

which we round up to  $4.90 \text{ m}$ .

### 7.6.7 Verification of Clearances, Flexibility, and Stability: Trial 2

As before, we will first check the clearance requirements; if they are met, we will then check the flexibility and the stability of the configuration; otherwise we will have to choose another..

#### 7.6.7.1 Clearances

We begin again by first computing the equilibrium position of the conductor under its own weight, using the procedure illustrated in Figure 7.12. The final position is now calculated in four main steps:

1. application of weight in 100 increments on a straight-line configuration equal to the total conductor length of 4.90 m
2. application of the horizontal displacement of  $-0.900 \text{ m}$  in 4000 increments to the right end support (left end is fixed) to get the desired span of 4.000 m
3. application of the vertical displacement of  $-0.090 \text{ m}$  in 500 increments to the right end support to get the vertical offset between the supports
4. application of the  $45^\circ$  rotations in 4000 increments to the right and left supports

The program input is given in Appendix B and the computational parameters are summarized in Table 7.10. Note here that a finer tolerance of  $1 \cdot 10^{-12}$  was required for the problem to converge under the application of the rotations; a tolerance of  $1 \cdot 10^{-8}$  used first did not lead to convergence.

**Table 7.10 Computational parameters for example 2 using *FEAP* software, trial 2**

Parameter	Value or description
Starting position	Straight line of length 4.900 m
Number of elements	64
Number of increments to apply weight of conductor	100
Number of increments to apply horizontal displacement	4000
Number of increments to apply vertical displacement	500
Number of increments to apply rotations	4000
Method used to reestablish equilibrium at each step	Newton-Raphson ( <i>tang</i> in <i>FEAP</i> )
Solution tolerance	$10^{-12}$

As before, the weight of the conductor was not input directly but replaced by an equivalent downward force at each node equivalent to the total weight of the conductor ( $5.470 \text{ kg/m} \times 9.81 \text{ m/s}^2 \times 4.90 \text{ m} = 262.9 \text{ N}$ ) divided by the number of elements:  $262.9 \text{ N} / 64 = 4.108 \text{ N}$ . This force was applied gradually in the first step discussed above.

As previously, we check the clearances graphically by plotting the equilibrium position, as illustrated in Figure 7.34. It is observed that the phase to ground clearance is now easily met, but the minimum safety distance is still violated, so the configuration is not adequate and we need to choose another shape.

### 7.6.8 Preliminary Shape: Trial 3

The only remaining choice is the inverse parabola shape, configuration 1 in Figure 7.1, where both ends are attached at  $90^\circ$ .

### 7.6.9 Required Conductor Length: Trial 3

The required length for the inverse parabola shape is given by Equation (7.2):

$$L_{0\_parabola} = \frac{\pi \cdot H}{2} + V$$

Using the values here for  $H$  and  $V$ , the required length is

$$L_{0\_parabola} = \frac{\pi \cdot H}{2} + V = \frac{\pi \cdot 4.000}{2} + 0.090 = 6.373$$

which we round up to  $6.37 \text{ m}$ .

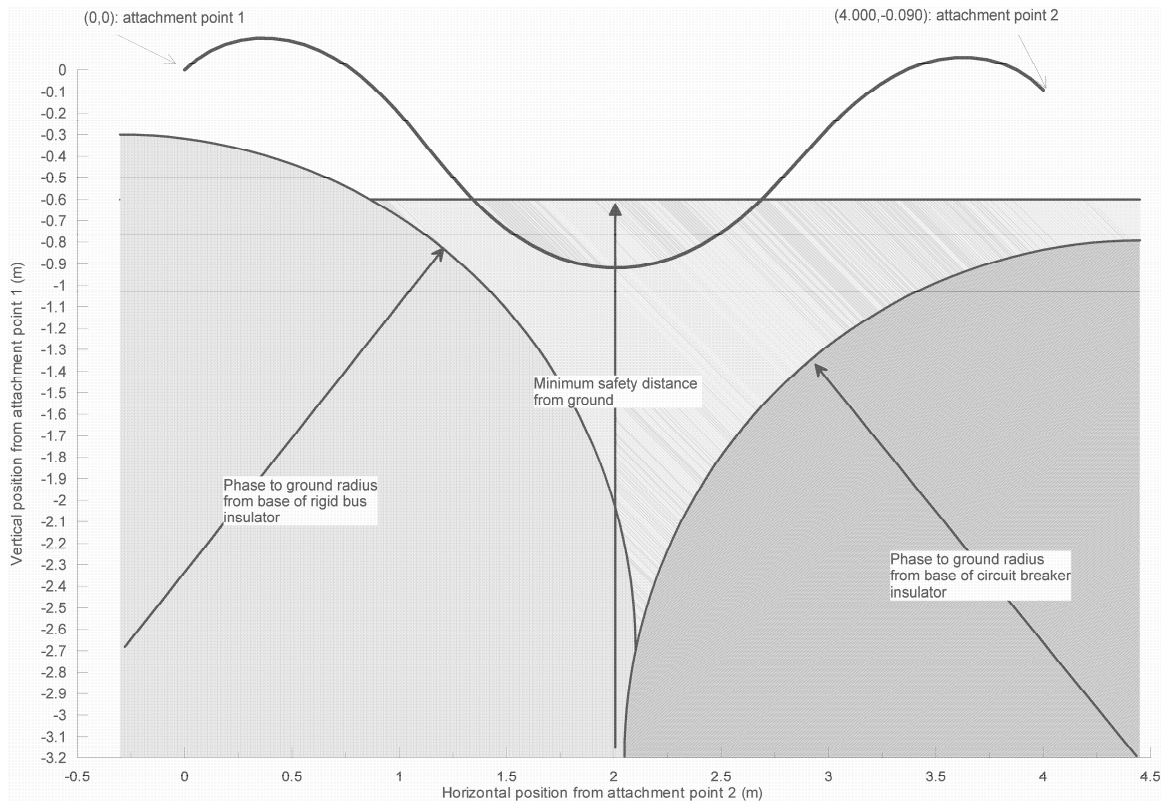


**Fig. 7.34 Verification of clearances for example 2, trial 2**

### 7.6.10 Verification of Clearances, Flexibility, and Stability: Trial 3

The inverse parabola will automatically meet all clearances as long as it is stable under its own weight. We will calculate the equilibrium position to illustrate it from the standpoint of clearances.

#### 7.6.10.1 Clearances

As before, we first compute the equilibrium position of the conductor under its own weight, using the procedure illustrated in Figure 7.12. The final position is now calculated in three main steps:

1. application of 2.5% of final rotations ( $2.0^\circ$ ) in 100 increments
2. simultaneous application of the horizontal displacement of 2.37 m, vertical displacement of -0.90 m, and the remaining rotations ( $98\% = 88^\circ$ ) in 3900 increments
3. application of the weight in 1000 increments

The first step consisting of applying a small portion of the rotations alone is to condition the conductor in moving as an inverse parabola before applying a horizontal displacement; indeed, the small rotations induce a moment that will move the conductor upward when we next apply the horizontal displacement along with the remaining rotations and the vertical displacement. If this step is omitted, then numerical convergence problems occur, probably because the conductor is stiff in the longitudinal direction. The upward conditioning here using the small rotations at both ends is similar to first applying the weight for the catenary shape before moving one end horizontally: the weight conditions the conductor to move downwards. Other paths also might have worked here. Note that this procedure corresponds physically to first forming the configuration in a flat plane parallel to the ground and then turning it in a vertical plane to install it; the weight is then applied after the configuration is first placed into shape.

The program input is given in Appendix B and the computational parameters are summarized in Table 7.11. Note here again that a finer tolerance of  $1 \cdot 10^{-12}$  was required for the problem to converge under the application of the rotations.

**Table 7.11 Computational parameters for example 2 using *FEAP* software, trial 3**

Parameter	Value or description
Starting position	Straight line of length 6.370 m
Number of elements	64
Number of increments to apply initially 5% of rotations	100
Number of increments to apply horizontal displacement, vertical displacement and remaining of rotations	3900
Number of increments to apply weight of conductor	100
Method used to reestablish equilibrium at each step	Newton-Raphson ( <i>tang</i> in <i>FEAP</i> )
Solution tolerance	$10^{-12}$

As before, the weight of the conductor was not input directly but replaced by an equivalent downward force at each node, equivalent to the total weight of the conductor divided by the number of elements.

The equilibrium position is illustrated in Figure 7.35. It is observed that all clearances are met as expected, and that the configuration is stable under its own weight.

### 7.6.10.2 Flexibility

To check the flexibility, we use the same finite element model, applying a cyclic displacement from the equilibrium position in a quasi-static fashion (without dynamic effects), equal to the elongation demand identified earlier to be 0.748 m. To do so, one end of the conductor is kept

fixed while the other end is moved back and forth by an amplitude equal to the elongation demand, similar to a push-pull test. The program input is given in Appendix B.

The force-elongation curve is presented in Figure 7.36. It is observed that the curve is close to being linear, without abrupt change of stiffness, so the configuration is adequate from the standpoint of flexibility. This was expected, as the inverse parabola is very flexible, and since we use only a small value of the available slack (low value of  $\beta=0.748/(6.37-4.00)=0.32$ ). The negative sign of the force here indicates that the configuration is in compression on the elongation range considered; this is normal and due to the bending stiffness of the conductor. Therefore, the configuration here applies a pushing force at both terminal ends in its installed position during the whole range of motion.

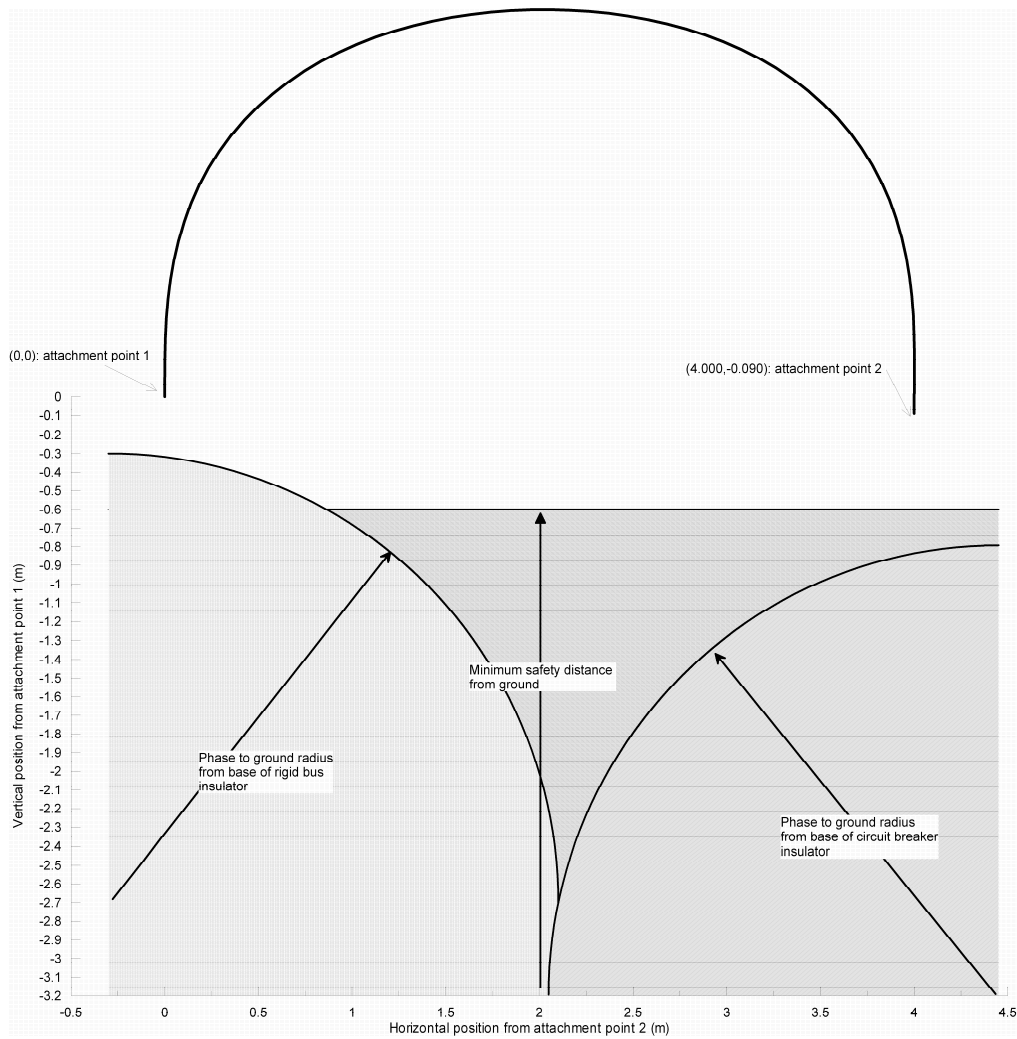


**Fig. 7.35 Verification of clearances for example 2, trial 3**

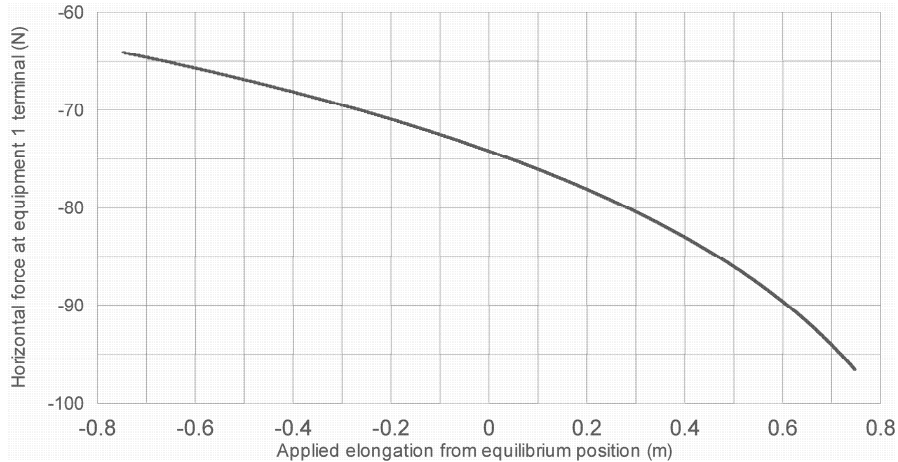


**Fig. 7.36 Force-elongation curve for example 2, trial 3, at equipment terminals**

### 7.6.10.3 Stability

It is necessary to check that the configuration studied will not collapse due to the effect of the 90 km/hr wind, and that it will maintain its clearances under it. As in the previous example, this load is considered as static (without dynamic effects). The effect of wind on the conductor is to generate a uniform lateral load.

Using Equation (7.17) and the values from Table 7.8 we obtain

$$F_w = CV^2 D_o C_f K_z G_f I = 0.613 \cdot 25.0^2 \cdot 0.05863 \cdot 1.0 \cdot 0.94 \cdot 0.95 \cdot 1 = 20.06 \text{ N/m}$$

The lateral displacement and deformed position is again obtained from finite element simulation, starting from the initial position calculated without ice. The wind force by unit length is replaced at each node by an equivalent point load, equal to the total force applied on the conductor divided by the number of elements. In the case here, the total force is given by  $20.06 \text{ N/m} \cdot 6.37 \text{ m} = 127.8 \text{ N}$  and, therefore, the nodal load is  $127.8 / 64 = 1.997 \text{ N}$ . This load is applied using 100 increments. The program input is given in Appendix B.

The obtained maximum lateral displacement is 1.02 m; the final equilibrium position under the wind is illustrated in Figure 7.37. It is observed that the configuration remains stable under the effect of wind. It is also observed that even though the lateral displacement is significant, it should not compromise the phase-to-phase clearance, as the other phases will experience the same displacement under the same wind at the same time.

#### 7.6.10.4 Conclusion on Example 2

It was observed here that due to the tight clearances and relatively large slack required, it took three trials before obtaining a suitable configuration. The inverse parabola retained has the advantage of easily meeting the necessary clearances while providing significant slack. It is observed that it remains stable under the action of wind loads without collapsing even if it is displaced significantly. It also meets the flexibility criterion and is therefore adequate.

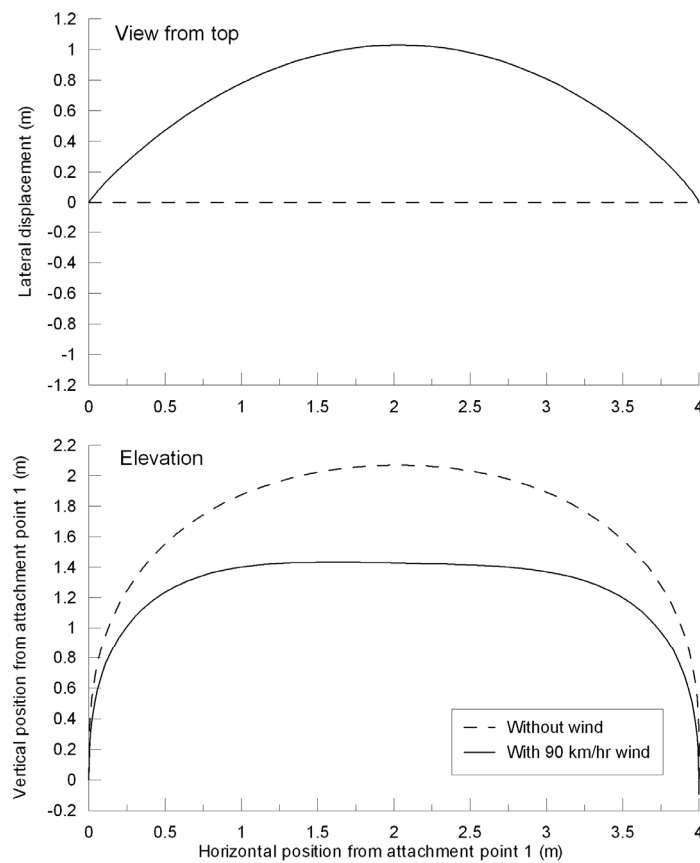


**Fig. 7.37 Equilibrium position for example 2, trial 3, with 90 km/hr wind**

### 7.7 FLEXIBLE CONNECTION DESIGN: EXAMPLE 3

A 245 kV capacitor bank—equipment 1, and a post insulator—equipment 2, need to be connected by a 4000 kcmil flexible conductor. The general description of the equipment and main dimensions are illustrated in Figure 7.38. Two attachment geometries are considered for equipment 1: horizontal or vertical. The configuration must also withstand the effects of ice and wind. The example basic data are given in Table 7.12. Detailed data will be given as needed. The

seismic input is defined according to the IEEE 693 high-performance level (1 g), corresponding to twice the spectra illustrated in Figure 4.4.

The capacitor bank and the post insulator are enclosed in a fenced area and therefore, only the phase to ground clearance for the station post insulator need to be met here.

We will follow the flowchart illustrated in Figure 3.3, along with certain steps considered for simplicity. The seismic input and basic connection geometry have already been described, so the next step is the determination of the elongation demand.

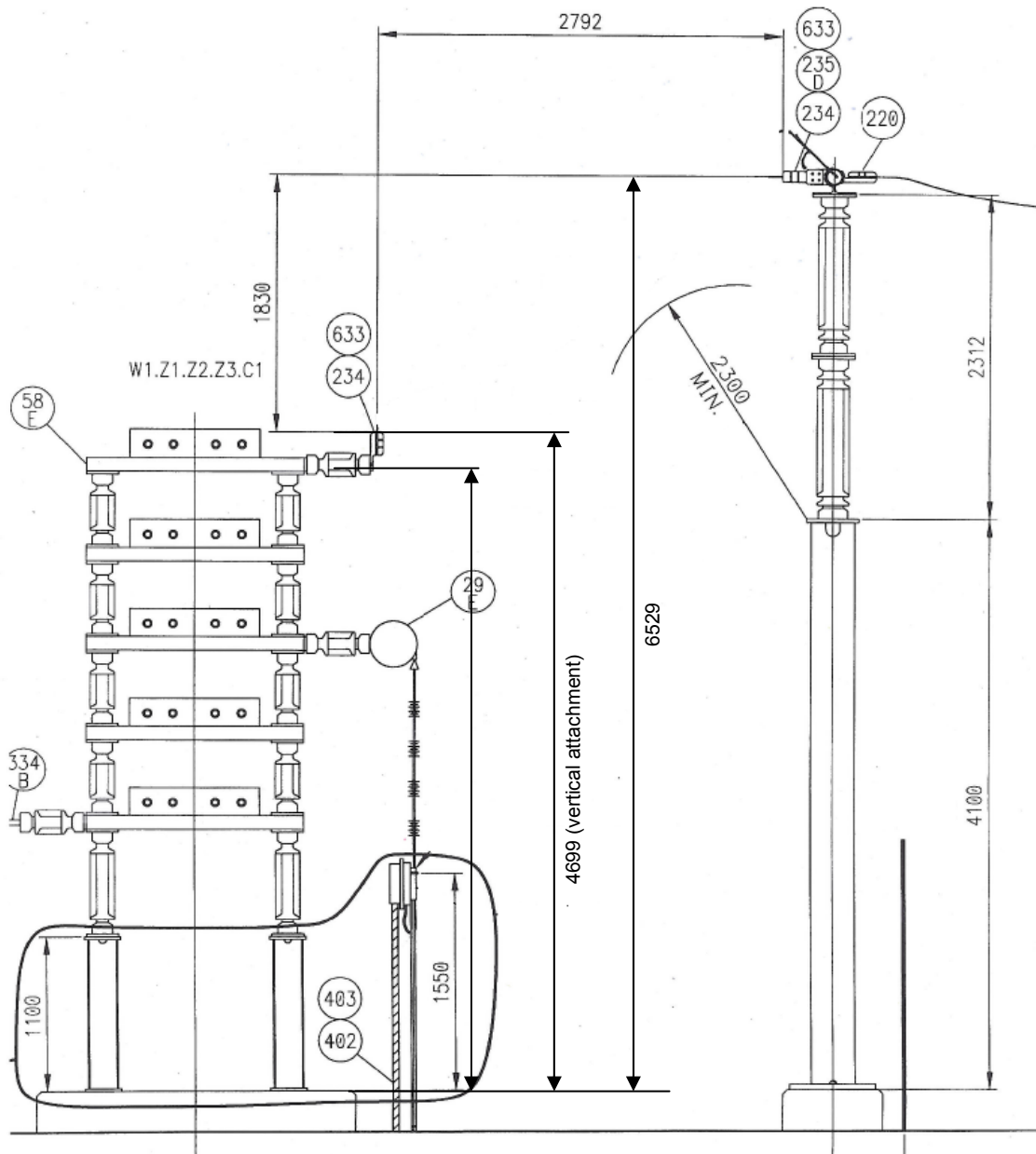


**Fig. 7.38 Example 3 general description and main dimensions (mm)**

**Table 7.12 Example 3: basic data**

Data		Description	Value
Basic connection geometry according to Figure 5.1	$h_1$	Height of attachment point 1 With horizontal attachment: With vertical attachment (90°)	4.470 m 4.699 m
	$h_2$	Height of attachment point 2	6.529 m
	L	Horizontal distance between attachment points	2.792 m
	H	Vertical distance between attachment points: With horizontal attachment at equipment 1: With vertical attachment at equipment 1:	2.059 m 1.830 m
Seismic input	-	Required response spectrum	IEEE 693 1 g performance level
Extreme wind	V	Extreme wind speed (30 mph)	48 km/h (13.33 m/s)
	$D_o$	Conductor diameter for wind force calculation	5.863 cm (2.308 in)
	-	Surface Roughness according to IEEE-605	C
		Height above ground for wind calculation	approximated to 7.6 m (25 ft) to use given values in IEEE-605
	$K_z$	Exposure factor according to IEEE-605 for surface roughness C and Height of 7.6 m	0.94
	$G_f$	Gust response factor according to IEEE-605 for wire and surface exposure C	0.95
	$C_f$	Force coefficient for cable (drag coefficient)	1.0
	I	Importance factor of structure for 2% annual probability of return and 50 year mean return period.	1.0
Ice thickness	$r_i$	radial ice thickness (.25 ")	6.35 mm

### 7.7.1 Determination of Elongation Demand

To determine the elongation demand, we use the stand-alone displacements of both equipment items from their seismic qualification reports for the IEEE 693 high-performance level spectrum:

- capacitor bank:  $f_1 = 3.20$  Hz,  $x_{\max,1} = 10.21$  cm
- post insulator:  $f_2 = 2.08$  Hz,  $x_{\max,2} = 30.12$  cm

where a critical damping ratio of 2% was assumed for both equipment items.

We will establish the elongation demand  $e_o$  using the maximum longitudinal displacement  $D_L$  between the equipment [Eq. (6.3)]:

$$e_o \approx D_L$$

The maximum differential displacement will be determined with the 1.25 factor recommended in Equation (6.16), using the SRSS rule, since the two fundamental frequencies are spaced by more than 20%:

$$D_L = 1.25 \cdot \sqrt{x_{\max,1}^2 + x_{\max,2}^2}$$

Hence, the elongation demand is given by

$$e_o \approx 1.25 \cdot \sqrt{x_{\max,1}^2 + x_{\max,2}^2} = 1.25 \cdot \sqrt{0.102^2 + 0.301^2} = 0.397 \text{ m}$$

### 7.7.2 Preliminary Shape: Trial 1

As preliminary shape, we will choose the flexible catenary configuration 3 from Figure 7.1 where both ends are attached at  $0^\circ$ .

### 7.7.3 Required Conductor Length: Trial 1

The required length is given by Equation (7.1):

$$L_0 = L_1 + e_o + L_2$$

$L_1$  is the straight-line distance between both attachment points and is given by Equation (5.1):

$$L_1 = \sqrt{L^2 + H^2}$$

Using the data from Figure 7.38 for the attachment point 1 in horizontal position, we obtain

$$L_1 = \sqrt{L^2 + H^2} = \sqrt{2.792^2 + 2.059^2} = 3.469 \text{ m}$$

Based on experience, we will choose a tentative value of  $L_2$  equal to 0.05 m; we will later check if this value procures sufficient flexibility.

Using the previous values, the required length is therefore:

$$L_0 = L_1 + e_o + L_2 = 3.469 + 0.397 + 0.05 = 3.916 \text{ m}$$

which we will round up to 3.92 m.

### 7.7.4 Verification of Clearances, Flexibility, and Stability: Trial 1

We will first check the clearance requirements; if met, then we check the flexibility and the stability; otherwise we must choose another configuration.

#### 7.7.4.1 Clearances

As discussed earlier, only the phase to ground clearance for the station post insulator needs to be met here, as illustrated in Figure 7.38, as 2.300 m for the 245 kV level.

To check whether this clearance is met, we establish the equilibrium position of the configuration using the nonlinear finite element method with the *FEAP* software; the conductor properties are the same as in the previous example (4000 kcmil conductor).

To check the clearances, we first compute the equilibrium position of the conductor under its own weight, using the procedure illustrated in Figure 7.12 and the *FEAP* software. The final position is calculated in three main steps:

1. application of weight on a straight horizontal line configuration equal to the total conductor length of 3.92 m
2. application of the horizontal displacement of right end support (left end fixed) of  $-1.128$  m to get the desired span of 2.792 m
3. application of the vertical displacement of right end support of  $+2.059$  m to get the vertical offset between supports

The program input is given in Appendix B, and the computational parameters are summarized in Table 7.13.

**Table 7.13 Computational parameters for example 3, trial 1, using *FEAP* software**

Parameter	Value or description
Starting position	Straight line of length 3.92 m
Number of elements	64
Number of increments to apply weight of conductor	100
Number of increments to apply horizontal displacement	2000
Number of increments to apply vertical displacement	1000
Method used to reestablish equilibrium at each step	Newton-Raphson ( <i>tang</i> in <i>FEAP</i> )
Solution tolerance	$10^{-12}$

As before, the weight of the conductor was not input directly but replaced by an equivalent downward force at each node equivalent to the total weight of the conductor ( $5.470 \text{ kg/m} \times 9.81 \text{ m/s}^2 \times 3.92 \text{ m} = 210.4 \text{ N}$ ) divided by the number of elements:  $210.4 \text{ N} / 64 = 3.287 \text{ N}$ . This force was applied gradually in the first step discussed above.

Once the calculation is done, we check the clearances graphically by plotting the obtained equilibrium position against the phase to ground radius from the base of equipment item 2. This is illustrated in Figure 7.39 where the (0,0) reference position is assumed to be the attachment point of the capacitor bank. It is observed that the required clearance is violated, so another tentative shape must be sought.

### 7.7.5 Preliminary Shape: Trial 2

As a second tentative shape, we will try a modified catenary (configuration 1—Fig. 7.1), by setting attachment point 1 at  $90^\circ$  and leaving point 2 at  $0^\circ$ . Since there is a large vertical offset

between the two points, it appears intuitively that the configuration will appear somewhat like a quarter circle.

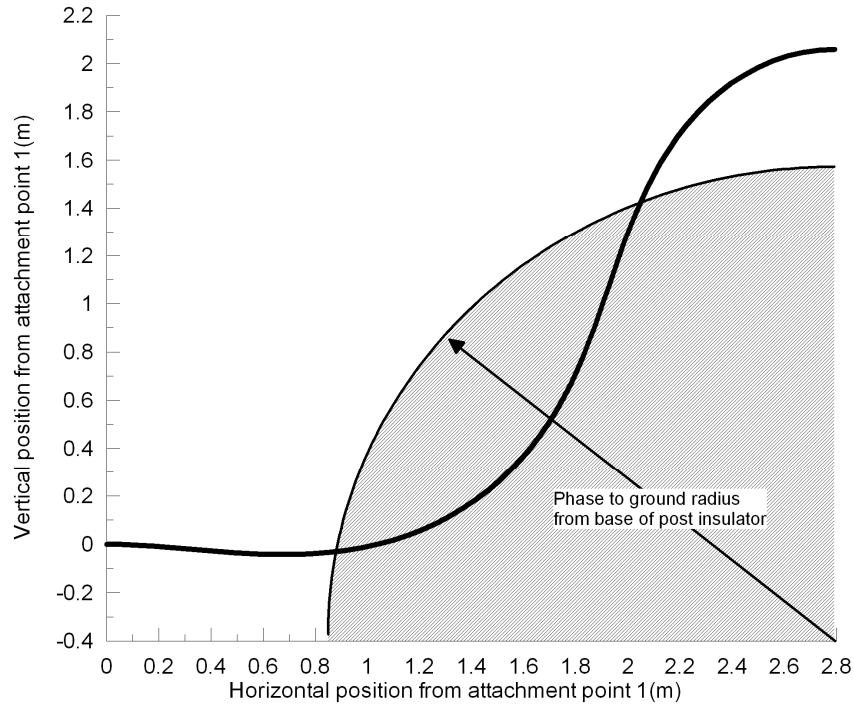


**Fig. 7.39 Verification of clearances for example 3, trial 1**

### 7.7.6 Required Conductor Length: Trial 2

The required length is given by Equation (7.1):

$$L_0 = L_1 + e_o + L_2$$

$L_1$  is the straight-line distance between both attachment points and is given by Equation (5.1):

$$L_1 = \sqrt{L^2 + H^2}$$

Using the data from Figure 7.38 for the attachment point 1 in a vertical position, we obtain

$$L_1 = \sqrt{L^2 + H^2} = \sqrt{2.792^2 + 1.830^2} = 3.338 \text{ m}$$

Based on experience, we will choose a tentative value of  $L_2$  equal to 0.10 m, since one end is at  $90^\circ$  and would therefore lead to more stiffness when the conductor is stretched extensively, as opposed to a configuration where the attachment point would be at  $0^\circ$ ; we will later check if this value procures sufficient flexibility.

Using the previous values, the required length is therefore

$$L_0 = L_1 + e_o + L_2 = 3.338 + 0.397 + 0.10 = 3.835 \text{ m}$$

which we will round up to 3.84 m.

### 7.7.7 Verification of Clearances, Flexibility, and Stability: Trial 2

We will first check clearance requirements; if met, then we will check the flexibility and the stability; otherwise we must choose another configuration shape.

#### 7.7.7.1 Clearances

As before, we compute the equilibrium position of the conductor under its own weight. Since this configuration is somehow like an inverse parabola, we will establish its equilibrium position in the same way used in the previous example for the parabola:

1. application of 2.5% of final rotations ( $2.0^\circ$ ) in 100 increments
2. simultaneous application of the horizontal displacement of 1.048 m, vertical displacement of 1.830 m, and the remaining rotation ( $98\% = 88^\circ$ ) in 3900 increments
3. application of the weight in 1000 increments

As previously, the first step consisting of applying a small portion of the rotation alone is to condition the conductor in moving as an inverse parabola before applying any horizontal displacement; indeed, the small rotation induces a moment that will move the conductor upward when we apply next the horizontal displacement along with the remaining rotations and the vertical displacement.

The program input is given in Appendix B and the computational parameters are summarized in Table 7.14. Note here again that a finer tolerance of  $1 \cdot 10^{-12}$  was required for the problem to converge under the application of the rotations.

**Table 7.14 Computational parameters for example 3 using *FEAP* software, trial 2**

Parameter	Value or description
Starting position	Straight line of length 3.840 m
Number of elements	64
Number of increments to apply initially 5% of rotations	100
Number of increments to apply horizontal displacement, vertical displacement and remaining of rotations	3900
Number of increments to apply weight of conductor	100
Method used to reestablish equilibrium at each step	Newton-Raphson ( <i>tang</i> in <i>FEAP</i> )
Solution tolerance	$10^{-12}$

As before, the weight of the conductor was not input directly but replaced by an equivalent downward force at each node, equivalent to the total weight of the conductor ( $5.470 \text{ kg/m} \times 9.81 \text{ m/s}^2 \times 3.84 \text{ m} = 206.1 \text{ N}$ ) divided by the number of elements:  $206.1 \text{ N} / 64 = 3.220 \text{ N}$ . This force was applied gradually in the first step discussed above.

Once the calculation is done, we check the clearances graphically by plotting the obtained equilibrium position against the phase to ground radius from the base of equipment item 2. This is illustrated in Figure 7.40. It is observed that the phase to ground clearance is now easily met.

#### **7.7.7.2 Flexibility**

As discussed, the required flexibility must be such that the force-elongation behavior of the conductor under the elongation demand must remain approximately linear without abrupt change of stiffness. To check that, we use the same finite element model as above, and starting from the computed equilibrium position, we apply a cyclic displacement in a quasi-static fashion (without dynamic effects), equal to the elongation demand of 0.397 m identified earlier. To do so, one end of the conductor is kept fixed in the simulation while the other is moved back and forth with an amplitude equal to the elongation demand, as in a push-pull test. The program input is given in Appendix B.

The resulting force-elongation curve is given in Figure 7.41. It is observed that although the curve is not linear over its entire range, no abrupt change of stiffness occurs with a force variation from -90 N to 140 N, which is relatively small; so we consider this configuration adequate from the standpoint of flexibility.

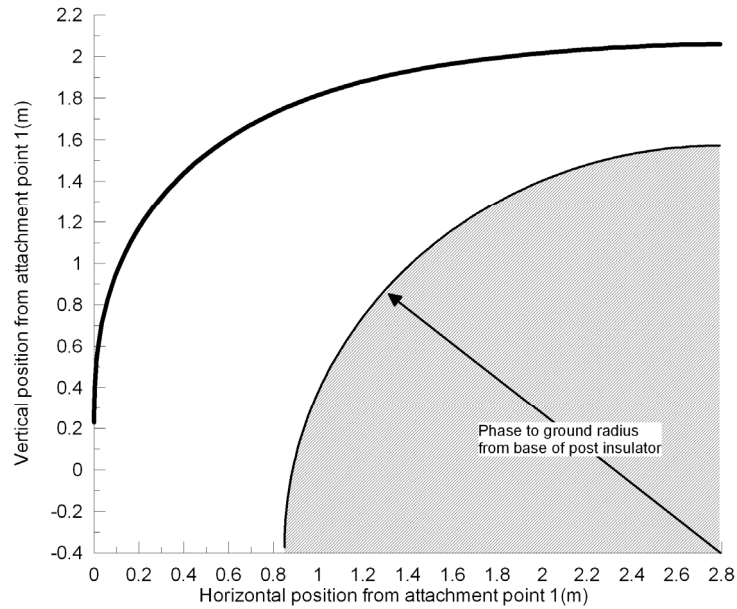


**Fig. 7.40 Verification of clearances for example 3, trial 2**

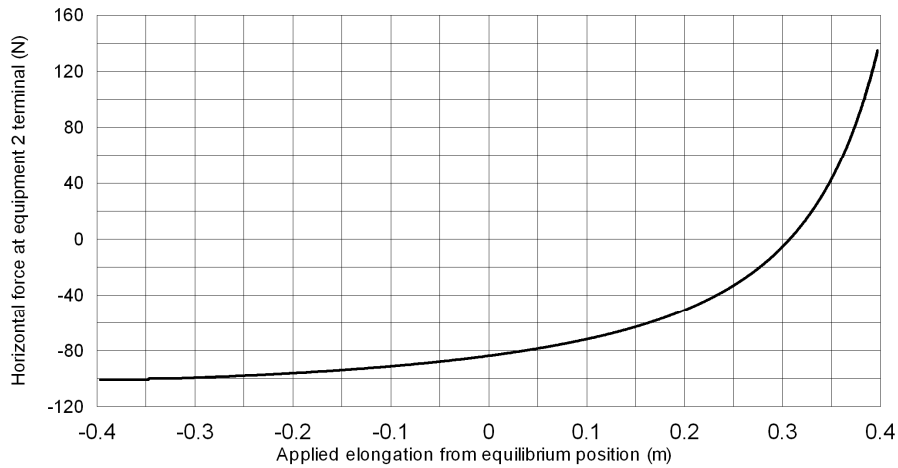


**Fig. 7.41 Force-elongation curve for example 3, trial 2, at equipment terminals**

### 7.7.7.3 Stability

It is necessary to check that the configuration studied will not collapse due to the effects of ice and wind, and that it will maintain its clearances under such effects. The climatic loads to consider in this example are the *concurrent* effects of 6.25 mm of ice (.25 in.) around the conductor and a wind of 48 km/h (30 mph).

Using Equation (7.15), the additional weight by unit length on the conductor is

$$F_I = \pi w_i r_i (D_o + r_i) = \pi \cdot 8820 \cdot 0.00635 \cdot (0.05863 + 0.00635) = 11.43 \text{ N/m}$$

Using Equation (7.18) and the values from Table 7.12, the effect of wind over a cross section covered by ice is given by

$$F_w = CV_i^2 (D_o + 2 \cdot r_i) C_f K_z G_f I = 0.613 \cdot 13.33^2 \cdot (0.05863 + 2 \cdot 0.00635) \cdot 1.0 \cdot 0.94 \cdot 0.95 \cdot 1 = 6.942 \text{ N/m}$$

To calculate the final shape of the conductor with the additional weight of ice and concurrent effect of wind, we will follow the same exact procedure as the one used before to calculate the equilibrium position, changing only the forces applied downward at all nodes to take account of the additional ice weight and adding an horizontal force due to the effect of the wind. Since we have 64 elements, the additional force applied at each node by the effect of ice will be equal to the ice unit weight times the conductor length divided by the number of elements:  $11.43 \text{ N/m} \times 3.84 \text{ m} / 64 = 0.686 \text{ N}$ . This force is added to the one simulating the weight of the conductor alone, for a total of  $3.906 \text{ N}$  at each node, downwards. The wind force by unit length is replaced at each node by an equivalent point load, equal to the total force applied on the conductor divided by the number of elements. In the case here, the total force is given by  $6.942 \text{ N/m} \times 3.84 \text{ m} = 26.66 \text{ N}$ , and therefore the nodal load by  $26.66 / 64 = 0.417 \text{ N}$ . Both loads are applied using 100 increments. The program input is given in Appendix B.

The result is illustrated in Figure 7.42 where the initial equilibrium position without ice and wind is also plotted. It is observed that the configuration is only slightly deformed by the additional ice weight and wind and that the clearance from the base of the insulator post is still met as needed. The corresponding maximum lateral displacement is  $0.191 \text{ m}$ .

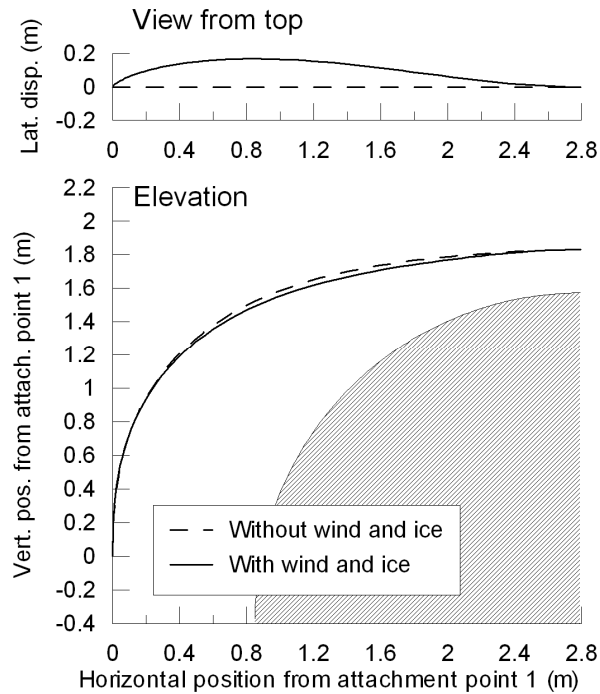


**Fig. 7.42 Equilibrium position for example 3 with 48 km/hr wind and 6.35 mm radial ice**

#### 7.7.7.4 Conclusion on Example 3

The tentative modified catenary shape with one end attached at  $90^\circ$  meets all requirements and is therefore accepted as final design.

## 7.8 STANDARDIZED DESIGN OF FLEXIBLE BUSWORK

The previous examples of flexible buswork design have demonstrated that individualized design on a case by case basis requires repeating several calculations each time: establishing the displacement demands of the two interconnected equipment, establishing the required slack, calculation of the equilibrium position to check clearances, verification of the flexibility of the conductor, and calculations to check the stability under climatic loading. While these calculations are relatively simple once the finite element methodology is mastered, they are nonetheless lengthy, especially if all pairs of equipment in a substation must be designed in this way. From a utility perspective, it is therefore preferable to use standardized (or universal) designs that can apply to most cases to avoid repeating such calculations and to facilitate the implementation of designs on a larger scale. Standardized designs may take the form of tables specifying shapes and conductor lengths satisfying the basic requirements (clearances, stability

to operation loads, etc.) for an array of distances between attachment points of a pair of equipment items.

Since, in general, electrical clearances are the same for a given voltage level, *it is best to design such tables according to specific voltage levels* (e.g., 245 kV, 330 kV, etc.). Also, generally, equipment at a given voltage level have fundamental frequencies within a given range, which in turn corresponds to a given range of expected differential displacements (for a given design response spectrum), and therefore to a given range of demand (minimum required slack). It is therefore recommended that such tables be based on a *design response spectrum that covers a wide area*, such that a limited set of these tables have a wide range of application, thus facilitating their implementation within a utility.

The main limitation of such tables is that since they aim at covering a wide range of interconnection possibilities and provide bounding values to cover most expected differential displacement values between possible pairs of equipment items, there is inherently a high level of conservatism in the available slack in most cases. This sometimes may lead to a given configuration that does not meet one or several criteria (such as the clearances) because the required slack is too large, even though such a shape could be applied for specific cases with lesser slack.

We present next the approach of designing standardized tables based on the voltage level for a given design response spectrum (i.e., for a specific area where such spectrum applies), followed by an example detailing the construction of a table.

## **7.8.1 How to Establish Standardized Design Tables**

We present in the following subclauses the steps required to establish standardized design tables.

### ***7.8.1.1 Determining Basic Dimensions to Check Clearances***

The recommended approach to design tables for a given voltage level is based on the dimensions of rigid bus bar structures *if the latter are standardized* within a given utility. Usually, rigid bus bar structures have standardized foundations, pedestal heights, and insulator lengths that can be used as a basis to verify the required electrical clearances; flexible configurations designed to meet clearances from these dimensions could therefore be applied to any pairs of equipment

items that have heights and dimensions equal or higher. Table 7.15 is an example of the standardized dimensions of rigid bus bars for some voltage levels used within a given utility. Also seen here is the maximum permitted sag from the total bus bar height, determined using the minimum safety distance.

**Table 7.15 Example of standardized rigid bus bar dimensions for a given utility**

Voltage level (kV)	Foundation height from ground (mm) (1)	Pedestal length (mm) (2)	Insulator length (mm) (3)	Total bus bar height (mm) (4)=(1)+(2)+(3)	Minimum safety distance (mm) (5)	Maximum permitted sag (mm) (5)-(4)	Phase to ground distance (mm) (6)
145	300	4000	1200	5500	4700	800	1124
170	300	4000	1700	6000	5200	800	1533
245	300	4000	2300	6600	5600	1000	1942
330	300	4000	2700	7000	6400	600	2401

### 7.8.1.2 Determining the Maximum Elongation Demand

The maximum elongation demand must be established to cover all possible pairs of interconnected equipment items; a maximum bound value is therefore sought. To do so, the following approach is recommended:

1. Perform a survey within your utility of the fundamental frequencies of equipment for the desired voltage level and determine the lower-bound value of frequency (denoted  $f_L$ ) that would cover most equipment items. This value will be used in the next step to establish a bound value of the maximum stand-alone displacement expected at that voltage level. It is therefore important to determine this value such that it is representative of most equipment items, while not necessarily being the lowest value found, as the corresponding stand-alone displacement will generally increase as the fundamental frequency decreases (see for example Fig. 6.11). This will lead to an overly conservative estimate of the demand, considering the added conservatism inherent in the next steps.
2. Using  $f_L$  and the required design spectrum, establish a bound value of the maximum stand-alone displacement,  $x_L$ , using Equation (6.9):

$$x_L = 1.62 \cdot S_d(f_L, \zeta)$$

A 2% value of damping  $\zeta$  is recommended. Note that Equation (6.9) covers 95% of equipment surveyed as discussed earlier. This value is considered adequate, as it already

introduces a high level of conservatism. Note also that the value of the stand-alone displacement to use as input could be determined directly from the survey done in step 1 if the stand-alone displacement is available with the fundamental frequency of the equipment surveyed. However, the advantage of using the 1.62 factor is that it would cover most new equipment that would be installed in the future.

3. Determine the elongation demand using Equation (6.16) with  $x_L$  for  $x_{max\_1}$  and  $x_{max\_2}$ .

$$e_o = D = 1.25 \cdot \sqrt{x_{max\_1}^2 + x_{max\_2}^2} = 1.25 \cdot \sqrt{2 \cdot x_L^2} = 1.77 \cdot x_L \quad (7.19)$$

The use of  $x_L$  for both  $x_{max\_1}$  and  $x_{max\_2}$  introduces conservatism in the elongation demand, as it is unlikely that both interconnected equipment items share this value. A less conservative value could be obtained by examining all possible combinations of equipment if a representative database is available, and by choosing the combination producing the maximum demand. In such a case, it is recommended to calculate the maximum elongation demand among those pairs using the CQC method given by Equation (6.14) and the 1.25 factor above, which should diminish the amount of conservatism.

### ***7.8.1.3 Checking a Shape over a Range of Spans between Equipment***

Using the elongation demand, the next step in establishing a standardized table is to check the possibility of using a chosen shape over a desired range of spans between equipment. Note that we use here the term span, since we will check the possibility of installing a configuration between equipment at the standardized bus bar height on both sides. However, once this is done for a given span, the configuration is valid for the same distance between equipment attachment points in the case when they are not at the same height, as long as both heights are equal or greater to the standardized bus bar height. Indeed, when equipment is not the same height, the elongation demand used will be conservative, as discussed in Section 6.1.

The steps to establish the validity of a shape over a range of spans are the following:

1. Establish the minimum and maximum attachment point horizontal distances required for the given voltage level—range of spans to cover; for example between 2 and 6 m.
2. Subdivide this range into a given number of increments, e.g., every 0.5 m: 2.0, 2.5, ... 6 m.

- Establish the additional required length  $L_2$  for the chosen shape, and using Equation (7.1), establish the required length for all spans in the range [note use Eq. (7.2) for the inverse parabola shape]:

$$L_0 = L_1 + e_o + L_2$$

- Calculate the equilibrium position for all spans in the range and check for clearance requirements graphically. If there is still a margin of slack for some, *it is recommended to increase the length for them to use the available margin and to match the required clearances as closely as possible*. This has the advantages of adding *additional flexibility* and conservatism in the design provided stability problems do not result.
- For all spans that meet the clearances, check the flexibility over the elongation and the stability under the climatic loading (wind and ice) selected for the area of application of the table. The spans for which the flexibility and the stability criteria are met are the ones that will be included in the table for that particular shape. Linear interpolation is to be used for values of spans between tabulated values.

## 7.8.2 Example of a Standardized Design Table for Flexible Configurations

This example addresses the design of a standardized table for the four different shapes presented in Figure 7.1 for a voltage level of 145 kV and a ground acceleration of 0.5 g, using a single 4000 kcmil conductor. We now present the different steps outlined above for the determination of this table.

### 7.8.2.1 Basic Dimensions

The basic dimensions used here are the values of the standardized bus bar dimensions for 145 kV presented in Table 7.15, and reproduced under and illustrated in Figure 7.43. The values that will be used to check clearances are the maximum permitted sag of 800 mm and the phase to ground distance of 1124 mm.

Voltage level (kV)	Foundation height from ground (mm) (1)	Pedestal length (mm) (2)	Insulator length (mm) (3)	Total bus bar height (mm) (4)=(1)+(2)+(3)	Minimum safety distance (mm) (5)	Maximum permitted sag (mm) (5)-(4)	Phase to ground distance (mm) (6)
145	300	4000	1200	5500	4700	800	1124

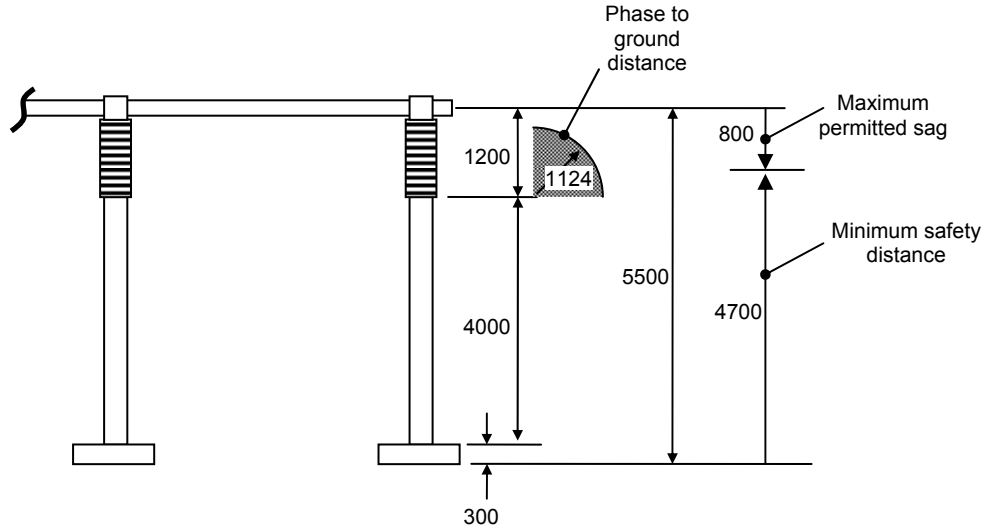


**Fig. 7.43 Bus bar dimensions for 145 kV standardized table example**

### 7.8.2.2 Maximum Elongation Demand

We suppose here that a survey of equipment for the 145 kV voltage level led to the identification of the lowest representative fundamental frequency of equipment as  $1.25 \text{ Hz}$  with a damping value of  $2\%$ .

The corresponding spectral displacement  $S_d(1.25, 2\%)$  from the  $0.5g$  response spectrum used is  $8.72 \text{ cm}$ . Using Equation (6.9) we obtain the maximum stand-alone displacement as

$$x_L = 1.62 \cdot S_d(f_L, \zeta) = 1.62 \cdot 8.72 = 14.12 \text{ cm}$$

The elongation demand is given using Equation (7.19) as

$$e_o = D = 1.77 \cdot x_L = 1.77 \cdot 14.12 = 25 \text{ cm}$$

### 7.8.2.3 Verification of Shapes over a Range of Spans

The range of spans retained for the 145 kV voltage level is from  $1.5$  to  $6.0 \text{ m}$ , with intervals of  $0.5 \text{ m}$ . We will check the application of the four basic shapes from Figure 7.1, as discussed. The calculations are identical to those presented in the case by case design examples earlier and will not be repeated here for sake of brevity. The wind and ice loads considered are  $6.35 \text{ mm}$  of ice ( $1/4 \text{ in.}$ ) with a concurrent wind of  $48 \text{ km/h}$  ( $30 \text{ mph}$ ). We will present only the final results, illustrating when necessary the respect of clearances for the different shapes, assuming that they meet all the other criteria.

### Configuration 1: Inverse Parabola

The required length  $L_o$  for this configuration is given by Equation (7.2). It was calculated that this configuration remains stable under the application of the ice and wind loads from 1.5 to 4.5 m only. The corresponding length to use and the corresponding availability is presented in Table 7.16; it is observed that the availability for all spans is much greater than the demand of 25 cm, since this configuration, as discussed earlier, requires more slack, as both attachment ends are at  $90^\circ$ . Since this configuration automatically meets all clearances, we will not plot the results here.

**Table 7.16 Length and availability for inverse parabola configuration**

<b>Span (m)</b>	1.5	2.0	2.5	3.0	3.5	4.0	4.5
<b><math>L_o</math> (m)</b>	2.36	3.14	3.93	4.71	5.5	6.28	7.07
<b>availability (m)</b>	0.86	1.14	1.43	1.71	2.0	2.28	2.57

### Configuration 2: Double Curvature

The required length  $L_o$  for this configuration is given by Equation (7.1), where the additional provision for the conductor shape under consideration,  $L_2$ , is chosen as 5 cm. Therefore, the minimum amount of slack to add to the span  $L_1$  is  $25 + 5 = 30$  cm. Due to the  $45^\circ$  angle of attachment at one end, it was found that clearances could be met while adding an additional amount of slack from 2 to 5 cm for the spans considered, in order to maximize flexibility as discussed earlier. However, it was established that this configuration can be applied only for spans 2.5 m and longer, as it is not flexible enough for shorter spans. The corresponding lengths and availability are presented in Table 7.17. Figure 7.44 presents the clearance requirements for spans between 2.5 and 6.0 m.

**Table 7.17 Length and availability for double-curvature configuration**

<b>Span (m)</b>	2.5	3.0	3.5	4.0	4.5	5.0	5.5	6.0
<b><math>L_o</math> (m)</b>	2.85	3.35	3.85	4.35	4.85	5.35	5.85	6.32
<b>availability (m)</b>	0.35	0.35	0.35	0.35	0.35	0.35	0.35	0.32

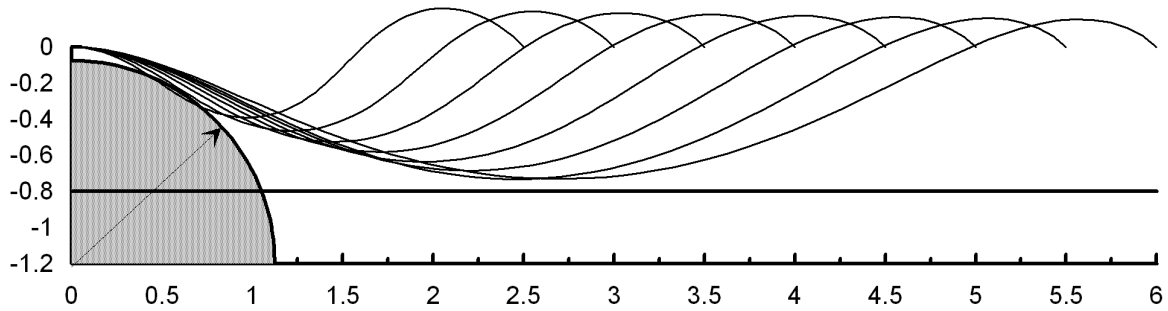


**Fig. 7.44 Double-curvature configurations for 145 kV standardized table example**

**Configuration 3: Triple Curvature**

The required length  $L_o$  for this configuration is given by Equation (7.1), where the additional provision for the conductor shape under consideration,  $L_2$ , is chosen as 10 cm. Therefore, the minimum amount of slack  $L_1$  is  $25 + 5 = 35$  cm. Due to the  $45^\circ$  angle of attachment at both ends, it was found that clearances could be met while adding an additional amount of slack from 15 to 35 cm for the spans considered, in order to maximize flexibility as discussed earlier. It was found that the greatest amount of added slack (35 cm) could be added to the shortest span (3.5 m) and then decreased onwards. However, it was established that this configuration can only be applied for spans 3.5 m or longer, as it is not sufficiently flexible for shorter spans. The corresponding lengths and availability are presented in Table 7.18. Figure 7.45 presents the clearance requirements between 3.5 and 6.0 m spans.

**Table 7.18 Length and availability for triple-curvature configuration**

Span (m)	3.5	4.0	4.5	5.0	5.5	6.0
$L_o$ (m)	4.20	4.68	5.15	5.60	6.05	6.50
availability (m)	0.70	0.68	0.65	0.60	0.55	0.50

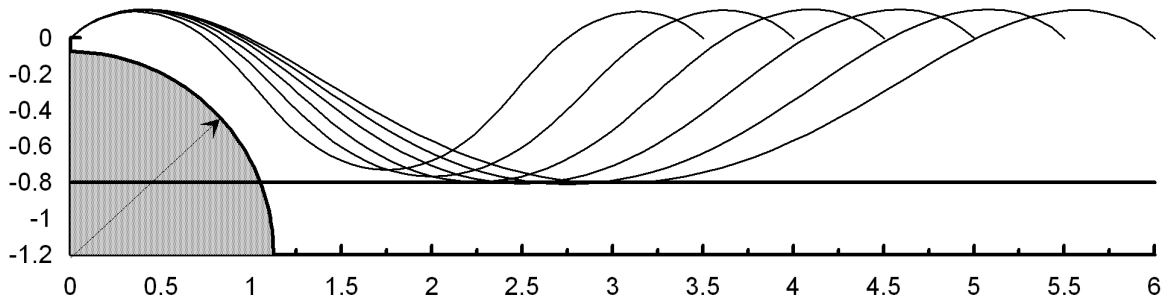


**Fig. 7.45 Triple-curvature configurations for 145 kV standardized table example**

#### Configuration 4: Catenary

The required length  $L_o$  for this configuration is given by Equation (7.1), where the additional provision for such shape,  $L_2$ , is chosen here as 5 cm. Therefore, the minimum amount of slack  $L_1$  is 30 cm. It was found that in order to meet clearances, this configuration could be applied only between 2.5 and 5.0 m spans. At 2.5 m, a slight violation in the phase to ground distance is observed. Nevertheless, this span is retained because usually the attachment point is not directly under the phase to ground origin, since the connection hardware length takes the conductor away from this point. The corresponding lengths and availability are presented in Table 7.19. Figure 7.46 presents the clearances required for spans between 2.5 to 5.0 m.

**Table 7.19 Length and availability for catenary configuration**

Span (m)	2.5	3.0	3.5	4.0	4.5	5.0
$L_o$ (m)	2.80	3.30	3.80	4.30	4.80	5.30
availability (m)	0.30	0.30	0.30	0.30	0.30	0.30

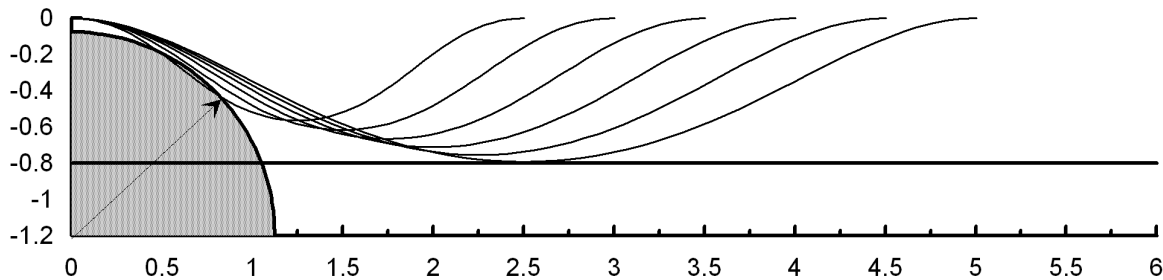


**Fig. 7.46 Catenary configurations for 145 kV standardized table example**

#### 7.8.2.4 Final Standardized Table

The final standardized table made from all the possible configurations between spans from 1.5 to 6.0 is shown in Table 7.20. This table gives, for the straight-line distance  $L_1$  between attachment points at 0.5 m intervals, the conductor length  $L_o$  to use according to the different shapes. For intermediate values of  $L_1$  between tabulated values, a linear interpolation is recommended to get the required value of  $L_o$ . The specified notes under the table are recommended to make sure such a table is used according to the assumptions from which it was built.

**Table 7.20 Standardized table for 145 kV example**

$L_1$ (m)	1.5	2.0	2.5	3.0	3.5	4.0	4.5	5.0	5.5	6.0
$L_o$ (m)—inverse parabola	2.36	3.14	3.93	4.71	5.50	6.28	7.07	n/a	n/a	n/a
$L_o$ (m)—double curvature	n/a	n/a	2.85	3.35	3.85	4.35	4.85	53.5	5.85	6.32
$L_o$ (m)—triple curvature	n/a	n/a	n/a	n/a	4.20	4.68	5.15	5.60	6.05	6.50
$L_o$ (m)—catenary	n/a	n/a	2.80	3.30	3.80	4.30	4.80	5.30	n/a	n/a

Notes:

1. Before using this table, make sure that
  - a. all equipment fundamental frequencies are greater than or equal to 1.25 Hz,
  - b. all equipment attachment points from the ground are higher than or equal to 5.500 m,
  - c. all equipment insulator (vertical) lengths are greater than or equal to 1.200 m.
2. For the inverse parabola, if a vertical difference  $H$  exists between attachment points, add this value to the length specified in the table [see Eq. (7.2)].

## 7.9 INSTALLATION OF FLEXIBLE BUSWORK

We provide here general guidance regarding the installation of flexible buswork. Typically, each utility has its own procedure. The general steps to install a flexible buswork are

1. Calculate and cut the required length of the conductor,  $L_C$ , consisting of the required length between the attachment points as specified in this guide (free conductor length  $L_o$ ) plus an additional length for the sections inside the connection hardware used ( $L_{c1}$  and  $L_{c2}$ ) as illustrated in Figure 7.47:

$$L_C = L_o + L_{c1} + L_{c2} \quad (7.20)$$

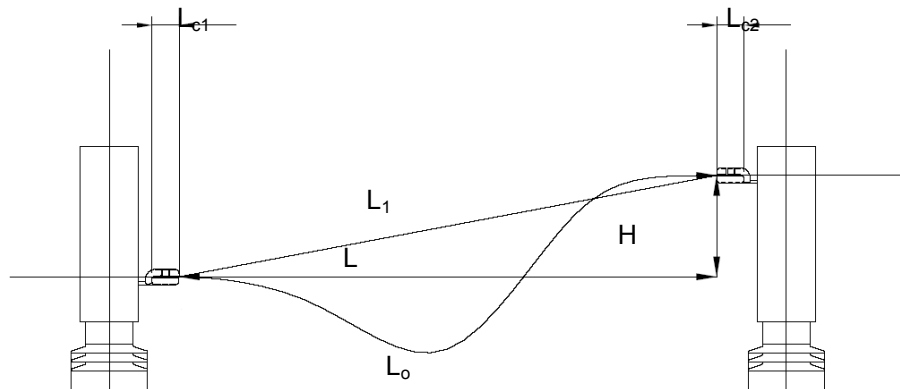


**Fig. 7.47 Geometry to determine length to cut for flexible connections**

2. It is recommended to attach hose clamps at the boundaries of the free conductor length so that the installation in the connection hardware will be done correctly. It is also recommended to use hose clamps on the extremities of the required length before cutting the cable from the conductor roll to prevent “bird caging” at or near the extremities. Proper care must be exercised to minimize manipulation on the conductor that may cause permanent deformation (e.g., kinks).
3. It is recommended to attach the conductor to the connection hardware on the ground before lifting the configuration to install between the equipment. It is also recommended to form the conductor according to the assumed shape sideways on the ground before attaching it to the hardware (e.g., forming an inverse parabola shape). If more than one conductor will be used with spacer(s), it is also recommended to attach the conductors together while resting sideways on the ground. The attachment of the conductor in the hardware should be done according to the hardware manufacturer’s specifications (e.g., required bolted torque).
4. The next step is to lift the configuration from the ground and bolt the attachment hardware to the equipment terminals. The support of a crane is recommended to hold the configuration while bolting the hardware to the terminals.

## 8 Seismic Design of Rigid Buswork

As an alternative to flexible buses, rigid buses may be used to interconnect substation equipment. This section discusses their seismic design in order to minimize the adverse interaction effect between the interconnected equipment.

### 8.1 INTRODUCTION

#### 8.1.1 General Description of Rigid Bus Connections

Rigid bus connections are usually made from a rigid conductor, as used in bus bar structures, connected at one end by a flexible connector to accommodate thermal expansion effects. An example is shown in Figure 8.1.



**Fig. 8.1 Rigid bus with flexible connector (Filiatrault et al. 1999)**

Different types of flexible connectors are commercially available. A common one is the flexible strap connector made of an assemblage of thin flat layers of conducting material (Fig. 8.2); another is the slider connector, which consists of a plunger connected by cables to the

receiving end that connects to the rigid conductor (Fig. 8.3). Custom-made flexible connectors can also be designed, such as the one made from three short cables, as shown in Figure 8.4.

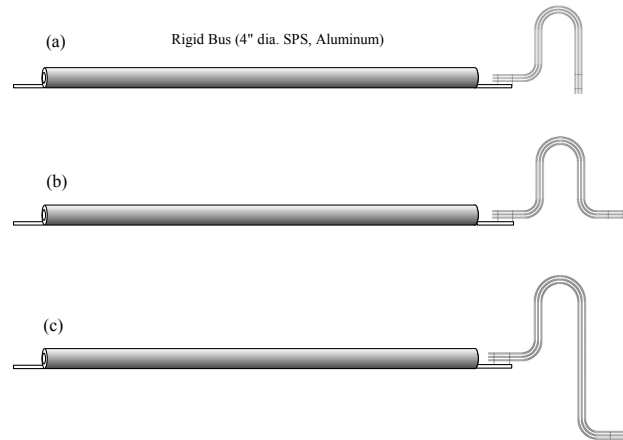


**Fig. 8.2 Flexible strap connectors (Song et al. 2006)**

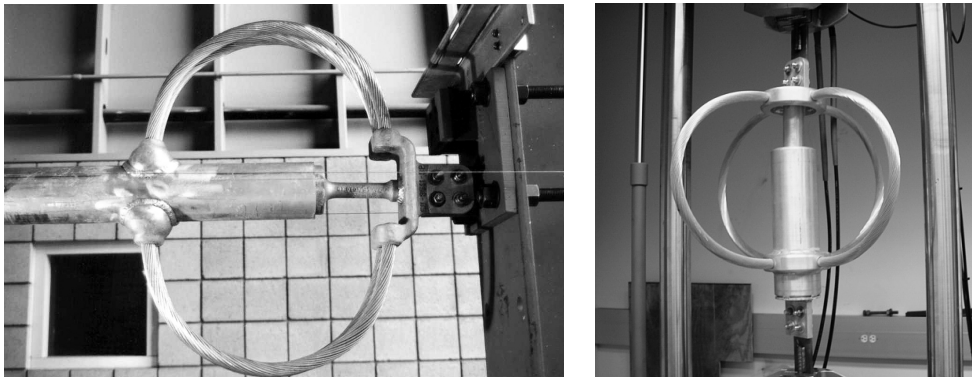


**Fig. 8.3 Slider connectors (Song et al. 2006)**

The main advantages of rigid bus conductors with a flexible connectors are

- Not having a sag, they easily meet required electrical clearances, thus requiring no verification on this aspect as opposed to flexible bus conductors.
- They provide a relatively high resistance and are therefore stable against transverse loads such as wind and short-circuit, as well as their own weight and ice in the downward direction, as long as the flexible connector has sufficient rigidity.
- The flexible connector may dissipate energy during a seismic event, depending on its construction and the amplitude of motion, and thus may increase the effective damping of the coupled interconnected equipment items.

- Depending on their dynamic properties, as well as those of the interconnected equipment and the seismic input, rigid bus conductors with flexible connectors may effectively uncouple the interconnected equipment.

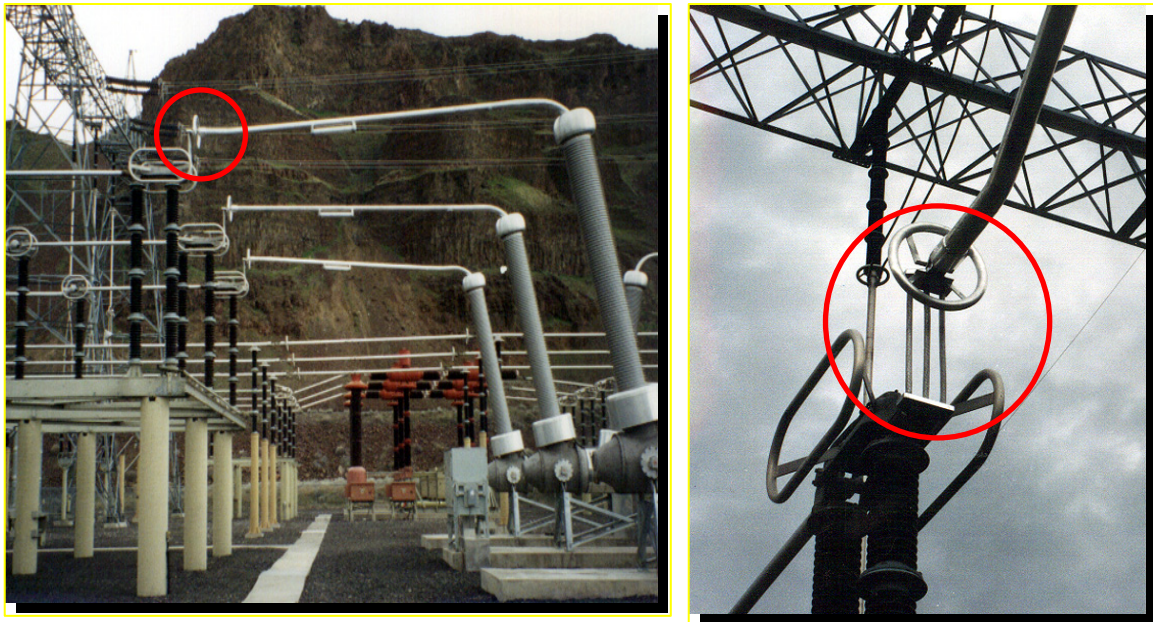


**Fig. 8.4 Custom-made BPA flexible connector (Courtesy of Leon Kempner, Bonneville Power Administration)**

The main disadvantages of rigid bus conductors are that

- depending on their construction, they may have limited capacity for differential displacement. Therefore, they generally are not well suited to accommodate large differential displacements that may occur with low-frequency equipment and high amplitude of ground motion.
- they may abruptly stiffen or become blocked, as with the slider connector when the plunger part ejects due to a displacement beyond its depth, or when all slack is used up in a flexible strap connector.
- under certain conditions they may significantly amplify the response of the higher-frequency equipment item as compared to its stand-alone response.
- under certain conditions, they can significantly alter the frequencies of the coupled equipment items as compared to their stand-alone frequencies.
- under high-intensity ground motion, the flexible connector may deform permanently and may need to be replaced afterwards.

### **8.1.2 Design Principles of Rigid Bus Conductors**

The seismic design of a rigid bus conductor is considerably different from that of a flexible bus conductor. The latter essentially requires the provision of sufficient slack to accommodate the expected differential displacement while meeting clearance and stability requirements under operational loads. Under such conditions, the interaction effect between interconnected components with flexible bus can be taken into account by specifying a design force applied at the terminals, and the dynamics of the coupled system then need not be explicitly considered. This simple approach, however, may lead to overly conservative designs in some cases.

Even though some of the same general principles apply to the design rigid bus (e.g., providing enough slack or flexibility), it has been shown that significant dynamic interaction can take place between interconnected components, often resulting in amplified response of the higher-frequency equipment in a pair, as compared to stand-alone response. Since clearance requirements are often automatically met with rigid buses, and since stability to operational loads is also not a critical issue due to the inherent high rigidity to lateral loads, the design of a rigid bus essentially amounts to *choosing the flexible connector properties such that the effect of interaction between the interconnected components is acceptably small*. It has been shown that to adequately evaluate this effect, the *dynamics of the coupled system must be considered*. To do so, the rigid bus–flexible connector properties must be determined beforehand, as they are critical in the evaluation of the interaction effect.

### **8.1.3 Available Methods to Evaluate the Interaction Effect**

The effect of interaction between equipment connected with rigid bus conductors may be determined either experimentally or through analytical and/or numerical means.

Experimental evaluation consists of exciting a pair of interconnected equipment items (or equivalent dummy items) with a given rigid bus connection on a shake table under a given seismic motion, and assessing if the response of the components is within design specifications. Such an approach is, however, costly and may lead to damaging the equipment items and/or the flexible connector itself, or may require repeated testing using different types of flexible connectors until a satisfactory performance is attained. Examples of such tests are given in references (Filiatrault et al. 1999; Strakel et al. 1998; Stearns and Filiatrault 2005) that provide representative examples of the possible behaviors of some of the different types of rigid bus

conductors discussed earlier. These experiments also validated the predicted behavior obtained through analytical/numerical methods as discussed below.

Analytical and/or numerical methods consist of modeling the coupled equipment-rigid bus system behavior and assessing the interaction effect through simulations. Due to the nonlinear behavior of most flexible connectors, the rigid bus–flexible connector assembly in general has a nonlinear response under dynamic action. Therefore, to obtain reliable predictions of the interaction effect, it is essential that an accurate model of the flexible connector is developed. Such a model can be developed by fitting to hysteresis loops developed under cyclic tests, or by finite element modeling. Der Kiureghian et al. (2000) and Hong (2003) include comparisons of hysteresis loops for flexible strap connectors obtained by cyclic testing and by finite elements, showing close agreement between the two methods. However, analytical methods have the considerable advantage of permitting easy and economical studies of the interaction effect, including parameter variations to explore the importance of various factors. Song et al. (2006) present an in-depth description of the available analytical/numerical methods, along with practical guidelines and examples. It is beyond the scope of this guide to describe in detail such methods, since some of them are quite complex. However, for the sake of the practicing engineer in an office setting, we present below an approximate and simplified method accounting for the nonlinear behavior of the rigid bus conductor, which provides results comparable to those obtained from the more complex methods mentioned above.

## **8.2 DETERMINATION OF RIGID BUS CONNECTION PROPERTIES**

In order to assess the seismic performance of a system of equipment items interconnected by a rigid bus/flexible connector, using the analytical method described below, the behavior of the bus under cyclic loading must first be determined. This behavior may be determined either experimentally or numerically through modeling and simulations.

### **8.2.1 Experimental Determination**

Experimental determination of rigid bus/flexible connector properties consists of obtaining the load-displacement curve of the connection under quasi-static cyclic tests. The ATC-24 loading protocol (or an adaptation of it) is recommended to perform the quasi-static tests on rigid bus

assemblies. This protocol consists of stepwise increase of displacement cycles, as illustrated in Figure 8.5.

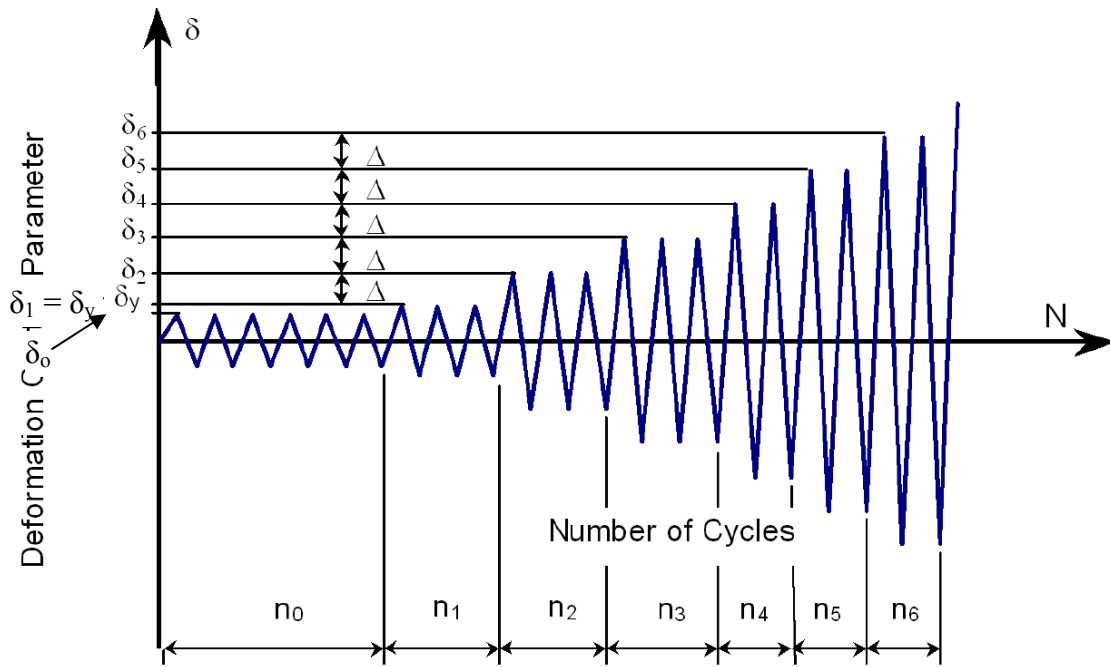


**Fig. 8.5 ATC-24 test protocol**

The loading history is defined by the following parameters:

$\delta_0$  is an initial displacement amplitude below yielding;

$\delta_y$  is the yield displacement across the connector ;

$\delta_j = \delta_y + (j-1)\Delta$  is the peak displacement across the connector in load step  $j$  ( $j \geq 1$ );

$n_j$  is the number of cycles to be performed in load step  $j$ ;

$\Delta$  is the increment in peak displacement between two consecutive steps.

As seen in the figure, the applied displacements  $\delta_j$  consist of multiples of the increment  $\Delta$ , which can be expressed in terms of the displacement ductility factor  $\mu$ , defined as

$$\mu = \frac{\delta}{\delta_y} \quad (8.1)$$

The yield displacement,  $\delta_y$ , is somewhat arbitrary for flexible connectors, as the transition from the linear behavior to the plastic behavior of the connector can vary greatly depending on the actual connector properties. The value of  $\delta_y$  is therefore chosen to obtain a representative value such that many load steps will be used in the elongation range of interest. In Filiatrault et al. (1999), the yield displacement was obtained by assuming that the yield took place at an

elongation of 0.2 %, while in Stearns and Filiatrault (2005), an arbitrary value of 1 in. was used. Some connectors do exhibit a sharp bilinear behavior. One example is the slider connector, which effectively “yields” once the friction force is overcome, and returns to elastic behavior when the direction of cyclic displacement is reversed. An example of a load-displacement curve obtained through such experiments is presented in Figure 8.6. It is observed that the behavior is hysteretic, typical of the behavior of flexible connectors that dissipate energy due to plastic deformation, geometric nonlinearities, contact, and friction. We will describe in Section 8.3 how the properties required for the analysis method presented in this guide can be extracted from such curves.

Load-displacement curves for rigid bus/flexible connectors that, to our knowledge, are available at this time are listed in Table 8.1 with the corresponding references.

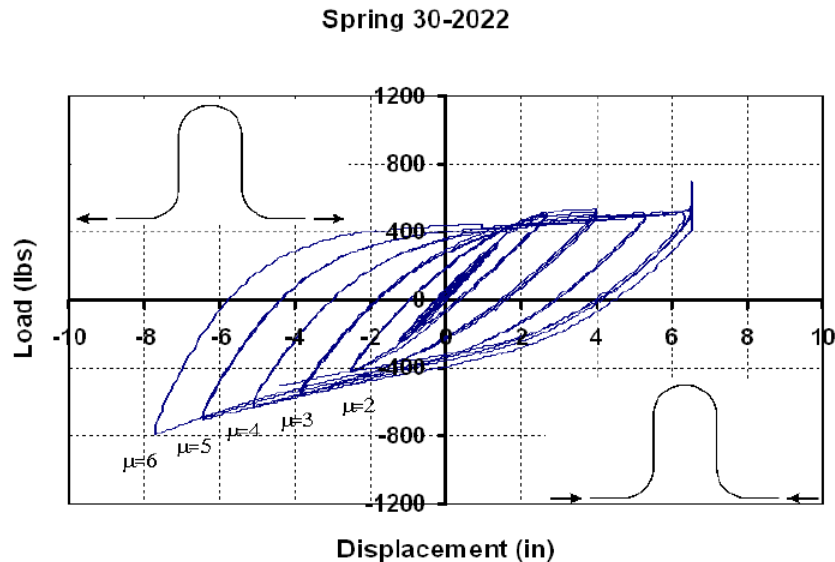


**Fig. 8.6 Load displacement response of a spring connector at different ductility levels (Filiatrault et al. 1999)**

**Table 8.1 Available load-displacement curves for rigid bus flexible connector**

Connector	Type	Reference
PG&E Part 30-2021	Flexible strap	Filiatrault et al. 1999; Stearns and Filiatrault 2005.
PG&E Part 30-2022	Flexible strap	
PG&E Part 30-2023	Flexible strap	
PG&E Part 30-4462	Bus Slider	
Custom S-FSC	Flexible strap (S-shape)	Stearns and Filiatrault 2005.
Improved from PG&E Part 30-4462	Bus slider	
SEFCOR WRLA290-1272-4B-60	Assembly of two 1272 kcmil rope lay aluminum conductors formed in an inverse parabola shape on a short span	

## 8.2.2 Numerical Determination

The load-displacement curves for a flexible connector can also be determined through numerical modeling. A nonlinear finite element model can be used, and it was found in Der Kiureghian et al. (2000) that the finite element analysis provided accurate estimates of the hysteretic behavior, as compared to experimental results, if material inelasticity and large deformation effects were properly accounted for. Once the finite element model is verified for a particular type of connector, it can be used to accurately predict the hysteretic behavior of similar connectors that are moderately different in shape, size, or material properties, thus avoiding costly experiments. Such models can be used in nonlinear finite element dynamic analysis of interconnected equipment as well. A global modeling of the connector behavior can also be obtained by fitting the results of tests or finite element analysis to analytical hysteresis models, such as the *Bouc-Wen* and *bilinear* models. Such analytical models then permit investigation of the interaction effect by nonlinear random vibration analysis; Figure 8.13 shows a comparison between a global analytical model and the results from experiments. However, for the purpose of the method described below, only the modeling of the hysteretic load-displacement curve is needed. Since it is beyond the scope of this guide to describe how to model connectors, as the procedure requires somewhat elaborate modeling techniques, the reader is referred to Der Kiureghian et al. (2000) and Song et al. (2006, 2007) for details and examples of how to establish representative models.

## 8.3 EVALUATION OF INTERACTION BETWEEN EQUIPMENT CONNECTED BY RIGID BUS USING SIMPLIFIED ANALYSIS METHODS

### 8.3.1 Basic Assumptions

The following basic assumptions are made regarding the analysis of equipment interconnected by rigid bus:

- The behavior of individual equipment items is linear and approximated by a unique displacement shape, corresponding to their first cantilever bending mode (or an approximation of it). As discussed in Section 6.2, this assumption is realistic for cantilever-type equipment, and attention must be paid to other types in order to identify the representative displacement shape. Song et al. (2007) also give further details on the recommended displacement shape to use.

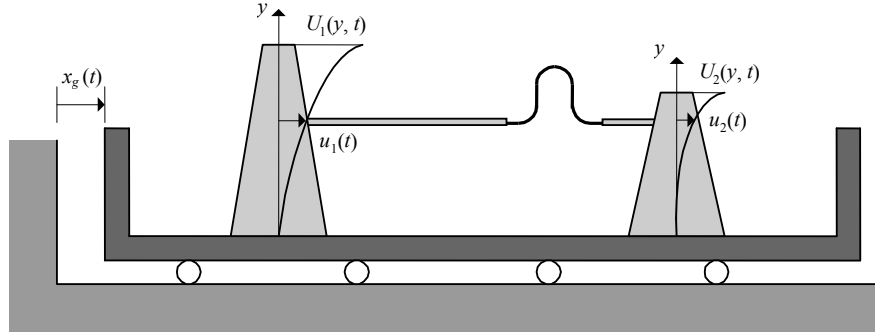
- The rigid connection transmits only a longitudinal force to the interconnected equipment. In practice some connections may also transfer torsional or bending moments, such as exemplified in the experiments presented in Filiatrault et al. (1999). These connections also transmit lateral loads as well. However, the influence of these additional loads on the interaction effect is insignificant.
- We consider only seismic motion in the longitudinal direction of the rigid bus connection and the effects of motions in the other orthogonal directions are neglected. Due to the flexibility of the rigid bus/flexible connector in directions orthogonal to its axis, dynamic interaction in these directions is not expected to be significant.
- Since the material presented below and developed so far is only for a pair of interconnected equipment items, we assume that the results obtained are valid for a series of interconnected equipment items with rigid buses as long as the interaction in each pair is within the acceptable design boundaries.

### 8.3.2 Seismic Interaction in Linearly Connected Equipment

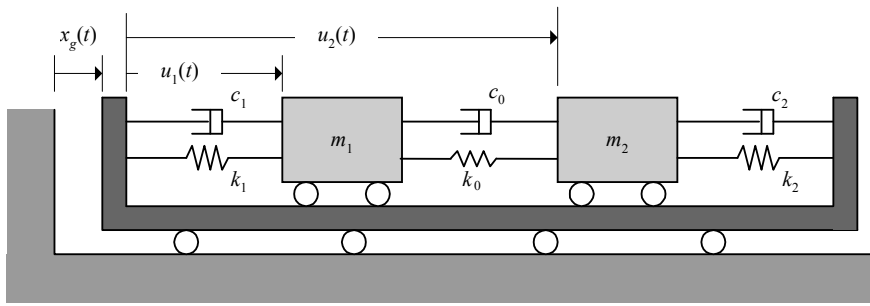
To derive the basic understanding necessary for the analysis of the interaction effect, we *first* consider the interaction between components connected by a linear rigid bus connection. By a *linear* rigid bus connection we assume that

- the force-elongation curve of the connection is linear for the entire range of motion;
- the damping of the connection is described by a linear viscous model, i.e., the damping force is proportional to the velocity.

We consider a system consisting of two equipment items connected by a rigid bus fitted with a flexible connector (a RB–FC assembly) that is subjected to a given base motion (Fig. 8.7). The RB–FC assembly is assumed to behave linearly and have negligible mass, constant stiffness  $k_0$  in the axial direction, and viscous damping coefficient  $c_0$ . The equipment items are idealized as generalized SDOF systems (Section 6.2.2) with natural circular frequencies  $\omega_1=2\pi f_1$  and  $\omega_2=2\pi f_2$ ; effective masses  $m_1$  and  $m_2$ ; viscous damping coefficients  $c_1=2\zeta_1\omega_1m_1$  and  $c_2=2\zeta_2\omega_2m_2$ , where  $\zeta_1$  and  $\zeta_2$  are the corresponding damping ratios; effective equipment stiffnesses  $k_1= m_1 (\omega_1)^2$  and  $k_2= m_2 (\omega_2)^2$ , and participation factors (Section 6.2.4)  $\alpha_1$  and  $\alpha_2$ . Without loss of generality we assume that  $\omega_1 \leq \omega_2$ , i.e., that the frequency of equipment 1 is lower than that of equipment 2.



(a) Two equipment items connected by a RB-FC assembly



(b) Idealized model of the connected system

**Fig. 8.7 Model of two equipment items connected by a linear RB-FC**

Expressions for the modal properties of the 2-DOF interconnected equipment system in terms of the above parameters have been derived in Der Kiureghian et al. (1999). The modal frequencies of the interconnected system,  $F_1$  and  $F_2$ , are obtained from their corresponding circular frequencies  $\Omega_1$  and  $\Omega_2$ :

$$\Omega_1 = 2\pi F_1 = \sqrt{\frac{a - \sqrt{a^2 - 4b}}{2}} \quad (8.2)$$

$$\Omega_2 = 2\pi F_2 = \sqrt{\frac{a + \sqrt{a^2 - 4b}}{2}} \quad (8.3)$$

where

$$a = \left(1 + \frac{k_0}{k_1 + k_2}\right)(\omega_1^2 + \omega_2^2) + \frac{k_0}{k_1 + k_2} \left(\frac{m_1}{m_2} \omega_1^2 + \frac{m_2}{m_1} \omega_2^2\right) \quad (8.4)$$

$$b = \left(1 + \frac{2k_0}{k_1 + k_2}\right) \omega_1^2 \omega_2^2 + \frac{k_0}{k_1 + k_2} \left(\frac{m_1}{m_2} \omega_1^4 + \frac{m_2}{m_1} \omega_2^4\right) \quad (8.5)$$

It can be verified that in general  $\omega_1 \leq \Omega_1 \leq \omega_2 \leq \Omega_2$  i.e., the first modal frequency of the connected system is bounded by the frequencies of the stand-alone equipment items, while the second

modal frequency is always greater than both stand-alone equipment frequencies. This results because by attaching the RB–FC, we have “stiffened” the system consisting of the two stand-alone equipment items. The mode shapes of the connected system (normalized to have a unit value at the attachment point of equipment item 1) are given by

$$\mathbf{\Phi} = \begin{bmatrix} 1 & 1 \\ \phi_1 & \phi_2 \end{bmatrix} \quad (8.6)$$

where

$$\phi_i = \frac{\Omega_i^2 - \omega_1^2}{\omega_2^2 - \Omega_i^2} \frac{m_1}{m_2}, \quad i = 1, 2 \quad (8.7)$$

The mode shapes associated with the interconnected system frequencies  $F_1$  and  $F_2$  are, respectively, the first and second columns in Equation (8.6). The first line of each column gives the displacement of equipment item 1, while the second line gives the displacement of equipment item 2. As stated above, these mode shapes are normalized such that the displacement of equipment item 1 is a unit value, so the values for equipment item 2 ( $\phi_1, \phi_2$ ) are relative to this unit displacement.

The connected system in general is nonclassically damped. However, it has been shown in Der Kiureghian et al. (2001) that a good approximation is obtained by neglecting the off-diagonal elements of the modal damping matrix. The result is that effective modal damping ratios of the interconnected equipment system,  $Z_1$  and  $Z_2$ , are given by

$$Z_i = \frac{c_0 + c_1 - 2c_0\phi_i + (c_0 + c_2)\phi_i^2}{2\Omega_i(m_1 + m_2\phi_i^2)}, \quad i = 1, 2 \quad (8.8)$$

With the modal properties known, the response spectrum method can be used to determine the responses of the equipment items in the connected system. Using the CQC combination rule, the maximum displacement responses of the interconnected equipment items  $j = 1$  (lower-frequency equipment item) and  $j = 2$  (higher-frequency equipment item) are given by

$$x_{\max,j} = \sqrt{A_{j,1}^2 S_d^2(F_1, Z_1) + 2\rho A_{j,1} A_{j,2} S_d(F_1, Z_1) S_d(F_2, Z_2) + A_{j,2}^2 S_d^2(F_2, Z_2)}, \quad j = 1, 2 \quad (8.9)$$

with  $\rho$  the modal correlation coefficient given by

$$\rho = \frac{8\sqrt{rZ_1Z_2}(rZ_1 + Z_2)r}{(1 - r^2)^2 + 4r(rZ_1 + Z_2)(rZ_2 + Z_1)} \quad (8.10)$$

where  $r = F_1 / F_2$  is the ratio of the modal frequencies.

In the above expressions,  $S_d(F_j, Z_j)$  is the spectral displacement for frequency  $F_j$  and damping ratio  $Z_j$  of equipment items  $j$ .  $A_{j,i}$  are the effective modal participation factors of equipment items  $j$  in the interconnected system and are given by

Equipment 1

$$A_{1,i} = \frac{\alpha_1 m_1 + \alpha_2 m_2 \phi_i}{m_1 + m_2 \phi_i^2}, \quad i = 1, 2 \quad (8.11)$$

Equipment 2

$$A_{2,i} = \left( \frac{\alpha_1 m_1 + \alpha_2 m_2 \phi_i}{m_1 + m_2 \phi_i^2} \right) \phi_i, \quad i = 1, 2 \quad (8.12)$$

To understand the effect of interaction between equipment items, we study the ratios of the maximum equipment responses in the connected system to the corresponding equipment responses in their stand-alone configurations. The latter, as derived in Section 6.2.2.2, are given by

$$x_{\max,0j} = \alpha_j S_d(f_j, \zeta_j), \quad j = 1, 2 \quad (8.13)$$

Shown in Figure 8.8 are the ratios of the maximum responses of the equipment items in the connected system to their corresponding stand-alone responses:

$$x_{\max,j} / x_{\max,0j}, \quad j = 1, 2 \quad (8.14)$$

These are plotted as a function of the ratio of equipment frequencies  $\omega_1/\omega_2 = f_1/f_2$  for selected values of the system parameters as noted in the caption of the figure. The IEEE 693 response spectrum for the moderate level (Fig. 4.4) is used.

A value greater than one for the ratio of responses implies that the seismic demand on the equipment item is amplified in account of the interaction effect; conversely, a value smaller than one indicates that the interaction tends to reduce the seismic demand on the equipment.

The following important observations can be made from Figure 8.8:

- On account of the dynamic interaction effect, the seismic demand on the lower-frequency equipment (equipment 1) is reduced relative to the demand in its stand-alone configuration, while the seismic demand on the higher-frequency equipment (equipment 2) is amplified compared to the demand in its stand-alone configuration. This is because the higher-frequency equipment item tends to act as an “anchor” for the lower-frequency equipment. The amplification in the seismic demand of the higher-frequency equipment item increases with increasing separation between the two frequencies, i.e., decreasing  $\omega_1/\omega_2$ , and with increasing stiffness of the RB–FC, i.e., increasing value of the ratio

$k_0/(k_1+k_2)$ . The amplification in the seismic demand of the higher-frequency equipment item can be as large as a factor of 4 or even higher.

- For  $\omega_1=\omega_2$ , provided  $\alpha_1=\alpha_2$ , no interaction occurs. The condition  $\alpha_1=\alpha_2$  implies that the equipment items have similar mass distributions and attachment configurations. In that case, when the equipment frequencies are identical, the two equipment items displace in phase, the RB–FC is not deformed and, hence, no interaction occurs.

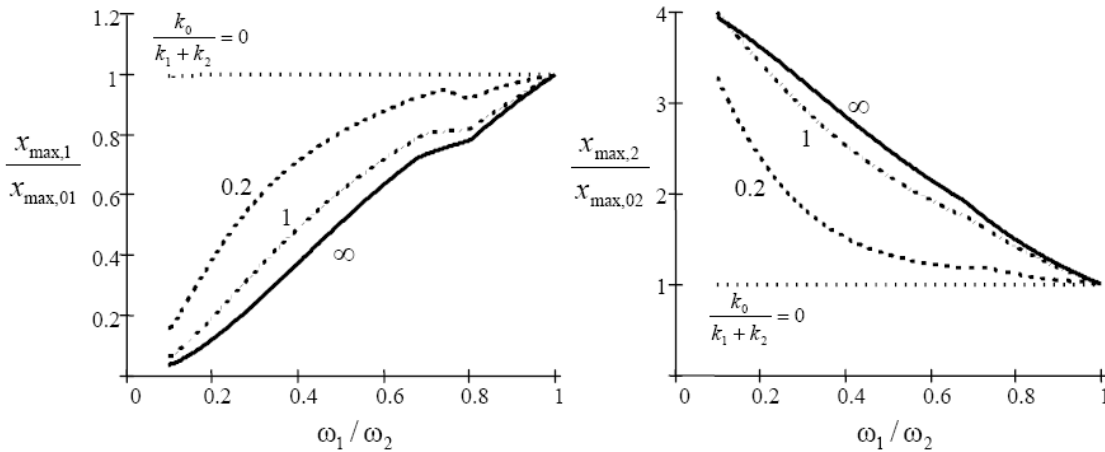


**Fig. 8.8 Influence of dynamic interaction on seismic demand of low-frequency (left) and high-frequency (right) equipment items. Parameter values are  $f_2 = \omega_2/2\pi = 10$  Hz,  $m_1/m_2 = 2$ ,  $\zeta_1 = \zeta_2 = 0.02$ ,  $\alpha_1 = \alpha_2 = 1$ , and  $c_0 = 0$ .**

Additional parametric studies reported in Der Kiureghian et al. (2001) show that the interaction effect is not significantly influenced by the shape of the response spectrum (or the locations of the equipment frequencies within the spectrum) and the damping ratios of the individual equipment items. However, the interaction effect is significantly influenced by the ratio of equipment masses, the damping of the RB–FC, and the relative magnitudes of the participation factors  $\alpha_1$  and  $\alpha_2$  of the two equipment items. Figures 8.9–8.11 show the influences of these parameters on the amplification of the seismic demand on the higher-frequency equipment item.

It can be seen from these figures that the seismic demand on the higher-frequency equipment item increases with

- increasing mass of the lower-frequency equipment item (more mass to be “anchored” by the higher-frequency equipment),
- decreasing damping of the RB–FC (less energy dissipation), and

- decreasing  $\alpha_2$  relative to  $\alpha_1$  (attachment configuration less favorable to the high-frequency equipment).

It is evident from the above analysis that the *dynamic interaction* between interconnected equipment *adversely affects the high-frequency equipment item*. While the benefit gained from the interaction for the low-frequency equipment cannot be exploited (since the equipment can be disconnected at the time of the earthquake event), the enhanced seismic demand on the high-frequency equipment must be addressed. This is done by increasing the required intensity of the support motion for the qualification of the equipment. The present section permits determining an approximation of the required amplification factor to be used in the qualification of the higher-frequency equipment under the assumption that the equipment items are interconnected by a linear rigid bus–flexible connector. The equations in this section can be used to derive graphs for any set of properties not addressed by the presented graphs.

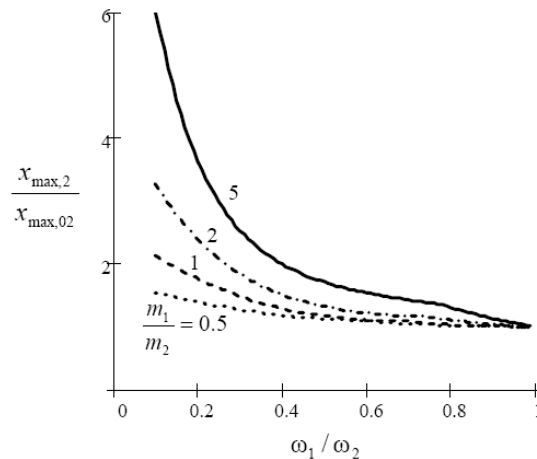


**Fig. 8.9 Influence of ratio of equipment masses on the seismic demand of high-frequency equipment. Parameter values are  $f_2 = \omega_2 / 2\pi = 10$  Hz,  $k_0 / (k_1 + k_2) = 0.2$ ,  $\zeta_1 = \zeta_2 = 0.02$ ,  $\alpha_1 = \alpha_2 = 1$ , and  $c_0 = 0$ .**

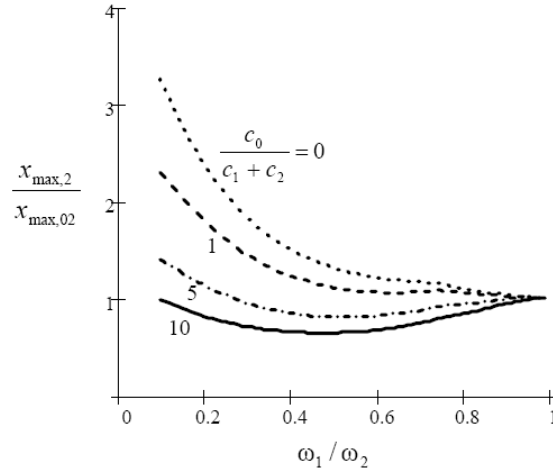


**Fig. 8.10 Influence of damping of RB–FC on the seismic demand of high-frequency equipment. Parameter values are  $f_2 = \omega_2 / 2\pi = 10$  Hz,  $k_0 / (k_1 + k_2) = 0.2$ ,  $m_1 / m_2 = 2$ ,  $\zeta_1 = \zeta_2 = 0.02$ , and  $\alpha_1 = \alpha_2 = 1$ .**

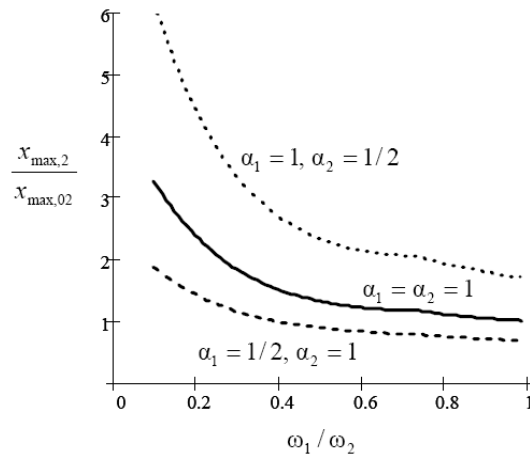


**Fig. 8.11 Influence of participation factors on the seismic demand of high-frequency equipment. Parameter values are  $f_2 = \omega_2 / 2\pi = 10$  Hz,  $k_0 / (k_1 + k_2) = 0.2$ ,  $m_1 / m_2 = 2$ ,  $\zeta_1 = \zeta_2 = 0.02$ , and  $c_0 = 0$ .**

### 8.3.3 Deformation of the Rigid Bus–Flexible Connector (RB–FC)

In addition to determining the amplification of the higher-frequency equipment as discussed above, it is important in the design to assess the deformation of the rigid bus–flexible connector. It is indeed necessary to check this deformation to determine if the adopted linear assumption is realistic and, subsequently, to determine if the applied deformation would in practice be permitted without stretching the connection beyond its limits, likely generating large impact forces. Contrary to the flexible connection case when the ratio of demand to availability,  $\beta$ ,

provided a good measure for design purposes, the elongation demand for a rigid bus–flexible connector cannot generally be well approximated using only the stand-alone displacements of the equipment items. This is because the frequencies of the two equipment items are substantially modified due to the coupling from the rigid bus connection. This is illustrated in what follows.

When the two equipment items are not connected, the maximum differential displacement (or elongation demand) can be determined in the manner described in Section 6.3, using either the SRSS method [Eq. (6.13) or (6.16)] or the CQC method [Eq. (6.14) or (6.17)]. For the sake of simplicity in the discussion that follows, we will make use of only the CQC method without the multiplication factor of 1.25 as used in Equation (6.17), so that we will be working with the mean value of the maximum differential displacement. Therefore, when the two equipment items are detached, the maximum differential displacement between them is given by Equation (6.14), which we repeat here for the sake of convenience:

$$\Delta x_{\max,0} = \sqrt{x_{\max,01}^2 - 2 \cdot \rho \cdot x_{\max,01} \cdot x_{\max,02} + x_{\max,02}^2}$$

where  $x_{\max,0j}$ ,  $j = 1,2$  are the maximum equipment displacements in their stand-alone configurations given by Equation (8.13) and  $\rho$  is the correlation coefficient between the two responses given by Equation (6.15) using the stand-alone frequencies and damping ratios.

As an example, for two equipment items with frequencies  $f_1=2$  Hz and  $f_2=5$  Hz, with damping ratios  $\zeta_1=\zeta_2=0.02$  and with modal participation factors  $\alpha_1=\alpha_2=1$ , one obtains using the IEEE 693 response spectrum for the moderate level (at the performance level):  $x_{\max,01}=0.101$  m,  $x_{\max,02}=0.016$  m and  $\Delta x_{\max,0}=0.102$  m.

In the connected system, the elongation demand (or maximum deformation) experienced by the RB–FC is obtained from the CQC modal combination rule as

$$\Delta x_{\max} = \sqrt{A_1^2 \cdot S_d^2(F_1, Z_1) + 2 \cdot \rho \cdot A_1 \cdot A_2 \cdot S_d(F_1, Z_1) \cdot S_d(F_2, Z_2) + A_2^2 \cdot S_d^2(F_2, Z_2)} \quad (8.15)$$

where  $A_i$  are the effective modal participation factors for the differential displacement given by

$$A_i = \left( \frac{\alpha_1 m_1 + \alpha_2 m_2 \phi_i}{m_1 + m_2 \phi_i^2} \right) (\phi_i - 1), \quad i = 1, 2 \quad (8.16)$$

and  $\rho$  is the cross-modal correlation coefficient given by Equation (8.10) using the interconnected system modal frequencies  $F_1, F_2$  with damping ratios  $Z_1, Z_2$ . As expected,  $\Delta x_{\max}$  is a fraction of the differential displacement between the stand-alone equipment items  $\Delta x_{\max,0}$ , as discussed at the beginning of this section. The fraction depends on the stiffness of the RB–FC and other parameters that influence the dynamic interaction between the two equipment items.

As an example, if the two equipment items described earlier have the mass ratio  $m_1/m_2=2$  and are connected with an RB–FC having the stiffness ratio  $k_0/(k_1+k_2)=0.2$ , from Equation (8.15) one obtains  $\Delta x_{\max}=0.054m$ , so that  $\Delta x_{\max}/\Delta x_{\max,0} = 0.528$ .

Figure 8.12 shows the ratio  $\Delta x_{\max}/\Delta x_{\max,0}$  as a function of the ratio of equipment frequencies for selected values of the ratio of stiffnesses  $k_0/(k_1+k_2)$ . It is observed that as the stiffness ratio  $k_0/(k_1+k_2)$  increases (i.e., the RB–FSC becomes stiffer), the ratio  $\Delta x_{\max}/\Delta x_{\max,0}$  decreases over the entire range of the ratio of frequencies.

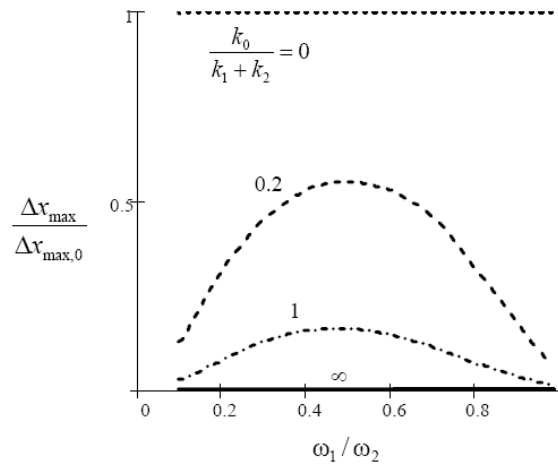


**Fig. 8.12 Deformation of the RB–FC relative to the differential displacement between stand-alone equipment items. Parameter values are  $f_2 = \omega_2/2\pi = 10$  Hz,  $m_1/m_2 = 2$ ,  $\zeta_1 = \zeta_2 = 0.02$ ,  $\alpha_1 = \alpha_2 = 1$  and  $c_0 = 0$ .**

### 8.3.4 Simplified Method to Analyze Interaction due to Nonlinear Rigid Bus Connections

Most flexible connectors used in practice with rigid buses exhibit inelastic behavior as they deform under earthquake load. Figure 8.13 shows the hysteresis loops of two flexible connectors under cyclic tests reported in Filiatrault et al. (1999) and Stearns and Filiatrault (2005). It is noted that significant inelastic action can occur even with a few centimeters of displacement. This inelastic deformation has two beneficial effects: (a) softening of the flexible connector, thereby reducing the adverse interaction effect on the high-frequency equipment and (b) dissipation of energy due to hysteretic effect, thereby reducing the overall response. These beneficial effects tend to increase with increasing intensity of the ground motion; therefore, neglecting these effects is conservative. On the other hand, inelastic action may permanently deform the flexible connector and, hence, retooling of the connector after each earthquake may

be necessary. Furthermore, the connector should be properly designed to allow the desired inelastic deformation to take place; otherwise large impact forces could be generated.

To investigate the effect of inelastic behavior on the seismic demand of the high-frequency equipment, the methods of nonlinear random vibration can be used as detailed in Song et al. (2006, 2007). In this reference, charts for the amplification factor  $x_{max,2}/x_{max,02}$  (ratio of the responses of the high-frequency equipment item in the connected and stand-alone configurations) have been developed for different sets of equipment properties, which can be used to estimate the required enhancement of the seismic demand on the equipment. Here, we suggest a simpler method based on response spectrum analysis and the formulations described in the preceding two clauses. The approach uses iterative calculations based on equivalent linear properties of the flexible connector.

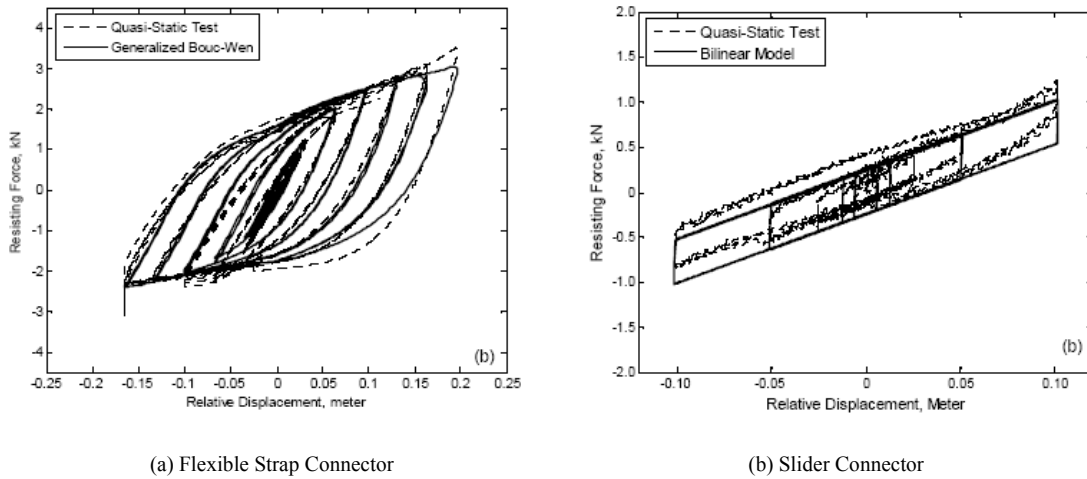


**Fig. 8.13 Hysteretic behavior of two FCs under quasi-static tests (Song et al. 2006)**

It is well known that the amount of energy dissipated in a linear viscous damper in one harmonic cycle of amplitude  $\Delta x$  and frequency  $\omega$  is

$$E_D = \pi \cdot c_0 \cdot \omega \cdot \Delta x^2 \quad (8.17)$$

where  $c_0$  is the damping coefficient (Chopra 2006).

For an inelastic RB–FC, we determine the equivalent viscous damping coefficient  $c_0$  by equating the dissipated energy  $E_D$  by the area enclosed by the force-deformation diagram of the RB–FC for a hysteresis loop having the amplitude  $\Delta x$ . Two parameters need to be determined in establishing this equivalence: the amplitude  $\Delta x$ , and the frequency  $\omega$ . From the response spectrum analysis, we have the mean maximum deformation of the RB–FC in the connected system as  $\Delta x_{max}$  from Equation (8.15). This is the mean of the maximum value over the entire

duration of the earthquake. Most cycles experienced by the RB–FC have amplitudes smaller than this maximum value. If we assume that the deformation response is a narrow-band, zero-mean Gaussian process, the local peak deformations have the Rayleigh distribution (Lutes and Sarkani 2004) with mean  $E[\Delta x] = \sqrt{\pi/2} \sigma_x$  and mean square value  $E[\Delta x^2] = 2\sigma_x^2$ , where  $\sigma_x$  is the standard deviation of the process. The latter is related to the maximum response through  $\sigma_x = \Delta x_{\max} / p$  where  $p$  is a peak factor that can be approximately set to 2 (Der Kiureghian 1980).

Thus, the expected amplitude of a cycle is

$$E[\Delta x] = \sqrt{\pi/8} \cdot \Delta x_{\max} \quad (8.18)$$

and its mean square is

$$E[\Delta x^2] = \Delta x_{\max}^2 / 2 \quad (8.19)$$

As for the second parameter, the frequency  $\omega$ , we note that the deformation of the RB–FC in the connected system is dominated by the first mode response. Hence,  $\omega = \Omega_1$  is used [Eq. (8.2)].

Thus, the expected value of the dissipated energy is

$$E_D = \pi \cdot c_0 \cdot \Omega_1 \cdot \Delta x_{\max}^2 / 2 \quad (8.20)$$

If  $A_{E[\Delta x]}$  denotes the area enclosed by the hysteresis loop of amplitude  $E[\Delta x]$ , the equivalent viscous damping coefficient is computed by setting  $A_{E[\Delta x]} = E_D$  as

$$c_0 = \frac{2 \cdot A_{E[\Delta x]}}{\pi \cdot \Omega_1 \cdot \Delta x_{\max}^2} \quad (8.21)$$

We also need to determine an equivalent stiffness  $k_0$  of the RB–FC. The hysteresis loops in Figure 8.13 clearly show softening of the RB–FC as the deformation increases. As an equivalent stiffness, we recommend using the “peak-to-peak” stiffness, as illustrated in Figure 8.14.

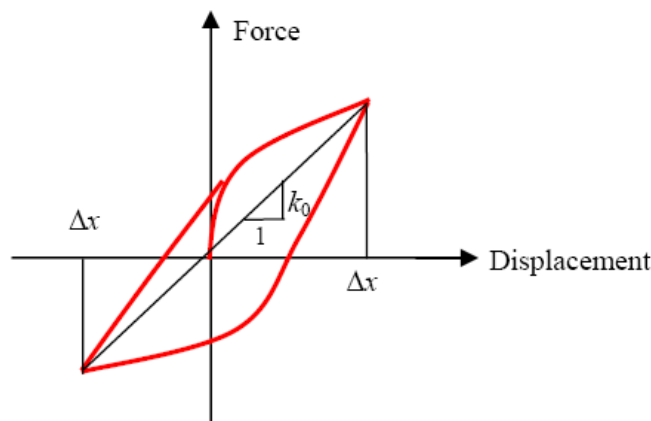


**Fig. 8.14** Definition of equivalent stiffness of RB–FC

From the results presented in the preceding section, it is clear that the parameters  $\Omega_1$  and  $\Delta x_{\max}$  are functions of the system properties, including the equivalent stiffness  $k_0$  and the damping coefficient  $c_0$ . As shown above, for a nonlinear connector the equivalent values of the latter parameters depend on the differential displacement  $\Delta x_{\max}$  as well as the shape of the hysteresis loop. Therefore, *an iterative scheme must be used* to compute these values, and the following procedure is recommended:

1. For the selected design response spectrum, use Equation (8.13) to compute the maximum displacements  $x_{\max,01}$  and  $x_{\max,02}$  of the stand-alone equipment items relative to the ground, and Equation (6.14) to compute the maximum differential displacement  $\Delta x_{\max,0}$  between the stand-alone equipment items.
2. Make an estimate of the maximum deformation  $\Delta x_{\max}$  of the RB–FC in the connected system as a fraction of  $\Delta x_{\max,0}$ . Figure 8.12 is useful for this purpose. As a rough estimate,  $\Delta x_{\max}=0.5 \cdot x_{\max,0}$  may be used.
3. Check the hysteresis loop (or the specifications of the flexible connector) to make sure that the value  $\Delta x_{\max}$  can be accommodated by the flexible connector without abrupt stiffening. If this is not the case and the estimate of  $\Delta x_{\max}$  is accurate, then a new flexible connector needs to be chosen and this step needs to be repeated.
4. Estimate the expected local peak  $E[\Delta x]$  using Equation (8.18) and determine the corresponding peak-to-peak equivalent stiffness  $k_0$  from the hysteresis loop, as exemplified in Figure 8.14 from either the experimental cyclic curve of the flexible connector or its numerical equivalent (see Song et al. 2006). Also compute the corresponding area,  $A_{E[\Delta x]}$ , of the hysteresis loop.
5. Use Equations (8.2)–(8.5), to compute the undamped modal frequencies  $\Omega_1$  and  $\Omega_2$  of the equivalent linearly connected system. Also compute the mode shapes from Equation 8.7. These calculations involve the estimated equivalent linear stiffness,  $k_0$ .
6. Compute the equivalent viscous damping coefficient of the RB–FC  $c_0$  using Equation (8.21). Using this value in Equation (8.8), compute the modal damping ratios of the equivalent linearly connected system  $Z_i, i=1,2$ .
7. With the modal properties of the equivalent system known, use Equation (8.15) to compute a new estimate for the maximum deformation of the RB–FC,  $\Delta x_{\max}$ . If this estimate is significantly different than from the last estimate, return to step 3 for a new

iteration cycle. Repeat these calculations until convergence in the computed value of  $\Delta x_{max}$  is achieved.

8. With the converged value of  $\Delta x_{max}$ , use Equation (8.9) to compute the response  $x_{max,2}$  of the higher-frequency equipment in the connected system. The ratio  $x_{max,2}/x_{max,02}$  represents the amplification in the seismic demand of the higher-frequency equipment item due to the effect of interaction between the two equipment items, approximately accounting for the nonlinear behavior of the connector. To safeguard against the adverse effect of interaction, the higher-frequency equipment item must be qualified for the design response spectrum amplified by this factor. If the amplification is too high, another flexible connector should be chosen as an alternative with enhanced structural properties that dissipate more energy and/or exhibit less stiffening; the procedure above from step 3 then needs to be repeated to evaluate the new corresponding amplification until a satisfactory design is attained.

#### 8.4 RIGID BUS CONNECTION DESIGN: EXAMPLE 1

Consider two equipment items having frequencies  $f_1 = 1$  Hz and  $f_2 = 5$  Hz, damping ratios  $\zeta_1 = \zeta_2 = 0.02$ , modal participation factors  $\alpha_1 = \alpha_2 = 1$ , and masses  $m_1 = 500$  kg and  $m_2 = 200$  kg. The corresponding stiffnesses of the equipment items are

$$k_1 = \omega_1^2 m_1 = (2\pi \times 1)^2 \times 500 = 19,740 \text{ N/m}$$

and

$$k_2 = \omega_2^2 m_2 = (2\pi \times 5)^2 \times 200 = 197,400 \text{ N/m}.$$

The corresponding viscous damping coefficients are

$$c_1 = 2\zeta_1 \omega_1 m_1 = 2 \cdot 0.02 \cdot 2\pi \cdot 1 \cdot 500 = 126 \text{ Ns/m}$$

and

$$c_2 = 2\zeta_2 \omega_2 m_2 = 2 \cdot 0.02 \cdot 2\pi \cdot 5 \cdot 200 = 251 \text{ Ns/m}$$

Suppose the equipment items are connected by an RB fitted with a flexible strap connector of the type shown in Figure 8.2b that has the hysteresis behavior shown in Figure 8.13a. The initial stiffness of this RB-FC is 35,600 N/m. We use the IEEE 693 response spectrum (Fig. 4.4) with PGA=0.5g.

### 8.4.1 Linear Analysis

Linear analysis<sup>6</sup> (Section 8.3.2) with the initial stiffness and using  $c_\theta=0$  (i.e., no damping in the RB–FC) results in the *amplification factor*  $x_{max,2}/x_{max,02}=2.07$  for the higher-frequency equipment item.

### 8.4.2 Nonlinear Analysis

In the following, we use the iterative scheme described above to obtain a more accurate estimation of the amplification factor by accounting for the inelastic behavior of the RB–FC.

#### Step 1

We calculate the stand-alone displacement of the equipment items, followed by the maximum differential displacement between them. From Equation (8.13) we calculate

$$x_{max,01} = \alpha_1 S_d(f_1, \zeta_1) = 1 \cdot S_d(1 \text{ Hz}, 0.02) = 1 \cdot 0.368 = 0.368 \text{ m}$$

and

$$x_{max,02} = \alpha_2 S_d(f_2, \zeta_2) = 1 \cdot S_d(5 \text{ Hz}, 0.02) = 1 \cdot 0.0161 = 0.0161 \text{ m}$$

From Equation (6.14) we calculate

$$\Delta x_{max,0} = \sqrt{x_{max,01}^2 - 2 \cdot \rho \cdot x_{max,01} \cdot x_{max,02} + x_{max,02}^2} = \sqrt{0.368^2 - 2 \cdot 0 \cdot 0.368 \cdot 0.0161 + 0.0161^2} \cong 0.368 \text{ m}$$

The correlation coefficient  $\rho$ , which when calculated precisely from Equation (8.10) is  $3.725 \times 10^{-4}$ , is here estimated to zero, since the frequencies of the equipment items are spaced by more than 20%. It is observed that the differential displacement is basically equal to the displacement of the lower-frequency equipment, since it is about 20 times larger than the one from the higher-frequency item.

#### Step 2

As an initial estimate of the maximum deformation in the RB–FC, we use 60% of  $\Delta x_{max,0}$ :

$$\Delta x_{max} = 0.6 \cdot x_{max,0} = 0.6 \cdot 0.368 = 0.221 \text{ m.}$$

#### Step 3: Iteration 1

We calculate the expected local peak amplitude using Equation (8.18) as

---

<sup>6</sup> We will present a more detailed linear analysis in the next example. However, the nonlinear analysis as exemplified in the following is basically a series of linear analyses.

$$E[\Delta x] = \sqrt{\pi/8} \cdot \Delta x_{\max} = 0.626 \cdot 0.221 = 0.138m .$$

For this peak deformation, using the hysteresis loop in Figure 8.13a, the peak-to-peak equivalent stiffness is estimated as

$$k_0 = 17,510 \text{ N/m}$$

and the area of the corresponding loop is estimated as

$$A_{E[\Delta x]} = 500 \text{ Nm.}$$

#### Step 4

We calculate the modal frequencies of the equivalent linearly connected system. From Equations (8.4) and (8.5) we first obtain the constants  $a$  and  $b$  using the stiffness ratio  $k_0/(k_1+k_2) = 17,510/(19,740+197,400) = 0.085$ :

$$\begin{aligned} a &= \left(1 + \frac{k_0}{k_1+k_2}\right)(\omega_1^2 + \omega_2^2) + \frac{k_0}{k_1+k_2} \left(\frac{m_1}{m_2}\omega_1^2 + \frac{m_2}{m_1}\omega_2^2\right) = \\ &= (1+0.081) \cdot ((2\pi)^2 + (10\pi)^2) + 0.081 \cdot \left(\frac{500}{200} \cdot (2\pi)^2 + \frac{200}{500} \cdot (10\pi)^2\right) = 1,149 \\ b &= \left(1 + \frac{2k_0}{k_1+k_2}\right)\omega_1^2\omega_2^2 + \frac{k_0}{k_1+k_2} \left(\frac{m_1}{m_2}\omega_1^4 + \frac{m_2}{m_1}\omega_2^4\right) = \\ &= (1+2 \cdot 0.081) \cdot ((2\pi)^2 \cdot (10\pi)^2) + 0.081 \cdot \left(\frac{500}{200} \cdot (2\pi)^4 + \frac{200}{500} \cdot (10\pi)^4\right) = 76,983 \end{aligned}$$

We then obtain the circular natural frequencies using Equations (8.2) and (8.3):

$$\Omega_1 = 2\pi F_1 = \sqrt{\frac{a - \sqrt{a^2 - 4b}}{2}} = \sqrt{\frac{1149 - \sqrt{1149^2 - 4 \cdot 76983}}{2}} = 8.452 \text{ rad/s}$$

and

$$\Omega_2 = 2\pi F_2 = \sqrt{\frac{a + \sqrt{a^2 - 4b}}{2}} = \sqrt{\frac{1149 + \sqrt{1149^2 - 4 \cdot 76983}}{2}} = 32.83 \text{ rad/s}$$

from which we obtain the modal frequencies of the linearly connected system:

$$F_1 = \frac{\Omega_1}{2\pi} = \frac{8.452}{2\pi} = 1.35 \text{ Hz}$$

and

$$F_2 = \frac{\Omega_2}{2\pi} = \frac{32.83}{2\pi} = 5.22 \text{ Hz}$$

Note that these frequencies are higher than the frequencies of the stand-alone equipment items.

### Step 5

We calculate the equivalent viscous damping ratio using Equation (8.21):

$$c_0 = \frac{2 \cdot A_{E[\Delta x]}}{\pi \cdot \Omega_1 \cdot \Delta x_{\max}^2} = \frac{2 \cdot 500}{\pi \cdot 8.452 \cdot 0.221^2} = 769 \text{ Ns/m.}$$

To obtain the modal damping ratios of the connected system  $Z_i$ , we first calculate the mode shape factors  $\phi_1$  and  $\phi_2$  using Equation (8.7):

$$\phi_1 = \frac{\Omega_1^2 - \omega_1^2}{\omega_2^2 - \Omega_1^2} \frac{m_1}{m_2} = \frac{8.452^2 - (2\pi)^2}{(10\pi)^2 - 8.452^2} \cdot \frac{500}{200} = 0.0873$$

$$\phi_2 = \frac{\Omega_2^2 - \omega_1^2}{\omega_2^2 - \Omega_2^2} \frac{m_1}{m_2} = \frac{32.83^2 - (2\pi)^2}{(10\pi)^2 - 32.83^2} \cdot \frac{500}{200} = -28.6$$

The modal damping ratios of the connected system are obtained using Equation (8.8):

$$Z_1 = \frac{c_0 + c_1 - 2c_0\phi_1 + (c_0 + c_2)\phi_1^2}{2\Omega_1(m_1 + m_2\phi_1^2)} = \frac{769 + 126 - 2 \cdot 769 \cdot 0.0873 + (769 + 251) \cdot 0.0873^2}{2 \cdot 8.452 \cdot (500 + 200 \cdot 0.0873^2)} = 0.0906$$

$$Z_2 = \frac{c_0 + c_1 - 2c_0\phi_2 + (c_0 + c_2)\phi_2^2}{2\Omega_2(m_1 + m_2\phi_2^2)} = \frac{769 + 126 - 2 \cdot 769 \cdot (-28.6) + (769 + 251) \cdot 28.6^2}{2 \cdot 32.83 \cdot (500 + 200 \cdot 28.6^2)} = 0.0816$$

These damping ratios are much higher than the modal damping ratios of the stand-alone equipment items due to the inelastic action in the RB-FC.

### Step 6

We calculate now a new estimate of the maximum deformation in the RB-FC. To do so we first calculate the spectral displacements of the connected system using the values of  $F_1$ ,  $F_2$ , and  $Z_1$ ,  $Z_2$  in the IEEE 693 response spectrum (see IEEE 2005 for calculation of the spectrum values using any value of damping) for PGA=0.5g. We obtain

$$S_d(1.35 \text{ Hz}, 0.083) = 0.139 \text{ m}$$

and

$$S_d(5.22 \text{ Hz}, 0.072) = 0.00959 \text{ m}$$

Next we calculate the effective modal participation factors for the differential displacement using Equation (8.16):

$$A_1 = \left( \frac{\alpha_1 m_1 + \alpha_2 m_2 \phi_1}{m_1 + m_2 \phi_1^2} \right) (\phi_1 - 1) = \left( \frac{1 \cdot 500 + 1 \cdot 200 \cdot 0.0873}{500 + 200 \cdot 0.0873^2} \right) \cdot (0.0873 - 1) = -0.942$$

and

$$A_2 = \left( \frac{\alpha_1 m_1 + \alpha_2 m_2 \phi_2}{m_1 + m_2 \phi_2^2} \right) (\phi_2 - 1) = \left( \frac{1 \cdot 500 + 1 \cdot 200 \cdot -28.6}{500 + 200 \cdot 28.6^2} \right) \cdot (-28.6 - 1) = 0.942$$

The new estimate for the maximum deformation is obtained using Equation (8.15):

$$\begin{aligned} \Delta x_{\max} &= \sqrt{A_1^2 \cdot S_d^2(F_1, Z_1) + 2 \cdot \rho \cdot A_1 \cdot A_2 \cdot S_d(F_1, Z_1) \cdot S_d(F_2, Z_2) + A_2^2 \cdot S_d^2(F_2, Z_2)} \\ &= \sqrt{0.942^2 \cdot 0.139^2 + 2 \cdot 0.011 \cdot -0.942 \cdot 0.942 \cdot 0.139 \cdot 0.00959 + 0.942^2 \cdot 0.00959^2} = 0.131 \text{ m} \end{aligned}$$

The correlation coefficient  $\rho$  has been calculated equal to 0.011.

It is observed that the first iteration produced an estimate of the maximum deformation, 0.131 m, significantly different from the initial estimate of 0.221 m. We therefore need to repeat the calculations from step 3 until convergence is attained, i.e., until the difference between the two iterations is small. A summary of these calculations is presented in Table 8.2. It is also observed that the converged deformation of the flexible connector, 0.0868 m, is easily within its maximum capacity, which is over 0.4 m, as also seen in Figure 8.13.

**Table 8.2 Summary of iterations for rigid bus design example 1**

Quantity	Source	Iteration 1	Iteration 2	Iteration 3	Iteration 4
$E[\Delta x]$ (m)	Equation (8.18)	0.138	0.082	0.064	0.056
$k_0$ (N/m)	Hysteresis loop	17510	25590	31880	34710
$A_{E_{flex}}$ (Nm)	Hysteresis loop	499	271	191	152
$F_1$ (Hz)	Equation (8.2)	1.35	1.46	1.54	1.57
$F_2$ (Hz)	Equation (8.3)	5.22	5.33	5.41	5.45
$c_0$ (Ns/m)	Equation (8.21)	769	1095	1220	1216
$Z_1$	Equation (8.8)	0.0906	0.105	0.105	0.0985
$Z_2$	Equation (8.8)	0.0816	0.108	0.118	0.118
$S_d(F_1, Z_1)$ (m)	Response spectrum	0.139	0.111	0.100	0.0893
$S_d(F_2, Z_2)$ (m)	Response spectrum	0.00959	0.00822	0.00767	0.00758
$A_1$	Equation (8.16)	-0.942	-0.914	-0.892	-0.882
$A_2$	Equation (8.16)	0.942	0.914	0.892	0.882
$\Delta x_{\max}$ (m)	Equation (8.15)	0.131	0.101	0.0896	0.0868

Next, using the modal properties of the converged linearized system, the responses of the two equipment items are obtained. We first evaluate the correlation coefficient  $\rho$  using Equation (8.10) with  $r = F_1/F_2 = 1.57/5.45 = 0.29$ :

$$\rho = \frac{8\sqrt{rZ_1Z_2}(rZ_2 + Z_2)r}{(1-r^2)^2 + 4r(rZ_1 + Z_2)(rZ_2 + Z_1)} = \frac{8\sqrt{0.29 \cdot 0.104 \cdot 0.118} \cdot (0.29 \cdot 0.104 + 0.118) \cdot 0.29}{(1-0.29^2)^2 + 4 \cdot 0.29 \cdot (0.29 \cdot 0.104 + 0.118)(0.29 \cdot 0.118 + 0.104)} = 0.0227$$

The modal participation factors in the interconnected system are given by Equations (8.11)–(8.12); we calculated beforehand the mode shape factors  $\varphi_1$  and  $\varphi_2$  using Equation (8.7) as  $\varphi_1 = 0.163$  and  $\varphi_2 = -15.3$ .

### Equipment 1

$$A_{1,i} = \frac{\alpha_1 m_1 + \alpha_2 m_2 \phi_i}{m_1 + m_2 \phi_i^2}, \quad i = 1, 2$$

$$A_{1,1} = \frac{\alpha_1 m_1 + \alpha_2 m_2 \phi_1}{m_1 + m_2 \phi_1^2} = \frac{1 \cdot 500 + 1 \cdot 200 \cdot 0.163}{500 + 200 \cdot 0.163^2} = 1.05$$

$$A_{1,2} = \frac{\alpha_1 m_1 + \alpha_2 m_2 \phi_2}{m_1 + m_2 \phi_2^2} = \frac{1 \cdot 500 + 1 \cdot 200 \cdot -15.3}{500 + 200 \cdot 15.3^2} = -0.0541$$

### Equipment 2

$$A_{2,i} = \left( \frac{\alpha_1 m_1 + \alpha_2 m_2 \phi_i}{m_1 + m_2 \phi_i^2} \right) \phi_i, \quad i = 1, 2$$

$$A_{2,1} = \left( \frac{\alpha_1 m_1 + \alpha_2 m_2 \phi_1}{m_1 + m_2 \phi_1^2} \right) \phi_1 = \left( \frac{1 \cdot 500 + 1 \cdot 200 \cdot 0.163}{500 + 200 \cdot 0.163^2} \right) \cdot 0.163 = 0.172$$

$$A_{2,2} = \left( \frac{\alpha_1 m_1 + \alpha_2 m_2 \phi_2}{m_1 + m_2 \phi_2^2} \right) \phi_2 = \left( \frac{1 \cdot 500 + 1 \cdot 200 \cdot -15.3}{500 + 200 \cdot 15.3^2} \right) \cdot -15.3 = 0.828$$

The required spectral displacements are extracted from the IEEE 693 response spectrum:

$$S_d(1.57 \text{ Hz}, 0.099) = 0.0983 \text{ m}$$

and

$$S_d(5.45 \text{ Hz}, 0.118) = 0.0758 \text{ m}$$

Using the results above, we can now evaluate the maximum displacement of each equipment item in its interconnected configuration, using Equation (8.9):

$$x_{\max,j} = \sqrt{A_{j,1}^2 S_d^2(F_1, Z_1) + 2\rho A_{j,1} A_{j,2} S_d(F_1, Z_1) S_d(F_2, Z_2) + A_{j,2}^2 S_d^2(F_2, Z_2)}, \quad j = 1, 2$$

$$x_{\max,1} = \sqrt{A_{1,1}^2 S_d^2(F_1, Z_1) + 2\rho A_{1,1} A_{1,2} S_d(F_1, Z_1) S_d(F_2, Z_2) + A_{1,2}^2 S_d^2(F_2, Z_2)}$$

$$= \sqrt{1.05^2 \cdot 0.0983^2 + 2 \cdot 0.0227 \cdot 1.05 \cdot -0.0541 \cdot 0.0983 \cdot 0.00758 + 0.0541^2 \cdot 0.00758^2} = 0.104 \text{ m}$$

$$x_{\max,2} = \sqrt{A_{2,1}^2 S_d^2(F_1, Z_1) + 2\rho A_{2,1} A_{2,2} S_d(F_1, Z_1) S_d(F_2, Z_2) + A_{2,2}^2 S_d^2(F_2, Z_2)}$$

$$= \sqrt{0.172^2 \cdot 0.0983^2 + 2 \cdot 0.0227 \cdot 0.172 \cdot 0.828 \cdot 0.0983 \cdot 0.00758 + 0.828^2 \cdot 0.00758^2} = 0.0182 \text{ m}$$

The response amplifications of the two equipment items in their interconnected configuration, under the assumption that the connector has the equivalent linear properties, are therefore:

$$x_{\max,1} / x_{\max,01} = 0.104 / 0.368 = 0.282$$

$$x_{\max,2} / x_{\max,02} = 0.0182 / 0.0161 = 1.13$$

It is observed that the response of the lower-frequency item is strongly de-amplified, while the response of the higher-frequency item is slightly amplified by the presence of the rigid bus/flexible connector. Based on the above analysis, the higher-frequency equipment item needs

to withstand a base motion that is 13% higher than the design ground motion used in stand-alone qualification.

It is also noted that the amplification obtained of 1.13 with the nonlinear analysis above is much lower than the value of 2.07 obtained under linear analysis, thus exemplifying the value of nonlinear analysis when the flexible connector has a hysteretic behavior, such as the one used in this example.

A detailed analysis as above may not always be necessary, e.g., when the interaction effect is small, as in many situations, or when the higher-frequency equipment item has significant reserve capacity. Charts in references Song et al. 2006, 2007) can be used to determine if the interaction effect needs special consideration.

## 8.5 RIGID BUS CONNECTION DESIGN: EXAMPLE 2

We consider here the same equipment items as in the flexible connection design example 1, Section 7.5, i.e., a 230 kV CVT (equipment item 1) interconnected with a 230 kV disconnect switch (equipment item 2). Suppose the items are connected by an RB fitted with a slider bus connector that has the hysteresis behavior shown in Figure 8.13b. In what follows, we use the properties of the bilinear model for this connector established in Song et al. (2006). This slider bus connector has a maximum stroke of  $\pm 12.7$  cm ( $\pm 5$  in.) and, preferably, its course should remain within  $\pm 10.2$  cm to ( $\pm 4$  in.) to avoid departure from the bilinear model at higher amplitudes (Stearns and Filiatrault 2005). We use the IEEE 693 response spectrum (Fig. 4.4) with  $PGA=0.5g$ .

The two equipment items have frequencies  $f_1=1.8$  Hz and  $f_2= 2.2$  Hz, damping ratios  $\zeta_1=\zeta_2=0.02$ , modal participation factors  $\alpha_1=\alpha_2=1.62$  (estimated), and masses  $m_1=1050$  kg and  $m_2=932$  kg. The corresponding stiffnesses are

$$k_1 = \omega_1^2 m_1 = (2\pi \times 1.8)^2 \times 1050 = 134,306 \text{ N/m}$$

and

$$k_2 = \omega_2^2 m_2 = (2\pi \times 2.2)^2 \times 932 = 178,082 \text{ N/m}.$$

The corresponding viscous damping coefficients are

$$c_1 = 2\zeta_1 \omega_1 m_1 = 2 \cdot 0.02 \cdot 2\pi \cdot 1.8 \cdot 1050 = 475 \text{ Ns/m}$$

and

$$c_2 = 2\zeta_2 \omega_2 m_2 = 2 \cdot 0.02 \cdot 2\pi \cdot 2.2 \cdot 932 = 515 \text{ Ns/m}.$$

### 8.5.1 Linear Analysis

We first perform a linear analysis as per Section 8.3.2 using  $c_\theta = 0$  (i.e., no damping in the RB–FC) and assuming that the linearized stiffness of the slider bus connector is equal to its post-yielding stiffness (i.e., after friction is overcome), equal to 7.71 kN/m (Song et al. 2006).

The stand-alone displacements of the equipment items have already been evaluated in Section 7.5 and are equal to

$$x_{\max,01} = 0.201 \text{ m}$$

and

$$x_{\max,02} = 0.135 \text{ m}$$

To obtain the displacements in the interconnected system, we first calculate the frequencies of the interconnected system as follows. From Equations (8.4) and (8.5) we first obtain the constants  $a$  and  $b$  using the stiffness ratio:

$$k_0 / (k_1 + k_2) = 7710 / (134306 + 178082) = 0.025$$

$$a = \left(1 + \frac{k_0}{k_1 + k_2}\right) (\omega_1^2 + \omega_2^2) + \frac{k_0}{k_1 + k_2} \left(\frac{m_1}{m_2} \omega_1^2 + \frac{m_2}{m_1} \omega_2^2\right) =$$

$$(1 + 0.025) \cdot ((2\pi \cdot 1.8)^2 + (2\pi \cdot 2.2)^2) + 0.025 \cdot \left(\frac{1050}{932} \cdot (2\pi \cdot 1.8)^2 + \frac{932}{1050} \cdot (2\pi \cdot 2.2)^2\right) = 335$$

$$b = \left(1 + \frac{2k_0}{k_1 + k_2}\right) \omega_1^2 \omega_2^2 + \frac{k_0}{k_1 + k_2} \left(\frac{m_1}{m_2} \omega_1^4 + \frac{m_2}{m_1} \omega_2^4\right) =$$

$$(1 + 2 \cdot 0.025) \cdot ((2\pi \cdot 1.8)^2 \cdot (2\pi \cdot 2.2)^2) + 0.025 \cdot \left(\frac{1050}{932} \cdot (2\pi \cdot 1.8)^4 + \frac{932}{1050} \cdot (2\pi \cdot 2.2)^4\right) = 26,902$$

We then obtain the circular natural frequencies using Equations (8.2) and (8.3):

$$\Omega_1 = 2\pi F_1 = \sqrt{\frac{a - \sqrt{a^2 - 4b}}{2}} = \sqrt{\frac{335 - \sqrt{335^2 - 4 \cdot 26933}}{2}} = 11.59 \text{ rad/s}$$

and

$$\Omega_2 = 2\pi F_2 = \sqrt{\frac{a + \sqrt{a^2 - 4b}}{2}} = \sqrt{\frac{335 + \sqrt{335^2 - 4 \cdot 26933}}{2}} = 14.15 \text{ rad/s}$$

from which we obtain the modal frequencies of the linearly connected system:

$$F_1 = \frac{\Omega_1}{2\pi} = \frac{11.58}{2\pi} = 1.84 \text{ Hz}$$

and

$$F_2 = \frac{\Omega_2}{2\pi} = \frac{14.15}{2\pi} = 2.25 \text{ Hz}$$

It is observed that the frequencies of the interconnected system are only slightly higher than the stand-alone frequencies, since the stiffness ratio  $k_0/(k_1+k_2)=0.025$  is relatively small here.

To evaluate the required effective modal damping ratios, we need to evaluate the mode shape factors  $\phi_1$  and  $\phi_2$  using Equation (8.7):

$$\phi_1 = \frac{\Omega_1^2 - \omega_1^2}{\omega_2^2 - \Omega_1^2} \frac{m_1}{m_2} = \frac{11.59^2 - (2\pi \cdot 1.8)^2}{(2\pi \cdot 2.2)^2 - 11.59^2} \cdot \frac{1050}{932} = 0.127$$

$$\phi_2 = \frac{\Omega_2^2 - \omega_1^2}{\omega_2^2 - \Omega_2^2} \frac{m_1}{m_2} = \frac{14.15^2 - (2\pi \cdot 1.8)^2}{(2\pi \cdot 2.2)^2 - 14.15^2} \cdot \frac{1050}{932} = -8.86$$

The modal damping ratios of the connected system are obtained using Equation (8.8):

$$Z_1 = \frac{c_0 + c_1 - 2c_0\phi_1 + (c_0 + c_2)\phi_1^2}{2\Omega_1(m_1 + m_2\phi_1^2)} = \frac{0 + 475 - 2 \cdot 0 \cdot 0.133 + (0 + 515) \cdot 0.127^2}{2 \cdot 11.59 \cdot (1050 + 932 \cdot 0.127^2)} = 0.0196$$

$$Z_2 = \frac{c_0 + c_1 - 2c_0\phi_2 + (c_0 + c_2)\phi_2^2}{2\Omega_2(m_1 + m_2\phi_2^2)} = \frac{0 + 475 - 2 \cdot 0 \cdot -8.86 + (0 + 515) \cdot 8.86^2}{2 \cdot 14.15 \cdot (1050 + 932 \cdot 8.86^2)} = 0.0195$$

The modal participation factors in the interconnected system are given by Equations (8.11)–(8.12):

#### Equipment 1

$$A_{1,i} = \frac{\alpha_1 m_1 + \alpha_2 m_2 \phi_i}{m_1 + m_2 \phi_i^2}, \quad i = 1, 2$$

$$A_{1,1} = \frac{\alpha_1 m_1 + \alpha_2 m_2 \phi_1}{m_1 + m_2 \phi_1^2} = \frac{1.62 \cdot 1050 + 1.62 \cdot 932 \cdot 0.127}{1050 + 932 \cdot 0.127^2} = 1.78$$

$$A_{1,2} = \frac{\alpha_1 m_1 + \alpha_2 m_2 \phi_2}{m_1 + m_2 \phi_2^2} = \frac{1.62 \cdot 1050 + 1.62 \cdot 932 \cdot -8.86}{1050 + 932 \cdot 8.86^2} = -0.157$$

#### Equipment 2

$$A_{2,i} = \left( \frac{\alpha_1 m_1 + \alpha_2 m_2 \phi_i}{m_1 + m_2 \phi_i^2} \right) \phi_i, \quad i = 1, 2$$

$$A_{2,1} = \left( \frac{\alpha_1 m_1 + \alpha_2 m_2 \phi_1}{m_1 + m_2 \phi_1^2} \right) \phi_1 = \left( \frac{1.62 \cdot 1050 + 1.62 \cdot 932 \cdot 0.127}{1050 + 932 \cdot 0.127^2} \right) \cdot 0.127 = 0.226$$

$$A_{2,2} = \left( \frac{\alpha_1 m_1 + \alpha_2 m_2 \phi_2}{m_1 + m_2 \phi_2^2} \right) \phi_2 = \left( \frac{1.62 \cdot 1050 + 1.62 \cdot 932 \cdot -8.86}{1050 + 932 \cdot 8.86^2} \right) \cdot -8.86 = 1.39$$

The required modal correlation coefficient is given by Equation (8.10) with  $r = F_1/F_2 = 1.84/2.25 = 0.819$ :

$$\rho = \frac{8\sqrt{rZ_1Z_2}(rZ_1 + Z_2)r^{3/2}}{(1-r^2)^2 + 4r(rZ_1 + Z_2)(rZ_2 + Z_1)} = \frac{8\sqrt{0.819 \cdot 0.0196 \cdot 0.0195} \cdot (0.819 \cdot 0.0196 + 0.0195) \cdot 0.819^{3/2}}{(1-0.819^2)^2 + 4 \cdot 0.819 \cdot (0.819 \cdot 0.0196 + 0.0195)(0.819 \cdot 0.0195 + 0.0196)} = 0.0365$$

The required spectral displacements are extracted from the IEEE 693 response spectrum:

$$S_d(1.84 \text{ Hz}, 0.0196) = 0.119 \text{ m}$$

and

$$S_d(2.25 \text{ Hz}, 0.0195) = 0.0798 \text{ m}$$

Using the results above and Equation (8.9), we can now evaluate the maximum displacement of each equipment item in its interconnected configuration:

$$\begin{aligned} x_{\max,j} &= \sqrt{A_{j,1}^2 S_d^2(F_1, Z_1) + 2\rho A_{j,1} A_{j,2} S_d(F_1, Z_1) S_d(F_2, Z_2) + A_{j,2}^2 S_d^2(F_2, Z_2)}, \quad j=1,2 \\ x_{\max,1} &= \sqrt{A_{1,1}^2 S_d^2(F_1, Z_1) + 2\rho A_{1,1} A_{1,2} S_d(F_1, Z_1) S_d(F_2, Z_2) + A_{1,2}^2 S_d^2(F_2, Z_2)} \\ &= \sqrt{1.78^2 \cdot 0.119^2 + 2 \cdot 0.0365 \cdot 1.78 \cdot -0.157 \cdot 0.119 \cdot 0.0798 + 0.157^2 \cdot 0.0798^2} = 0.211 \text{ m} \\ x_{\max,2} &= \sqrt{A_{2,1}^2 S_d^2(F_1, Z_1) + 2\rho A_{2,1} A_{2,2} S_d(F_1, Z_1) S_d(F_2, Z_2) + A_{2,2}^2 S_d^2(F_2, Z_2)} \\ &= \sqrt{0.226^2 \cdot 0.119^2 + 2 \cdot 0.0365 \cdot 0.226 \cdot 1.39 \cdot 0.119 \cdot 0.0798 + 1.39^2 \cdot 0.0798^2} = 0.115 \text{ m} \end{aligned}$$

The amplification factors of the two equipment items in their interconnected configuration, under the assumption that the connector is linear without damping, are therefore

$$\begin{aligned} x_{\max,1} / x_{\max,01} &= 0.211 / 0.201 = 1.05 \\ x_{\max,2} / x_{\max,02} &= 0.115 / 0.135 = 0.857 \end{aligned}$$

We observe here that the low-frequency equipment is slightly amplified, while the higher-frequency equipment is de-amplified. (There is a slight error in these results due to the neglect of non-classical damping effects. This is the reason for the slight amplification of the lower-frequency equipment item response and de-amplification of the higher-frequency equipment item response. This effect, however, is insignificant from a practical standpoint.)

We now obtain the deformation of the connector in the connected system under the linear assumption, without damping. We calculate first the effective modal participation factors for the differential displacement using Equation (8.16):

$$A_1 = \left( \frac{\alpha_1 m_1 + \alpha_2 m_2 \phi_1}{m_1 + m_2 \phi_1^2} \right) (\phi_1 - 1) = \left( \frac{1.62 \cdot 1050 + 1.62 \cdot 932 \cdot 0.127}{1050 + 932 \cdot 0.127^2} \right) \cdot (0.127 - 1) = -1.55$$

and

$$A_2 = \left( \frac{\alpha_1 m_1 + \alpha_2 m_2 \phi_2}{m_1 + m_2 \phi_2^2} \right) (\phi_2 - 1) = \left( \frac{1.62 \cdot 1050 + 1.62 \cdot 932 \cdot -8.86}{1050 + 932 \cdot 8.86^2} \right) \cdot (-8.86 - 1) = 1.55$$

The estimate for the maximum deformation is obtained using Equation (8.15):

$$\begin{aligned} \Delta x_{\max} &= \sqrt{A_1^2 \cdot S_d^2(F_1, Z_1) + 2 \cdot \rho \cdot A_1 \cdot A_2 \cdot S_d(F_1, Z_1) \cdot S_d(F_2, Z_2) + A_2^2 \cdot S_d^2(F_2, Z_2)} \\ &= \sqrt{1.55^2 \cdot 0.119^2 + 2 \cdot 0.0365 \cdot -1.55 \cdot 1.55 \cdot 0.119 \cdot 0.0198 + 1.55^2 \cdot 0.0798^2} = 0.218 \text{ m} \end{aligned}$$

### 8.5.2 Nonlinear Analysis

In the following, we use the iterative scheme described earlier to obtain a more accurate estimation of the amplification factor by accounting for the inelastic behavior of the rigid bus/slider connector. We use for  $k_0$  the peak-to-peak stiffness as defined in Figure 8.14, based on the maximum deformation in the rigid bus/slider connector. As an initial estimate of this quantity, we use 60% of the value of the deformation in the connected system under the linear assumption without damping obtained above:  $\Delta x_{max}=0.60 \cdot \Delta x_{max} = 0.6 \cdot 0.218 = 0.131$  m.

Since most of the calculations are similar to the ones presented in the linear analysis (as well as in the preceding example), only a summary of the results is presented in Table 8.3. The values of  $k_0$  and  $A_{E[x]}$  are estimated from the hysteresis loop in Figure 8.13b.

**Table 8.3 Summary of iterations for rigid bus design example 2**

Quantity	Source	Iteration 1	Iteration 2	Iteration 3
$E[\Delta x]$ (m)	Equation (8.18)	0.0821	0.118	0.123
$k_0$ (N/m)	constant	11.5e3	10.4e3	10.3e3
$A_{E[x]}$ (Nm)	Hysteresis loop	65.5	94.0	98.0
$F_1$ (Hz)	Equation (8.2)	1.86	1.86	1.86
$F_2$ (Hz)	Equation (8.3)	2.28	2.27	2.27
$c_0$ (Ns/m)	Equation (8.21)	207.7	145.1	139.2
$Z_1$	Equation (8.8)	0.0249	0.0235	0.0233
$Z_2$	Equation (8.8)	0.0294	0.0263	0.0260
$S_d(F_1, Z_1)$ (m)	Response spectrum	0.110	0.112	0.112
$S_d(F_2, Z_2)$ (m)	Response spectrum	0.0699	0.0726	0.0728
$A_1$	Equation (8.16)	-1.49	-1.51	-1.51
$A_2$	Equation (8.16)	1.49	1.51	1.51
$\Delta x_{max}$ (m)	Equation (8.15)	0.188	0.196	0.197

It is observed that the initial estimate was of  $\Delta x_{max}=0.131$  m was too low, as we converged afterwards to the value of 0.197 for the maximum deformation in the connector. This is lower than the value assumed without damping (0.218 m). This is understandable because the actual damping of the slider bus connector (which arises only from friction) is small if we compare the value of  $c_0$  here with the values obtained in the previous example with the flexible connector undergoing inelastic deformation. This can also be seen by comparing the areas in the hysteresis loops in Figure 8.13(a)–(b). For this reason the values of the damping ratios in the connected system,  $Z_1=0.0233$  and  $Z_2=0.0260$ , are only slightly higher than those of the stand-alone equipment items ( $\zeta_{1,2} = 0.02$ ). We also observe that the maximum deformation of 0.197 m is within the acceptable range permitted for this connector.

Next, using the modal properties of the converged linearized system, the responses of the two equipment items are obtained. We first evaluate the correlation coefficient  $\rho$  using Equation (8.10) with  $r=F_1/F_2=1.86/2.27=0.819$  and  $Z_1=0.0233$  and  $Z_2=0.0260$ :

$$\begin{aligned}\rho &= \frac{8\sqrt{rZ_1Z_2}(rZ_1+Z_2)r}{(1-r^2)^2+4r(rZ_1+Z_2)(rZ_2+Z_1)} \\ &= \frac{8\sqrt{0.819 \cdot 0.0233 \cdot 0.0260} \cdot (0.819 \cdot 0.0233 + 0.02260)0.819}{(1-0.819^2)^2 + 4 \cdot 0.819 \cdot (0.819 \cdot 0.0233 + 0.0260)(0.819 \cdot 0.0260 + 0.0233)} = 0.0562\end{aligned}$$

The modal participation factors in the interconnected system are different than those obtained during the linear analysis, as we note that the value of  $k_0$  was changed in the nonlinear analysis.

The required spectral displacements are extracted from the IEEE 693 response spectrum:

$$S_d(1.86 \text{ Hz}, 0.0233) = 0.112 \text{ m}$$

and

$$S_d(2.27 \text{ Hz}, 0.0260) = 0.0728 \text{ m}$$

Using the results above, we can now evaluate the maximum displacement of each equipment item in its interconnected configuration, using Equation (8.9):

$$\begin{aligned}x_{\max,j} &= \sqrt{A_{j,1}^2 S_d^2(F_1, Z_1) + 2\rho A_{j,1} A_{j,2} S_d(F_1, Z_1) S_d(F_2, Z_2) + A_{j,2}^2 S_d^2(F_2, Z_2)}, \quad j=1,2 \\ x_{\max,1} &= \sqrt{A_{1,1}^2 S_d^2(F_1, Z_1) + 2\rho A_{1,1} A_{1,2} S_d(F_1, Z_1) S_d(F_2, Z_2) + A_{1,2}^2 S_d^2(F_2, Z_2)} \\ &= \sqrt{1.82^2 \cdot 0.112^2 + 2 \cdot 0.0562 \cdot 1.82 \cdot -0.195 \cdot 0.112 \cdot 0.0728 + 0.195^2 \cdot 0.0728^2} = 0.203 \text{ m} \\ x_{\max,2} &= \sqrt{A_{2,1}^2 S_d^2(F_1, Z_1) + 2\rho A_{2,1} A_{2,2} S_d(F_1, Z_1) S_d(F_2, Z_2) + A_{2,2}^2 S_d^2(F_2, Z_2)} \\ &= \sqrt{0.302^2 \cdot 0.112^2 + 2 \cdot 0.0562 \cdot 0.302 \cdot 1.32 \cdot 0.112 \cdot 0.0728 + 1.32^2 \cdot 0.0728^2} = 0.104 \text{ m}\end{aligned}$$

The amplification of both equipment items in their interconnected configuration with damping is therefore:

$$\begin{aligned}x_{\max,1} / x_{\max,01} &= 0.203 / 0.201 = 1.01 \\ x_{\max,2} / x_{\max,02} &= 0.104 / 0.135 = 0.770\end{aligned}$$

As with the linear analysis above, we observe that the low-frequency equipment is slightly amplified, while the higher-frequency equipment is de-amplified. Therefore, we can conclude that the rigid bus/slider connector has little influence on the responses of the two equipment items. This example also shows that the interaction effect does not always result in the amplification of the higher-frequency item.

## 9 Other Considerations

### 9.1 CONSIDERATIONS OF INTEREST IN OTHER STANDARDS

IEEE Std 1527 (IEEE 2006) discusses the following other considerations that might be of interest to the users of this guide:

- type of material to use: copper versus aluminum
- corona losses
- current-carrying capacity
- fault conditions
- connection hardware

IEEE Std 605 (IEEE 2008) discusses the following that may also be of interest:

- field bending of rigid conductors
- bolted connections
- loads on bus structure including short-circuit force calculations for rigid and flexible connections
- maximum allowable spans for rigid buses
- induced vibrations and vibration attenuation

IEEE Std 693 (IEEE 2005) discusses the following that may also be of interest:

- analysis and testing methods for seismic qualification
- seismic performance criteria for electrical substation equipment

ASCE Manual No. 113 (ASCE 2008) discusses the following that may also be of interest:

- design of substation structures
- terminal connection loads for electrical equipment
- wind and ice loads
- deflection criteria

## 9.2 BIRD CAGING OF FLEXIBLE CONDUCTORS

Bird caging, or basketing, of flexible conductors is the unraveling or untwisting of outer and inner strands. It can be caused by the following:

- minimum bending radius violated
- ends being twisted opposite to direction of lay angle
- overloading of conductors due to exceptional ice or wind loads

Although not desirable, bird caging has not been found to be a cause of concern for substation operation, except at the 500 kV voltage level and up, where it can cause corona discharges. Bird caging is often present to some degree in most installations, as it may be induced during installation or over time from wind and other operational loads. It may be prevented by reinforcing the ends of the conductor near the attachment points using clamps and/or stiffeners, as shown in Figure 9.1.



**Fig. 9.1 Clamps used to prevent bird caging**

## 9.3 PREVENTION OF CLEARANCE VIOLATION WITH FLEXIBLE BUS USING RIGID BUS EXTENSIONS

As discussed in Section 3.1.2, a flexible bus must meet clearance requirements. As seen, the required slack may sometimes lead to phase to ground violation when terminal loads are horizontal. One way shown in this guide to prevent this is to use other configurations with terminal ends at 45° or 90° upward. Whenever possible, an alternative method is to extend the rigid bus past the center line of the support in the case of connections to rigid bus sections. In the case of equipment, a hybrid connection made of a short section of a rigid bus connected on one end to the terminal and on the other to a flexible bus spanning the remaining distance to the next equipment item may be a valid design as well. However, extension by rigid bus reduces the flexible bus length, since the span is shorter, and may thus reduce the available slack in the

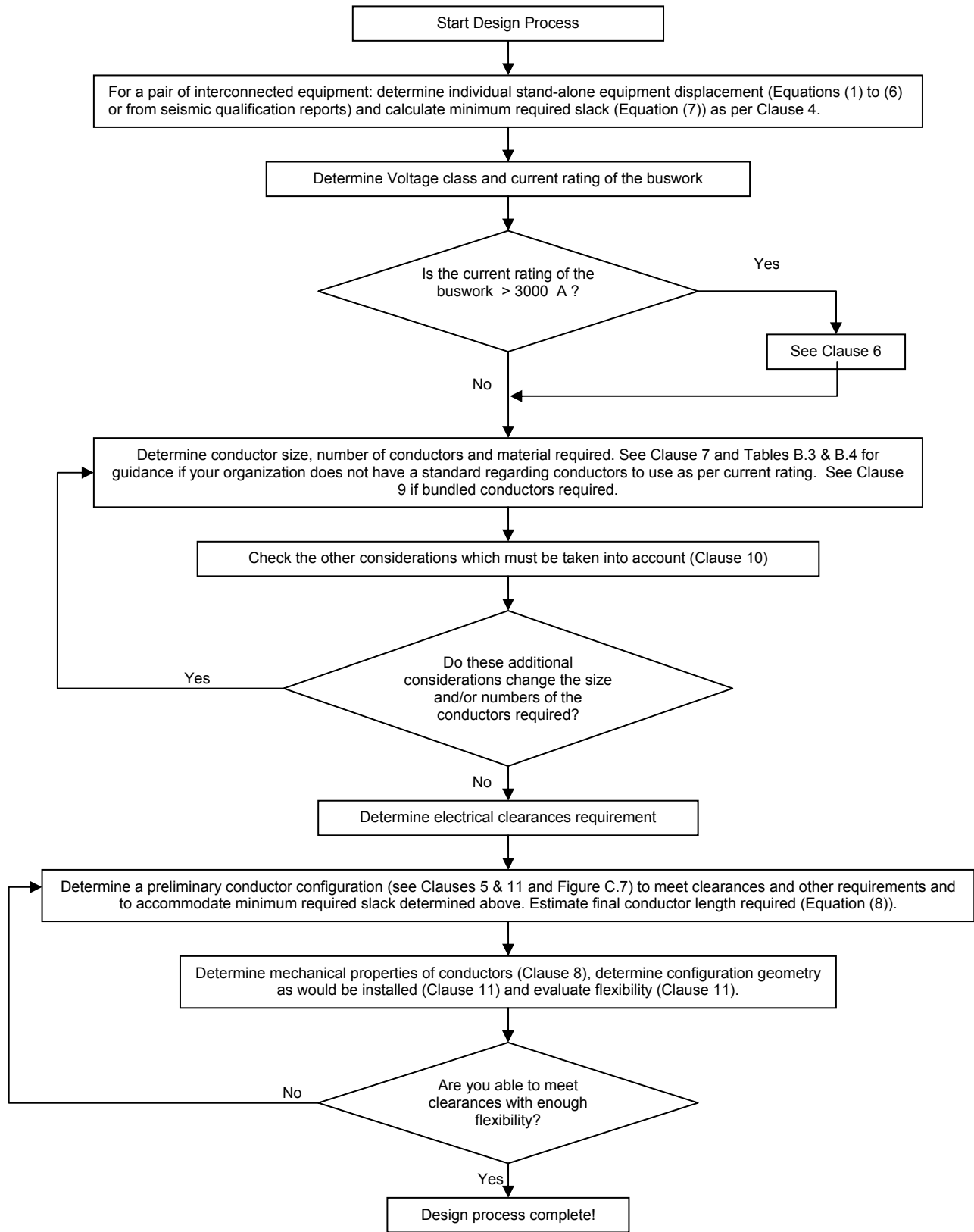
conductor. Also, this may transfer additional bending moment to the base of the insulator, as compared to a flexible bus attached directly at the terminal pad.

## REFERENCES

- ASCE 2008. *Substation Structure Design Guide*. ASCE Manuals and Reports on Engineering Practice No. 113, American Society of Civil Engineers.
- Bhuyan, G.S., H. Rainer, H. Ghalibafian, et al. 2001. *Verification of flexible conductor seismic designs*, Project report no. 2 – Project No: 12028-36, BC Hydro, Canada.
- Chopra, A. 2006. *Dynamics of structures, 3rd Edition*. New York: Prentice Hall.
- Clough, R. V., and J. Penzien. 1975. *Dynamics of Structures*. New York: McGraw-Hill.
- Dastous, J.-B. 2007. Guidelines for seismic design of flexible buswork between substation equipment. *Earthquake Engng. Struct. Dyn.*, 36(2): 191-208.
- Dastous, J.-B. 2005. Nonlinear finite-element analysis of stranded conductors with variable bending stiffness using the tangent stiffness method. *IEEE Transactions on Power Delivery*, 20(12): 328-337.
- Dastous, J.-B., A. Filiatrault, and J.-R. Pierre. 2004. Estimation of Displacement at Interconnection Points of Substation Equipment Subjected to Earthquakes. *IEEE Transactions on Power Delivery*, 19(2): 618-628.
- Dastous, J.-B., and J.-Y. Paquin. 2003. Testing and Development of Alternative Flexible-Bus Geometries for Interconnected Substation Equipment Subjected to Earthquakes. *IEEE Transactions on Power Delivery*, 18(3): 772-780.
- Dastous, J.-B., and J.-R. Pierre. 1996. Experimental investigation on the dynamic behavior of flexible conductors between substation equipment during an earthquake. *IEEE Transactions on Power Delivery*, 11(2): 801-807.
- Der Kiureghian, A., J. L. Sackman, and K.-J. Hong. 2001. Seismic interaction in linearly connected electrical substation equipment. *Earthquake Engineering and Structural Dynamics*, 30(3): 327-347.
- Der Kiureghian, A., K.-J. Hong, and J. L. Sackman. 2000. *Further studies on seismic interaction in interconnected electrical substation equipment*. Report PEER 2000/01. Berkeley, Calif.: Pacific Earthquake Engineering Research Center, University of California.
- Der Kiureghian, A., J. L. Sackman, and K.-J. Hong. 1999. *Interaction in interconnected electrical substation equipment subjected to earthquake ground motions*. Report PEER 1999/01. Berkeley, Calif.: Pacific Earthquake Engineering Research Center, University of California.
- Der Kiureghian, A. 1980. Structural response to stationary excitation. *J. Eng. Mech. Div.*, ASCE, 106(6): 1195-1213.
- EPRI. 1998. *The 1986 North Palm Springs Earthquake: Effects on Power Facilities*, EPRI report NP-5607. Palo Alto, Calif.: Electric Power Research Institute.
- Filiatrault, A., and C. Stearns. 2002. *Electrical Substation Equipment Interaction – Experimental Flexible Conductor Studies*. Report SSRP-2002/09. San Diego, Calif.: Department of Structural Engineering, Structural Systems Research Project, University of California.
- Filiatrault, A., S. Kremmidas, A. Elgamal, and F. Seible. 1999. *Substation Equipment Interaction – Rigid and Flexible Conductor Studies*. Report SSRP-99/09. San Diego, Calif.: Department of Structural Engineering, Structural Systems Research Project, University of California.
- Gualifabian, H., G. Bhuyan, et al. 2004. Seismic Behavior of Flexible Conductors connecting Substation Equipment, Part2: Shake Table Tests. *IEEE Transactions on Power Delivery*, 19(4): 1680-1687.
- Hong, K.-J., A. Der Kiureghian, and J. L. Sackman. 2005. Bending behavior of helically wrapped cables. *Journal of Engineering Mechanics (ASCE)*, 131(5):500-511. Discussion and Closure, 132(7): 790-792.
- Hong, K.-J. 2003. *Dynamic interaction in cable-connected equipment*. Ph.D. Thesis. Berkeley, Calif.: University of California.
- Hong K.-J., Der Kiureghian, A., Sackman, J. L. 2001. Seismic interaction in cable-connected equipment items. *Journal of Engineering Mechanics (ASCE)*. 127(11):1096-1105.

- IEEE 2008. *IEEE Std 605-2008, IEEE Guide for Design of Substation Bus Structures*. Institute of Electrical and Electronics Engineers. Piscataway. NJ.
- IEEE 2006. *IEEE Std 1527-2006. IEEE Recommended Practice for the Design of Flexible Buswork Located in Seismically Active Areas*. Institute of Electrical and Electronics Engineers. Piscataway. NJ.
- IEEE 2005. *IEEE Std 693-2005, IEEE Recommended Practice for Seismic Design of Substations*. Institute of Electrical and Electronics Engineers. Piscataway. NJ.
- IEEE 2001. *IEEE Std. C2-2002- National Electrical Safety Code* . Institute of Electrical and Electronics Engineers. Piscataway. NJ.
- Lutes, L.D., and S. Sarkani. 2004. *Random Vibrations: Analysis of Structural and Mechanical Systems*, Burlington, Mass.: Elsevier Butterworth-Heinemann.
- NIST 1996. *The January 17, 1995 Hyogoken-Nanbu (Kobe) Earthquake: Performance of Structures, Lifelines, and Fire Protection Systems*. NIST Special Publication 901.
- Okada, T., T. Misaki, et alter. 1986. *Seismic design of connecting leads in open-air type substations*. Report 23-04, Paris: CIGRE.
- Opsetmoen, T., 1998. *Aluminum Stranded Bus Connection – Flexibility Investigation*. BC Hydro, Canada.
- Pierre, J.-R. 1991. First experience concerning the seismic behavior of an electric power system in Eastern North America. *Proceedings of the 3<sup>rd</sup> U.S. Conference on Lifeline Earthquake Engineering*. pp.266-274.
- Schiff, A. 1998. *Guide to Improved Earthquake Performance of Electric Power Systems*, Report NIST GCR 98-757.
- Song, J., A. Der Kiureghian, and J. L. Sackman. 2007. Seismic interaction in electrical substation equipment connected by nonlinear rigid bus conductors. *Earthquake Engineering and Structural Dynamics*, 36(2): 167-190.
- Song, J., A. Der Kiureghian, and J. L. Sackman. 2006. *Seismic Response and Reliability of Electrical Substation Equipment and Systems*. Report PEER 2005/16. Berkeley, Calif.: Pacific Earthquake Engineering Research Center, University of California.
- Starkel, D. L., M. Wendelin, and L. Kempner. 1998. *Seismic Evaluation – Seismic Connection with Rigid Bus Conductor*. Portland. Wa.: Dept. of Civil Engineering. Portland State University.
- Stearns, C., and A. Filiatrault. 2005. *Electrical Substation Equipment Interaction – Experimental rigid conductor studies*. Report PEER 2004/09. Berkeley, Calif.: Pacific Earthquake Engineering Research Center, University of California.
- Stevenson, R.B., and G. J. Beattie. 1990. *In-plane stiffness tests and wind simulation tests on a quad cicada stranded conductor and twin cicada stranded conductor*. Central Laboratories report 90-25239. New Zealand.
- Zienkiewicz, O.C. and R. L. Taylor, R.L. 2000. *The finite element method. Volume 2. Solid mechanics. Fifth edition*, Oxford: Butterworth-Heinemann.

**Appendix A: General Design Tree for Flexible  
Connection from IEEE Std 1527-  
2006**



Note: Not shown in this Figure from IEEE-1527 is the need to check terminal pad connection capacities in regards to the estimated terminal loads.

## **Appendix B: FEAP Input Files for Flexible Configuration Examples**

## Example of stability of inverse parabola of 6 m — *Newton-Raphson* equilibrium method

```

ex_stability.txt                                2008-12-15

FEAP * example 3 trial #2 equilibrium position
0,0,0,3,6,2      ! 3D problem with 6 dof/node and 2 nodes/element
GLOB
FINITE ! finite deformation formulation for beam element (large displ.)
reference,node,1,1,1

COOR           ! initial coordinates
1 1 0 0 0
65 0 9.425 0 0

ELEM           ! element definition
1 1 1 1 2
64 0 1 64 65

BOUN           ! boundary conditions
1 0 1 1 1 1 1 1
65 0 1 1 1 1 1 1

DISP           ! displacements applied at beginning and end nodes
1 0 0.000 0.000 0 0 0 1.57080
65 0 -3.425 0.000 0 0 0 -1.57080

FORCE         ! vertical force for weight
2 1 0 -7.902 0
64 0 0 -7.902 0

FPRO          ! reference to function numbers for displacements and forces applied
1 0 0 0 0 0 0 30
2 1 0 5 0 0 0 0
64 0 0 5 0 0 0 0
65 0 10 20 0 0 0 30

MATE, 1,4000 kcmil
FRAME
ELASTIC ISOTROPIC 69.9e9 0.3
CROSS SECTION 0.203E-02 0.117E-08 0.117E-08 0.000E+00 0.234E-08

END

batch
plot,mesh
prop,,5      ! function to apply weight
prop,,10     ! function to apply horizontal displacement of end#2
prop,,20     ! function to apply vertical displacement of end#2
prop,,30     ! function to apply rotatino of end#1
tol,,1.d-12  ! solution tolerance
dt,,1
loop,time,4000 !we only apply the duration to apply the displacements
time
loop,iter,20
tang,,1      ! Newton-Raphson method
next,iter

next,time
disp,all
end
2,4          ! function 5 definition
0,0,4000,0,4100,1,0,0
2,5          ! function 10 definition
0,0,100,0,4000,1,4100,1,0,0
2,5          ! function 20 definition
0,0,100,0,4000,1,4100,1,0,0
2,4          ! function 30 definition
0,0,4000,1,4100,1,0,0
end
inter
stop

```

## Example of stability of inverse parabola of 6 m — *Arc length* equilibrium method

```
ex_stability_arc_method.txt                                2008-12-15

FEAP * example 3 trial #2 equilibrium position
0,0,0,3,6,2      ! 3D problem with 6 dof/node and 2 nodes/element
GLOB
FINITE ! finite deformation formulation for beam element (large displ.)
reference,node,1,1,1

COOR          ! initial coordinates calculated from ex_stability.txt
1      0      0      0      0
2      0      3.62E-03 0.14722      0
3      0      1.44E-02 0.29409      0
4      0      3.25E-02 0.44025      0
5      0      5.76E-02 0.58535      0
6      0      8.99E-02 0.72904      0
7      0      0.12913 0.87097 0
8      0      0.17535 1.0108 0
9      0      0.22827 1.1482 0
10     0      0.288 1.2829 0
11     0      0.3542 1.4144 0
12     0      0.4267 1.5426 0
13     0      0.5055 1.667 0
14     0      0.5903 1.7874 0
15     0      0.6808 1.9035 0
16     0      0.777 2.015 0
17     0      0.8786 2.1217 0
18     0      0.9852 2.2233 0
19     0      1.0967 2.3195 0
20     0      1.2127 2.4101 0
21     0      1.3331 2.4949 0
22     0      1.4576 2.5737 0
23     0      1.5856 2.6463 0
24     0      1.7172 2.7126 0
25     0      1.8518 2.7723 0
26     0      1.9892 2.8253 0
27     0      2.129 2.8715 0
28     0      2.271 2.9108 0
29     0      2.4146 2.943 0
30     0      2.5598 2.9682 0
31     0      2.7059 2.9863 0
32     0      2.8527 2.9971 0
33     0      3 3.0007 0
34     0      3.1473 2.9971 0
35     0      3.2941 2.9863 0
36     0      3.4402 2.9682 0
37     0      3.5854 2.943 0
38     0      3.729 2.9108 0
39     0      3.871 2.8715 0
40     0      4.0108 2.8253 0
41     0      4.1482 2.7723 0
42     0      4.2828 2.7126 0
43     0      4.4144 2.6463 0
44     0      4.5424 2.5737 0
45     0      4.6669 2.4949 0
46     0      4.7873 2.4101 0
47     0      4.9033 2.3195 0
48     0      5.0148 2.2233 0
49     0      5.1215 2.1217 0
50     0      5.223 2.015 0
51     0      5.3192 1.9035 0
52     0      5.4097 1.7874 0
53     0      5.4945 1.667 0
54     0      5.5733 1.5426 0
55     0      5.6458 1.4144 0
56     0      5.712 1.2829 0
57     0      5.7717 1.1482 0
58     0      5.8246 1.0108 0
```

```

59      0      5.8709  0.87097  0
60      0      5.9102  0.72904  0
61      0      5.9423  0.58535  0
62      0      5.9675  0.44025  0
63      0      5.9856  0.29409  0
64      0      5.9964  0.14722  0
65      0      6      0      0

ELEM      ! element definition
  1      1      2      1      2
64      0      2      64      65

BOUN      ! boundary conditions
  1      0      1      1      1      1      1      1
65      0      1      1      1      1      1      1

DISP      ! displacements applied at beginning and end nodes
  1      0      0.000      0.000  0  0  0  0.
65      0      0.000      0.000  0  0  0  0.

FORCE     ! vertical force for weight
  2      1      0      -7.902  0
64      0      0      -7.902  0

MATE, 2,4000 MC
FRAME
ELASTIC ISOTROPIC 69.9e9 0.3
CROSS SECTION 0.203E-02 0.117E-08 0.117E-08 0.000E+00 0.233E-08

END

batch
plot,mesh
tplot
tol,,1d-16
arclength      ! arc length method
dt,,0.01
loop,time,2157      ! number of steps to obtain a prop. load of 1.
                    time
                    loop,iter,100
                    tang,,1
                    next,iter

next,time
disp,all
end
arcl,33,2      !output of proportional load vs mid-span displacement
stop

```

## Example 1: Calculation of equilibrium position

```
exl_equilibrium.txt                                2008-11-11

FEAP * example 1 equilibrium position
0,0,0,3,6,2      ! 3D problem with 6 dof/node and 2 nodes/element
GLOB
FINITE ! finite deformation formulation for beam element (large displ.)
reference,node,1,1,1

COOR           ! initial coordinates
1  1  0  0  0
65 0  3.320 0  0

ELEM           ! element definition
1  1  1  1  1  2
64 0  1  64 65

BOUN           ! boundary conditions
1  0  1  1  1  1  1  1
65 0  1  1  1  1  1  1

DISP           ! displacements applied at beginning and end nodes
1  0  0.000  0.000  0  0  0  0
65 0  -0.362  0.246  0  0  0  0

FORCE ! vertical force for weight
2  1  0  -1.606  0
64 0  0  -1.606  0

FPRO ! reference to function numbers for displacements and forces applied
1  0  0  0  0  0  0  0
2  1  0  5  0  0  0  0
64 0  0  5  0  0  0  0
65 0  10 20 0  0  0  0

MATE, 1,2300 kcmil
FRAME
ELASTIC ISOTROPIC 69.9e9 0.3
CROSS SECTION 0.117E-02 0.178E-08 0.178E-08 0.000E+00 0.356E-08

END

batch
plot,mesh
prop,,5      ! function to apply weight
prop,,10     ! function to apply horizontal displacement of end#2
prop,,20     ! function to apply vertical displacement of end#2
tol,,1.d-8   ! solution tolerance
dt,,1
loop,time,2600
            time
            loop,iter,20
            tang,,1      ! Newton-Raphson method
            next,iter

next,time
disp,all
end
2,4      ! function 5 definition
0,0,100,1,1100,1,0,0
2,5      ! function 10 definition
0,0,100,0,2100,1,2600,1,0,0
2,4      ! function 20 definition
0,0,2100,0,2600,1,0,0
end
inter
stop
```

## Example 1: Calculation of elongation curve under cyclic displacement of +/- 0.297 m

```
ex1_elongation.txt                                2008-11-11

FEAP * example 1 elongation curve under cyclic displ.of +/- 0.297 m
0,0,0,3,6,2      ! 3D problem with 6 dof/node and 2 nodes/element
GLOB
FINITE ! finite deformation formulation for beam element (large displ.)
reference,node,1,1,1

COOR           ! initial coordinates
1  1  0  0  0
65 0  3.320 0 0

ELEM           ! element definition
1  1  1  1  1  2
64 0  1  64 65

BOUN           ! boundary conditions
1  0  1  1  1  1  1  1
65 0  1  1  1  1  1  1

DISP           ! displacements applied at beginning and end nodes
1  0  0.000  0.000 0 0 0 0
65 0 -0.362  0.246 0 0 0 0

FORCE ! vertical force for self-weight
2  1  0 -1.606  0
64 0  0 -1.606  0

FPRO ! reference to function numbers for displacements and forces applied
1  0  0  0  0  0  0  0
2  1  0  5  0  0  0  0
64 0  0  5  0  0  0  0
65 0  10 20 0  0  0  0

MATE, 1,2300 kcmil
FRAME
ELASTIC ISOTROPIC 69.9e9 0.3
CROSS SECTION 0.117E-02 0.178E-08 0.178E-08 0.000E+00 0.356E-08

END

batch
plot,mesh
prop,,5      ! function to apply weight and ice
prop,,10     ! function to apply horizontal displacement of end#2
prop,,20     ! function to apply vertical displacement of end#2
tol,,1.d-8   ! solution tolerance
dt,,1
loop,time,10600
    time
    loop,iter,20
        tang,,1      ! Newton-Raphson method
    next,iter
next,time
disp,all
end
2,4          ! function 5 definition
0,0,100,1,10600,1,0,0
2,8          ! function 10 definition
0,0,100,0,2100,1,2600,1,4600,1.8204,8600,0.1796,10600,1,0,0
2,5          ! function 20 definition
0,0,2100,0,2600,1,10600,1,0,0
end
inter
stop
```

## Example 1: Calculation of equilibrium position under 45 mm radial ice

```
exl_ice_45mm.txt                                2008-11-11

FEAP * example 1 equilibrium position under 45 mm radial ice
0,0,0,3,6,2      ! 3D problem with 6 dof/node and 2 nodes/element
GLOB
FINITE ! finite deformation formulation for beam element (large displ.)
reference,node,1,1,1

COOR           ! initial coordinates
1  1  0  0  0
65 0  3.320 0 0

ELEM           ! element definition
1  1  1  1  1  2
64 0  1  64 65

BOUN           ! boundary conditions
1  0  1  1  1  1  1  1
65 0  1  1  1  1  1  1

DISP           ! displacements applied at beginning and end nodes
1  0  0.000  0.000 0 0 0 0
65 0 -0.362  0.246 0 0 0 0

FORCE ! vertical force for self-weight and ice
2  1  0 -7.395  0
64 0  0 -7.395  0

FPRO ! reference to function numbers for displacements and forces applied
1  0  0  0  0  0  0  0
2  1  0  5  0  0  0  0
64 0  0  5  0  0  0  0
65 0  10 20 0  0  0  0

MATE, 1,2300 kcmil
FRAME
ELASTIC ISOTROPIC 69.9e9 0.3
CROSS SECTION 0.117E-02 0.178E-08 0.178E-08 0.000E+00 0.356E-08

END

batch
plot,mesh
prop,,5      ! function to apply weight and ice
prop,,10     ! function to apply horizontal displacement of end#2
prop,,20     ! function to apply vertical displacement of end#2
tol,,1.d-8   ! solution tolerance
dt,,1
loop,time,2600
    time
    loop,iter,20
        tang,,1      ! Newton-Raphson method
    next,iter
next,time
disp,all
end
2,4          ! function 5 definition
0,0,100,1,1100,1,0,0
2,5          ! function 10 definition
0,0,100,0,2100,1,2600,1,0,0
2,4          ! function 20 definition
0,0,2100,0,2600,1,0,0
end
inter
stop
```

## Example 1: Calculation of equilibrium position under a 160 km/hr wind

```

ex1_wind_160kmhr.txt                                2008-11-11

FEAP * example 1 equilibrium position under 160 km/hr wind
0,0,0,3,6,2      ! 3D problem with 6 dof/node and 2 nodes/element
GLOB
FINITE ! finite deformation formulation for beam element (large displ.)
reference,node,1,1,1

COOR              ! initial coordinates
1  1  0  0  0
65 0  3.320 0 0

ELEM              ! element definition
1  1  1  1  1  2
64 0  1  64 65

BOUN              ! boundary conditions
1  0  1  1  1  1  1  1
65 0  1  1  1  1  1  1

DISP              ! displacements applied at beginning and end nodes
1  0  0.000  0.000 0 0 0 0
65 0 -0.362  0.246 0 0 0 0

FORCE             ! vertical force for weight; lateral force for wind
2  1  0  -1.606  2.496
64 0  0  -1.606  2.496

FPRO              ! reference to function numbers for displacements and forces applied
1  0  0  0  0  0  0  0
2  1  0  5  30 0 0 0
64 0  0  5  30 0 0 0
65 0  10 20 0  0 0 0

MATE, 1,2300 kcmil
FRAME
ELASTIC ISOTROPIC 69.9e9 0.3
CROSS SECTION 0.117E-02 0.178E-08 0.178E-08 0.000E+00 0.356E-08

END

batch
plot,mesh
prop,,5          ! function to apply weight
prop,,10         ! function to apply horizontal displacement of end#2
prop,,20        ! function to apply vertical displacement of end#2
prop,,30        ! function to apply wind force
tol,,1.d-8      ! solution tolerance
dt,,1
loop,time,4700
    time
    loop,iter,20
        tang,,1          ! Newton-Raphson method
    next,iter

next,time
disp,all
end
2,5              ! function 5 definition
0,0,100,1,5000,1,50000,1,0,0
2,5              ! function 10 definition
0,0,100,0,3600,1,5000,1,0,0
2,5              ! function 20 definition
0,0,3600,0,4600,1,5000,1,0,0
2,5              ! function 30 definition
0,0,3600,0,4600,0,4700,1,0,0
end
inter
stop

```

## Example 2, trial 1: Calculation of equilibrium position

```

ex2#1_equilibrium.txt                                2008-11-11

FEAP * example 2 trial #1 equilibrium position
0,0,0,3,6,2      ! 3D problem with 6 dof/node and 2 nodes/element
GLOB
FINITE ! finite deformation formulation for beam element (large displ.)
reference,node,1,1,1

COOR           ! initial coordinates
1  1  0  0  0
65 0  4.800 0  0

ELEM           ! element definition
1  1  1  1  1  2
64 0  1  64 65

BOUN           ! boundary conditions
1  0  1  1  1  1  1  1
65 0  1  1  1  1  1  1

DISP           ! displacements applied at beginning and end nodes
1  0  0.000  0.000  0  0  0  0
65 0 -0.800 -0.090  0  0  0  0

FORCE ! vertical force for weight
2  1  0 -4.025  0
64 0  0 -4.025  0

FPRO ! reference to function numbers for displacements and forces applied
1  0  0  0  0  0  0  0
2  1  0  5  0  0  0  0
64 0  0  5  0  0  0  0
65 0  10 20 0  0  0  0

MATE, 1,4000 kcmil
FRAME
ELASTIC ISOTROPIC 69.9e9 0.3
CROSS SECTION 0.203E-02 0.117E-08 0.117E-08 0.000E+00 0.234E-08

END

batch
plot,mesh
prop,,5      ! function to apply weight
prop,,10     ! function to apply horizontal displacement of end#2
prop,,20     ! function to apply vertical displacement of end#2
tol,,1.d-8   ! solution tolerance
dt,,1
loop,time,4600
      time
      loop,iter,20
            tang,,1      ! Newton-Raphson method
      next,iter
next,time
disp,all
end
2,4      ! function 5 definition
0,0,100,1,4600,1,0,0
2,5      ! function 10 definition
0,0,100,0,4100,1,4600,1,0,0
2,4      ! function 20 definition
0,0,4100,0,4600,1,0,0
end
inter
stop

```

## Example 2, trial 2: Calculation of equilibrium position

```

ex2#2_equilibrium.txt                                2008-11-11

FEAP * example 2 trial #2 equilibrium position
0,0,0,3,6,2      ! 3D problem with 6 dof/node and 2 nodes/element
GLOB
FINITE ! finite deformation formulation for beam element (large displ.)
reference,node,1,1,1

COOR           ! initial coordinates
1  1  0  0  0
65 0  4.900 0  0

ELEM           ! element definition
1  1  1  1  1  2
64 0  1  64 65

BOUN           ! boundary conditions
1  0  1  1  1  1  1  1
65 0  1  1  1  1  1  1

DISP           ! displacements applied at beginning and end nodes
1  0  0.000  0.000  0  0  0  0.7854
65 0 -0.900 -0.090  0  0  0 -0.7854

FORCE         ! vertical force for weight
2  1  0  -4.108  0
64 0  0  -4.108  0

FPRO         ! reference to function numbers for displacements and forces applied
1  0  0  0  0  0  0  30
2  1  0  5  0  0  0  0
64 0  0  5  0  0  0  0
65 0  10 20 0  0  0  30

MATE, 1,4000 kcmil
FRAME
ELASTIC ISOTROPIC 69.9e9 0.3
CROSS SECTION 0.203E-02 0.117E-08 0.117E-08 0.000E+00 0.234E-08

END

batch
plot,mesh
prop,,5      ! function to apply weight
prop,,10     ! function to apply horizontal displacement of end#2
prop,,20     ! function to apply vertical displacement of end#2
prop,,30     ! function to apply rotations at both ends
tol,,1.d-12  ! solution tolerance
dt,,1
loop,time,8600
      time
      loop,iter,20
            tang,,1      ! Newton-Raphson method
      next,iter

next,time
disp,all
end
2,4      ! function 5 definition
0,0,100,1,8600,1,0,0
2,5      ! function 10 definition
0,0,100,0,4100,1,8600,1,0,0
2,5      ! function 20 definition
0,0,4100,0,4600,1,8600,1,0,0
2,5      ! function 30 definition
0,0,4100,0,4600,0,8600,1,0,0
end
inter
stop

```

## Example 2, trial 3: Calculation of equilibrium position

```

ex2#3_equilibrium.txt                                2008-11-12

FEAP * example 2 trial #3 equilibrium position
0,0,0,3,6,2      ! 3D problem with 6 dof/node and 2 nodes/element
GLOB
FINITE ! finite deformation formulation for beam element (large displ.)
reference,node,1,1,1

COOR           ! initial coordinates
1 1 0 0 0
65 0 6.731 0 0

ELEM           ! element definition
1 1 1 1 2
64 0 1 64 65

BOUN           ! boundary conditions
1 0 1 1 1 1 1 1
65 0 1 1 1 1 1 1

DISP           ! displacements applied at beginning and end nodes
1 0 0.000 0.000 0 0 0 1.57080
65 0 -2.731 -0.090 0 0 0 -1.57080

FORCE ! vertical force for weight
2 1 0 -5.564 0
64 0 0 -5.564 0

FPRO ! reference to function numbers for displacements and forces applied
1 0 0 0 0 0 0 30
2 1 0 5 0 0 0 0
64 0 0 5 0 0 0 0
65 0 10 20 0 0 0 30

MATE, 1,4000 kcmil
FRAME
ELASTIC ISOTROPIC 69.9e9 0.3
CROSS SECTION 0.203E-02 0.117E-08 0.117E-08 0.000E+00 0.234E-08

END

batch
plot,mesh
prop,,5      ! function to apply weight
prop,,10     ! function to apply horizontal displacement of end#2
prop,,20     ! function to apply vertical displacement of end#2
prop,,30     ! function to apply rotations at both ends
tol,,1.d-12  ! solution tolerance
dt,,1
loop,time,4100
      time
      loop,iter,20
            tang,,1      ! Newton-Raphson method
      next,iter

next,time
disp,all
end
2,4      ! function 5 definition
0,0,4000,0,4100,1,0,0
2,5      ! function 10 definition
0,0,100,0,4000,1,4100,1,0,0
2,5      ! function 20 definition
0,0,100,0,4000,1,4100,1,0,0
2,4      ! function 30 definition
0,0,4000,1,4100,1,0,0
inter
stop

```

## Example 2, trial 3: Calculation of elongation curve under cyclic displacement of +/- 0.748 m

```

ex2#3_elongation.txt                                2008-11-12

FEAP * example 2 elongation curve under cyclic displ.of +/- 0.748 m
0,0,0,3,6,2      ! 3D problem with 6 dof/node and 2 nodes/element
GLOB
FINITE ! finite deformation formulation for beam element (large displ.)
reference,node,1,1,1

COOR          ! initial coordinates
1 1 0 0 0
65 0 6.731 0 0

ELEM          ! element definition
1 1 1 1 2
64 0 1 64 65

BOUN          ! boundary conditions
1 0 1 1 1 1 1 1
65 0 1 1 1 1 1 1

DISP          ! displacements applied at beginning and end nodes
1 0 0.000 0.000 0 0 0 1.57080
65 0 -2.731 -0.090 0 0 0 -1.57080

FORCE ! vertical force for weight
2 1 0 -5.564 0
64 0 0 -5.564 0

FPRO ! reference to function numbers for displacements and forces applied
1 0 0 0 0 0 0 30
2 1 0 5 0 0 0 0
64 0 0 5 0 0 0 0
65 0 10 20 0 0 0 30

MATE, 1,4000 kcmil
FRAME
ELASTIC ISOTROPIC 69.9e9 0.3
CROSS SECTION 0.203E-02 0.117E-08 0.117E-08 0.000E+00 0.234E-08

END

batch
plot,mesh
prop,,5      ! function to apply weight
prop,,10     ! function to apply horizontal displacement of end#2
prop,,20     ! function to apply vertical displacement of end#2
prop,,30     ! function to apply rotations at both ends
tol,,1.d-12  ! solution tolerance
dt,,1
loop,time,12100
      time
      loop,iter,20
            tang,,1      ! Newton-Raphson method
      next,iter

next,time
disp,all
end
2,5      ! function 5 definition
0,0,4000,0,4100,1,12100,1,0,0
2,8      ! function 10 definition
0,0,100,0,4000,1,4100,1,6100,1.31548,10100,0.68542,12100,1,0,0
2,5      ! function 20 definition
0,0,100,0,4000,1,12100,1,0,0
2,4      ! function 30 definition
0,0,4000,1,12100,1,0,0
inter
stop

```

## Example 2, trial 3: Calculation of equilibrium position under a 90 km/hr wind

```

ex2#3_wind_90kmhr.txt                                2008-11-12

FEAP * example 2 trial #3 equilibrium position under 90 km/hr wind
0,0,0,3,6,2      ! 3D problem with 6 dof/node and 2 nodes/element
GLOB
FINITE ! finite deformation formulation for beam element (large displ.)
reference,node,1,1,1

COOR           ! initial coordinates
1  1  0  0  0
65 0  6.731 0 0

ELEM           ! element definition
1  1  1  1  1  2
64 0  1  64 65

BOUN           ! boundary conditions
1  0  1  1  1  1  1  1
65 0  1  1  1  1  1  1

DISP           ! displacements applied at beginning and end nodes
1  0  0.000  0.000  0  0  0  1.57080
65 0  -2.731  -0.090  0  0  0  -1.57080

FORCE ! vertical force for weight; lateral force for wind
2  1  0  -5.564  1.997
64 0  0  -5.564  1.997

FPRO ! reference to function numbers for displacements and forces applied
1  0  0  0  0  0  0  30
2  1  0  5  40  0  0  0
64 0  0  5  40  0  0  0
65 0  10  20  0  0  0  30

MATE, 1,4000 kcmil
FRAME
ELASTIC ISOTROPIC 69.9e9 0.3
CROSS SECTION 0.203E-02 0.117E-08 0.117E-08 0.000E+00 0.234E-08

END

batch
plot,mesh
prop,,5      ! function to apply weight
prop,,10     ! function to apply horizontal displacement of end#2
prop,,20     ! function to apply vertical displacement of end#2
prop,,30     ! function to apply rotations at both ends
prop,,40     ! function to apply wind force
tol,,1.d-12 ! solution tolerance
dt,,1
loop,time,4200
                time
                loop,iter,20
                    tang,,1      ! Newton-Raphson method
                next,iter

next,time
disp,all
end
2,5      ! function 5 definition
0,0,4000,0,4100,1,4200,1,0,0
2,5      ! function 10 definition
0,0,100,0,4000,1,4200,1,0,0
2,5      ! function 20 definition
0,0,100,0,4000,1,4200,1,0,0
2,4      ! function 30 definition
0,0,4000,1,4200,1,0,0
2,4      ! function 40 definition
0,0,4100,0,4200,1,0,0

```

### Example 3, trial 1: Calculation of equilibrium position

```

ex3#1_equilibrium.txt                                2008-11-14

FEAP * example 3 trial #1 equilibrium position
0,0,0,3,6,2      ! 3D problem with 6 dof/node and 2 nodes/element
GLOB
FINITE ! finite deformation formulation for beam element (large displ.)
reference,node,1,1,1

COOR           ! initial coordinates
1  1  0  0  0
65 0  3.920 0 0

ELEM           ! element definition
1  1  1  1  1  2
64 0  1  64 65

BOUN           ! boundary conditions
1  0  1  1  1  1  1  1
65 0  1  1  1  1  1  1

DISP           ! displacements applied at beginning and end nodes
1  0  0.000  0.000 0 0 0 0
65 0 -1.128  2.059 0 0 0 0

FORCE          ! vertical force for weight
2  1  0  -3.287  0
64 0  0  -3.287  0

FPRO          ! reference to function numbers for displacements and forces applied
1  0  0  0  0  0  0  0
2  1  0  5  0  0  0  0
64 0  0  5  0  0  0  0
65 0  10 20 0  0  0  0

MATE, 1,4000 kcmil
FRAME
ELASTIC ISOTROPIC 69.9e9 0.3
CROSS SECTION 0.203E-02 0.117E-08 0.117E-08 0.000E+00 0.234E-08

END

batch
plot,mesh
prop,,5      ! function to apply weight
prop,,10     ! function to apply horizontal displacement of end#2
prop,,20     ! function to apply vertical displacement of end#2
tol,,1.d-12  ! solution tolerance
dt,,1
loop,time,3100
    time
    loop,iter,20
        tang,,1      ! Newton-Raphson method
    next,iter
next,time
disp,all
end
2,4          ! function 5 definition
0,0,100,1,100000,1,0,0
2,5          ! function 10 definition
0,0,100,0,2100,1,10000,1,0,0
2,5          ! function 20 definition
0,0,2100,0,3100,1,0,0
end
inter
stop

```

### Example 3, trial 2: Calculation of equilibrium position

```

ex3#2_equilibrium.txt                                2008-11-17

FEAP * example 3 trial #2 equilibrium position
0,0,0,3,6,2      ! 3D problem with 6 dof/node and 2 nodes/element
GLOB
FINITE ! finite deformation formulation for beam element (large displ.)
reference,node,1,1,1

COOR           ! initial coordinates
1  1  0  0  0
65 0  3.840 0  0

ELEM           ! element definition
1  1  1  1  1  2
64 0  1  64 65

BOUN           ! boundary conditions
1  0  1  1  1  1  1  1
65 0  1  1  1  1  1  1

DISP           ! displacements applied at beginning and end nodes
1  0  0.000  0.000  0  0  0  1.5708
65 0  -1.048  1.830  0  0  0  0

FORCE         ! vertical force for weight
2  1  0  -3.220  0
64 0  0  -3.220  0

FPRO         ! reference to function numbers for displacements and forces applied
1  0  0  0  0  0  0  30
2  1  0  5  0  0  0  0
64 0  0  5  0  0  0  0
65 0  10 20 0  0  0  0

MATE, 1,4000 kcmil
FRAME
ELASTIC ISOTROPIC 69.9e9 0.3
CROSS SECTION 0.203E-02 0.117E-08 0.117E-08 0.000E+00 0.234E-08

END

batch
plot,mesh
prop,,5      ! function to apply weight
prop,,10     ! function to apply horizontal displacement of end#2
prop,,20     ! function to apply vertical displacement of end#2
prop,,30     ! function to apply rotatino of end#1
tol,,1.d-12 ! solution tolerance
dt,,1
loop,time,4100
      time
      loop,iter,20
            tang,,1      ! Newton-Raphson method
      next,iter

next,time
disp,all
end
2,4      ! function 5 definition
0,0,4000,0,4100,1,0,0
2,5      ! function 10 definition
0,0,100,0,4000,1,4100,1,0,0
2,5      ! function 20 definition
0,0,100,0,4000,1,4100,1,0,0
2,4      ! function 30 definition
0,0,4000,1,4100,1,0,0
end
inter
stop

```

### Example 3, trial 2: Calculation of elongation curve under cyclic displacement of +/- 0.397 m

```

ex3#2_elongation.txt                                2008-11-17

FEAP * example 3 elongation curve under cyclic displ.of +/- 0.397 m
0,0,0,3,6,2      ! 3D problem with 6 dof/node and 2 nodes/element
GLOB
FINITE ! finite deformation formulation for beam element (large displ.)
reference,node,1,1,1

COOR           ! initial coordinates
1  1  0  0  0
65 0  3.840 0 0

ELEM           ! element definition
1  1  1  1  1  2
64 0  1  64 65

BOUN           ! boundary conditions
1  0  1  1  1  1  1  1
65 0  1  1  1  1  1  1

DISP           ! displacements applied at beginning and end nodes
1  0  0.000  0.000 0 0 0 1.5708
65 0 -1.048  1.830 0 0 0 0

FORCE ! vertical force for weight
2  1  0 -3.220 0
64 0  0 -3.220 0

FPRO ! reference to function numbers for displacements and forces applied
1  0  0  0  0  0  0  30
2  1  0  5  0  0  0  0
64 0  0  5  0  0  0  0
65 0  10 20 0  0  0  0

MATE, 1,4000 kcmil
FRAME
ELASTIC ISOTROPIC 69.9e9 0.3
CROSS SECTION 0.203E-02 0.117E-08 0.117E-08 0.000E+00 0.234E-08

END

batch
plot,mesh
prop,,5      ! function to apply weight
prop,,10     ! function to apply horizontal displacement of end#2
prop,,20     ! function to apply vertical displacement of end#2
prop,,30     ! function to apply rotation at end#1
tol,,1.d-12  ! solution tolerance
dt,,1
loop,time,12100
      time
      loop,iter,20
            tang,,1      ! Newton-Raphson method
      next,iter

next,time
disp,all
end
2,5      ! function 5 definition
0,0,4000,0,4100,1,12100,1,0,0
2,8      ! function 10 definition
0,0,100,0,4000,1,4100,1,6100,1.3788,10100,0.6212,12100,1,0,0
2,5      ! function 20 definition
0,0,100,0,4000,1,12100,1,0,0
2,4      ! function 30 definition
0,0,4000,1,12100,1,0,0
inter
stop

```

### Example 3, trial 2: Calculation of equilibrium position under a 48 km/hr wind and 6.35 mm radial ice

```

ex3#2_wind&ice.txt                                2008-11-17

FEAP * example 3 trial #2 equilibrium position under concurrent wind and ice
0,0,0,3,6,2    ! 3D problem with 6 dof/node and 2 nodes/element
GLOB
FINITE ! finite deformation formulation for beam element (large displ.)
reference,node,1,1,1

COOR          ! initial coordinates
1  1  0      0  0
65 0  3.840  0  0

ELEM          ! element definition
1  1  1  1  1  2
64 0  1  64 65

BOUN          ! boundary conditions
1  0  1  1  1  1  1  1
65 0  1  1  1  1  1  1

DISP          ! displacements applied at beginning and end nodes
1  0  0.000  0.000  0  0  0  1.5708
65 0  -1.048  1.830  0  0  0  0

FORCE        ! vertical force for weight (including ice); lateral force for wind
2  1  0  -3.906  -0.417
64 0  0  -3.906  -0.417

FPRO        ! reference to function numbers for displacements and forces applied
1  0  0  0  0  0  0  0  30
2  1  0  5  40  0  0  0
64 0  0  5  40  0  0  0
65 0  10  20  0  0  0  0

MATE, 1,4000 kcmil
FRAME
ELASTIC ISOTROPIC 69.9e9 0.3
CROSS SECTION 0.203E-02 0.117E-08 0.117E-08 0.000E+00 0.234E-08

END

batch
plot,mesh
prop,,5      ! function to apply weight
prop,,10     ! function to apply horizontal displacement of end#2
prop,,20     ! function to apply vertical displacement of end#2
prop,,30     ! function to apply rotatino of end#1
prop,,40     ! function to apply wind force
tol,,1.d-12 ! solution tolerance
dt,,1
loop,time,4200
                time
                loop,iter,20
                    tang,,1      ! Newton-Raphson method
                next,iter

next,time
disp,all
end
2,5           ! function 5 definition
0,0,4000,0,4100,0.8244,4200,1,0,0
2,5           ! function 10 definition
0,0,100,0,4000,1,4200,1,0,0
2,5           ! function 20 definition
0,0,100,0,4000,1,4200,1,0,0
2,4           ! function 30 definition
0,0,4000,1,4200,1,0,0
2,4           ! function 40 definition
0,0,4100,0,4200,1,0,0

```

## PEER REPORTS

PEER reports are available individually or by yearly subscription. PEER reports can be ordered at [http://peer.berkeley.edu/publications/peer\\_reports.html](http://peer.berkeley.edu/publications/peer_reports.html) or by contacting the Pacific Earthquake Engineering Research Center, 1301 South 46<sup>th</sup> Street, Richmond, CA 94804-4698. Tel.: (510) 665-3448; Fax: (510) 665-3456; Email: [peer\\_editor@berkeley.edu](mailto:peer_editor@berkeley.edu)

- PEER 2010/04** *Application Guide for the Design of Flexible and Rigid Bus Connections between Substation Equipment Subjected to Earthquakes.* Jean-Bernard Dastous and Armen Der Kiureghian. September 2010.
- PEER 2010/03** *Shear Wave Velocity as a Statistical Function of Standard Penetration Test Resistance and Vertical Effective Stress at Caltrans Bridge Sites.* Scott J. Brandenburg, Naresh Bellana, and Thomas Shantz. June 2010.
- PEER 2010/02** *Stochastic Modeling and Simulation of Ground Motions for Performance-Based Earthquake Engineering.* Sanaz Rezaeian and Armen Der Kiureghian. June 2010.
- PEER 2010/01** *Structural Response and Cost Characterization of Bridge Construction Using Seismic Performance Enhancement Strategies.* Ady Aviram, Božidar Stojadinović, Gustavo J. Parra-Montesinos, and Kevin R. Mackie. March 2010.
- PEER 2009/03** *The Integration of Experimental and Simulation Data in the Study of Reinforced Concrete Bridge Systems Including Soil-Foundation-Structure Interaction.* Matthew Dryden and Gregory L. Fenves. November 2009.
- PEER 2009/02** *Improving Earthquake Mitigation through Innovations and Applications in Seismic Science, Engineering, Communication, and Response. Proceedings of a U.S.-Iran Seismic Workshop.* October 2009.
- PEER 2009/01** *Evaluation of Ground Motion Selection and Modification Methods: Predicting Median Interstory Drift Response of Buildings.* Curt B. Haselton, Ed. June 2009.
- PEER 2008/10** *Technical Manual for Strata.* Albert R. Kottke and Ellen M. Rathje. February 2009.
- PEER 2008/09** *NGA Model for Average Horizontal Component of Peak Ground Motion and Response Spectra.* Brian S.-J. Chiou and Robert R. Youngs. November 2008.
- PEER 2008/08** *Toward Earthquake-Resistant Design of Concentrically Braced Steel Structures.* Patxi Uriz and Stephen A. Mahin. November 2008.
- PEER 2008/07** *Using OpenSees for Performance-Based Evaluation of Bridges on Liquefiable Soils.* Stephen L. Kramer, Pedro Arduino, and HyungSuk Shin. November 2008.
- PEER 2008/06** *Shaking Table Tests and Numerical Investigation of Self-Centering Reinforced Concrete Bridge Columns.* Hyung IL Jeong, Junichi Sakai, and Stephen A. Mahin. September 2008.
- PEER 2008/05** *Performance-Based Earthquake Engineering Design Evaluation Procedure for Bridge Foundations Undergoing Liquefaction-Induced Lateral Ground Displacement.* Christian A. Ledezma and Jonathan D. Bray. August 2008.
- PEER 2008/04** *Benchmarking of Nonlinear Geotechnical Ground Response Analysis Procedures.* Jonathan P. Stewart, Annie On-Lei Kwok, Youssef M. A. Hashash, Neven Matasovic, Robert Pyke, Zhiliang Wang, and Zhaohui Yang. August 2008.
- PEER 2008/03** *Guidelines for Nonlinear Analysis of Bridge Structures in California.* Ady Aviram, Kevin R. Mackie, and Božidar Stojadinović. August 2008.
- PEER 2008/02** *Treatment of Uncertainties in Seismic-Risk Analysis of Transportation Systems.* Evangelos Stergiou and Anne S. Kiremidjian. July 2008.
- PEER 2008/01** *Seismic Performance Objectives for Tall Buildings.* William T. Holmes, Charles Kircher, William Petak, and Nabih Youssef. August 2008.
- PEER 2007/12** *An Assessment to Benchmark the Seismic Performance of a Code-Conforming Reinforced Concrete Moment-Frame Building.* Curt Haselton, Christine A. Goulet, Judith Mitrani-Reiser, James L. Beck, Gregory G. Deierlein, Keith A. Porter, Jonathan P. Stewart, and Ertugrul Taciroglu. August 2008.
- PEER 2007/11** *Bar Buckling in Reinforced Concrete Bridge Columns.* Wayne A. Brown, Dawn E. Lehman, and John F. Stanton. February 2008.
- PEER 2007/10** *Computational Modeling of Progressive Collapse in Reinforced Concrete Frame Structures.* Mohamed M. Talaat and Khalid M. Mosalam. May 2008.
- PEER 2007/09** *Integrated Probabilistic Performance-Based Evaluation of Benchmark Reinforced Concrete Bridges.* Kevin R. Mackie, John-Michael Wong, and Božidar Stojadinović. January 2008.
- PEER 2007/08** *Assessing Seismic Collapse Safety of Modern Reinforced Concrete Moment-Frame Buildings.* Curt B. Haselton and Gregory G. Deierlein. February 2008.

- PEER 2007/07** *Performance Modeling Strategies for Modern Reinforced Concrete Bridge Columns.* Michael P. Berry and Marc O. Eberhard. April 2008.
- PEER 2007/06** *Development of Improved Procedures for Seismic Design of Buried and Partially Buried Structures.* Linda Al Atik and Nicholas Sitar. June 2007.
- PEER 2007/05** *Uncertainty and Correlation in Seismic Risk Assessment of Transportation Systems.* Renee G. Lee and Anne S. Kiremidjian. July 2007.
- PEER 2007/04** *Numerical Models for Analysis and Performance-Based Design of Shallow Foundations Subjected to Seismic Loading.* Sivapalan Gajan, Tara C. Hutchinson, Bruce L. Kutter, Prishati Raychowdhury, José A. Ugalde, and Jonathan P. Stewart. May 2008.
- PEER 2007/03** *Beam-Column Element Model Calibrated for Predicting Flexural Response Leading to Global Collapse of RC Frame Buildings.* Curt B. Haselton, Abbie B. Liel, Sarah Taylor Lange, and Gregory G. Deierlein. May 2008.
- PEER 2007/02** *Campbell-Bozorgnia NGA Ground Motion Relations for the Geometric Mean Horizontal Component of Peak and Spectral Ground Motion Parameters.* Kenneth W. Campbell and Yousef Bozorgnia. May 2007.
- PEER 2007/01** *Boore-Atkinson NGA Ground Motion Relations for the Geometric Mean Horizontal Component of Peak and Spectral Ground Motion Parameters.* David M. Boore and Gail M. Atkinson. May 2007.
- PEER 2006/12** *Societal Implications of Performance-Based Earthquake Engineering.* Peter J. May. May 2007.
- PEER 2006/11** *Probabilistic Seismic Demand Analysis Using Advanced Ground Motion Intensity Measures, Attenuation Relationships, and Near-Fault Effects.* Polsak Tothong and C. Allin Cornell. March 2007.
- PEER 2006/10** *Application of the PEER PBEE Methodology to the I-880 Viaduct.* Sashi Kunnath. February 2007.
- PEER 2006/09** *Quantifying Economic Losses from Travel Forgone Following a Large Metropolitan Earthquake.* James Moore, Sungbin Cho, Yue Yue Fan, and Stuart Werner. November 2006.
- PEER 2006/08** *Vector-Valued Ground Motion Intensity Measures for Probabilistic Seismic Demand Analysis.* Jack W. Baker and C. Allin Cornell. October 2006.
- PEER 2006/07** *Analytical Modeling of Reinforced Concrete Walls for Predicting Flexural and Coupled-Shear-Flexural Responses.* Kutay Orakcal, Leonardo M. Massone, and John W. Wallace. October 2006.
- PEER 2006/06** *Nonlinear Analysis of a Soil-Drilled Pier System under Static and Dynamic Axial Loading.* Gang Wang and Nicholas Sitar. November 2006.
- PEER 2006/05** *Advanced Seismic Assessment Guidelines.* Paolo Bazzurro, C. Allin Cornell, Charles Menun, Maziar Motahari, and Nicolas Luco. September 2006.
- PEER 2006/04** *Probabilistic Seismic Evaluation of Reinforced Concrete Structural Components and Systems.* Tae Hyung Lee and Khalid M. Mosalam. August 2006.
- PEER 2006/03** *Performance of Lifelines Subjected to Lateral Spreading.* Scott A. Ashford and Teerawat Juirnarongrit. July 2006.
- PEER 2006/02** *Pacific Earthquake Engineering Research Center Highway Demonstration Project.* Anne Kiremidjian, James Moore, Yue Yue Fan, Nesrin Basoz, Ozgur Yazali, and Meredith Williams. April 2006.
- PEER 2006/01** *Bracing Berkeley. A Guide to Seismic Safety on the UC Berkeley Campus.* Mary C. Comerio, Stephen Tobriner, and Ariane Fehrenkamp. January 2006.
- PEER 2005/16** *Seismic Response and Reliability of Electrical Substation Equipment and Systems.* Junho Song, Armen Der Kiureghian, and Jerome L. Sackman. April 2006.
- PEER 2005/15** *CPT-Based Probabilistic Assessment of Seismic Soil Liquefaction Initiation.* R. E. S. Moss, R. B. Seed, R. E. Kayen, J. P. Stewart, and A. Der Kiureghian. April 2006.
- PEER 2005/14** *Workshop on Modeling of Nonlinear Cyclic Load-Deformation Behavior of Shallow Foundations.* Bruce L. Kutter, Geoffrey Martin, Tara Hutchinson, Chad Harden, Sivapalan Gajan, and Justin Phalen. March 2006.
- PEER 2005/13** *Stochastic Characterization and Decision Bases under Time-Dependent Aftershock Risk in Performance-Based Earthquake Engineering.* Gee Liek Yeo and C. Allin Cornell. July 2005.
- PEER 2005/12** *PEER Testbed Study on a Laboratory Building: Exercising Seismic Performance Assessment.* Mary C. Comerio, editor. November 2005.
- PEER 2005/11** *Van Nuys Hotel Building Testbed Report: Exercising Seismic Performance Assessment.* Helmut Krawinkler, editor. October 2005.
- PEER 2005/10** *First NEES/E-Defense Workshop on Collapse Simulation of Reinforced Concrete Building Structures.* September 2005.

- PEER 2005/09** *Test Applications of Advanced Seismic Assessment Guidelines.* Joe Maffei, Karl Telleen, Danya Mohr, William Holmes, and Yuki Nakayama. August 2006.
- PEER 2005/08** *Damage Accumulation in Lightly Confined Reinforced Concrete Bridge Columns.* R. Tyler Ranf, Jared M. Nelson, Zach Price, Marc O. Eberhard, and John F. Stanton. April 2006.
- PEER 2005/07** *Experimental and Analytical Studies on the Seismic Response of Freestanding and Anchored Laboratory Equipment.* Dimitrios Konstantinidis and Nicos Makris. January 2005.
- PEER 2005/06** *Global Collapse of Frame Structures under Seismic Excitations.* Luis F. Ibarra and Helmut Krawinkler. September 2005.
- PEER 2005/05** *Performance Characterization of Bench- and Shelf-Mounted Equipment.* Samit Ray Chaudhuri and Tara C. Hutchinson. May 2006.
- PEER 2005/04** *Numerical Modeling of the Nonlinear Cyclic Response of Shallow Foundations.* Chad Harden, Tara Hutchinson, Geoffrey R. Martin, and Bruce L. Kutter. August 2005.
- PEER 2005/03** *A Taxonomy of Building Components for Performance-Based Earthquake Engineering.* Keith A. Porter. September 2005.
- PEER 2005/02** *Fragility Basis for California Highway Overpass Bridge Seismic Decision Making.* Kevin R. Mackie and Božidar Stojadinović. June 2005.
- PEER 2005/01** *Empirical Characterization of Site Conditions on Strong Ground Motion.* Jonathan P. Stewart, Yoojoong Choi, and Robert W. Graves. June 2005.
- PEER 2004/09** *Electrical Substation Equipment Interaction: Experimental Rigid Conductor Studies.* Christopher Stearns and André Filiatrault. February 2005.
- PEER 2004/08** *Seismic Qualification and Fragility Testing of Line Break 550-kV Disconnect Switches.* Shakhzod M. Takhirov, Gregory L. Fenves, and Eric Fujisaki. January 2005.
- PEER 2004/07** *Ground Motions for Earthquake Simulator Qualification of Electrical Substation Equipment.* Shakhzod M. Takhirov, Gregory L. Fenves, Eric Fujisaki, and Don Clyde. January 2005.
- PEER 2004/06** *Performance-Based Regulation and Regulatory Regimes.* Peter J. May and Chris Koski. September 2004.
- PEER 2004/05** *Performance-Based Seismic Design Concepts and Implementation: Proceedings of an International Workshop.* Peter Fajfar and Helmut Krawinkler, editors. September 2004.
- PEER 2004/04** *Seismic Performance of an Instrumented Tilt-up Wall Building.* James C. Anderson and Vitelmo V. Bertero. July 2004.
- PEER 2004/03** *Evaluation and Application of Concrete Tilt-up Assessment Methodologies.* Timothy Graf and James O. Malley. October 2004.
- PEER 2004/02** *Analytical Investigations of New Methods for Reducing Residual Displacements of Reinforced Concrete Bridge Columns.* Junichi Sakai and Stephen A. Mahin. August 2004.
- PEER 2004/01** *Seismic Performance of Masonry Buildings and Design Implications.* Kerri Anne Taeko Tokoro, James C. Anderson, and Vitelmo V. Bertero. February 2004.
- PEER 2003/18** *Performance Models for Flexural Damage in Reinforced Concrete Columns.* Michael Berry and Marc Eberhard. August 2003.
- PEER 2003/17** *Predicting Earthquake Damage in Older Reinforced Concrete Beam-Column Joints.* Catherine Pagni and Laura Lowes. October 2004.
- PEER 2003/16** *Seismic Demands for Performance-Based Design of Bridges.* Kevin Mackie and Božidar Stojadinović. August 2003.
- PEER 2003/15** *Seismic Demands for Nondeteriorating Frame Structures and Their Dependence on Ground Motions.* Ricardo Antonio Medina and Helmut Krawinkler. May 2004.
- PEER 2003/14** *Finite Element Reliability and Sensitivity Methods for Performance-Based Earthquake Engineering.* Terje Haukaas and Armen Der Kiureghian. April 2004.
- PEER 2003/13** *Effects of Connection Hysteretic Degradation on the Seismic Behavior of Steel Moment-Resisting Frames.* Janise E. Rodgers and Stephen A. Mahin. March 2004.
- PEER 2003/12** *Implementation Manual for the Seismic Protection of Laboratory Contents: Format and Case Studies.* William T. Holmes and Mary C. Comerio. October 2003.
- PEER 2003/11** *Fifth U.S.-Japan Workshop on Performance-Based Earthquake Engineering Methodology for Reinforced Concrete Building Structures.* February 2004.

- PEER 2003/10** *A Beam-Column Joint Model for Simulating the Earthquake Response of Reinforced Concrete Frames.* Laura N. Lowes, Nilanjan Mitra, and Arash Altoontash. February 2004.
- PEER 2003/09** *Sequencing Repairs after an Earthquake: An Economic Approach.* Marco Casari and Simon J. Wilkie. April 2004.
- PEER 2003/08** *A Technical Framework for Probability-Based Demand and Capacity Factor Design (DCFD) Seismic Formats.* Fatemeh Jalayer and C. Allin Cornell. November 2003.
- PEER 2003/07** *Uncertainty Specification and Propagation for Loss Estimation Using FOSM Methods.* Jack W. Baker and C. Allin Cornell. September 2003.
- PEER 2003/06** *Performance of Circular Reinforced Concrete Bridge Columns under Bidirectional Earthquake Loading.* Mahmoud M. Hachem, Stephen A. Mahin, and Jack P. Moehle. February 2003.
- PEER 2003/05** *Response Assessment for Building-Specific Loss Estimation.* Eduardo Miranda and Shahram Taghavi. September 2003.
- PEER 2003/04** *Experimental Assessment of Columns with Short Lap Splices Subjected to Cyclic Loads.* Murat Melek, John W. Wallace, and Joel Conte. April 2003.
- PEER 2003/03** *Probabilistic Response Assessment for Building-Specific Loss Estimation.* Eduardo Miranda and Hesameddin Aslani. September 2003.
- PEER 2003/02** *Software Framework for Collaborative Development of Nonlinear Dynamic Analysis Program.* Jun Peng and Kincho H. Law. September 2003.
- PEER 2003/01** *Shake Table Tests and Analytical Studies on the Gravity Load Collapse of Reinforced Concrete Frames.* Kenneth John Elwood and Jack P. Moehle. November 2003.
- PEER 2002/24** *Performance of Beam to Column Bridge Joints Subjected to a Large Velocity Pulse.* Natalie Gibson, André Filiatrault, and Scott A. Ashford. April 2002.
- PEER 2002/23** *Effects of Large Velocity Pulses on Reinforced Concrete Bridge Columns.* Greg L. Orozco and Scott A. Ashford. April 2002.
- PEER 2002/22** *Characterization of Large Velocity Pulses for Laboratory Testing.* Kenneth E. Cox and Scott A. Ashford. April 2002.
- PEER 2002/21** *Fourth U.S.-Japan Workshop on Performance-Based Earthquake Engineering Methodology for Reinforced Concrete Building Structures.* December 2002.
- PEER 2002/20** *Barriers to Adoption and Implementation of PBEE Innovations.* Peter J. May. August 2002.
- PEER 2002/19** *Economic-Engineered Integrated Models for Earthquakes: Socioeconomic Impacts.* Peter Gordon, James E. Moore II, and Harry W. Richardson. July 2002.
- PEER 2002/18** *Assessment of Reinforced Concrete Building Exterior Joints with Substandard Details.* Chris P. Pantelides, Jon Hansen, Justin Nadauld, and Lawrence D. Reaveley. May 2002.
- PEER 2002/17** *Structural Characterization and Seismic Response Analysis of a Highway Overcrossing Equipped with Elastomeric Bearings and Fluid Dampers: A Case Study.* Nicos Makris and Jian Zhang. November 2002.
- PEER 2002/16** *Estimation of Uncertainty in Geotechnical Properties for Performance-Based Earthquake Engineering.* Allen L. Jones, Steven L. Kramer, and Pedro Arduino. December 2002.
- PEER 2002/15** *Seismic Behavior of Bridge Columns Subjected to Various Loading Patterns.* Asadollah Esmaeily-Gh. and Yan Xiao. December 2002.
- PEER 2002/14** *Inelastic Seismic Response of Extended Pile Shaft Supported Bridge Structures.* T.C. Hutchinson, R.W. Boulanger, Y.H. Chai, and I.M. Idriss. December 2002.
- PEER 2002/13** *Probabilistic Models and Fragility Estimates for Bridge Components and Systems.* Paolo Gardoni, Armen Der Kiureghian, and Khalid M. Mosalam. June 2002.
- PEER 2002/12** *Effects of Fault Dip and Slip Rake on Near-Source Ground Motions: Why Chi-Chi Was a Relatively Mild M7.6 Earthquake.* Brad T. Aagaard, John F. Hall, and Thomas H. Heaton. December 2002.
- PEER 2002/11** *Analytical and Experimental Study of Fiber-Reinforced Strip Isolators.* James M. Kelly and Shakhzod M. Takhirov. September 2002.
- PEER 2002/10** *Centrifuge Modeling of Settlement and Lateral Spreading with Comparisons to Numerical Analyses.* Sivapalan Gajan and Bruce L. Kutter. January 2003.
- PEER 2002/09** *Documentation and Analysis of Field Case Histories of Seismic Compression during the 1994 Northridge, California, Earthquake.* Jonathan P. Stewart, Patrick M. Smith, Daniel H. Whang, and Jonathan D. Bray. October 2002.

- PEER 2002/08** *Component Testing, Stability Analysis and Characterization of Buckling-Restrained Unbonded Braces™*. Cameron Black, Nicos Makris, and Ian Aiken. September 2002.
- PEER 2002/07** *Seismic Performance of Pile-Wharf Connections*. Charles W. Roeder, Robert Graff, Jennifer Soderstrom, and Jun Han Yoo. December 2001.
- PEER 2002/06** *The Use of Benefit-Cost Analysis for Evaluation of Performance-Based Earthquake Engineering Decisions*. Richard O. Zerbe and Anthony Falit-Baiamonte. September 2001.
- PEER 2002/05** *Guidelines, Specifications, and Seismic Performance Characterization of Nonstructural Building Components and Equipment*. André Filiatrault, Constantin Christopoulos, and Christopher Stearns. September 2001.
- PEER 2002/04** *Consortium of Organizations for Strong-Motion Observation Systems and the Pacific Earthquake Engineering Research Center Lifelines Program: Invited Workshop on Archiving and Web Dissemination of Geotechnical Data, 4–5 October 2001*. September 2002.
- PEER 2002/03** *Investigation of Sensitivity of Building Loss Estimates to Major Uncertain Variables for the Van Nuys Testbed*. Keith A. Porter, James L. Beck, and Rustem V. Shaikhutdinov. August 2002.
- PEER 2002/02** *The Third U.S.-Japan Workshop on Performance-Based Earthquake Engineering Methodology for Reinforced Concrete Building Structures*. July 2002.
- PEER 2002/01** *Nonstructural Loss Estimation: The UC Berkeley Case Study*. Mary C. Comerio and John C. Stallmeyer. December 2001.
- PEER 2001/16** *Statistics of SDF-System Estimate of Roof Displacement for Pushover Analysis of Buildings*. Anil K. Chopra, Rakesh K. Goel, and Chatpan Chintanapakdee. December 2001.
- PEER 2001/15** *Damage to Bridges during the 2001 Nisqually Earthquake*. R. Tyler Ranf, Marc O. Eberhard, and Michael P. Berry. November 2001.
- PEER 2001/14** *Rocking Response of Equipment Anchored to a Base Foundation*. Nicos Makris and Cameron J. Black. September 2001.
- PEER 2001/13** *Modeling Soil Liquefaction Hazards for Performance-Based Earthquake Engineering*. Steven L. Kramer and Ahmed-W. Elgamal. February 2001.
- PEER 2001/12** *Development of Geotechnical Capabilities in OpenSees*. Boris Jeremi . September 2001.
- PEER 2001/11** *Analytical and Experimental Study of Fiber-Reinforced Elastomeric Isolators*. James M. Kelly and Shakhzod M. Takhirov. September 2001.
- PEER 2001/10** *Amplification Factors for Spectral Acceleration in Active Regions*. Jonathan P. Stewart, Andrew H. Liu, Yoojoong Choi, and Mehmet B. Baturay. December 2001.
- PEER 2001/09** *Ground Motion Evaluation Procedures for Performance-Based Design*. Jonathan P. Stewart, Shyh-Jeng Chiou, Jonathan D. Bray, Robert W. Graves, Paul G. Somerville, and Norman A. Abrahamson. September 2001.
- PEER 2001/08** *Experimental and Computational Evaluation of Reinforced Concrete Bridge Beam-Column Connections for Seismic Performance*. Clay J. Naito, Jack P. Moehle, and Khalid M. Mosalam. November 2001.
- PEER 2001/07** *The Rocking Spectrum and the Shortcomings of Design Guidelines*. Nicos Makris and Dimitrios Konstantinidis. August 2001.
- PEER 2001/06** *Development of an Electrical Substation Equipment Performance Database for Evaluation of Equipment Fragilities*. Thalia Agnanos. April 1999.
- PEER 2001/05** *Stiffness Analysis of Fiber-Reinforced Elastomeric Isolators*. Hsiang-Chuan Tsai and James M. Kelly. May 2001.
- PEER 2001/04** *Organizational and Societal Considerations for Performance-Based Earthquake Engineering*. Peter J. May. April 2001.
- PEER 2001/03** *A Modal Pushover Analysis Procedure to Estimate Seismic Demands for Buildings: Theory and Preliminary Evaluation*. Anil K. Chopra and Rakesh K. Goel. January 2001.
- PEER 2001/02** *Seismic Response Analysis of Highway Overcrossings Including Soil-Structure Interaction*. Jian Zhang and Nicos Makris. March 2001.
- PEER 2001/01** *Experimental Study of Large Seismic Steel Beam-to-Column Connections*. Egor P. Popov and Shakhzod M. Takhirov. November 2000.
- PEER 2000/10** *The Second U.S.-Japan Workshop on Performance-Based Earthquake Engineering Methodology for Reinforced Concrete Building Structures*. March 2000.

- PEER 2000/09** *Structural Engineering Reconnaissance of the August 17, 1999 Earthquake: Kocaeli (Izmit), Turkey.* Halil Sezen, Kenneth J. Elwood, Andrew S. Whittaker, Khalid Mosalam, John J. Wallace, and John F. Stanton. December 2000.
- PEER 2000/08** *Behavior of Reinforced Concrete Bridge Columns Having Varying Aspect Ratios and Varying Lengths of Confinement.* Anthony J. Calderone, Dawn E. Lehman, and Jack P. Moehle. January 2001.
- PEER 2000/07** *Cover-Plate and Flange-Plate Reinforced Steel Moment-Resisting Connections.* Taejin Kim, Andrew S. Whittaker, Amir S. Gilani, Vitelmo V. Bertero, and Shakhzod M. Takhirov. September 2000.
- PEER 2000/06** *Seismic Evaluation and Analysis of 230-kV Disconnect Switches.* Amir S. J. Gilani, Andrew S. Whittaker, Gregory L. Fenves, Chun-Hao Chen, Henry Ho, and Eric Fujisaki. July 2000.
- PEER 2000/05** *Performance-Based Evaluation of Exterior Reinforced Concrete Building Joints for Seismic Excitation.* Chandra Clyde, Chris P. Pantelides, and Lawrence D. Reaveley. July 2000.
- PEER 2000/04** *An Evaluation of Seismic Energy Demand: An Attenuation Approach.* Chung-Che Chou and Chia-Ming Uang. July 1999.
- PEER 2000/03** *Framing Earthquake Retrofitting Decisions: The Case of Hillside Homes in Los Angeles.* Detlof von Winterfeldt, Nels Roselund, and Alicia Kitsuse. March 2000.
- PEER 2000/02** *U.S.-Japan Workshop on the Effects of Near-Field Earthquake Shaking.* Andrew Whittaker, ed. July 2000.
- PEER 2000/01** *Further Studies on Seismic Interaction in Interconnected Electrical Substation Equipment.* Armen Der Kiureghian, Kee-Jeung Hong, and Jerome L. Sackman. November 1999.
- PEER 1999/14** *Seismic Evaluation and Retrofit of 230-kV Porcelain Transformer Bushings.* Amir S. Gilani, Andrew S. Whittaker, Gregory L. Fenves, and Eric Fujisaki. December 1999.
- PEER 1999/13** *Building Vulnerability Studies: Modeling and Evaluation of Tilt-up and Steel Reinforced Concrete Buildings.* John W. Wallace, Jonathan P. Stewart, and Andrew S. Whittaker, editors. December 1999.
- PEER 1999/12** *Rehabilitation of Nonductile RC Frame Building Using Encasement Plates and Energy-Dissipating Devices.* Mehrdad Sasani, Vitelmo V. Bertero, James C. Anderson. December 1999.
- PEER 1999/11** *Performance Evaluation Database for Concrete Bridge Components and Systems under Simulated Seismic Loads.* Yael D. Hose and Frieder Seible. November 1999.
- PEER 1999/10** *U.S.-Japan Workshop on Performance-Based Earthquake Engineering Methodology for Reinforced Concrete Building Structures.* December 1999.
- PEER 1999/09** *Performance Improvement of Long Period Building Structures Subjected to Severe Pulse-Type Ground Motions.* James C. Anderson, Vitelmo V. Bertero, and Raul Bertero. October 1999.
- PEER 1999/08** *Envelopes for Seismic Response Vectors.* Charles Menun and Armen Der Kiureghian. July 1999.
- PEER 1999/07** *Documentation of Strengths and Weaknesses of Current Computer Analysis Methods for Seismic Performance of Reinforced Concrete Members.* William F. Cofer. November 1999.
- PEER 1999/06** *Rocking Response and Overturning of Anchored Equipment under Seismic Excitations.* Nicos Makris and Jian Zhang. November 1999.
- PEER 1999/05** *Seismic Evaluation of 550 kV Porcelain Transformer Bushings.* Amir S. Gilani, Andrew S. Whittaker, Gregory L. Fenves, and Eric Fujisaki. October 1999.
- PEER 1999/04** *Adoption and Enforcement of Earthquake Risk-Reduction Measures.* Peter J. May, Raymond J. Burby, T. Jens Feeley, and Robert Wood.
- PEER 1999/03** *Task 3 Characterization of Site Response General Site Categories.* Adrian Rodriguez-Marek, Jonathan D. Bray, and Norman Abrahamson. February 1999.
- PEER 1999/02** *Capacity-Demand-Diagram Methods for Estimating Seismic Deformation of Inelastic Structures: SDF Systems.* Anil K. Chopra and Rakesh Goel. April 1999.
- PEER 1999/01** *Interaction in Interconnected Electrical Substation Equipment Subjected to Earthquake Ground Motions.* Armen Der Kiureghian, Jerome L. Sackman, and Kee-Jeung Hong. February 1999.
- PEER 1998/08** *Behavior and Failure Analysis of a Multiple-Frame Highway Bridge in the 1994 Northridge Earthquake.* Gregory L. Fenves and Michael Ellery. December 1998.
- PEER 1998/07** *Empirical Evaluation of Inertial Soil-Structure Interaction Effects.* Jonathan P. Stewart, Raymond B. Seed, and Gregory L. Fenves. November 1998.
- PEER 1998/06** *Effect of Damping Mechanisms on the Response of Seismic Isolated Structures.* Nicos Makris and Shih-Po Chang. November 1998.

- PEER 1998/05** *Rocking Response and Overturning of Equipment under Horizontal Pulse-Type Motions.* Nicos Makris and Yiannis Roussos. October 1998.
- PEER 1998/04** *Pacific Earthquake Engineering Research Invitational Workshop Proceedings, May 14–15, 1998: Defining the Links between Planning, Policy Analysis, Economics and Earthquake Engineering.* Mary Comerio and Peter Gordon. September 1998.
- PEER 1998/03** *Repair/Upgrade Procedures for Welded Beam to Column Connections.* James C. Anderson and Xiaojing Duan. May 1998.
- PEER 1998/02** *Seismic Evaluation of 196 kV Porcelain Transformer Bushings.* Amir S. Gilani, Juan W. Chavez, Gregory L. Fenves, and Andrew S. Whittaker. May 1998.
- PEER 1998/01** *Seismic Performance of Well-Confined Concrete Bridge Columns.* Dawn E. Lehman and Jack P. Moehle. December 2000.

## ONLINE REPORTS

The following PEER reports are available by Internet only at [http://peer.berkeley.edu/publications/peer\\_reports.html](http://peer.berkeley.edu/publications/peer_reports.html)

- PEER 2010/109** *Report of the Seventh Joint Planning Meeting of NEES/E-Defense Collaboration on Earthquake Engineering. Held at the E-Defense, Miki, and Shin-Kobe, Japan, September 18–19, 2009.* August 2010.
- PEER 2010/107** *Performance and Reliability of Exposed Column Base Plate Connections for Steel Moment-Resisting Frames.* Ady Aviram, Božidar Stojadinovic, and Armen Der Kiureghian. August 2010.
- PEER 2010/106** *Verification of Probabilistic Seismic Hazard Analysis Computer Programs.* Patricia Thomas, Ivan Wong, and Norman Abrahamson. May 2010.
- PEER 2010/105** *Structural Engineering Reconnaissance of the April 6, 2009, Abruzzo, Italy, Earthquake, and Lessons Learned.* M. Selim Günay and Khalid M. Mosalam. April 2010.
- PEER 2010/104** *Simulating the Inelastic Seismic Behavior of Steel Braced Frames, Including the Effects of Low-Cycle Fatigue.* Yuli Huang and Stephen A. Mahin. April 2010.
- PEER 2010/103** *Post-Earthquake Traffic Capacity of Modern Bridges in California.* Vesna Terzic and Božidar Stojadinović. March 2010.
- PEER 2010/102** *Analysis of Cumulative Absolute Velocity (CAV) and JMA Instrumental Seismic Intensity ( $I_{JMA}$ ) Using the PEER–NGA Strong Motion Database.* Kenneth W. Campbell and Yousef Bozorgnia. February 2010.
- PEER 2010/101** *Rocking Response of Bridges on Shallow Foundations.* Jose A. Ugalde, Bruce L. Kutter, Boris Jeremic
- PEER 2009/109** *Simulation and Performance-Based Earthquake Engineering Assessment of Self-Centering Post-Tensioned Concrete Bridge Systems.* Won K. Lee and Sarah L. Billington. December 2009.
- PEER 2009/108** *PEER Lifelines Geotechnical Virtual Data Center.* J. Carl Stepp, Daniel J. Ponti, Loren L. Turner, Jennifer N. Swift, Sean Devlin, Yang Zhu, Jean Benoit, and John Bobbitt. September 2009.
- PEER 2009/107** *Experimental and Computational Evaluation of Current and Innovative In-Span Hinge Details in Reinforced Concrete Box-Girder Bridges: Part 2: Post-Test Analysis and Design Recommendations.* Matias A. Hube and Khalid M. Mosalam. December 2009.
- PEER 2009/106** *Shear Strength Models of Exterior Beam-Column Joints without Transverse Reinforcement.* Sangjoon Park and Khalid M. Mosalam. November 2009.
- PEER 2009/105** *Reduced Uncertainty of Ground Motion Prediction Equations through Bayesian Variance Analysis.* Robb Eric S. Moss. November 2009.
- PEER 2009/104** *Advanced Implementation of Hybrid Simulation.* Andreas H. Schellenberg, Stephen A. Mahin, Gregory L. Fenves. November 2009.
- PEER 2009/103** *Performance Evaluation of Innovative Steel Braced Frames.* T. Y. Yang, Jack P. Moehle, and Božidar Stojadinovic. August 2009.
- PEER 2009/102** *Reinvestigation of Liquefaction and Nonliquefaction Case Histories from the 1976 Tangshan Earthquake.* Robb Eric Moss, Robert E. Kayen, Liyuan Tong, Songyu Liu, Guojun Cai, and Jiaer Wu. August 2009.
- PEER 2009/101** *Report of the First Joint Planning Meeting for the Second Phase of NEES/E-Defense Collaborative Research on Earthquake Engineering.* Stephen A. Mahin et al. July 2009.
- PEER 2008/104** *Experimental and Analytical Study of the Seismic Performance of Retaining Structures.* Linda Al Atik and Nicholas Sitar. January 2009.
- PEER 2008/103** *Experimental and Computational Evaluation of Current and Innovative In-Span Hinge Details in Reinforced Concrete Box-Girder Bridges. Part 1: Experimental Findings and Pre-Test Analysis.* Matias A. Hube and Khalid M. Mosalam. January 2009.
- PEER 2008/102** *Modeling of Unreinforced Masonry Infill Walls Considering In-Plane and Out-of-Plane Interaction.* Stephen Kadysiewski and Khalid M. Mosalam. January 2009.
- PEER 2008/101** *Seismic Performance Objectives for Tall Buildings.* William T. Holmes, Charles Kircher, William Petak, and Nabih Youssef. August 2008.
- PEER 2007/101** *Generalized Hybrid Simulation Framework for Structural Systems Subjected to Seismic Loading.* Tarek Elkhoraibi and Khalid M. Mosalam. July 2007.
- PEER 2007/100** *Seismic Evaluation of Reinforced Concrete Buildings Including Effects of Masonry Infill Walls.* Alidad Hashemi and Khalid M. Mosalam. July 2007.